UNDERSTANDING ANATOMICAL PERFUSION AND STRATEGIES TO OPTIMIZE VASCULARITY IN FREE TISSUE TRANSFER FOR AUTOLOGOUS BREAST RECONSTRUCTION USING THE DEEP INFERIOR EPIGASTRIC ARTERY PERFORATOR (DIEP) FLAP

ANITA TANNIRU MOHAN

CLARE COLLEGE

DEPARTMENT OF SURGERY

UNIVERSITY OF CAMBRIDGE

THIS DISSERATION IS SUBMITTED FOR THE DEGREE OF DOCTOR OF PHILOSOPHY

MARCH 2019

"What interests me in life is curiosity, challenges, the good fight with its victories and defeats."

Paulo coehlo

DECLARATION

I, Anita T Mohan declare that this dissertation is the result of my own work and includes nothing, which is the outcome of work done in collaboration except where specifically indicated in the text. It has not been previously submitted, in part or whole, to any university of institution for any degree, diploma, or other qualification.

In accordance with the Department of Surgery guidelines, this thesis is does not exceed 80,000 words, and it contains less than 150 figures.

Anita T Mohan MRCS(Eng), MBBS, BSc(Hons)

ABSTRACT

Understanding Anatomical Perfusion and Strategies to Optimize Vascularity in Free Tissue Transfer for Autologous Breast Reconstruction using the Deep Inferior Epigastric Artery Perforator Flap

Anita T Mohan

Breast cancer is the commonest cancer that affects women in the United Kingdom (UK). Autologous free tissue transfer using abdominal tissue remains an excellent option for breast reconstruction following mastectomy, given greater availability of tissue and lower donor site morbidity associated with muscle-sparing approaches (perforator-based). This research evaluated microvascular anatomy of Deep Inferior Epigastric Artery Perforator (DIEP) flaps, the role of linking vessels on dynamic perfusion in bilateral breast reconstruction and strategies to augment flap vascularity.

For the ex-vivo anatomical studies, three and four-dimensional computed tomographic angiography (CTA) were used to evaluate patterns of the microvascular blood supply of individual perforators and corresponding perfusion patterns in the hemi-abdomen. This was combined with an in-vivo clinical study of women undergoing bilateral DIEP breast reconstruction following mastectomy, where both preoperative CTA and intra-operative Laser-Assisted Indocyanine Green Fluorescence Angiography (LA-ICGFA) were used to evaluate perforator anatomy and dynamic perfusion zones of individual perforators. Finally, an experimental in-vivo animal model was used to investigate strategies of pre-treatment of perforator flaps with negative pressure wound therapy to augment vascularity of perforator flaps prior to flap harvest.

The vascular territories of individual perforator within hemi-DIEP flaps demonstrated variable patterns with unique patterns of perfusion. Concepts including early capture of large calibre direct linking vessels to adjacent perforators or the superficial inferior epigastric artery (SIEA) territories, mostly found in the supra-scarpa's and subdermal layers of the flap, played a key role in defining overall perfusion area and dynamic perfusion patterns not previously described.

In conclusion, this work reported the characterization of the microvasculature within abdominal-based perforator flaps to better understand the variation in dynamic perfusion. It also explored the potential role of non-invasive negative pressure treatment to augment flap perfusion that may be translated into the clinical setting.

ACKNOWLEDGEMENTS

I would like to thank Professor Michel Saint-Cyr for his kind supervision, wisdom and mentorship. His profound enthusiasm, generation of ideas and concepts provided the foundation of my skills as a scientist, and encouraged me to continually work hard, and appraise current surgical practices to identify avenues to develop new ideas that can be transformed into the clinical environment to optimize management of our patients. It was an overwhelming privilege to have you as my clinical supervisor during my PhD and I thank you for your support and making my PhD a challenging and enriching experience.

This opportunity would not have been possible without the mentorship of Professor Charles M Malata. You have provided incredible support and inspiration throughout my clinical training and during my PhD, sharing your vast knowledge and experience, that gave me the inspiration to succeed in both my clinical and academic training. Furthermore, I am grateful for the academic support and guidance of my academic supervisor Professor Nicholson at the University of Cambridge.

I have tremendous gratitude to the members and technical staff of the Department of Anatomy at Mayo Clinic who facilitated my anatomical work and always were there to help, provide guidance and created a wonderful working environment even during stressful times. Dr Nirusha Lachman, thank you for your mentorship, friendship, and sharing your vast expertise in the field of anatomical research. I would like to also acknowledge the noble generosity of the Mayo Clinic's whole-body donors whose altruistic gift made this study possible.

I would like to thank the collaboration with the Department of Radiology to build protocols for the research, brainstorming and providing technical assistance to carry out my work. Thank you Dr Gregory Michalak and Andrew Vercnoeke for your time and dedication over the last three years in refining our protocols and providing your great expertise for image analysis. Thank you to Jill Anderson for welcoming me to Mayo Clinic, your kind heart, willingness to teach and assist me in the early stages of my research was profound.

Thank you to Drs Cheng Chen and TB Ferguson for your collaboration to develop novel approaches to assessment of dynamic perfusion and your expertise for image post-processing and analysis.

I would also like to thank the Department of Comparative Medicine, Department of Surgical Research and Department of Orthopaedic Research, in particular Dr Allen Bishop and Patrician Friedrich, Bruce Knudson and Professor Chungfeng Zhao in welcoming me to labs, operative assistance, training, brainstorming the hurdles and challenges and facilitating the completion of my animal studies. None of this would have been possible without your expertise, collaboration and support.

A huge thank you to my friends and family for their patience and invaluable support, listening to me, guiding me, and giving me the love, strength and encouragement throughout my PhD studies and clinical training.

TABLE OF CONTENTS

LIST OF FIGURES ***10***

LIST OF TABLES ***20***

CHAPTER 1: INTRODUCTION ***21***

1.1 Overview **22**

1.2 Rationale **26**

1.3 Hypothesis and Aims **28**

CHAPTER 2: LITERATURE REVIEW ***29***

2.1 Anatomy and Physiology of the Deep Inferior Epigastric Artery Perforator Flaps in Bilateral Breast Reconstruction **30**

2.1.1 Perforator Anatomy and Flap Design in Perforator Flap Surgery 30

2.1.2 Autologous free tissue transfer in breast reconstruction 32

2.1.3 Vascular anatomy of the Deep Inferior Epigastric Artery Perforator (DIEP) Flap in breast reconstruction 34

2.1.4 Zonal perfusion of the Deep Inferior Epigastric Artery Perforator (DIEP) Flap 38

2.1.5 Imaging Techniques in DIEP Breast Reconstruction 43

2.1.6 Computed Tomographic Angiography to Assess DIEP Vascular Anatomy 44

2.1.7 Magnetic Resonance Angiography to Assess DIEP Vascular Anatomy 46

Table 2.1: Overview of advantages and Disadvantages of Computer Tomographic Angiography (CTA) and Magnetic Resonance Angiography (MRA) to assess vascular anatomy in breast reconstruction. 48

Advantages 48

Disadvantages 48

2.1.8 Laser Assisted Indocyanine Green Fluorescence Angiography (LA-ICGFA) in Breast Reconstruction 49

2.1.9 Dynamic Infrared Thermography (DIRT) to Assess DIEP Perfusion 50

2.2 Topical Negative Pressure Pre-treatment and Implications on Flap Vascularity **53**

2.2.1 Overview of strategies to augment flap perfusion 53

2.2.2 The Delay Phenomenon 54

2.2.3 Ischemic Preconditioning 55

2.2.4 Alternative Preconditioning Techniques 56

2.2.5 Negative Pressure Therapy Pre-treatment to Augment Vascularity 57

2.2.6 Experimental Animal Flap Models 59

CHAPTER 3: MATERIALS AND METHODS ***60***

3.1 Evaluation of the microcirculation anatomy and flap physiology of the deep inferior epigastric artery perforator flaps in bilateral breast reconstruction **61**

3.1.1 Anatomical Cadaveric Study of the Perfusion Territories (Perforasomes) of DIEA perforators in the Hemi-Abdomen 61

3.1.1.1 Preliminary Cadaveric Studies 62

3.1.1.2 Deep Inferior Epigastric Artery Perforator Cadaveric Study 64

3.1.1.3 Three-dimensional Computed Tomographic Angiography (3D-CTA) 66

3.1.1.4 Four-dimensional Computed Tomographic Angiography (4D-CTA) 68

3.1.1.5 CTA Analysis 69

3.1.2 Clinical Study to Evaluate of Anatomy and Dynamic DIEA Perfusion Territories (Perforasomes) of Hemi-DIEP Flaps in Breast reconstruction 71

3.1.2.1 Patient Population 71

3.1.2.2 Analysis of Pre-operative Computed Tomographic Angiography 72

3.1.2.3 Analysis of Laser-Assisted Indocyanine Green Fluorescence Angiography 78

3.1.2.4 Statistical Analysis 84

3.2 An Experimental Small Animal Model to Evaluate Topical Negative Pressure Pre-treatment and Implications on Flap Vascularity 85
3.2.1 Preliminary Work 85
3.2.2 Experimental animals 87
3.2.3 Pilot studies 87
3.2.4 Overview of Experimental Methods 89
3.2.5 Animal Procedures 91
3.2.6 Outcome Assessment of 4D dynamic perfusion CT imaging 97
3.2.7 Outcomes Assessment of Indocyanine Green Fluorescence Laser Angiography 99
3.2.8 Outcomes Assessment of Micro CT 99
3.2.9 Outcomes Assessment of Histology 101
3.2.10 Statistical analysis 102

CHAPTER 4: RESULTS 103

4.1: Anatomical Cadaveric Study of the Perfusion Territories (Perforasomes) of DIEA perforators in the Hemi-Abdomen 104
4.1.1 DIEA Perforator Mapping in Hemi-Abdominal Flap 104
4.1.2 Assessment of Perforator Vascular Territories (Perforasome) 105
4.1.3 Assessment of Linking Vessels on Perforator Territories 109
4.1.4 Qualitative analysis of dominant axiality of flow within the perforasome 112
4.1.5 Qualitative analysis of 4-Dimensional perforator vascular territory 114

4.2: Clinical Study to Evaluate of Anatomy and Dynamic DIEA Perfusion Territories (Perforasomes) of Hemi-DIEP Flaps in Breast Reconstruction 118
4.2.1 Patient Population 118
4.2.2 Evaluation of Preoperative Computed Tomographic Angiography 119
4.2.3 Analysis of Hemi-DIEP perforasome with Laser Assisted Indocyanine Green Fluorescence Angiography 119
4.2.4 Analysis of Computed Tomographic Angiography and Hemi-DIEP perforasome with Laser Assisted Indocyanine Green Fluorescence Angiography 125
4.2.4.1 Medial versus Lateral Row perforators 125
4.2.4.2 Course and characteristics of the DIEA perforator 125
4.2.4.3 Branching patterns of the perforator in the Hemi-DIEP flap 126
4.2.4.4 Presence of dominant linking vessels in the Hemi-DIEP flap 128
4.2.4.5 Characteristics of perforator anatomy, branching patterns and linking vessels on SPY perfusion patterns 129
4.2.4.6 Surgical outcomes of DIEP Breast 136

4.3 An Experimental Small Animal Model to Evaluate Topical Negative Pressure Pre-treatment and Implications on Flap Vascularity 137
4.3.1 Animal Experiment and Data Acquisition 137
4.3.2 Outcome Measurements of Dynamic Computed Tomographic Angiography 138
4.3.3 Outcome Measurements of Laser Assisted ICG Fluorescence Angiography 142
4.3.4 Outcome Measurements of Micro-Computed Tomography Angiography 145
4.3.5 Outcome Measurements of Clinical Flap Viability 146
4.3.6 Outcome Measurements of Histological Assessment 148
4.3.6.1 Epidermis: H&E Stain 149
4.3.6.2 Dermis: H&E Stain 151
4.3.6.3 CD 31 Immunohistochemical staining 153

CHAPTER 5: DISCUSSION 157

5.1 Anatomy and Physiology of the Perforasome of Deep Inferior Epigastric Artery Perforators in bilateral breast reconstruction 158
5.1.1 Perforator Anatomy and Perforasomes of Hemi-DIEP flaps 158
5.1.2 A Novel Approach to Evaluate Dynamic Perforasomes of DIEP Flaps in Bilateral Breast Reconstruction In-Vivo 160

5.1.3 Bridging the Gap Between Microvascular Anatomy and Impact on Dynamic Perforasomes of DIEP flaps in Bilateral Breast Reconstruction 164

5.2 Topical Negative Pressure Pre-treatment and Implications on Flap Vascularity 167

5.2.1 The Concept of Delay and Pre-conditioning Flaps 167

5.2.2 Biological Mechanisms of Negative Pressure Wound Therapy 169

5.2.3 The Role of Negative Pressure Wound Therapy Pre-Treatment in Flap Surgery 170

5.3 Limitations 171

5.4 General Conclusions 174

5.5 Future Work 175

BIBLIOGRAPHY 176

APPENDIX 204

APPENDIX 1: List of Products 205

APPENDIX 2: List of Presentations 206

APPENDIX 3: Publications 209

APPENDIX 4: Preoperative CTA DIEP protocol 210

LIST OF FIGURES

Figure Number	**Caption**	Page Number
	SECTION 2: LITERATURE REVIEW	
2.1	Pictorial representation of Taylor and Palmer Angiosomes and predicted vascular arterial territories of the source arteries	31
2.2	Illustration of the DIEP flap harvest of only skin and subcutaneous fat, with a dissection of the pedicle through the rectus muscle	33
2.3	Schematic illustrations of the arterial systems of the anterior torso demonstrating the angiosome concept and dotted lines representing the choke vessels of adjacent territories (*Left)* and general angiosome territories and their representative source vessels (*Right*).	35
2.4	Three dimensional computed tomographic angiography (CTA) and demonstration of DIEP perforators in the paraumbilical area	37
2.5	Illustration and patient demonstration of location of dominant perforators of the deep inferior epigastric vessels in relation to the umbilicus (left); and representation of key areas of dominant perforators (hot spots) in red, and areas of deficient dominant perforators (cold spots) in blue	38
2.6	Representation of Hartrampf zones of perfusion of Deep Inferior Epigastric Artery Perforator (DIEP) in the lower abdomen	39
2.7	Micro-CT analysis of an injected perforator and presence of direct linking vessels and indirect linking vessels via the subdermal plexus, with connections to an adjacent perforator. The upper portion of the image represents the perforator and deep surface of the flap and the inferior portion of the image represents the skin.	40
2.8	Left Hemi-DIEP based on a medial row single dominant perforator, however large linking vessel can be identified on CT between medial	42

	and lateral row perforator using timing map SPYQC ® analysis from the ICG fluorescence angiography captured with SPY® Elite system.	
2.9	New proposed model of perforasome perfusion of the lower abdomen following sequential pattern between adjacent perforasome.	43
	SECTION 3: MATERIALS AND METHODS	
3.1	Set up of Harvard pump and tubing (large, intermediate and small diameters) to simulate trials for development of initial 4D injection protocol	63
3.2	Anatomical dissection outline for flap harvest on a fresh female cadaveric specimen (left); Hemi-abdominal flap raised with perforators marked on skin and the dominant perforators dissected for subsequent cannulation, red arrow (centre) and hemi-abdominal flap with perforators mapped (right).	65
3.3	Preparation of hemi-abdominal flap for CT scanning (left) and example of injection of a medial row perforator and mapping of perforator territory within the hemi-abdominal flap (right).	67
3.4	3D CTA reconstruction of individual perforator territories and comparison of medial and lateral rows territories in the hemi-abdominal integument	68
3.5	Example of an axial image of Maximum Intensity Projection reconstruction in a patient following contrast CTA. Marker set at level of umbilicus in the midline. Scarpa's fascia can be identified and traced (orange arrow) and dominant traversing inking vessel in suprascarpa's fascia (blue arrow).	75
3.6	Example of an axial image of Maximum Intensity Projection reconstruction in a patient following contrast CTA. Marker set at level of umbilicus in the midline. Degree and layer of arborisation assessed through multi-plane views and type of pattern of contribution to supply the subdermal plexus characterized. Multiple branching at the layer of the fascia shown (green arrow).	76

3.7	Example of scoring used for branching of perforator in the subscarpa's layer shown in an axial slice image in a patient following contrast CTA: 1=none, 2=minimal (1-2 branches) and 3=multiple branches.	76
3.8	Two examples of a sagittal slice images of Maximum Intensity Projection reconstruction in a patient following contrast CTA. Marker set at level of umbilicus and direct linking vessel could be traced to the SIEA (blue arrow), and contributions to the subdermal plexus can be visualised from the dominant perforator (red arrows).	77
3.9	Example of a axial slice image of Maximum Intensity Projection reconstruction in a patient following contrast CTA, illustrating a lateral linking vessel in the suprascarpa's layer (blue arrow) and additional linking vessel in the subdermis could be traced directly to DCIA perforator passing through the external oblique muscle (green arrow).	77
3.10	Three angiographic phases of perfusion captured using the SPY Elite® system camera, starting with arterial, microvascular (ingress) and venous (egress)	80
3.11	Graphic illustration of software calculation and capture of total concentration (intensity) of indocyanine green injected detected over total time of the recording pixel by pixel over the entire Region of Interest (ROI) or flap area to create intensity maps	82
3.12	Graphic illustration of software calculation and capture of rate of inflow (ingress of indocyanine green detected over total time, pixel by pixel, over the entire Region of Interest (ROI) or flap area to creating timing maps	83
3.13	Example of LA-ICGFA cumulative perfusion mapping during image capture with SPY Elite® of a hemi-DIEP flap based on a single dominant perforator and graphs of cranio-caudal and medial to lateral perfusion on timing maps (left) and intensity perfusion maps	83

	(right)	
3.14	Cadaveric dissection of the dorsal rat skin to identify perforators; Cranial Deep Circumflex Iliac Artery (DCIA) perforators arose next to the gluteal maximus (GM) muscle. The caudal biceps femoris (BF) perforators were also consistent but located to caudal to provide a reliable location for NPWT application	86
3.15	Planned gluteal perforator flap design based on the DCIA vessels following hair removal. Two flaps representing the control (rat's left side) and intervention flap (rat's right side) were designed	87
3.16	Overview of methods to show animals, groups and outcome measures used at each stage of the study	90
3.17	Illustration of muscle anatomy and location of perforator vessel exiting proximal to the superficial gluteus and biceps femoris muscles and running in the caudal direction to be included in the flap design (*black dotted square)*	92
3.18	Inhalation anaesthesia set up for induction and maintenance (left); materials for application of VAC dressing (right)	93
3.19	Application of VAC Granufoam ™ sponge dressing (A); occlusive dressing applied and Sensa TRAC ™ pad applied (B); further Tegaderm ™ to accommodate rat's movement and maintain seal and flexible spring coil placed to protect tubing (C), and application of a light torso waterproof tape (right)	94
3.20	Each animal was singly housed and closely monitored to ensure it could freely mobilize around its cage following application of the VAC® dressing	94
3.21	Flap outlines and SPY imaging demonstrating perfusion during image acquisition for control on the rat's left side and the preconditioned side on the rat's left hand side	95
3.22	Flaps marked, incised and raised over the gluteal region of rat, and finally re-sutured	97

3.23	An axial image of the 4DCT with an Region of Interest (ROI) drawn over the preconditioned area (pink) and control area (red). Graphs represent absolute quantity of contrast detected in Hounsfield units, in the respective ROI, against time in seconds	98
3.24	Example of 3D reconstruction of microvessel architecture of skin flaps control versus preconditioned	100
	SECTION 4: RESULTS	
4.1	Maximal Intensity Projection (MIP) images of two perforator injections of a lateral row (left) and medial row (right) perforator in the same flap analyzed using the Syngo® CT workplace (Siemens). Perforator injection areas (perforasomes) were superimposed onto one another and perforasome area, flap area and degree of overlap could be compared	105
4.2	Graph to show comparison of perforasome as a percentage of the total hemi-abdominal flap area in medial and lateral row DIEA perforators.	106
4.3	Graph to illustrate correlation between body mass index (BMI, kg/m^2) and total number of DIEA perforators of the anterior hemi-abdomen and line of best fit	108
4.4	3D maximal intensity projection (MIP) images of a right hemi-abdominal flap and comparison of a medial and lateral row perforator injection studies; Orange arrows demonstrate capture of dominant linking vessel that courses through the integument.	110
4.5	3D Maximal Intensity Projection (MIP) images of a left hemi-abdominal flap and comparison of medial and lateral row DIEA injection studies highlighting how linking vessels course through the integument and overlap with potential adjacent source artery territories of the DCIA and SIEA	110
4.6	Graph to show median and interquartile ranges of perforasome area (cm^2) between different combination of dominant linking vessels (inter-row, intra-row and lateral) captured following DIEA	112

	perforator injection	
4.7	Graph to show impact of dominant axiality of flow / perforasome distribution on total perforasome area (cm^2)	113
4.8	Two examples (A and B) of computed tomographic angiography coronal images captured from 4D scanning following initial 0.5ml injection of contrast into a medial row perforator in left hemi-abdominal flaps. Figures demonstrate initial distribution (left) and final perforasome distribution and area (right).	115
4.9	Two examples (A and B) of computed tomographic angiography axial images captured from 4D scanning following initial 0.5ml injection of contrast into a medial row perforator in left hemi-abdominal flaps. Figures demonstrate initial distribution (left) and final perforasome distribution and area (right). Initial direction of direct and recurrent flow and capture of principle linking vessels and filling patterns are shown (red arrows)	116
4.10	Example of computed tomographic angiography coronal (top image) and axial (bottom image) screenshots captured from 4D scanning following initial 1ml injection of contrast into a medial row perforator in a right hemi-abdominal flap. Dominant direction of flow and filling distributions shown (*red arrows)*	117
4.11	Illustration of the three angiographic phases captures on SPY Elite System® (Novadaq Technologies, Inc.), Image provided by Dr. C Chen and TB Ferguson with permissions.	120
4.12	Three broad categories of perfusion of single dominant hemi-DIEP flaps illustrated on review of timing maps captured using LA-ICGFA using the SPY Elite System ® (Novadaq Technologies, Inc): Single (*right*), Co-dominance (*centre),* and Diffuse (*left*).	121

4.13	An example of imaging captured on LA-ICGFA and analysis using SPYQc ® software (Novadaq Technologies, Inc) reproducing intensity map (left) and timing map (right). Cephalad-caudal and medial-lateral gradients of perfusion were assessed on each axis of the map and area under the curve represents area across the flap and marked to show area than is >75% relative to the reference value. Bottom left recorded areas of perfusion that were >75%, >50% and >25% of perfusion relative to the reference value.	123
4.14	Graph to demonstrate impact of contribution to dermal plexus on the area of flap perfusion above the 25% threshold relative to the perforator.	128
4.15	Example of imaging technologies used to evaluate a right hemi-DIEP flap and assessment of preoperative perforator anatomy (A) axial slice of preoperative DIEP CTA scan demonstrating a single medial dominant row perforator with minimal lateral linking vessels and minimal branching, however an oblique orientation of one of the subscarpa's branches; (B) sagittal image of direct longitudinal connection with the territory of the SIEA territory within the superficial scarpa's layer; (C-E) Video capture of LA-ICGFA at 6 seconds, 12 seconds and 18 seconds (reaching peak of arterial phase); (F) Timing map during the arterial and microvascular phases demonstrating lateralized dominant perfusion of a single medial row perforator hemi-DIEP and centralized hot spot "single pattern"	133
4.16	Example of imaging technologies used to evaluate a right hemi-DIEP flap and assessment of preoperative perforator anatomy (A) axial slice of preoperative DIEP CTA scan demonstrating a single medial dominant row perforator with large bifurcation at the level of the Scarpa's fascia with an oblique orientation of one of the subscarpa's branches that continues laterally (*green arrow*) with multiple contributions to the subdermal plexus (*orange arrows)* (B)	135

	axial magnified image of direct branch from the dominant perforator and connection to the lateral adjacent perforator at the level of the subdermal plexus; (C) Timing map capturing the arterial and microvascular phases demonstrating two initial dominant hot spots of perfusion of a single medial row perforator hemi-DIEP in a "co-dominant pattern", and (D) Video capture of LA-ICGFA at 5 seconds, 10 seconds and 15 seconds (reaching peak of arterial phase).	
4.17	Example of Screenshot of DynEva enhancement curves recording mean Hounsfield Units (HU) detected over time at 0.25cm in the control (red ROI 1) and NPWT treated (pink ROI 2) pre-harvest flap regions	139
4.18	Graph to show mean peak of contrast in Hounsfield Units (HU) during dynamic CT angiography, detected at different distances along the flap in control and NPWT treated flaps**.**	140
4.19	Graph to Show Comparison of Mean Perfusion in Control and NPWT treated flaps at all distances along the flap	141
4.20	Colour maps captured at single time point acquired during LA-ICGFA video assessment in three animals (A-C) prior to surgery, following NPWT treatment. The right flap marked (left of image) was the NPWT treated flap.	143
4.21	Example of an average intensity curve and images of control and NPWT flap captured during the different phases of LA-ICGFA assessment following application of NPWT prior to flap harvest.	143
4.22	Video capture using SPY® Elite during LA-ICGFA assessment at seven days following flap procedure. Area of lower or slower perfusion are represented by the darker region (over the control flap) compared to NPWT pre-conditioned flap**.**	144
4.23	Example of assessment of Micro CT using three-dimensional volume rendered skin flaps with microvasculature demonstrating transverse cross-section and longitudinal views of control and NPWT skin flaps.	145

4.24	Photograph example of one case demonstrating evidence of hyperaemia on the treated side immediately following removal of the VAC® following 7 days of therapy	146
4.25	Photograph to demonstrate control and NPWT pre-treated flap at 7 days post procedure with 100% flap survival	147
4.26	Photograph to demonstrate example of case of significant flap necrosis with comparison of control and NPWT pre-treated flaps at 7 days post procedure	148
4.27	Representative H&E stained section to demonstrate layers within a longitudinal cross-section of dorsal rat skin of a control flap.	149
4.28	Representative H&E stained sample in control flap to demonstrate layers of the epidermis in the dorsal rat skin	150
4.29	Histogram of mean epidermal thickness and standard deviation in control and NPWT pre-treated skin flaps	151
4.30	Representative figure of H&E stained sections showing NPWT pre-treated flaps (right) qualitatively demonstrated greater collagen organization that was more densely arranged compared to control flap (left)	152
4.31	Histological representative views to show example of high-powered views x20 magnification regions for comparison of different semi-quantitative scoring assigned	153
4.32	CD31 quantification based on mean area fraction % per high-power field showing increase in the marker following NPWT removal at Day 7, but this difference was smaller 7 days following surgery, at Day 14	155
	SECTION 5: DISCUSSION	
5.1	(A) Example of an assessment of zonal perfusion as measured using LA-ICGFA. (B) An example of an assessment of zonal perfusion as measured using tissue oximetry	161
5.2	An example of LA-ICGFA used intraoperatively following perforator dissection and flap harvest, just prior to start of ischemia time (A)	162

	Screen shot of the grey scale video visualized during image capture where by perforators, subdermal linking vessels and flow into the flap can be qualitatively assessed; (B) Intensity maps during the arterial and microcirculatory phases with application of color scaled to the amount of ICG detected per pixel; (C) Timing maps during the arterial and microcirculatory phases with application of color scaled to rate of ingress into the flap detected per pixel.	
5.3	Examples of LA-ICGFA timing maps produced using SPY-Qc software® (Novadaq Technologies, Inc). (A-C) Demonstrate different perfusion patterns in single medial row hemi-DIEP flaps with predicted adjacent perforators (blue arrows) & inter-perforator zones (small black arrow); (D) MS-TRAM flap exhibiting traditional Hartrampf zonal perfusion.	163

LIST OF TABLES

Table Number	Caption	Page
2.1	Overview of advantages and Disadvantages of Computer Tomographic Angiography (CTA) and Magnetic Resonance Angiography (MRA) to assess vascular anatomy in breast reconstruction.	48
4.1	Comparison of vascular injection territories of individual perforators (perforasomes) between medial row, lateral row and DCIA perforators in a hemi-abdominal flap	105
4.2	Table to summarize the perfusion limits and areas on LA-ICGFA as analysed by SPY-Qc ® (Novadaq Technologies, Inc).	124
4.3	Summary of the different parameters analysed on preoperative CTA and categories of perfusion patterns defined on SPY-Qc® (single, co-dominant, diffuse).	131
4.4	Summary of successful data points acquired and available for each outcome assessment	138

CHAPTER 1: INTRODUCTION

1.1 Overview

Breast cancer affects 50,000 women in the United Kingdom (UK) and over 250,000 women in the United States (USA) per year, with a lifetime risk of 1 in 8 (1,2). Second to skin cancer, it is the most commonly diagnosed cancer among women and men worldwide, and the commonest cancer affecting women in the UK (3), representing almost one third of newly diagnosed cancers in women in 2017. It is the second leading cause of cancer-related death after lung cancer.(3) Treatment for breast cancer involves surgery with adjuvant therapy. The goal of surgery is to remove the cancer and determine the stage of disease and this may be through breast-conserving therapy (BCS) or mastectomy.

In most cases BCS is followed by radiation. Mastectomy involves the removal of all the breast tissue resulting in the loss of the entire breast. Mastectomy may be required for high tumour size to breast ratio, multi-centric disease, locally advanced or inflammatory cancers. Additional driving forces postulated for women who are eligible for BCS but opt to undergo mastectomy include the need for radiation, fear of recurrence, women under 40 years, women with larger tumours and those who live remote to a treatment facility.(4) The rate of women receiving a mastectomy as their primary therapeutic procedure is approximately 40% in the UK (5) and in the USA 45% receive a mastectomy.(6)

There has been a growing trend in contralateral prophylactic mastectomy (CPM) and simultaneous bilateral reconstruction has been a rising trend in the United States. (7) Indications for bilateral prophylactic mastectomy and CPM include patients with high risk from genetic susceptibility gene mutations including BRCA, a very strong family history and those with aggressive disease based on histology. However in the United States the use of CPM has become prevalent in all stages of breast cancer and low risk disease: 10-15% of women undergoing mastectomy for breast cancer also received CPM in 2006, compared to a decade later, where CPM rates represented nearly 50% of all women undergoing mastectomies and 90% of these women proceed with a reconstruction.(8)

The rise in bilateral mastectomy procedures is largely attributed to patient-driven motivators and in one study by the United States National Cancer Registry revealed that

over 30% of women under the age of 40 underwent CPM. (9) This trend has also been seen in the United Kingdom with the proportion of women without cancer undergoing bilateral mastectomy rising from 12% to 20% between 2002 and 2009 and an estimated annual increase in women with cancer undergoing CPM of 7%. (10) Similar to the United States, 91% of women undergo prophylactic risk reduction surgery, with the majority under 40 years, and 41% of women undergoing CPM proceeded with bilateral immediate breast reconstruction. It is pertinent for the reconstructive and oncologic surgeon to be aware of the rising incidence of bilateral procedures and demand for reconstruction. Bilateral mastectomy in women undergoing CPM, with or without reconstruction, has double the risk of surgical complications compared to unilateral mastectomy(11), therefore risk and morbidity may increase when associated with immediate reconstruction.

Breast reconstruction has become an important consideration for women after mastectomy. The goal is to re-create a breast mound that is naturally soft, durable, looks and feels like a normal breast, and can mature and naturally change with the patient over time. Greater satisfaction in breast appearance in addition to improved physical/emotional wellbeing has been recognized in women who undergo reconstruction compared to those who have a mastectomy alone.(12,13) Women undergoing breast cancer surgery have become younger over the years and so reconstructive options ought to place greater emphasis on longevity. In the 2011 National Mastectomy and Breast Reconstruction audit (UK)(5) it was shown that satisfaction in breast appearance was consistently lower in implant-only reconstructions in both delayed and immediate reconstruction.

The use of autologous tissue is less commonly performed compared to implant-based reconstruction, but still seen as a preferable choice in many circumstances and has gained increasing popularity over the years. A systematic review by Tsoi and colleagues (2014)(14) on patient satisfaction with cosmesis showed that autologous reconstruction provided consistent, stable results that were consistent over time in the follow up period.(14) Documented trends include changes in patient demands and expectations; the disadvantages of implant reconstruction being better understood, and the results with autologous reconstruction being more widely recognized (15,16). The increasing proportion

of young women undergoing mastectomy, secondary to screening programs, education and family history risks, has meant that a durable and natural reconstruction is becoming an increasing important aspect in the reconstructive decision-making process. Autologous tissue can behave very much like normal breast tissue, but the surgery is considered to be more complex and lengthier in comparison to prosthetic based reconstruction. The lower abdomen is the preferred donor site for microvascular reconstruction as it remains unmatched for tissue quality, texture and quantity.(17) In addition, the advancement of microsurgery, reconstructive techniques, and incorporation of enhanced recovery protocols, has significantly reduced the associated morbidity of autologous microvascular breast reconstruction.

The use of abdominal tissue for autologous breast reconstruction has been long and widely practiced, with similar characteristics to breast tissue and an aesthetic donor site scar. The Deep Inferior Epigastric Perforator (DIEP) free flap evolved from the traditional transverse rectus myocutaneous (TRAM) flap that was used for pedicled breast reconstruction based on the superior epigastric artery.(18) The DIEP is harvested as a perforator flap, that is based on small "perforating" vessels that supply the skin and subcutaneous fat and sparing harvest of the underlying rectus muscle. The use of perforator flaps affords considerable improvement in donor site morbidity compared to its predecessor. Abdominal tissue is widely considered the first choice for donor site for unilateral or bilateral autologous microvascular breast reconstruction and the DIEP flap now plays the dominant role in abdominal tissue transfer in autologous reconstruction and often considered the 'gold standard'.(19)

The blood supply of tissue and adequate wound healing potential are pivotal to successful flap harvest and reconstructive surgery. The reconstructive surgeon would attempt to safely harvest the maximum amount of tissue in the lower abdomen, and this is more pertinent in bilateral autologous reconstructions where the donor site is more limited compared to unilateral procedures. Although there have been extraordinary anatomical, technical and technological advances in plastic surgery, there is still an existing problem in clinical practice

to accurately plan and predict the amount of well perfused tissue that can be safely harvested during flap preparation or following transfer.

Complications may be a result of persistent ischemia, hypoxia, post-ischemic reperfusion injury, venous insufficiency of the tissue, or thrombosis that may lead to total or partial flap necrosis. Flaps that are transferred as a free-tissue that require microsurgery experience have a 1-5% flap loss rate in experienced hands, however partial flap necrosis rates can occur in pedicled and free flaps of over 30% (20). It has been recognized that rates of fat necrosis within the flap are higher in DIEP flaps in comparison to pedicled TRAM. (21) However, the use of pedicled TRAM has also notable rates of ischemic complications and partial necrosis.(22)(23,24) These complications can result in considerable morbidity, further reconstructive challenges and increased healthcare costs.

Autologous breast reconstruction has made substantial progress over the years and the evolution of refinements over the last 30 years has allowed flaps to be based on specific perforators. This revolutionary concept can preserve underlying muscle; reducing donor site morbidity, and the ability to tailor the flap to reconstruct exactly the tissues that are missing at the recipient site. The ultimate goal of breast reconstruction following mastectomy is to match optimal tissue replacement with minimal donor-site expenditure. In parallel surgeons will seek ways to ensure safe flap design and harvest while maintaining predictability and reliable tissue perfusion.

Saint-Cyr et al. (2009) highlighted that each perforator has a unique and complex vascular territory and that a single perforator can capture multiple adjacent territories through direct and indirect linking vessels. (25) The same group, published further anatomical studies of vascular territories of the abdominal flaps in breast reconstruction, that raised awareness of differences in branching patterns and perfusion of pedicled TRAM, full TRAM and DIEP flaps(19), and characterized patterns of perfusion and variation of individual perforators in the lower abdomen.(26–28) This anatomical work laid the basis for understanding the implications of individual perforator territories on flap design in unilateral breast reconstruction.

1.2 Rationale

Previous anatomical research has focused on the anterior abdominal wall vascular supply, perfusion based on pedicled TRAM flaps and more recent years further examination of perfusion based on individual perforasomes that are relevant for DIEP breast reconstruction. These exemplary studies have provided the foundation of our knowledge on perforator anatomy, linking vessels and perfusion to a lesser degree. Many of these studies focused on the entire lower abdomen and the use of central tissue and the perfusion based on unilateral breast reconstruction. There are no studies that focus specifically on bilateral reconstructions, which require a different perspective and understanding of specific anatomy pertinent to optimize hemi-DIEP flap design and harvest. Flap complications such as fat necrosis and partial flap loss may be multifactorial, but generally related to blood supply, thus a better understanding may aid in the predictability and reliability of flap harvest. This knowledge provides one approach to augment flap viability through inclusion of dominant perforators found in “hot spots” in the body and optimize flap design through understanding axiality of flow and capture of direct linking vessels. The use of preoperative imaging, such as computed tomographic angiography, has been widely adopted for assessment of perforator anatomy preoperatively but technologies to assess of intraoperative perfusion and flap physiology are varied and have not been as well established.

The proposed research aims to bridge the gap between microvascular anatomy and flap physiology that can aid in decision making for flap design and perforator choice with or without adjunct intraoperative imaging technologies. The recognized rise in bilateral mastectomy and demand for reconstruction provides justification to re-evaluate perforasome anatomy and flap physiology in the context of bilateral microvascular breast reconstruction.

The ability to extend the dynamic vascular territory and render tissue more resistant to ischemia during flap harvest is one proposed mechanism that plays a role in surgical delay and ischemic preconditioning to enhance the microcirculation of the flap. Clinical and experimental studies have demonstrated some effectiveness in techniques to augment flap

viability but there are still significant gaps in existing and new knowledge that deserve further investigation. Preconditioning techniques may have the capability to improve flap survival at varying ischemia times, and increase the critical ischemia time which induces 50% flap necrosis in both skin and muscle(29). There is a critical gap in knowledge and applications of targeted approaches, supported by scientific rigor, to “mimic” ischemic preconditioning which may enhance the safety and reliability of flap design, harvest and the potential to minimize associated complications. The proposed research will add new scientific knowledge that will help develop protocols and optimize strategies for flap preconditioning which can be clinically applied with the aim to reduce morbidity from complications. Key innovations for this research include (1) the use of a perforator flap model and topical negative pressure therapy, which has different blood flow dynamics compared to random pattern skin flap designs and clinically relevant to reconstructive surgery, and (2) develop an innovative strategy for flap preconditioning and measure its impact on flap perfusion, vascularity and flap survival.

1.3 Aims

The proposed research seeks to better understand the arterial territories of abdominal perforator flaps of the anterior abdominal wall in the context of bilateral breast reconstruction. It aims to explore the relationship of microvascular anatomy, including the presence of direct and indirect linking vessels within the integument of the skin and subcutaneous fat, and its impact on overall perfusion zones. Furthermore, this research will explore how microvascular anatomy in the integument may correlate overall flap physiology that may allow greater predictability in flap design to reduce potential complications. Finally, the scope for this research will determine the use of non-invasive approach of negative pressure wound therapy (NPWT) pre-treatment for perforator flap preconditioning and its influence on capillary recruitment, vasculogenesis, angiogenic growth factor release, flap perfusion and lower flap complications compared to control flaps.

The **aims of this study** include:

1. To qualitatively define the patterns of the microcirculation of individual deep inferior epigastric artery perforators for bilateral breast reconstruction.

2. Evaluate the role of linking vessels and microvascular anatomy on the dynamic microcirculation and flap physiology in bilateral DIEP breast reconstruction

3. Evaluate the role of negative pressure wound therapy preconditioning to augment flap vascularity prior to flap harvest.

CHAPTER 2: LITERATURE REVIEW

2.1 Anatomy and Physiology of the Deep Inferior Epigastric Artery Perforator Flaps in Bilateral Breast Reconstruction

2.1.1 Perforator Anatomy and Flap Design in Perforator Flap Surgery

Sir Harold Gillies wrote that surgeons are "faced with a constant battle between vascular supply and beauty,". (30) Throughout the evolution of reconstructive and modern microsurgical practice, surgeons have continued to face the same challenges and goals to optimize safe, successful tissue transfer that is reliant on a robust blood supply. Milton's work on flap survivability in random pattern flaps demonstrated flap survival and length was dependent on the inclusion of a pedicle containing a large vessel. (31) The anatomical territory of a vessel has been characterized by the structure of vessels and their branches, and the pattern in which they ramify before anastomosing with adjacent vessels. Cormack and Lamberty (1984) (32) extended the works of Salmon in detailed examination of the skin integument and several systems of perforating vessels which contribute to the blood supply, and the axiality of flow from these perforators in different parts of the corpus (32). Taylor and Palmer (1987) (33) described that the vasculature of the human body was a continuous three-dimensional network of interconnecting vessels, fed by cutaneous perforators. The whole body is compartmentalized into vascular building blocks referred to as "angiosomes", defined by a block of composite tissue (from deep tissues to the skin) supplied by a source vessel; adjacent angiosomes can be linked by true anastomoses or via small calibre "choke vessels" (33). Each angiosome territory describes the immediate vascular territory supplied by a source vessel and a perimeter of choke vessels, which connect with neighbouring source arteries. (33)

These traditional studies were succeeded by exemplary works that have contributed to knowledge of cutaneous blood supply and individual perforator anatomy providing the framework for perforator flap design, harvest and developing modifications(31–37) Saint-Cyr et al. focused on the perforator itself and not the source vessel through a series of anatomical studies, to define individual vascular territories through three- and four-dimensional computed tomographic angiography (19,38,39). The "perforasome" concept, coined by Saint-Cyr et al. in their original article, also referred to as a "perforator

angiosome" or "cutaneous angiosome" (25), characterized the unique individual perforator vascular territory or "perforasome" and the relationship to dominant axiality of blood flow, connections with adjacent perforators through direct and indirect linking vessels, and the contribution of the subdermal plexus. (25,32) Large filling pressures through a single dominant perforator can allow for large perforator flap harvest based on linking vessels that may connect multiple perforasomes to one another. (40) With over 350 clinically relevant perforators in the body, this has created new flap options and a sense of creative freedom for reconstruction tailored towards a specific defect, without the constraints of specific landmarks and using a "free-style" approach.

Figure 2.1: Pictorial representation of the Taylor and Palmer Angiosomes and predicted vascular arterial territories of the source arteries. (From Taylor GI, Palmer JH. The vascular territories [angiosomes] of the body: experimental study and clinical applications. Br J Plast Surg. 1987;40:113)(33)

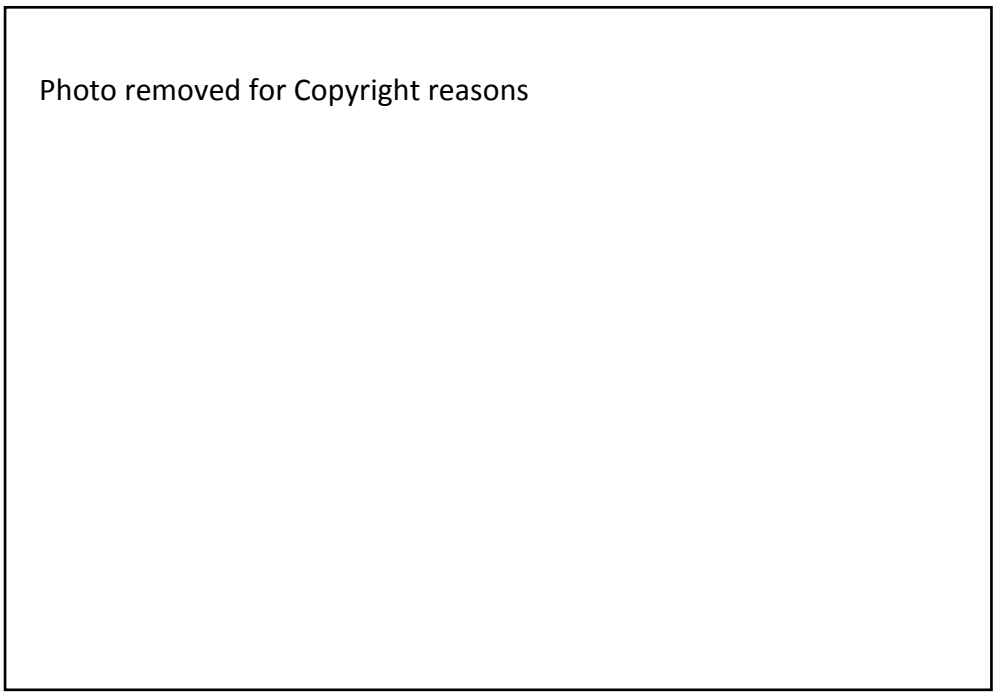

1)Thyroid 2) Facial 3)Buccal 4) ophthalmic 5) superficial temporal 6) occipital 7)deep cervical 8)transverse cervical 9)acromiothoracic 10) suprascapular) 11)posterior circumflex humeral 12) circumflex scapular 13) profunda brachii 14) brachial 15) ulnar 16) radial 17) posterior intercostals 18) lumbar 19) superior gluteal 20) inferior gluteal 21) profunda femoris 22) popliteal 23) descending genicular 23) sural 24) peroneal 25) lateral plantar 26) anterior tibial 27) lateral femoral circumflex 28) adductor 29) medial plantar 30) posterior tibial 31) superficial femoral 32) common femoral 33) deep circumflex iliac 34) deep inferior epigastric 35) internal thoracic 36) lateral thoracic 37) thoracodorsal 38) posterior interosseous 39) anterior interosseous 40) internal pudendal.

A dynamic territory, is considered the extended the territory which can be supplied by a source vessel into an area of decreased pressure or watershed. The principle of a dynamic territory implies that there has been a resultant alteration in intravascular pressures and readjustment of flow and change in the area perfused. This concept was elaborated in the studies of McGregor and Morgan (1973), which provide distinction between random and axial pattern flaps and more in depth understanding of the cutaneous blood supply. (41) Cormack and Lamberty (1994) believed that selective single injection of arteries to the skin integument in a fresh cadaver would more estimate a dynamic territory in-vivo, because the lack of surrounding intravascular pressure in vessel would have shifted the boundary of the injection territory. Therefore, the limits of the injected contrast medium or dye is likely to reflect the limits of a flap that could be immediately harvested in clinical practice based on that vessel. (32) The factors that may influence dynamic territories were largely unknown and have been subject to on-going research to elucidate the possible mechanisms.

Better understanding of the vascular anatomy and physiology of the cutaneous circulation within soft tissues, and that of patterns of blood flow from individual perforator has provided insight to advance perforator flap harvest and modifications in flap design. A comprehensive understanding of the vascular anatomy is critical to evidence-based perforator selection and optimizing flap design.

2.1.2 Autologous free tissue transfer in breast reconstruction

Breast reconstruction has become an important consideration for women after mastectomy. The goal is to re-create a breast mound that is naturally soft, durable, looks and feels like a normal breast, and can mature and naturally change with the patient over time. Women undergoing breast cancer surgery have become younger over the years and so reconstructive options ought to place greater emphasis on longevity. Documented trends include changes in patient demands and expectations; the disadvantages of implant reconstruction being better understood and the results through autologous reconstruction being more widely recognized. (15,16)

The deep inferior epigastric artery perforating vessels supply the overlying the skin and muscle in the lower abdomen. Hartrampf (1982) recognized that the breast is largely a fat gland therefore reconstruction with vascularized fat, taken from an area of excess, and transposition to the chest wall would be a desirable and attractive concept. (18) The lower abdomen potentially provides the greatest area of skin in the free-flap surgery. (42)The use of abdominal tissue for autologous breast reconstruction has been long and widely practiced, with similar characteristics to breast tissue and an aesthetic donor site scar. The Deep Inferior Epigastric Perforator (DIEP) flap had evolved from the traditional transverse rectus myocutaneous (TRAM) flap that was used for pedicled breast reconstruction, based on the superior epigastric artery. (18) However, the inferior epigastric artery plays the dominant role in abdominal tissue transfer in autologous reconstruction. (19) Koshima and Soeda first described the DIEP flap in 1989 (43) and Allen and Treece popularized its use in breast reconstruction in 1994. (44) This flap has been studied extensively and is a safe reliable option in breast reconstruction with low morbidity.

Figure 2.2: Illustration of the DIEP flap harvest of only skin and subcutaneous fat, with a dissection of the pedicle through the rectus muscle. (*Source: Saint-Cyr M. Assessing perforator architecture. Clin Plast Surg 2011; 38: 175–202).*

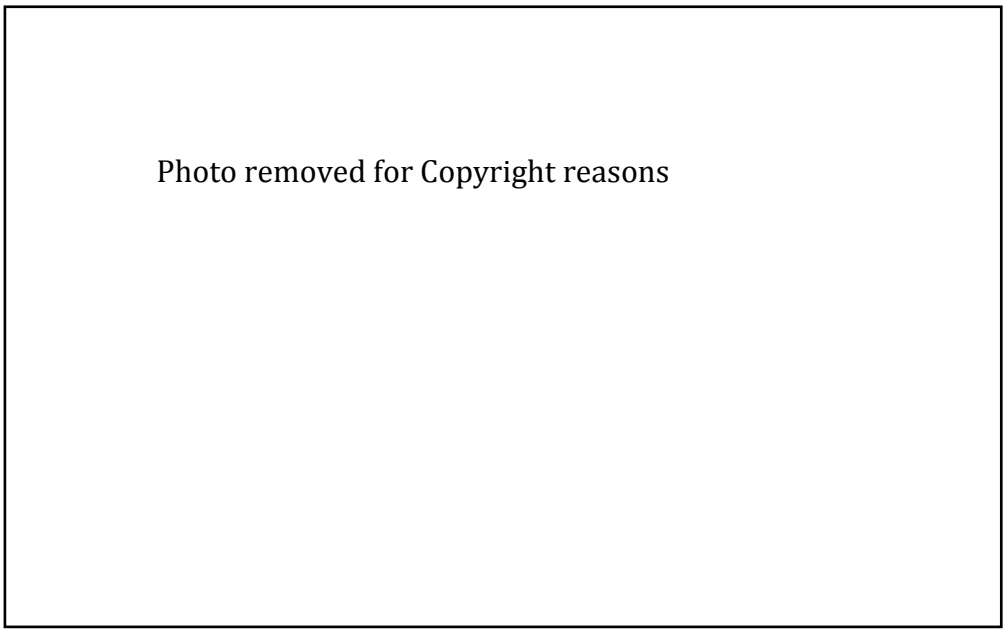

2.1.3 Vascular anatomy of the Deep Inferior Epigastric Artery Perforator (DIEP) Flap in breast reconstruction

The deep inferior epigastric artery is a paired artery that forms the dominant supply to the anterior abdominal wall. The artery arises from the external iliac artery, just above the inguinal ligament, and courses cephalad and medially to approach the rectus muscle on its lateral edge and travels towards the arcuate line on its deep surface. The artery pierces the fascia transversalis, and enters the rectus sheath in front of the arcuate line. (45) At this level the main artery will form one of three typical branching patterns. (46) The commonest branching pattern is a type II (57-89%), which is a simple bifurcation and perforators arising from the medial or lateral row of the DIEA. Type I vascular pattern involves a single inferior vessel (27-29%) and type III pattern (14-16%) is a trifurcating pattern above the arcuate line. (47) Variations in anatomy include absent unilateral DIEA (48), duplicate systems and intra-abdominal origin of the DIEA. (47)

The deep vascular system of the anterior abdominal wall includes the inferior epigastric and this continues cephalad to anastomose with the deep superior epigastric vessels. Branches from these two systems extend laterally to anastomose with the intercostal territories. In anatomical studies of the anterior abdominal wall, prominent connections between different vascular territories and networks have been studied and described as a system of longitudinal and transverse arcades. (45). Lateral branches provide a series of fasciocutaneous perforators that emerge from the external oblique aponeurosis and anastomose with the intercostal vessels. (45) The lowermost lateral branches are interposed with perforators from the Deep Circumflex Iliac Artery (DCIA) ascending branch which together can form a continuous network. This ascending branch of the DCIA, which is a branch of the external iliac artery, courses cephalad between the transversus abdominis and internal oblique muscles to anastomose with the lateral branches of the DIEA and intercostal arteries laterally. (45,49) Figure 2.3 is an illustration to highlight the angiosome concept as described by Taylor et al (1991).(45)

Figure 2.3: Schematic illustrations of the arterial systems of the anterior torso demonstrating the angiosome concept and dotted lines representing the choke vessels of adjacent territories (*Left)* and general angiosome territories and their representative source vessels (*Right*). (*Source: Taylor et al 1991. Vascular Anatomy of the Anterior Abdominal Wall and Flap Design. Semin Plast Surg. 2008 Jun 19;5(1):1–28)*

Photo removed for copyright reasons

The DIEA during its course gives rise to muscular, musculocutaneous, lateral segmental, peritoneal and a large umbilical artery. (42) The perforators may take an intramuscular course, which can be short (most common), perpendicular or a long oblique course, or they may have a completely extra-muscular course. After exiting the rectus muscle, the perforators may directly pierce the anterior rectus sheath or travel a short distance in the sub-fascial plane before penetrating the anterior rectus sheath. Cutaneous perforators have been classically divided into three groups including medial fasciocutaneous perforators from the linea alba (paraumbilical), middle musculocutaneous perforators from the anterior rectus sheath, and lateral fasciocutaneous arising through the external oblique aponeurosis. (42). Medial musculocutaneous perforators have been described as the larger branches that arise from the main DIEA vascular axis to supply the overlying skin and subcutaneous tissue,

with minor contributions to the muscle. Classical anatomical studies of the DIEA perforators have shown that large DIEA perforators are clustered in the medial and periumbilical area(42,46) and there is a lower concentration of perforators over the lateral third of the rectus muscle.

In a systematic review by Iretan et al. (2014) the course of these perforators had a considerable anatomical variation in that 20 up to 67% had a direct course on exiting the fascia, and around 33% and 50% may have a sub-fascial course between 0.5 up to 3cm from the collated studies. Perforators that had a more direct course were found usually within 3cm of the umbilicus, and those lower in the abdomen were more likely to have a longer sub-fascial course. (47,50) In the subcutaneous layer, lateral row perforators have a more oblique course through this layer, whilst the medial row perforators a more direct path. Once the perforators reach the subcutaneous and dermal layers there is considerable branching and anastomoses; midline perforators have a high degree of midline crossover, in contrast to the lateral row perforators, that have little midline crossover of their vascular territories, and this has been demonstrated on cadaveric anatomical studies. (27,51) Larger dominant perforators are typically seen in the medial row, and within 3-5 cm of the umbilicus, representing a “hot spot” of dominant perforators in DIEP flap harvest.

The anterior abdominal wall is a rich anastomotic network connecting the source vessels. They form rich plexuses in the subdermal region, adjacent to the Scarpa’s fascia, within the deep layer of subcutaneous fat and on the surface of the rectus sheath. (45) Perforators pierce the anterior rectus fascia and branch out in a cranial, caudal, and lateral directions to join an arterial community of linking vessels. These linking vessels may form direct communication with the superficial systems from the superficial inferior epigastric artery (SIEA) and superficial circumflex iliac artery (SCIA) territories.(42) The dominant axiality of flow from the SIEA is directed cranially and laterally to join the intercostal system. (42) The superficial systems from the superficial inferior epigastric artery (SIEA) and superficial circumflex iliac arteries (SCIA) mimic the patterns of the deep systems (DIEA and DCIA). (52) The territory of the SIEA is defined as just beyond the lateral border of the rectus muscle

and this can extend towards the anterior axillary line and can be captured by an ipsilateral DIEA perforator.(42)

Linking vessels within the integument are comprised of a series of reduced calibre vessels, termed “choke” vessels, which help to determine the anastomotic territories of the arteries. (33). Angiosome concepts have been used to predict the borders of potential necrosis of flaps. Taylor and Palmer (1987) described the ability to safely capture adjacent vascular territories that include one set of choke vessels, but attempts to harvest any subsequent angiosomes (more than one series of choke vessels), would lead to flap necrosis. (33)

Figure 2.4: Three-dimensional computed tomographic angiography (CTA) in-vivo and demonstration of DIEP perforators in the paraumbilical area*. (Image source provided by Prof Michel Saint-Cyr based on prior research).*

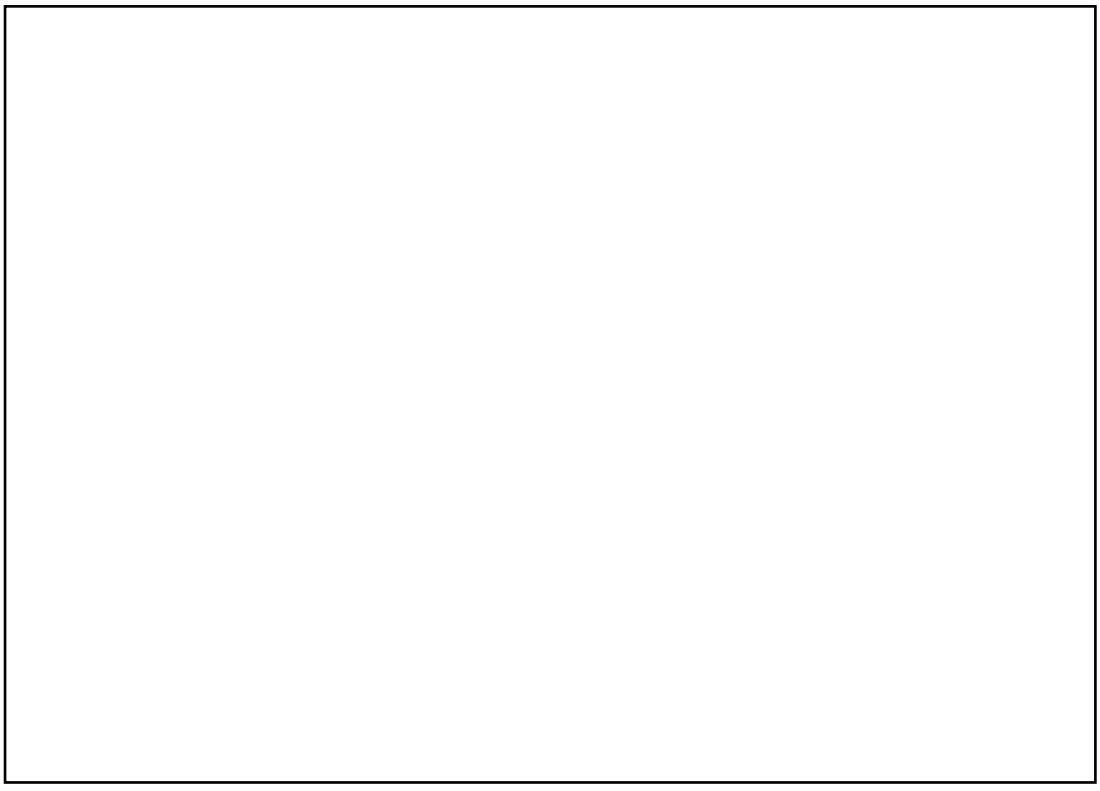

Figure 2.5: Illustration and patient demonstration of location of dominant perforators of the deep inferior epigastric vessels in relation to the umbilicus (left); and representation of key areas of dominant perforators (hot spots) in red, and areas of deficient dominant perforators (cold spots) in blue.

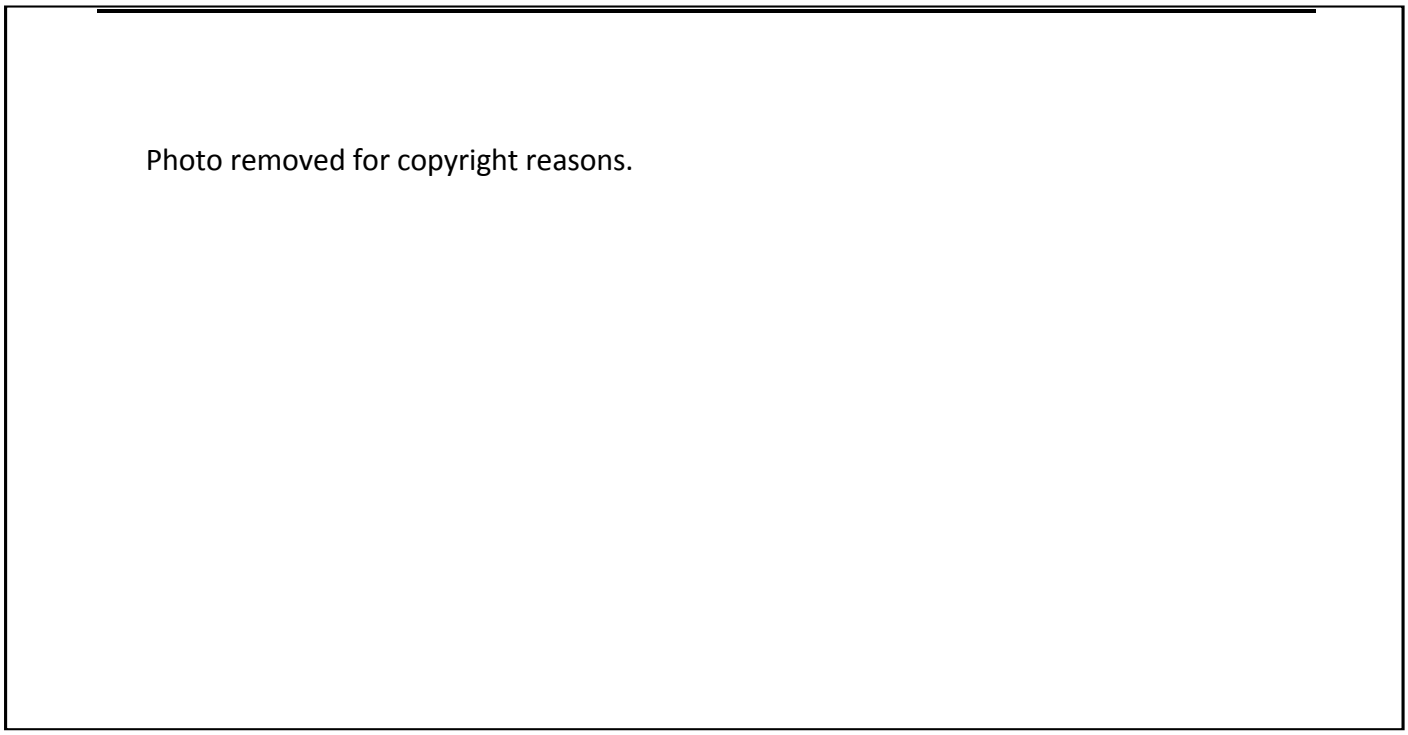

2.1.4 Zonal perfusion of the Deep Inferior Epigastric Artery Perforator (DIEP) Flap

There have been a considerable degree of anatomical, radiological and clinical studies using a variety of intraoperative technologies, to determine the perfusion patterns of perforators following DIEP flap harvest. In the harvest of the TRAM flap, where most of the DIEP perforators are included, it has been accepted that the perfusion of the flap integument occurs in zones.

Four zones have been typically described for vascular perfusion of the lower abdominal wall, with sequential filling of each zone. (18)(53)(54,55) The first zone universally represents the highest degree of perfusion found on the ipsilateral side of the DIEA perforator. The Hartrampf zones of perfusion (I to IV) are familiar to most plastic surgeons. The Hartrampf zones II and III were proposed to be reversed following earlier clinical studies by Dinner et al

(1983)(56) and recommended by Holm et al (2006) using intraoperative fluorescence imaging. (55) There is contention in the literature of the characteristics of these zones and the application of these traditional zones to perforator flaps based on a single dominant perforator. It is recognized that lateral and medial row perforator have different vascular perfusion patterns through clinical, radiological and cadaveric anatomical studies. (26,28,55,57)

Medial row perforators generally are larger in calibre, with more extensive branching patterns and greater perfusion patterns compared to lateral row perforators. (19,26,27,57) The medial row perforators can reliably perfuse across the midline and provide a robust vascularity to flaps raised on a single dominant perforator in the central two zones. (27) Cadaveric studies by Moon and Taylor (1988) demonstrated that midline perfusion occurred predominantly at the subdermal and superficial scarpa's level to fill the perforator of the contralateral DIEA, but with limited capture of the deep scarpa's tissue on the contralateral side, and no filling of the contralateral SIEA. (46)

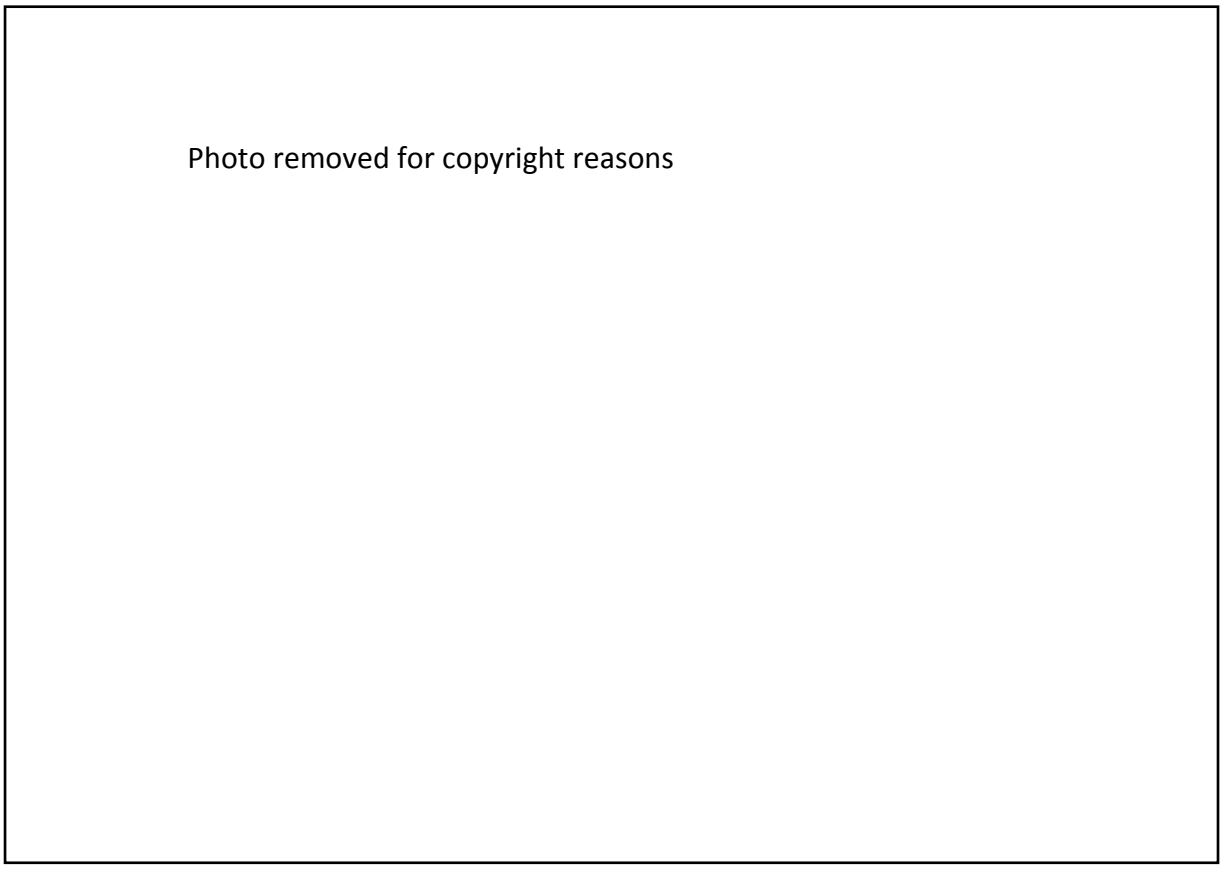

Figure 2.7: Micro-CT analysis of an injected perforator and presence of direct linking vessels and indirect linking vessels via the subdermal plexus, with connections to an adjacent perforator. The upper portion of the image represents the perforator and deep surface of the flap and the inferior portion of the image represents the skin. (*Source: Laungani AT, Van et al. Three-dimensional CT angiography assessment of the impact of the dermis and the subdermal plexus in DIEP flap perfusion. J Plast Reconstr Aesthet Surg. 2015*)(58)

The medial row perforators are found to have a more direct course through the anterior rectus sheath (47) and to Scarpa's fascia compared to lateral row perforators. The medial row perforasome can be classified using the traditional zone concepts and through anatomical studies have demonstrated perfusion patterns similar to Hartrampf zones of perfusion. In contrast, the lateral row perforasome is more representative of Holm's zones of perfusion. (26)

For unilateral reconstruction the medial row perforators perfuse more medially supplying the central portion of lower abdomen, and lateral perforators perfuse laterally therefore preferentially supplying the ipsilateral hemi-abdomen (57), and they share a similar territory to the ipsilateral superficial inferior epigastric artery (SIEA). (26) The DIEP flap's vascular territory could be potentially augmented with the inclusion of a second perforator. It was

often found that the lateral row perforators of the DIEA during flap harvest were usually the more dominant (larger) in the lower abdomen, and ran a more rectilinear course permitting an easier dissection. (59) However, if the medial row perforators were dominant, it would be recommended to harvest a flap based on a dominant medial row perforator, particularly if a larger flap is being required (as an alternative to muscle-sparing TRAM flap). Although in the past it was advocated that if a flap was reconstructed with only a hemi-abdominal flap, a lateral row perforator DIEA or SIEA could be considered. However, perfusion territories can vary between medial and lateral row, the decision for perforator choice should be based on the largest and dominant perforator in the hemi-abdomen, regardless of row. In the hemi-abdomen, the medial and lateral row are connected by direct linking vessels and indirect linking vessels via the subdermal plexus.

For medial row perforators, there are large linking vessels, which connect with the lateral row and additional intra-row perforators; linkage with the contralateral medial row perforators across the midline is obtained via the subdermal plexus. These linking vessels are similar to the choke vessels described by Taylor. The use of preoperative Computed Tomographic Angiography (CTA) can be used preoperatively, to review the presence of dominant perforators and linking vessels, and the course of the dominant perforators to plan the dissection and flap harvest. (60,61) The addition of intraoperative use of indocyanine green (ICG) laser fluorescence angiography has provided a useful tool for an early assessment of flap perfusion and micro-anastomotic flow.

Figure 2.8: Left Hemi-DIEP based on a medial row single dominant perforator, however large linking vessel can be identified on CT between medial and lateral row perforator using timing map SPYQC ® analysis from the ICG fluorescence angiography captured with SPY® Elite system.

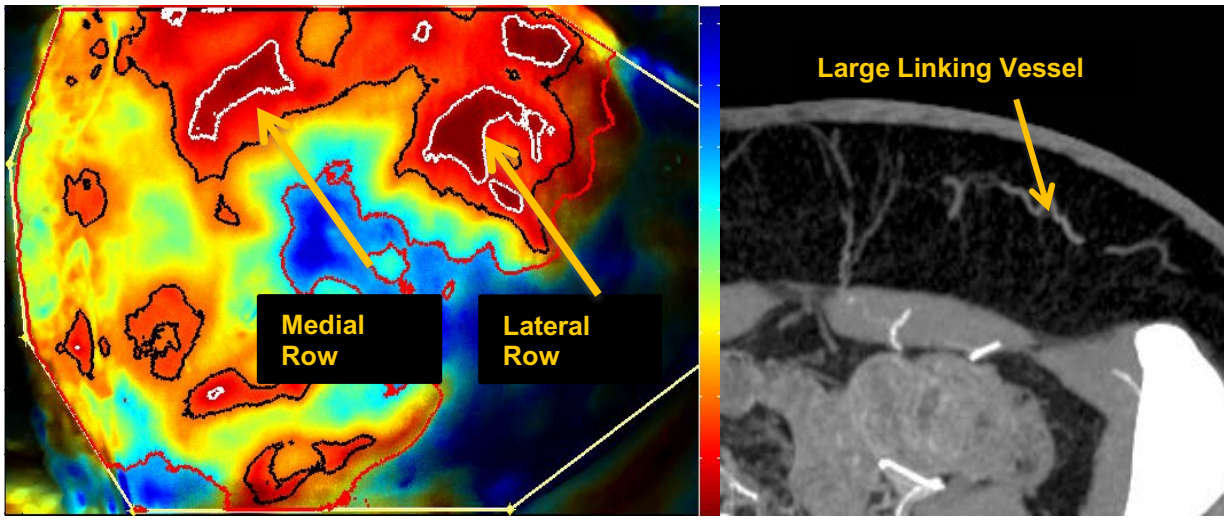

A newer proposal of perforator perfusion is a radial distribution of zones that is centred on the selected dominant perforator, and the perfusion sequentially falls in both directions between adjacent perforasomes. (40,57) For example, if zone I is supplied by a selected medial row DIEA perforator, the immediate adjacent perforasome zone II is captured by the ipsilateral lateral row DIEA and contralateral medial row DIEA; zone III, refers to the second captured zone extending further out, which would be the contralateral lateral row and ipsilateral SIEA territory, and Zone IV refers to the contralateral SIEA territory that is the farthest away. (25,40)

Linking vessels in the trunk are commonly directed perpendicular to the midline and follow an oblique transverse direction, parallel to the cutaneous dermatomes. Flow from these perforator angiosomes can be multidirectional and cross the midline in many cases, but preferential flow is normally directed away from the midline to maintain adequate blood supply to adjacent regions, which are populated with fewer perforators. The degree of branching in DIEA perforators are highly variable in number and calibre between perforators, even within the same row. It has been recognized that an individualized

approach in mapping the vascular territories of individual perforators indicates the high variability in the ability of a perforator to perfuse a given tissue volume. (62)

Figure 2.9: New proposed model of perforasome perfusion of the lower abdomen following sequential pattern between adjacent perforasome. *Source: Saint-Cyr M. Assessing peforator architecture. Clin Plast Surg 2011; 38: 175–202*

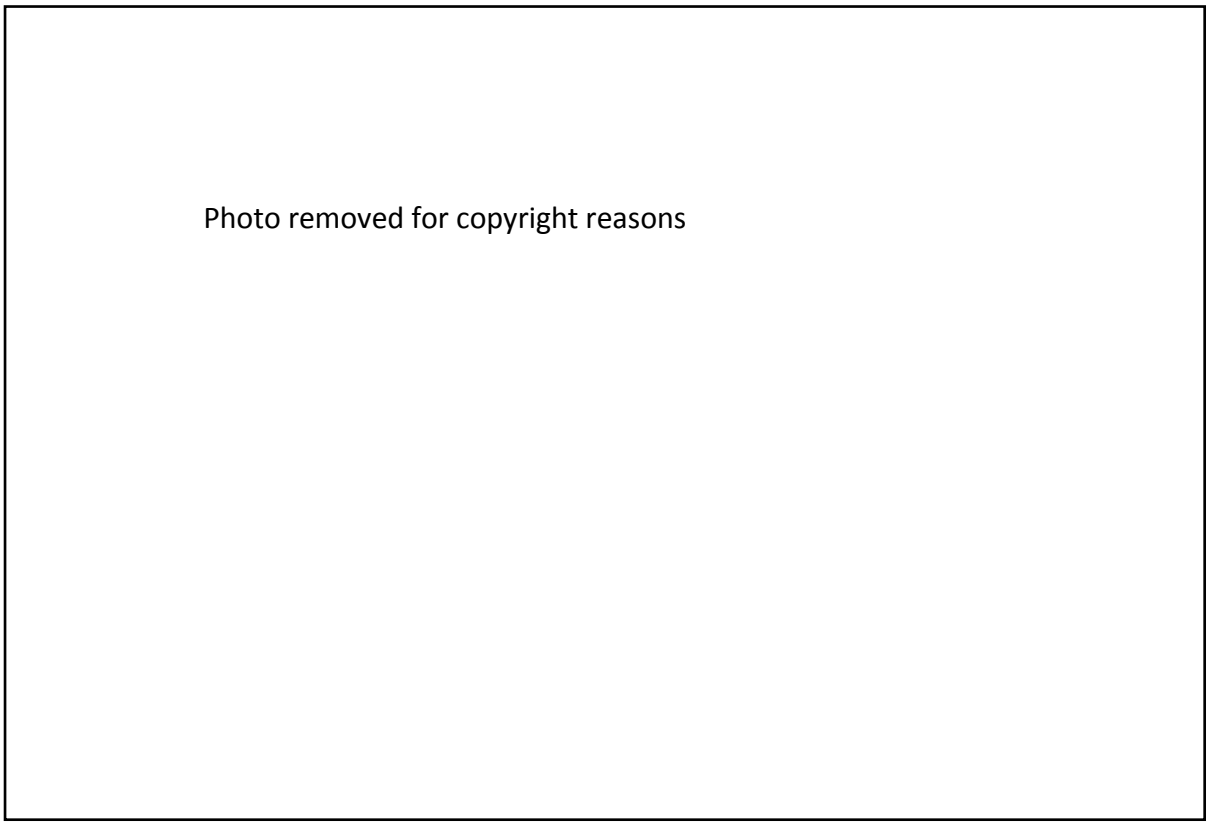

2.1.5 Imaging Techniques in DIEP Breast Reconstruction

(This section is based on previously published work on review of imaging techniques has been previously published by Mohan et al(63))

Computed tomographic angiography (CTA) and magnetic resonance angiography (MRA) have played a valuable role in the advance of anatomical research of perforator flaps(38,62), and preoperative planning of patients in breast reconstruction, providing a three-dimensional representation of the vascular architecture. The use of sophisticated imaging tools both in clinical practice and research has advanced our understanding of flap

physiology, microcirculatory architecture, vascular territories, axiality of flow of dominant perforators and role of linking vessels within the soft tissue integument.(25,26,38–40,58,64–69) Despite the knowledge of regional "hot spots" of dominant perforators, it is recognized that anatomy is highly variable, even between individual sides of a patient.(64,70) Flap harvest is a highly technical procedure associated with a steep learning curve and therefore knowledge of the location and anatomy of the underlying perforators can shorten the learning curve; increase the predictability and intraoperative decision-making in choosing the appropriate perforator and technique in an individual patient; (71,72) and anticipated dissection time.(73)

The handheld Doppler and Colour Duplex Ultrasonography have been traditionally used to detect the location of perforators and their characteristics of flow(74–77). However, although these techniques are less expensive and obviate radiation exposure, they have been associated with significant inter-observer variability, conducted over 45-60 minutes by highly experienced personnel, have high false positive rates, may be limited by difficulty in interpretation of findings, reproducibility, patient body habitus and only provide a two dimensional picture of the underlying vascular architecture.(73) Although CTA has superseded Doppler US in many institutions, it is not universally considered as a first-line preoperative imaging choice.(78,79) Agreement between colour Doppler US and CTA has been reported to be good. Cina et al. (2010)(79) reported in a study of 45 patients who had both CTA and Colour Doppler US, that both modalities were accurate in perforator mapping and had their associated strengths and weaknesses in assessing artery calibres and estimating the intramuscular courses.

2.1.6 Computed Tomographic Angiography to Assess DIEP Vascular Anatomy

Masia et al. (2006)(80) and Alonso-Burgos et al. (2006)(81) were among the first to report preoperative CTA in planning of free tissue transfer and it has become widely adopted into clinical practice and considered to some extent as the gold standard for preoperative imaging in DIEP breast reconstruction.(60,64,69,71,82–85) It allows for highly accurate perforator mapping, including the course of dominant perforators and it is non-invasive,

highly reproducible, has a short scanning time (less than 5 minutes), high spatial resolution and concordance with intraoperative findings.(85)(64,86)(87,88) Furthermore, preoperative imaging can reveal uncommon congenital absence or iatrogenic ligation of the deep inferior epigastric source vessels, aberrant communication of perforators with underlying source vessels, or absence of suitable DIEP perforators.(84,89) It has a valuable role in women who have had previous abdominal surgery who could be a potential candidate for DIEP reconstruction, allowing assessment of scarring and the availability of perforators. (90) Although CTA does not provide details on flow characteristics and perfusion, the ability to examine the linking vessels and branching pattern in the subcutaneous tissue and connection with adjacent perforator territories, may allow the surgeon to make inferences on the potential perfusion territories.(84) Similarly, connections between the superficial and deep systems, and communicating vessels across the midline can be examined. (59)

It is important that if CTA is to be incorporated into the preoperative planning of microsurgical breast reconstruction that a dedicated protocol is established within the institution specific to the device being used. Similarly, there is valuable role in collaborating with radiology colleagues to create a reporting procedure to highlight crucial and relevant details specific to DIEP flap surgery. Radiation exposure has been a limitation or sometimes concern for preoperative planning, however the advancement of CT protocols which have been developed for more focused exams has limited the radiation exposure on average around 5mSv per scan, which is equivalent to two abdominal radiographs and lower than a standard abdominal CT.(80,91–94) Sensitivity to iodinated contrast materials or its nephrotoxicity can be the main limitation associated with CTA in selected patients with known allergies or renal impairment.

As reconstructive algorithms evolve it has been shown that these techniques, such as adaptive statistical iterative reconstruction protocols that have been incorporated into commercial CT scanners, can now achieve reproducable high quality comparable images without amplification of noise in the imaging.(95) Other developments include 3D perforator anatomy models for the patient from preoperative imaging. Real-time projection guidance tools for intraoperative perforator identification have also been investigated, but

require further detailed studies.(88,89,96) Hummelink et al. (2015) reported the use of a handheld projection tool intra-operatively to map the perforators and anatomical course of the vessel to the source DIEA from the preoperative CTA directly onto the abdomen. This new tool was to demonstrate the combination of a minimalist operative room compatible projection system and CTA reconstructed images. A comparison was made with localization with a handheld Doppler, demonstrating better localization, and with a potential benefit in patients with a high Body Mass Index (BMI) >30. (96)

2.1.7 Magnetic Resonance Angiography to Assess DIEP Vascular Anatomy

In 1994, Ahn et al. first described the use of MR imaging for delineating perforators of the lower abdomen for TRAM flap selection without contrast.(97) The use of a Contrast-Enhanced MR angiography (CE-MRA) protocol in examination of the DIEA vascular anatomy is a relatively newer imaging modality and represents the next generation in preoperative DIEP planning. The protocol has been previously described by Chernyak.(98–100) Rozen et al. (2009) who reported a low specificity with MRA (50%) despite a high sensitivity (100%), which suggested that it was still inferior to preoperative CTA. However significant advances have been seen in imaging acquisition, processing, contrast agents and the scanners themselves. MRA has notable advantages over CTA as it obviates the exposure to ionizing radiation but can still provide high imaging quality and accurate localization of perforators with high concordance with intraoperative findings.(98,101,102) MRA is considered to have lower spatial resolution but higher contrast resolution, permitting a better delineation of the intramuscular course of perforators.(103) Schaverien et al. (2011)(101) assessed the role of contrast-enhanced MRA (CE-MRA) for assessment of DIEP venous anatomy providing information on the connections between perforator vena comitantes and the superficial inferior epigastric vein (SIEV) and the incidence of diffuse venous congestion ($P<0.0001$).(104)

CE-MRA with Gadolinium has a better safety risk profile, and lower hypersensitivity compared to the iodinating contrast media used in CTA, but is associated with a rare

syndrome of nephrogenic systemic fibrosis in patients with severe renal impairment. (101) Some of the advances in MRA have been the introduction of newer contrast agents and scanners with higher field strength for better quality image acquisition including extracellular contrast agents such as gadobenate dimeglumine, and newer blood pool contrast agents such as gadofosveset trisodium.(85,105)

Limitations with MRA in preoperative planning in breast reconstruction include the higher costs compared to CTA, limitation in detecting perforators less than 0.8mm in diameter, susceptibility to motion artefact and the requirement for the patient to breath-hold for longer periods, which may not be feasible in some patients.(85) MRA is contraindicated in severe obesity, patients with implanted defibrillators, implanted metallic devices or foreign bodies. It is a relative contraindication in patients with artificial heart valves, and in patients who cannot lay still, or have severe anxiety or claustrophobia. Currently the higher cost, availability and timing for the examination, is a major drawback to the adoption of MRA in breast reconstruction. The actual scanning time required for CE-MRA is around 20-30 seconds, compared to MD-CTA which is less than 20 seconds(101), although total examination time may be up to 40 minutes. As MRA becomes more accessible it may become considered as a first line imaging modality for preoperative planning in the near future, in particular for younger patients, iodine hypersensitivity or renal impairment.(85) CTA and MRA both provide a three-dimensional map and are reported as superior techniques in localization and characterization of perforator anatomy (Table 2.1).(69,106,107)

Table 2.1: Overview of advantages and Disadvantages of Computer Tomographic Angiography (CTA) and Magnetic Resonance Angiography (MRA) to assess vascular anatomy in breast reconstruction.

	Advantages	**Disadvantages**
CTA	• Considered current gold standard • Fast image acquisition • Widely available • Can image larger BMI patients • Accurate localization and course of perforator • Can identify vessels down to 0.3mm • Excellent spatial resolution • Easy interpretation with 2D and 3D reconstructions. • Images can be reviewed independently	• Ionization radiation exposure • Risk of hypersensitivity or nephrotoxicity
MRA	• Contrast agents may have safer risk profiles e.g. gadolinium • No ionizing radiation • Arterial and venous image acquisition in single scan. • Greater muscle to vessel contrast resolution • Easy interpretation of 2D and 3D reconstructions • Images can be reviewed independently	• Longer scan time • Need for MR contrast agent • Contraindications e.g. implantable defibrillator, metallic foreign bodies and claustrophobia

2.1.8 Laser Assisted Indocyanine Green Fluorescence Angiography (LA-ICGFA) in Breast Reconstruction

Fluorescent angiography has been used in other specialties but its utility in reconstructive surgery is relatively new and still developing. Indocyanine green absorbs green light in the near infrared spectral range at 805nm and emits fluorescence with a maximum of 835nm. (55). Following a peripheral injection through an intravenous catheter, ICG binds to plasma proteins immediately and remains almost completely bound.(108) A light wavelength of 800nm in the near-infrared spectrum is minimally absorbed by water or haemoglobin and minimally scattered in surrounding tissues and allows the capture of blood flow in the microcirculation of the subdermal plexus and subcutaneous fat up to depth of 2cm approximately. (23,108)Following the injection of indocyanine green through peripheral injection, at a dilution typically of 2.5mg/ml, the cutaneous vascularity is captured within 15 seconds to 2.5 minutes using infrared energy to excite the ICG, and recorded with inbuilt video and analysis software algorithms to generate quantitative data. (85,109) It has a short half-life of 3-4 minutes and is excreted in the bile, which makes repeat measurements possible intra-operatively without reaching toxic levels. This type of laser has no potential for local tissue damage. Its role in preoperative imaging is still limited and the information it can provide is limited in depth of penetration from the skin. (110) LA-ICGFA can characterize flow and perfusion in flaps and its use has focused on intraoperative assessment of flap perfusion, patency of the anastomosis, and on occasion postoperative monitoring.(111–114) It is safe to use, with very few reports of anaphylaxis but its use is contraindicated in patients with allergies to iodine.(108)

New quantitative algorithms may have the potential of identifying cutaneous perforators in a 2D map using ingress/ egress calculations per pixel to create timing maps to locate dominant perforators. However, the 3D mapping and detailed knowledge of underlying anatomy is absent. This technology is considered better at assessing flap physiology and perfusion used intra-operatively as an adjunct to clinical judgment, and in conjunction with other preoperative imaging technologies to improve predictability and reduced complications in breast reconstruction. Its main impact has been seen in the early

identification of mastectomy skin necrosis reducing its subsequent complications, and has sometimes necessitated changes to the approach in breast reconstruction.(112,115)

2.1.9 Dynamic Assessment of DIEP Perfusion

The use of dynamic infrared thermography (DIRT) to assess the cutaneous circulation was introduced in the 1980s but its application in preoperative planning of perforator flaps is more novel. (116–119) There is limited evidence on the efficacy and comparison of this imaging modality as a tool for preoperative perforator selection in breast reconstruction. The technique is based on surface cooling followed by a period of rewarming, and during the rewarming phase, the cutaneous perfusion is analysed with an infrared camera and hot spots correlate with perforator location. This technology is non-invasive and requires no contrast agents, however the accuracy of this technology has been compared with Doppler (116) and findings were dependent on the pattern of rewarming. This technology, although non-invasive and with a low patient risk profile, can only provide moderate and variable data on perforator location through a 2D map. Compared to the 3D architectural mapping from CTA and MRA, it is considered an inferior preoperative imaging choice. It is not widely available and although it may be associated with lower costs, there is a dearth of evidence to support its utility for preoperative planning and limited evidence intra-operatively that would support decision-making in breast reconstruction. (120)

The development of some of these technologies serve as an aid to assist to reduce the learning curve, potentially decrease surgery time and operative stress and may translate to improved clinical outcomes. Any imaging technique should aspire to have the lowest risk of harm to the patient, acquisition of the highest quality images providing the greatest amount of information, and be performed within the short duration and minimal burden to the patient. Current imaging modalities should still be considered as an adjunct and not a replacement for clinical judgment in planning and intra-operative decision-making in breast reconstruction. The evolution of technology has facilitated the ability to improve the predictability and reproducibility of outcomes in autologous breast reconstruction (71) and

translate to improved patient outcomes and efficiency, although large prospective clinical data are still required in this area. (71,73,82,88,101,103,108,111,112,125–128)

There are limited clinical studies that specifically review the perforasomes and the assessment of zonal perfusion in DIEP flaps in-vivo. The use of ICG fluorescence angiography has been used as a method to assess intraoperative dynamic perfusion of both TRAM and DIEP flaps intraoperatively. Yamaguchi et al (2004) evaluated the perfusion patterns intraoperatively of 10 TRAM flaps in breast reconstruction and demonstrated that perfusion zones can be objectively analysed intraoperatively using ICGFA had areas of hypo-perfusion, but did not apply any objective quantifiable data to their assessment.(114) Holm et al (2006) in 15 patients (13 unilateral flaps, 2 hemi-DIEP flaps) used ICGFA to assess these zones of perfusion as originally described by Hartrampf to compare a perfusion index and inflow in each of these zones.(53) Flaps were harvested on 2 (n=12 flaps) or 3 perforators (n=3 flaps). Losken et al (2012) evaluated perfusion of TRAM (n=37) and DIEP (n=18) flaps using 12 data points in each Hartrampf zone of the flap. Absolute values of ICG perfusion were averaged in each zone, in order to quantify and compare zones of perfusion. Only 15 flaps were based on single row perforators and a comparison of medial and lateral row perforators did not appreciate a difference in median perfusion in zones I-IV. It was recognized that real-time assessment of perfusion is possible with this technique that is quantifiable, reproducible and dynamic. (121)

Laser Doppler imaging has also been described in the assessment of dynamic intraoperative perfusion of DIEP flaps. This technology has been used to assess microcirculatory changes in DIEP flaps and compare assessments postoperatively in breast reconstruction. (21,122). In one study by Van den Heuvel (2011), the author evaluated perfusion in DIEP flaps intraoperatively in 16 DIEP flaps. In this study a 15cm x 10cm area was marked on the flap from the midline, in addition to a 2cm x 2cm area for subsequent analysis. In this study there was no evaluation of zonal perfusion of DIEP flaps but a more rudimentary assessment of central and peripheral flow that was evaluated preoperatively, following transplantation to the chest wall and 24 hours post operatively. (122) There was no difference in the central and peripheral flow preoperatively and immediately following flap

harvest, and there was no significant change in peripheral perfusion when the flap was isolated on the vascular pedicle. However, changes in flow occurred after transplantation to the chest wall. Tindholt et al (2011) compared intraoperative zonal perfusion, using traditional Hartrampf zones with changes in perfusion post operatively in 20 unilateral breast reconstructions following resection of zone IV. (123) In this case series 16 flaps were based on single medial row and 2 flaps were based on lateral row perforators. They identified that preoperatively all four zones had uniform perfusion, but following flap harvest zone IV significantly dropped in comparison to zone I, zone III also dropped significantly but zones I and II remained unaffected. Comparison of medial and lateral perforator location was not performed. (121).

The characteristics between clinical and quantitative assessment of DIEP zonal perfusion continues to be under further debate and investigation. Other example modalities used in clinical studies to evaluate zonal perfusion include the use of dynamic infrared thermography (DIRT) and tissue oxygenation. The use of thermography has been proposed as a new modality to bridge the gap in identifying perforators but in addition, identify the pattern of interconnections. (124) Chubb et al (2013) proposed that the use of DIRT can be used to evaluate true and choke anastomoses between perforator angiosomes in flaps and that patterns of the interconnections seen on thermographic images correlated with patterns seen in the group's previous anatomical cadaveric studies. (124) Rahmanian-Schwarz et al (2011) performed a combined anatomical and clinical study to assess the DIEP microcirculation using a micro-lightguide spectrophotometer that combines tissue oxygen and laser doppler flowmetry. Quantitative analysis of the traditional Hartrampf zones of DIEP flap perfusion was assessed intraoperatively using several measurement points within each zone. (17) The results of their study did not show significant changes in perfusion in zones II and III when the flaps were isolated on their vascular pedicle and regardless of perforator row.

The characterization of dynamic perforasomes is still not fully understood. A few limited studies to appreciate intraoperative perfusion dynamics of DIEP perforasomes have often used traditional zonal perfusion as a reference but many highlighted the residual gap in

knowledge, that there is high variability in perforasomes and that the traditionally used Hartrampf zones are still in debate in the context of DIEP flaps.

2.2 Topical Negative Pressure Pre-treatment and Implications on Flap Vascularity

2.2.1 Overview of strategies to augment flap perfusion

Successful flap reconstruction relies on the presence of adequate blood supply and wound healing potential. Angiogenesis is controlled by a complex regulatory system and is important for wound and tissue repair. Complications may be a result of persistent ischemia, hypoxia, post-ischemic reperfusion injury, venous insufficiency of the tissue, or thrombosis that may lead to total or partial flap necrosis. Augmented neovascularization would theoretically decrease the likelihood of flap loss or skin necrosis while increasing the amount of potential well-vascularized tissue harvested. This would have the potential benefit to reduce the risks of complications associated with poor blood supply, including flap loss, partial necrosis and fat necrosis.

Knowledge of perforator anatomy and microvascular architecture has improved the understanding of vascular territories of individual perforators for more predictable flap design and harvest, however the concomitant use of additional interventions in clinical and experimental models has shown potential to augment flap viability to improve survival. These strategies may alter the microvascular flow with early and late effects through changes in metabolism, blood flow and density of blood vessels within the tissue(20). Mechanisms that are involved in surgical delay / preconditioning to result in increased flap survival is thought to represent a combination of anatomical, physiological and molecular factors. The ability to extend the vascular territory of a perforator flap and render tissue more resistant to ischemia during flap harvest is one proposed mechanism that plays a role in surgical delay and ischemic preconditioning that have been traditionally used to augment flap perfusion. These treatment strategies are applied prior to flap surgery in order to improve survival and adapt tissue to the subsequent stress of the surgery by improving

overall tissue tolerance. Other strategies to apply stressors to develop tissue tolerance against ischemia may now include for example hyperthermia, hypothermia, drugs and application of growth factors.(116,117)

2.2.2 The Delay Phenomenon

The technique of surgical delay refers to a staged surgical approach that has been used for many years, traditionally for pedicled skin flaps, to augment their blood supply and viability. Delay is a well-recognized method of increasing vascularity in pedicled flaps and has been a technique studied in numerous experiments in animals(118–124) and used clinically. (125–127) One type of surgical delay technique for fasciocutaneous flaps is based on incising the longitudinal sides of the flap followed by flap undermining, to create a bi-pedicled flap and suturing it back into the donor site. In perforator or musculocutaneous perforator flaps this the delay technique is performed with incisions along the flap and elimination of additional feeding vascular pedicle. This manoeuvre promotes hypertrophy and reorganization of vessels to promote axiality of flow along the length of the flap. (128) At 2-3 weeks following the first stage, the distal end of the flap is cut and a single pedicled flap can be completely harvested and transferred to the recipient site for wound coverage. Surgical delay increases the survival length of a flap by allowing the choke vessels to dilate between adjacent perforators. Similarly, an alternative to incising the perimeter of the flap is the technique of vascular delay achieved by dividing distal perforating arteries at 1-2 weeks prior to raising the flaps. Similarly, ligation of the distal vessels or additional perforators in to a flap is a technique of vascular delay that can also augment the blood supply to pedicled flaps prior to transfer. This has been used in the clinical setting in transverse rectus abdominis myocutaneous (TRAM) flaps for breast reconstruction. (125,126,129,130)

These traditional mechanisms of surgical and vascular delay are still poorly understood but have been clinically proven to increase the vascularity of the flap. It is postulated that changes seen in vascular delay can be divided into early and late effects. On completion of the surgical delay procedure, there is an immediate effect of alteration of sympathetic tone, followed by dilation and reorientation of choke vessels within the flap.(131,132)

2.2.3 Ischemic Preconditioning

Ischemic and remote preconditioning techniques, involving pre-clamping of pedicles followed by reperfusion of the tissue, can lead to metabolic changes that give rise to an increase in ischemic tolerance and are considered a more sophisticated form of vascular delay. A later potential benefit of vascular and surgical delay stems from the increase in angiogenesis (development of micro-vessels from a pre-existing capillary network) and vasculogenesis (the formation of new blood vessels). The effect of ischemia on vascular growth has been extensively studied across other medical and surgical specialties, including myocardial ischemia(133), brain, skeletal muscle, gastrointestinal tract, lung and kidney(116), but parallels can be drawn from these conditions to propose mechanisms underpinning the delay phenomenon.(20) Murry et al. (1986) were the first to describe the ischemic preconditioning through repeated occlusion of the afferent vessels to the heart that was shown to delay or prevent lethal injury after a subsequent ischemic insult(133).

Experimental studies have also demonstrated success of ischemic preconditioning in flaps. A large variety of cellular mechanisms including vasodilating nitric oxide, protein kinase C, ATP signal transduction pathways, adenosine, cyclooxygenase-2, bradykinin through sensory nerve stimulation and growth factors, have been investigated for their role in ischemic preconditioning(134). The biological mechanisms of new vessel formation (vasculogenesis) and the growth of pre-existing vessels (angiogenesis) are still subjects of ongoing research (20,116,135). Some of the proposed mechanisms associated with ischemic preconditioning include a reduction in arteriolar vasospasm, a decrease in capillary no-reflow and an increase in blood flow response that have been investigated through experimental in-vivo models(116). Remote ischemic preconditioning of flaps has been shown to enhance flap survival by induction of an ischemic/perfusion event in an area distant from the flap; this indicates that this phenomenon has a systemic component to it and not merely a local tissue reaction (136,137). Remote ischemic preconditioning (acute and late) has been investigated in limb ischemia experimental models demonstrating the sequential use of a tourniquet on the limb can enhance flap survival by enhancing perfusion in the microcirculation (134). In experimental studies the ischemic preconditioning has shown to have some benefit,

including when combined with delay procedures for pedicled and free flaps, however, it still has had limited translation into clinical practice. In experimental animal models preconditioning has been shown to be slightly more effective for the myocutaneous flap model when compared with the skin (fasciocutaneous) flap models, but in both flap types there has been a demonstrable reduction in the rate of total flap necrosis.(29)

2.2.4 Alternative Preconditioning Techniques

Multiple overlapping factors are recognized to contribute to the delay phenomenon to increase blood flow within tissue. This involves a combination of dilation of vessels, reorientation of choke vessels, the impact of ischemic preconditioning and promotion of neovascularization (20). Some factors that induce stress such as ischemia, heat, toxins, hypoxia and hypoglycaemia (138) may provide beneficial changes to the flap microcirculation. There have been a host of strategies for alternative non-invasive preconditioning include hyperbaric oxygen (139,140), Botulinum toxin injections (141), supra-physiological heat treatment (138,142), hypothermic preconditioning (143), Isoflurane exposure (144), pharmacological agents (116) and growth factors.(116) Tissue expansion has also been described to instigate changes in microvascular perfusion through the dilation of choke or linking vessels and reorientation of the microvasculature that is seen during vascular delay procedures. It represents a form of delay through surgical manipulation that may lead to localized ischemia and vessel hypertrophy. (20) Successions of diverse experimental protocols have been created but are not necessarily reproducible in the clinical setting. The disadvantages of surgical and ischemic preconditioning include the need for additional surgical procedures, time, anaesthesia and both are relatively invasive. There is a need for targeted protective measures, supported by scientific rigor, to “mimic” ischemic preconditioning which can enhance the safety and reliability of flap design, harvest and minimize patient complications.

2.2.5 Negative Pressure Therapy Pre-treatment to Augment Vascularity

In the last 20 years topical negative pressure therapy, originally referred to as a sub-atmospheric pressure technique, has revolutionized clinical practice for acute, chronic and complex wound management. (138)(139,140) As a basic concept, the atmosphere at sea level exerts a pressure of 760mmHg, and the application of a vacuum results in a lower value or sub-atmospheric pressure. Gauge pressure (measuring pressure differences) compares the pressure of a system with that to a reference (usually atmospheric pressure), and is reported with a negative value for vacuum systems.(141) Negative pressure wound therapy (NPWT) is now well established in clinical practice and can increase blood flow, reduce oedema and bacterial contamination, improve granulation and encourage the formation of more physiological blood vessels. (138,139,142–144) Foam-mediated external suction or external volume expansion, are alternative terms described in the literature to represent negative pressure therapy. Despite the extensive research that has been carried out in basic science models and clinical practice, there is still a deficiency of large randomized controlled trial and a knowledge gap in the underlying biological mechanisms.

Our current knowledge indicates that NPWT can improve vascularization in *wound healing* both within clinical studies and experimental animal models. The mechanisms of action in wound healing focus on blood flow changes and increased perfusion to the wound; fluid removal;(145) stimulation of cellular proliferation, and macrodeformations promoting wound size reduction and maintenance of wound homeostasis.(138) In wound healing models the application of NPWT has demonstrated increased capillary vessel calibre, capillary density and increased blood flow. (146,147)

Angiogenesis is an intricate process involving the interaction of multiple genes expressed by a variety of cell types, which interact in a complex process. Hypoxia is thought to pay a pivotal role as a regulator for the expression of Hypoxia Induced Factor (HIF) 1-alpha, and the physical interactions between cells and extracellular matrix and angiogenic factors including VEGF. (144,148–150) The inflammatory microenvironment is another important modulator of wound angiogenesis, with macrophages becoming an important source of growth factors and cytokines, including VEGF and other angiogenic factors. It has been

shown that static forces through external suction applied to skin in murine or rodent models can induce vascular modelling and promote angiogenesis through increased vessel density, epidermal proliferation and hyperplasia, and increased expression of hypoxia induction factor alpha (HIF-1alpha) and related angiogenic factors such as vascular endothelial growth factor (VEGF). (143,147,151) VEGF and its receptor VEGFR2 are considered essential in normal blood vessel development and angiogenesis, which can be influenced by changes in the extracellular matrix microenvironment, cell shape and cell structures. (149) VEGF and its mediation of angiogenic activity is essential to wound repair. (152) CD-31 is a known marker in immunohistochemistry staining which can identify endothelium and allow for identification of vessels and an assessment of vessel density and morphology in histological sections. (144,151) Cells are able to sense mechanical forces and may respond through the regulation of specific genes and different interaction pathways.(141) Microdeformational transductive forces can influence the microenvironment and stimulate transcriptional cellular mechanisms that controls angiogenesis, but these underlying mechanisms are still poorly understood.(149) There is limited knowledge about the impact of negative pressure or external suction and the resultant microdeformational forces on neovascularization in wound healing (144), and the role in preconditioning has not been extensively explored.

Although the role of NPWT in as a pre-treatment to improve flap survival was originally among a small series of experimental swine model studies described by Morykwas (1997), there is limited further evaluation of its role to augment flap vascularity, and these have been primarily in small animal studies. (147,153,154)The potential however to treat compromised tissues with a modality such as NPWT that can be applied to a limited area, pre- and post-flap surgery, may have a greater value than more elaborate interventions and pharmacological agents.

2.2.6 Experimental Animal Flap Models

Animal models for negative pressure therapy have been based on wound healing models in murine, rodent, rabbit and swine models. Flap models have been mainly based on random pattern flaps (155), such as the basic science foundations of the role of negative pressure in a swine model by Morykwas et al (1997). (156) Perforator flap models in rodent animal experiments have focused primarily on abdominal based flaps. (157–160) A few alternative perforator flap models in rodents have been described in the posterior thigh (161), medial thigh (162), and other small potential perforator flaps.(163) Dorsally based flaps have been examined through animal studies of dorsal skin perforator flaps, which have identified three principle perforators: a posterior intercostal artery, lateral intercostal and iliolumbar artery which usually is a branch from the deep circumflex iliac artery. (163–167) The extended vascular territories of the deep circumflex iliac artery which gives off the iliolumbar artery perforator has been examined to look at the extent of its vascular territory in a rat model.(165)

CHAPTER 3: MATERIALS AND METHODS

3.1 Evaluation of the microcirculation anatomy and flap physiology of the deep inferior epigastric artery perforator flaps in bilateral breast reconstruction

The **overall aims** in the first section of my PhD research were:

1. Evaluate anatomical microvasculature and predicted perfusion territories of individual perforators in hemi-abdominal DIEP flaps.
2. Correlate dynamic perfusion of specific perforators to the underlying microvascular anatomy in hemi-DIEP flaps in-vivo.

3.1.1 Anatomical Cadaveric Study of the Perfusion Territories (Perforasomes) of DIEA perforators in the Hemi-Abdomen

The first aim was to assess characteristics of DIEA arterial perforators and the microvasculature on perfusion territory areas and patterns of perfusion within the integument of hemi-abdominal flaps.

The **hypotheses** were:

1. DIEA perforator location and size will influence overall perfusion area of a hemi-abdomen, regardless of perforator origin (medial versus lateral row).
2. The presence of linking vessels between perforators and adjacent territories will influence the resultant overall perfusion territory of the flap
3. Dynamic computed tomographic angiography (4D CTA) methods can be applied to characterize the presence and relevance of dominant linking vessels in the hemi-abdominal DIEP integument and demonstrate how dynamic perfusion patterns may influence overall perforator perfusion territories.

3.1.1.1 Preliminary Cadaveric Studies

To develop the dissection and injection techniques, preliminary work was completed to inform protocol development. A study of Profunda Artery Perforator (PAP) flaps and Superficial Femoral Artery Perforator (SFAP) flaps of the lower limb helped to develop and refine skills in flap harvest, preparation and injection for CTA.

Specific skills that were developed included: careful dissection of the perforator and pedicle with medium and small ligatures to prevent leaks from injection; cannulation with 4.5x loupe magnification of 0.7-2mm perforating vessels using micro-instruments; careful flushing of the flap with heparinized saline; methylene blue injection (3ml) to identify leaks which can be sealed with diathermy or ligatures, and careful preparation and optimization of the flap for vascular injection with Omnipaque 240 ®. Vascular injection techniques that were originally trialled included:

- Slow individual freehand injection of 3ml of contrast.
- Injection with Harvard pump apparatus at slow infusion rate (0.5ml/min, 1ml/min, 2ml/min).
- Injection with Harvard pump with pressure monitoring using an arterial line system and transducer) and assessment of imaging following each injection at 30, 40, 60, 80 and 100mmHg to evaluate the impact of pressure as a confounder to the intravascular injection. This step was critical in optimization of the injection protocol.
- Development and refinement of a 4D protocol using varying diameter tubing to simulate the flap injection. A shuttle mode protocol was utilized for image capture during the injection at a rate of 3ml/min.

Further refinements of the 4D imaging protocol were then performed. Injections at different rates and image sampling intervals were compared for image resolution and feasibility of the protocol. In a pilot study using 3 hemi-DIEP flaps were assessed using 1) injection at 0.5ml/min, sampled every 5 seconds for 1 min; 2) injection at 1ml/min sampled every 2.5 seconds for 1 minute, and 3) injection at 0.5ml/min sampled every 15 seconds for a duration of 90 seconds.

Figure 3.1: Set up of Harvard pump and tubing (large, intermediate and small diameters) to simulate trials for development of initial 4D injection protocol

The quality and results of the imaging techniques were reviewed. Based on previous experience of the clinical supervisor and confirmed with this preliminary work, it was decided that a slow injection of 3 ml of iodinated contrast injected slowly over 90 seconds, produced high quality imaging with no additional resultant extravasation or vessel damage. For adequate injection and contrast intensity, a mixture of 1:1 Omnipaque 240 ® was used with normal heparinized saline, warmed to 38 Celsius prior to injection. Fresh specimens and fresh frozen specimens which were not frozen for a long period of time provided the best quality in terms of imaging of the vessel architecture.

This preliminary work and studies of the SFAP, PAP and lower extremity flaps provided initial technique and development of protocols used in cadaveric imaging studies of perforator anatomy and subsequently published. (168,169) A sample of 10-11 cadavers was considered adequate for the anatomical study based on previous published data of individual arterial perforasomes of DIEA vessels. These studies use the entire lower abdominal skin as a single flap, but the inclusion of multiple perforator injections simulated 20-48 DIEP flaps. (26–28,170,171) A sample size of at least 10 female fresh torsos would provide 20 hemi-abdominal flaps for assessment and potential for a much higher number of simulated DIEP flaps through injection studies.

3.1.1.2 Deep Inferior Epigastric Artery Perforator Cadaveric Study

A total of 22 hemi-abdominal flaps were used in the study of arterial perforators from fresh human cadavers acquired through the Mayo Clinic Whole Body Donor Program. The anatomical study was performed at the department of Anatomy, Mayo Clinic, Rochester MN and received approval by the Bio-Specimens Committee. All imaging was performed in the Opus Radiology Research Core, Mayo Clinic, Rochester MN.

Anatomical Dissection

Standardized markings were drawn on each torso using a pre-designed template. Markings were drawn to highlight the midline, umbilicus, superior border of the pubic bone, ASIS, mid-axillary line, subchondral margin and the xiphoid process. These markings represent the borders of the hemi-abdominal flaps that were harvested. This flap design was selected to better evaluate the extent of perforator vascular territories in relation to the entire anterior abdominal wall and better capture the territories of the DCIA and SIEA more consistently. Measurements were taken for each torso: xiphoid process to midpoint of umbilicus; xiphoid process to superior border of pubic; mid-axillary to contralateral mid-axially line at the level of the umbilicus, and mid-axial line to midline. These represented the reference lines used in measurements of the perforator and their location within each hemi-abdominal flap.

An inferior incision was made and dissection and recording of the size, pattern of branching of the superficial inferior epigastric vein, including the presence of a medial venous branch, was documented and then subsequently ligated. The superficial inferior epigastric artery was ligated. The inferior incision was carried out laterally past the mid-axial line. A midline incision was made followed by the superior incision of the abdominal flap that was made down to the muscle. Dissection was carried out under x4.5 loupe magnification. The dissection was commenced from the superior portion of the abdominal flap in an inferior dissection. All perforators greater than 0.5mm in size were measured using digital fine callipers (Mitutoyo®, Mitutoyo American Corp., Illinois), marked on the skin flap with ink

and electrocautery to reference where the perforators entered the flap. Their diameter was measured using electronic callipers. Perforators were numbered and mapped onto the template simultaneously for accurate record keeping. Dissection was continued to the level of the umbilicus. The lateral dissection (lateral to the rectus abdominis muscle) was continued through the superior incision as this area is deficient in perforators. Dissection then proceeded through the inferior incision in a superior direction.

Figure 3.2: Anatomical dissection outline for flap harvest on a fresh female cadaveric specimen (left); Hemi-abdominal flap raised with perforators marked on skin and the dominant perforators dissected for subsequent cannulation, red arrow (centre) and hemi-abdominal flap with perforators mapped (right).

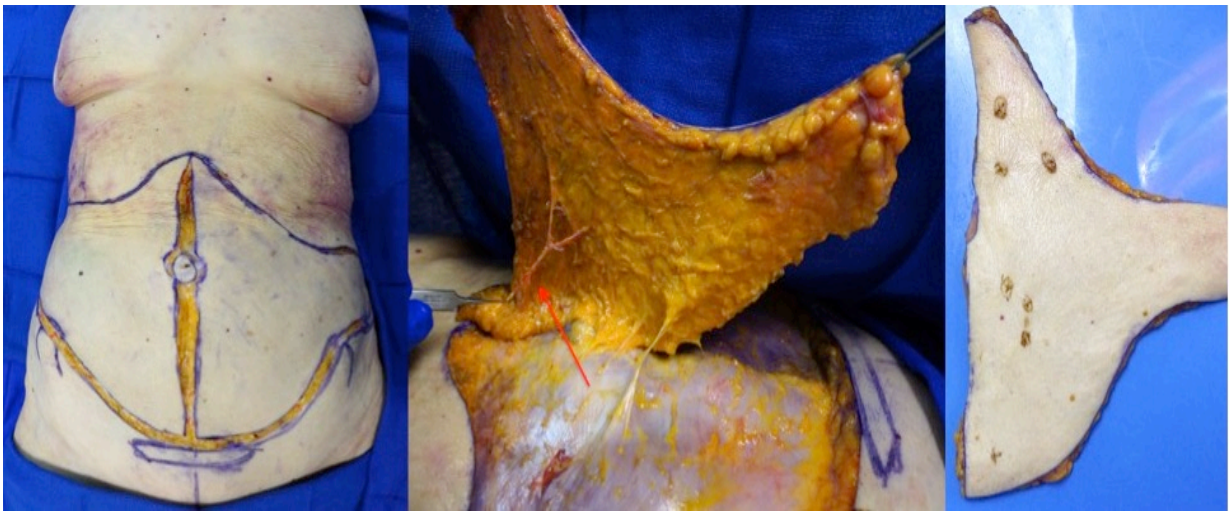

The largest dominant perforators from the medial and lateral row that would be suitable for hemi-DIEP flap harvest were then assessed and selected. The flap was released medially and the selected perforators were then meticulously dissected out through an initial fascial incision and their course was followed to the deep inferior epigastric source vessel. All side branches along the vascular pedicle of each perforator were ligated. A suitable length of the pedicle was then harvested to assist with subsequent cannulation of the perforator. Flap dissection then continued laterally towards the mid-axillary line. Identification of additional

perforators through the external oblique arising from the deep circumflex iliac artery (DCIA) were then documented. If a suitable perforator was found, the perforator was dissected for additional cannulation to compare the overlap of the vascular territory with the DIEA perforators. If no suitable DCIA perforator was identified the flap was incised at the mid-axillary line. If a DCIA perforator was identified for cannulation, the flap was extended posteriorly for 10cm or the posterior midline, depending on the size of the torso.

The selected perforators from each flap were recorded on the template. Measurements were carried out to map all the arterial perforators on each hemi-abdominal flap. The selected perforators were cannulated with 24-gauge intravenous catheters (BD Insyte™, Becton Dickinson, Franklin 95 Lakes, NJ) for Computed Tomographic Angiography (CTA) evaluation. The remaining perforators were sealed with metal vessel clips (Horizon™ Teleflex, Wayne, PA) or electrocautery. The flaps were injected with dilute heparinized (10U/ml) methylene blue to enable remaining vascular leaks to be identified and sealed with diathermy or clip ligation. This provided an estimate and correlated with the final volume of contrast volume that would be used for CTA evaluation.

3.1.1.3 Three-dimensional Computed Tomographic Angiography (3D-CTA)

At first, initial scout scanning was performed to obtain baseline images. To maintain the shape and orientation of the flap during repeated scanning, the outer margin of the flap was marked on the disposable base-board. A 50:50 mixture of 0.9% Normal Saline and iodinated contrast medium (OmnipaqueTM 240, GE Healthcare, Little Chalfont, UK) was injected into the chosen perforator and the flap was scanned. The iodinated contrast medium mixture had a calculated osmolality of 350 mOsm/kg water (approximately 1.2 times that of normal body fluid) and heated to 37°C to reduce the viscosity and improve vascular filling. A volume of 3 ml injected using a Harvard pump system (Harvard Apparatus, MA) at a rate of 1.66ml/minute to achieve optimal filling of the vascular territory of each perforator. Next, 36 ml of warm saline (37°C) containing heparin (10 U/ml) was infused into the same perforator to flush the iodinated contrast medium out of the flap, and the flap was re-scanned to verify the absence of iodinated contrast medium. The same process was

repeated for the next perforator. The 3D-CTA Images were generated using a dual-source CT system (127 SOMATOM® Definition FLASH, Siemens Healthcare, Forchheim, Germany). Given the high HU value within the iodinated vessels surrounded by low HU value of the fat and dermis, single-energy Dual- source scanning was performed using an ultra-high resolution technique typically used for temporal bone and joint imaging. This technique entails a tube potential of 120 kV, detector collimation of 16 x 0.3 mm, and scan FOV of 30 cm. The highest allowable tube current was used to maximize image quality. Axial images were reconstructed at 0.4 mm thickness and 0.4 mm increments using a very sharp kernel to preserve small details. Iterative reconstruction (SAFIRETM, Siemens Healthcare, Forchheim, Germany) was used to reduce the image noise.

Figure 3.3: Preparation of hemi-abdominal flap for CT scanning (left) and example of injection of a medial row perforator and mapping of perforator territory within the hemi-abdominal flap (right).

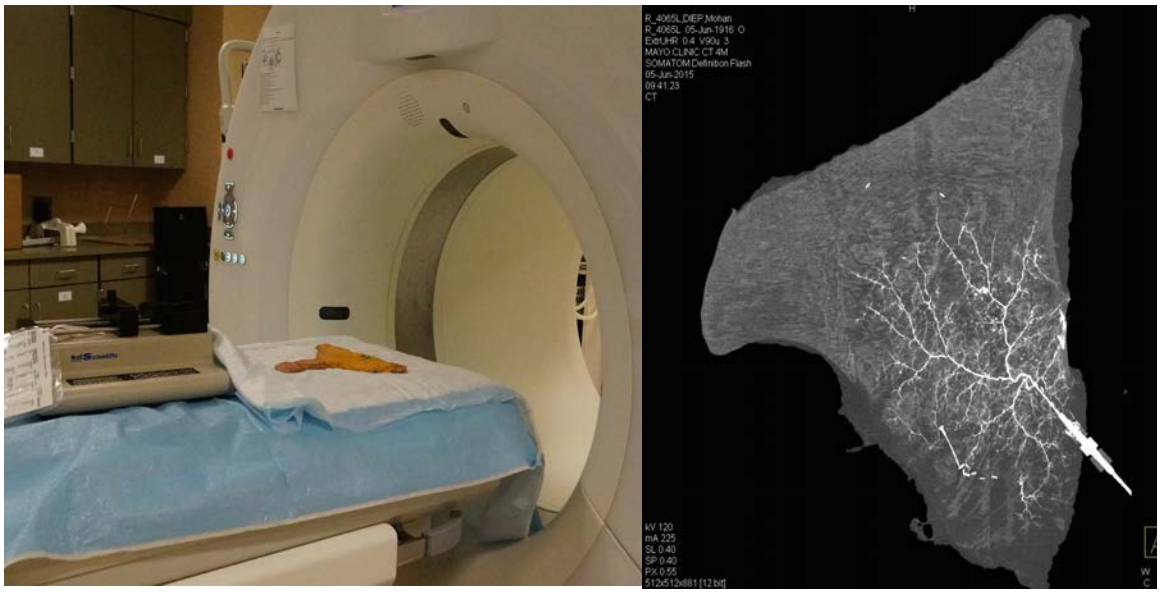

Figure 3.4: 3D CTA reconstruction of individual perforator territories and comparison of medial and lateral rows territories in the hemi-abdominal integument

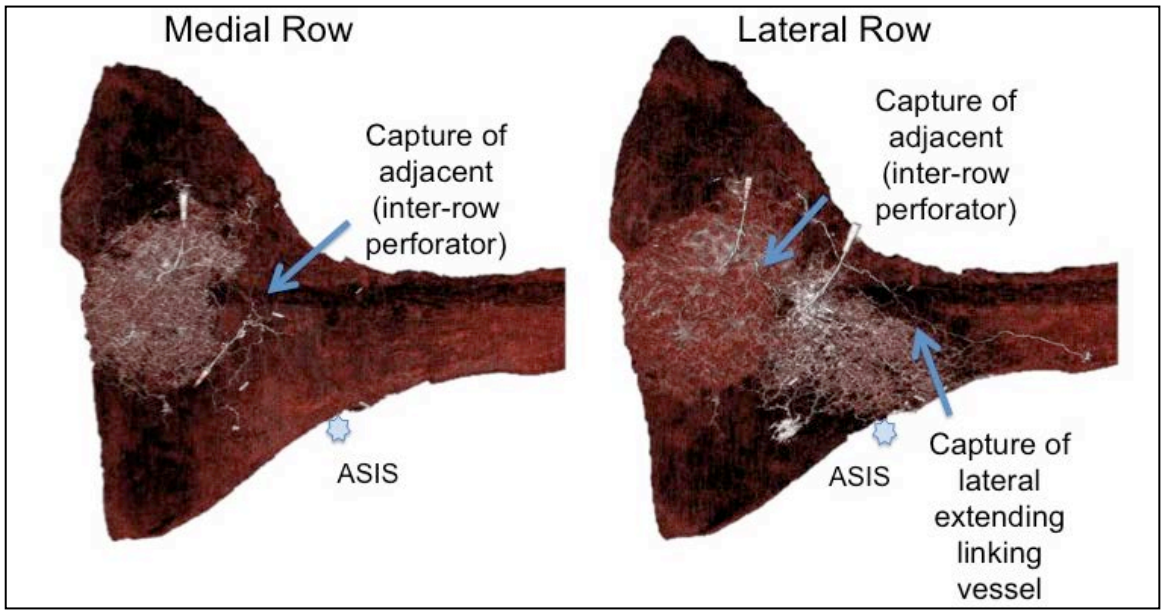

3.1.1.4 Four-dimensional Computed Tomographic Angiography (4D-CTA)

Although flap injections were carried out with previously established protocol, we subsequently were able to apply an evaluation of contrast injection over time using the developed protocol from the preliminary studies. CT scanning of the flaps was performed using both a 4D and high-resolution protocol. For 4D scanning, the flap was placed in the gantry and upon initiating the infusion of the contrast agent, the scanner began continuous imaging of the flap in “shuttle” mode. This entails irradiating the flap while the table moved in and out of the gantry a distance of 28.4 cm every 2.5 seconds for a total scan time of approximately 90 seconds, resulting in 35 total scans. The kV was set to 100, the mAs was set to 150, and the detector collimation was set to 32 x 1.2 mm. Images were reconstructed using a slice thickness and increment of 1.5 mm using a medium/sharp kernel. Since these data were time resolved, the total image volume over time was imported into post processing software (InSpace, Siemens) and movies depicting the perfusion of the contrast media into the flap were generated. This imaging protocol was done twice per flap during

the injection of the first 2ml of contrast. A final scan was performed as described above to obtain the final overall dynamic territory with the full volume of contrast.

3.1.1.5 CTA Analysis

All images were processed using software capable of both 3D rendering and volume calculation designed for 3D rendering (syngo® 133 MultiModality Workplace, Siemens Healthcare, Forchheim, Germany). Maximum intensity projection images were generated in the coronal plane. A freehand area tool was used to measure the total flap area and perfused areas and an independent reviewer was provided the assessment and measurements of each injection (GM)[1]. The perfused area was estimated by outlining the vascular structures that contained iodinated contrast medium, using the baseline images and recently flushed images as a reference. For consistency, the window level and magnification settings between perfused and reference images were linked during each measurement. 3D images were also generated using a volume rendering technique. Perfused volume was determined by drawing a volume of interest around the entire flap and setting a segmentation threshold of 100 HU. Any voxels above this value were summed to produce the total volume perfused. Injection and total flap areas and volumes were recorded and compared. Measurements for this part of the analysis were calculated by an independent experienced reviewed (GM)[1] using a previously developed protocol through our preliminary studies. (168,169)

Thickness of the flap at the level of the umbilicus, number of perforators and location in reference to surface anatomy were recorded to map all perforators greater than 0.5mm in the hemi-abdomen. The largest perforators were selected and prepared for injection, and when possible, multiple perforators were cannulated. This allowed simulation of multiple hemi-DIEP flaps. Following the injection studies and post processing of the CT imaging, the total area and volume of the vascular territory was outlined and compared to the total flap area. When more than one perforator was injected within the same hemi-abdominal flap, the percentage overall was recorded.

[1] GM= Gregory J Michalak

The percentage of cephalad extent and the caudal extend of the perforator territory towards the pubis was calculated from the perforator along this longitudinal axis of the hemi-abdominal flap. The relative extent of lateral perfusion was also compared along a horizontal axis from the midline towards the anterior superior iliac spine (ASIS). In addition to measurement of the flap perfusion territories and perforator mapping, 3D reconstructions were further assessed qualitatively using the 3D rendering (Syngo® Multimodality Workplace, Siemens Healthcare, Forcheim, Germany). Principle pattern and axiality of the vascular distribution was then documented from each perforator (medial, lateral, superior, or radial). The perforasome distribution laterally was assessed separately, and in particular, the capture of a dominant laterally orientated linking vessel was documented (yes/no) and whether there was capture of the superficial SIEA vascular territory (yes/no). On examination of the microvascular territory, the presence of direct linking vessels from the injected perforator and between perforators of the same row (intra-row) and perforators of adjacent row (inter-row) (yes/no) were documented. Finally, it was noted whether there was a dominant linking vessel and flow into to the superficial SIEA territory (yes/no) and when applicable, the degree of overlap with the DCIA perforator territory.

3.1.2 Clinical Study to Evaluate the Anatomy and Dynamic DIEA Perfusion Territories (Perforasomes) of Hemi-DIEP Flaps in Breast reconstruction

The **aim** of this study was to characterize the dynamic perfusion territories (perforasomes) of an individual perforator and then correlate dynamic perfusion of specific perforators to the underlying microvascular anatomy in hemi-DIEP flaps in-vivo.

The **hypotheses** were:

1. The use of LA-ICG-FA can be used to characterize the dynamic perforasome of dominant perforators used in hemi-DIEP flaps for breast reconstruction
2. DIEA perforator row does not influence overall perfusion area of a hemi-abdominal DIEP flap
3. The dynamic perforasome on LA-ICG-FA can be characterized by underlying microvascular anatomy based on perforator course, perforator location, linking vessels and branching patterns within the different layers of the integument, and presence of dominant linking vessels as seen on preoperative CTA imaging.
4. The patterns of the dynamic perforasome can determine overall perfusion areas within hemi-DIEP flaps in breast reconstruction

3.1.2.1 Patient Population

A prospective review was conducted of consecutive women who underwent bilateral breast reconstruction following mastectomy with DIEP or MS-TRAM flaps between January 2014 and June 2016 performed by a single surgeon (M.S-C)[2] at the Mayo Clinic, Rochester, MN. The study received approval by the Institutional Review Board, (IRB #14-003174). Patient characteristics, operative details of flap characteristics, selected perforator size and correlation with preoperative CT, flap weight, intraoperative findings and complications were abstracted from the electronic medical record. Preoperative Computed Tomographic Angiography (CTA) imaging that was performed using a dedicated institutional DIEP protocol was reviewed to identify dominant perforators and correlation with intraoperative findings.

[2] M.S-C = Michel Saint-Cyr

Following dissection of the selected perforator and the pedicle for the flap, the flaps are routinely left in-situ for at least ten minutes and allow for better assessment of any areas of concern regarding perfusion, which is performed clinically and with the use of intraoperative imaging techniques. We developed a protocol for routine assessment of individual flaps prior to free tissue transfer. Therefore, perfusion was assessed on a single perforator, using Laser-Assisted Indocyanine Green Fluorescence Angiography (LA-ICGFA) using the SPY Elite® system (Novadaq Technologies Inc.) and based on an intraoperative protocol for image capture. Intraoperative hemodynamic parameters at the time of imaging and concentration of ICG injected were recorded.

Exclusion criteria included women who underwent unilateral DIEP reconstruction, transverse rectus abdominis myocutaneous flaps (TRAM), those who did not have prior CTA imaging and women who did not have adequate LA-ICGFA imaging once reviewed for quality control by a blinded reviewer (CC)[3].

3.1.2.2 Analysis of Pre-operative Computed Tomographic Angiography

Preoperative CTA was reviewed to assess the location of dominant perforator in each hemi-abdomen from the DIEA, its origin from the medial or lateral row, its anatomical course and the branching pattern of the DIEA. This information was correlated with the imaging report performed by an independent expert consultant radiologist. Further detailed analysis of the vasculature was then performed using reconstructed maximum intensity projection (MIP) reconstructions and 3D rendering using TeraRecon® imaging software (TeraRecon Inc, California).

Subsequent detailed analysis of the CTA images was based on the perforator selected for DIEP flap harvest. Abdominal thickness in millimetres was recorded at the level of the umbilicus. Maximum Intensity Projection images were reconstructed to optimize evaluation

[3] CC= Cheng Chen

of perforator course and course of communicating vessels in the coronal, axial and sagittal planes. Details recorded included the type of branching pattern of the DIEA, level this branching occurred and the dominant row; the external diameter of the dominant perforator; size and location of the dominant perforator, and length intramuscular course. The origin of the dominant perforator from the medial or lateral row was recorded. The perforator row was classified as medial, lateral or paraumbilical. The number of perforators within each hemi-abdomen and the presence of a single dominant perforator in the hemi-abdomen (yes/no) were recorded. These types of assessments have been previously described in the literature and provide a standard description of the DIEA vascular pedicle and the anatomical course of the perforator.

To perform more detailed analysis of the perforator and microvascular anatomy there is a lack of standardized methodology or approaches in the literature. Previous research by Prof M. Saint-Cyr characterized the microvasculature in cadaveric models using high resolution imaging, with recognition for the importance of direct or indirect linking vessels between perforator, and the contribution of the dermal plexus, to the perfusion of the flap. (19,26,39,58,65) To date there is no consensus to further classify the branching patterns at the level of the perforator, therefore it was necessary to establish a new series of qualitative and semi-quantitative measurements to analyse the microvasculature of the perforator and its branching patterns. The analysis was developed after initial review of 10 patient abdominal CTAs, following the perforator along its course, and reviewing microvasculature contributions to the dermal plexus in addition to any dominant linking vessels in the integument. Patterns observed were documented and when applicable, semi-quantitative classifications were created. The system designed for the proposed approach for the analysis was reviewed with a senior Consultant Radiologist, together with CT scans to determine if the methodology was appropriate. This is notable limitation in this study, as the methodology has not been validated, yet it provided an initial schema for evaluation or the microvasculature using patient CT scans that would need further studies for validation for a novel classification system. This study, however, will provide the initial data to inform further development, reproducibility and validation for this new classification of the DIEA microvasculature

The degree of branching of the perforator from the either the lateral or medial row of the DIEA was then recorded: perforators were seen to follow a “direct” course with none to minimal branches to the rectus muscle and fat towards the subdermis; perforators with an “indirect” course had multiple branches to the rectus muscle, and fat before reaching the subdermal plexus. The angle of the perforator exiting the anterior rectus fascia was assessed based on its orientation through the integument towards the subdermal plexus (direct=0-45 degrees or oblique=45-90 degrees). The distance of the perforator course within the fat was also measured prior to arborisation and the main layer or arborisation of the perforator was recorded (subscarpa’s, suprascarpa’s, subdermal) were documented. The degree of branching in the subscarpa’s and suprascarpa’s layer was assessed semi-quantitatively as none, minimal (1-2 larger calibre branches) or multiple (>2), around the dominant perforator.

The microvasculature and contribution to the subdermal plexus was then analysed on axial and sagittal slices of the CT scan. These assessments were made through semi-quantitative or subjective assessment of the microvasculature, but reviewed with a Consultant Radiologist[4] following review of a sample of reconstructed images. Specifically, the density of vertical communicating vessels from the dominant perforator to the subdermal plexus was categorised semi-quantitatively as minimal, moderate, or multiple. Characterization of the pattern of contribution to the subdermal plexus from the dominant perforator was then assessed subjectively according to patterns identified following review of coronal and sagittal MIP reconstructions. These patterns were variable but were classified as: presence of a direct dominant linking vessel from the perforator with small communicating branches to the subdermis; multiple fine communicating vessels from the perforator to the subdermis; a direct course of the perforator to the subdermis without additional branching; a direct course of the perforator to the subdermis in addition to the presence of a dominant direct linking vessel from perforator, and a combination of a direct course of the perforator to the subdermis with multiple additional fine communicating branches.

[4] Dr. Robert Maxwell, Consultant Radiology, Department of Radiology, Mayo Clinic, Rochester.

The presence of a direct linking vessel (yes/no) in the subscarpa's, suprascarpa's or subdermal level from the dominant perforator. The presence of linking vessels to the SIEA territory was then evaluated and the principle layer this occurred was documented (yes/no), or whether direct communicating branches were present. Direct linking vessels towards the DCIA lateral territory was also assessed (yes/no) and layer in which these linking vessels course were also documented. These assessments were performed initially using coronal planes of the MIP reconstructions and characterized using all three planes. Finally, the presence of a direct linking vessel between the dominant perforator in the flap to an adjacent inter-row or intra-row perforator was documented (yes/no). The layer in which these large direct linking vessels course was then reported. Examples of CTA image slices from MIP reconstructions to evaluate the microvasculature of the lower abdomen shown in Figures 3.5-3.9.

Figure 3.5: Example of an axial image of Maximum Intensity Projection reconstruction in a patient following contrast CTA. Marker set at level of umbilicus in the midline. Scarpa's fascia can be identified and traced (orange arrow) and dominant traversing inking vessel in suprascarpa's fascia (blue arrow).

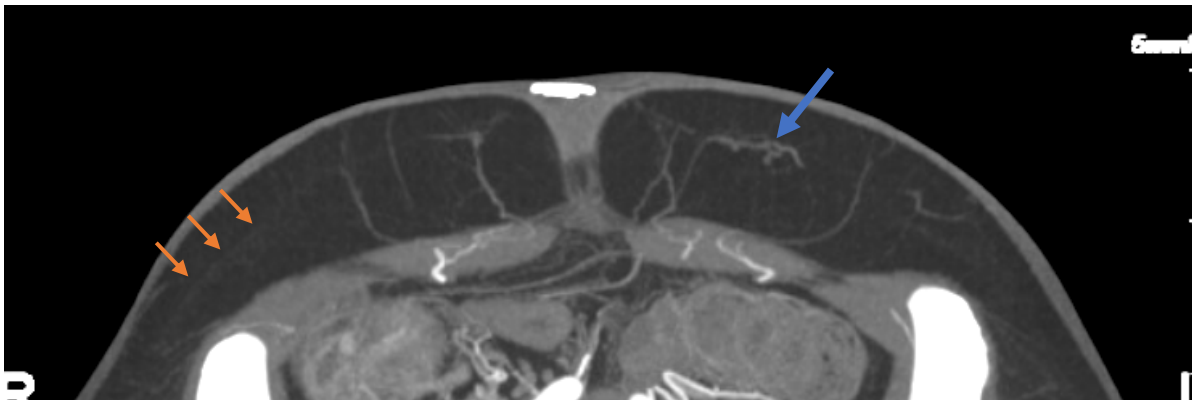

Figure 3.6: Example of an axial image of Maximum Intensity Projection reconstruction in a patient following contrast CTA. Marker set at level of umbilicus in the midline. Degree and layer of arborisation assessed through multi-plane views and type of pattern of contribution to supply the subdermal plexus characterized. Multiple branching at the layer of the fascia shown (green arrow).

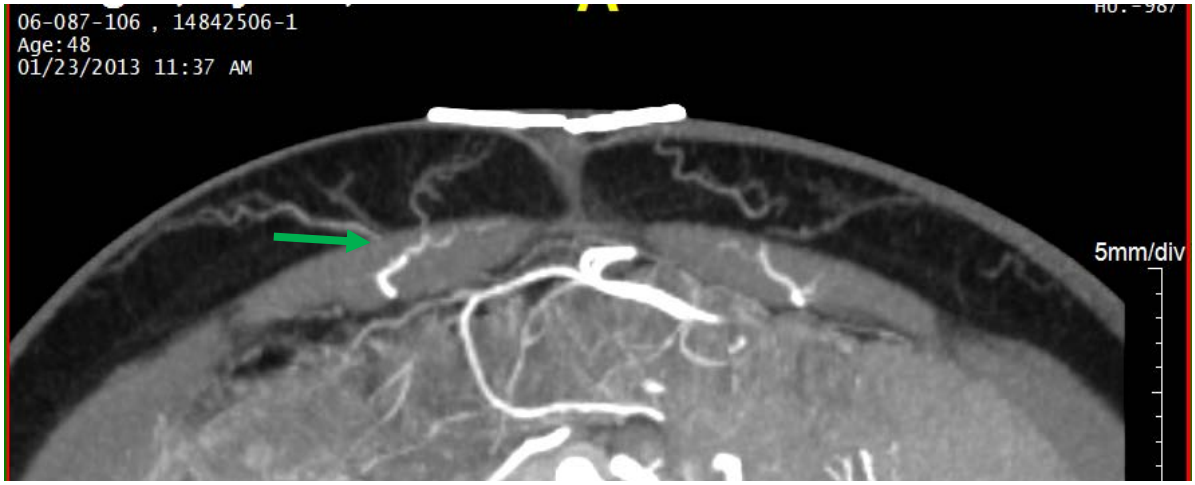

Figure 3.7: Example of scoring used for branching of perforator in the subscarpa's layer shown in an axial slice image in a patient following contrast CTA: 1=none, 2=minimal (1-2 branches) and 3=multiple branches.

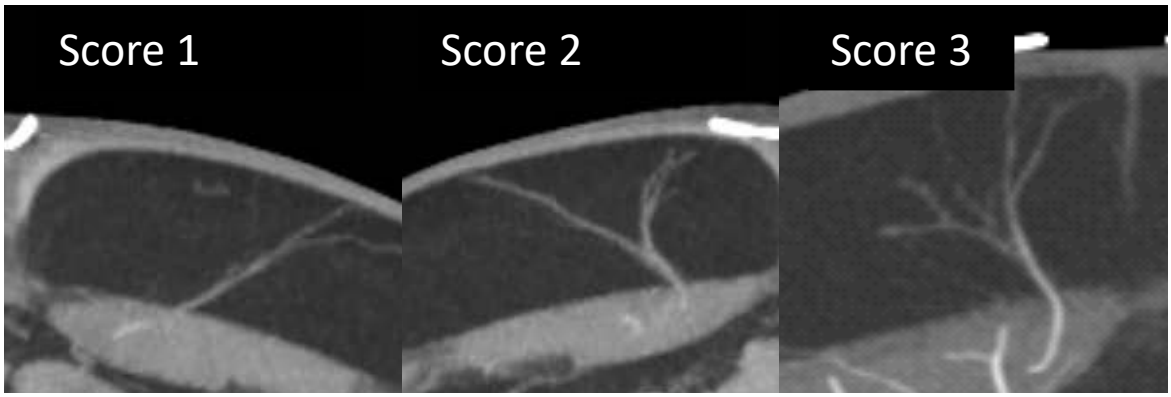

Figure 3.8: *Two examples* of a sagittal slice images of Maximum Intensity Projection reconstruction in a patient following contrast CTA. Marker set at level of umbilicus and direct linking vessel could be traced to the SIEA (blue arrow), and contributions to the subdermal plexus can be visualised from the dominant perforator (red arrows).

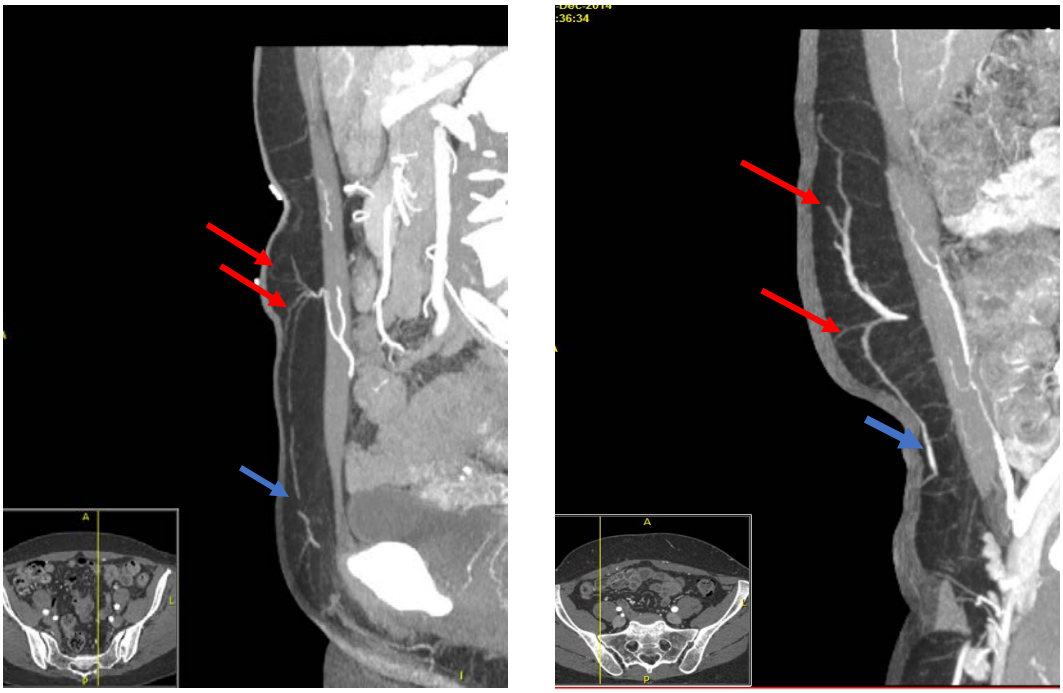

Figure 3.9: Example of a axial slice image of Maximum Intensity Projection reconstruction in a patient following contrast CTA, illustrating a lateral linking vessel in the suprascarpa's layer (blue arrow) and additional linking vessel in the subdermis could be traced directly to DCIA perforator passing through the external oblique muscle (green arrow).

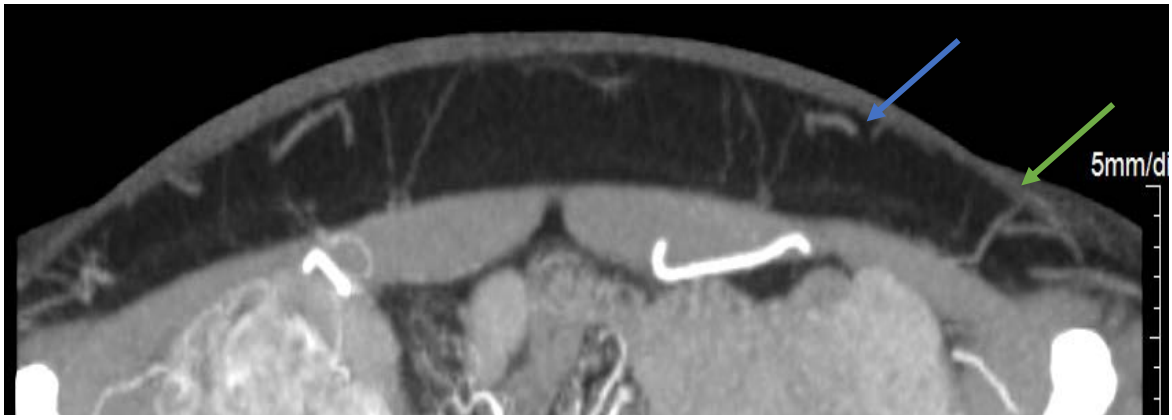

3.1.2.3 Analysis of Laser-Assisted Indocyanine Green Fluorescence Angiography

Following perforator dissection flaps were assessed for perfusion using Laser-Assisted Indocyanine Green Fluorescence Angiography (LA-ICGFA) using the SPY® Elite system (Novadaq Technologies Inc). The camera was set up centred over the hemi-DIEP flap with a maximum field of view (FOV) of 25 x 25cm., with the camera parallel to the flap surface. Images were orientated in a standardized fashion with the upper screen representing the cephalad border, and the inferior portion of the screen correlating with the caudal border of the flap. 5ml of indocyanine green (ICG) was injected through a peripheral intravenous catheter followed by a saline flush. Image capture was commenced following the injection and continued to the maximum length of recording time, 180 seconds, to capture the initial inflow of dye (ingress), the plateau phase, and beginning of outflow (egress) phase. The location of the perforator was marked on the flap at the start of the image capture for reference for the final analysis.

A protocol was developed in collaboration with Drs C Chen and TB Ferguson (see acknowledgements) and using SPY-Qc beta software that they developed designed specifically for the SPY® Elite system. Drs Chen and Ferguson developed the original software that most surgeons are familiar, the SPY-Q analysis program, that is available on the device. Attempts of analysis using LAICGFA with this device has been previously performed with random selection of points within the flap and zone, but these values can change depending on the timing the measurement was taken, or area that is limited in shape to a simple rectangle. The use of multiple arbitrary points throughout the flap was considered, however, previous published data typically would still divide the flap into traditional DIEP zones and average these points within each zone. Other options included using a series of values along two principle axes, medial to lateral and cephalad to caudal, to evaluate changes along them. Both the previously described methodology are limited by bias in selection of the placement of markers to extrapolate data, and that with the current proprietary software, these measurements can only be performed at a single time point, therefore can impact the overall result depending on timing of the angiographic phase used.

Based on the literature and direct peer to peer consultation with multiple experts who published their initial experience in the USA with the device, there is no recognised standardization for using this software to evaluate *whole* flap dynamics. Surgeons commonly use the video image alone to assess areas of ischemia, or refer to the absolute or relative measurements using the analysis tool for areas of concern. Therefore, in collaboration with the software developers, we were able to use a more advanced program to try an establish a more comprehensive approach for this study. It is acknowledged that this is an early pilot of this analysis tool and would require further studies to validate our analysis protocol.

Video images were reviewed to qualitatively assess perfusion into the flap, which represents the surgeon's view that is captured intra-operatively and used for immediate assessment of overall perfusion in the flap, and identification of the areas of hypo-perfusion. A curve is reproduced during the recording that represents the detection of the ICG in the FOV, that provides information of rate of ingress into the flap, plateau and subsequent egress of the ICG that is visually represented on a graph over time (Figure 3.10).

For quantitative analysis, a protocol was developed as a novel approach to evaluate flap perfusion dynamics within the flap. This analysis was completed by a blinded reviewer who developed the both the original and new software. The first step in the quantitative analysis was a quality assessment of the videos captured to permit the analysis. This improved with development of a prospective data collection protocol following flap harvest. The flap area was marked out freehand as the region of interest (ROI) for the analysis.

Intensity and timing maps were created to provide qualitative and quantitative results to evaluate perfusion in the ROI, which was marked as the peripheral border of the hemi-DIEP flap. The software allowed analysis of concentration of dye captured throughout the flap region (intensity) and the rate at which dye was detected throughout the flap (timing). Contour maps were created for both intensity and timing modalities. Intensity maps, provided an average of the cumulated concentration of the ICG detected in every pixel of the image captured in the ROI (Figure 3.11) and can vary based on the amount of ICG

injected. This provided further supportive evidence on the role of using relative values, to allow comparison of quantitative analysis between patients. Timing maps, in contrast, provide a visual colour map of the average ingress (inflow) of ICG detected in the ROI (the hemi-DIEP) flap (Figure 3.12). Timing maps characterize the microcirculatory flow and are independent of the amount of ICG injected. The developers of the new proprietary software, in their experience, deemed that timing maps may better record and map perforators on the abdomen in comparison to traditional intensity maps. These visual colour maps record these values that are averaged over the arterial and microcirculatory angiographic phases (Figure 3.13). Evaluating the ROI as the whole flap afforded the ability to capture perfusion comprehensively, pixel by pixel over all three angiographic phases, instead of multiple arbitrary points in the flap at a single time point. An average rate of ingress or total contrast detected (intensity) was calculated for each pixel within the ROI.

Figure 3.10: Three angiographic phases of perfusion captured using the SPY Elite® system camera, starting with arterial, microvascular (ingress) and venous (egress) phase.

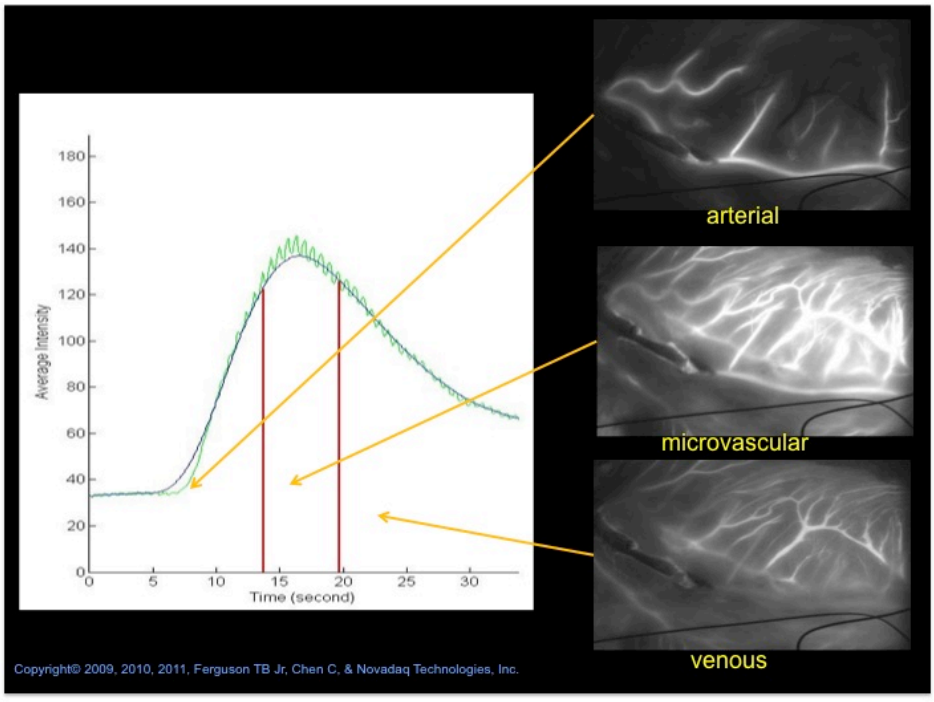

The use of absolute values of ICG detected, or relative values of ICG detected by selecting the 100% reference value, could have been used for the basis of the final quantitative analysis. It was determined on development of the protocol, that relative perfusion values of ICG detected would be the most reliable for comparative analysis between different patients. The absolute values of ICG detected on the SPY® Elite System camera can be influenced by multiple patient factors and physiological parameters, including haemoglobin concentration, heart rate, blood pressure, and patient BMI. Use of relative values would evaluate areas of perfusion within the hemi-DIEP flap and therefore allow better comparison between patients. Measurements were recorded using the dominant perforator harvested as the 100% reference point. The location of the perforator on the flap surface, that was indicated by the surgeon on the video, was used as the 100% reference value and to represent the point of maximal perfusion into the flap (for example within a traditional Hartrampf zone I). Since each patient and flap dimensions could not be measured, we calculated areas relative to the total flap area (ROI). Using the 100% reference point as the maximal threshold at the site of the single dominant perforator selected for flap harvest, the perfusion of the flap was then evaluated.

Prior to finalization of the protocol for analysis, preliminary assessments and trials for analysis were performed and discussed sequentially. This provided an iterative approach to these new methods of assessment. Flap perfusion was assessed qualitatively to evaluate general patterns of perfusion on intensity and timing maps, which were generated from average values of each pixel within the ROI. Next, three perfusion thresholds of decreasing value (75%, 50% and 25%), all relative to the 100% reference point, were used to semi-quantitatively assess the magnitude of the perfusion within the flap and created “contour” maps at for each threshold: thus, the areas of the flap at each threshold value *and greater* were documented. For example, the area of the flap representing perfusion thresholds of 75% and above, in either the intensity or timing map, would indicate how much of the flap had strong degree of perfusion (to the skin and superficial layers), and that may be representative of e.g. zone I type perfusion. Relative values below 20% are considered areas of poor perfusion, and would be expected values in DIEP zone IV perfusion, and areas of concern that would have typically been resected. The approach of using the three intervals

was thought to provide a good depiction of trends in perfusion changes with respect to the perforator location, and the lower value is close to the 20% value which is used as a clinical reference. It is acknowledged that this technique has not been validated as new proprietary software tools was used for analysis and assumptions were made on use of the selected threshold values, but it provided a novel and systematic approach to evaluate zones of perfusion from a new perspective.

Timing maps represented the rate of ingress and egress within the flap that correlated with the angiographic phases during LA-ICGFA previously described. For both timing and intensity maps, values within every pixel across the region of interest (ROI) and value were taken collected over the arterial and microvascular phases therefore an average trend could be calculated along both cephalad-caudal and horizontal axes over time. Using timing maps, average perfusion gradients were calculated in the cephalad-caudal axis and the medial-lateral axis across each flap, and were illustrated graphically. The area of under curves created for the perfusion gradients was representative of the area of the entire flap (ROI). The degree of cephalad-caudal and medial-lateral perfusion was evaluated based on the area under the curve that represented threshold values of 75% and above. This provided a level of comparison along both axes for the most intense perfusion within the flap relative to the perforators.

Figure 3.11: Graphic illustration of software calculation and capture of total concentration (intensity) of indocyanine green injected detected over total time of the recording pixel by pixel over the entire Region of Interest (ROI) or flap area to create intensity maps.

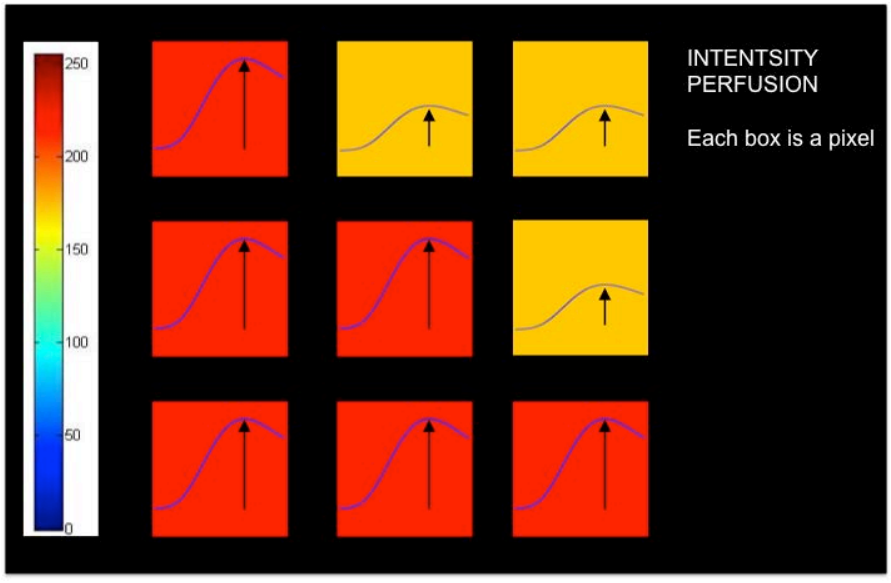

Figure 3.12: Graphic illustration of software calculation and capture of rate of inflow (ingress of indocyanine green detected over total time, pixel by pixel, over the entire Region of Interest (ROI) or flap area to creating timing maps.

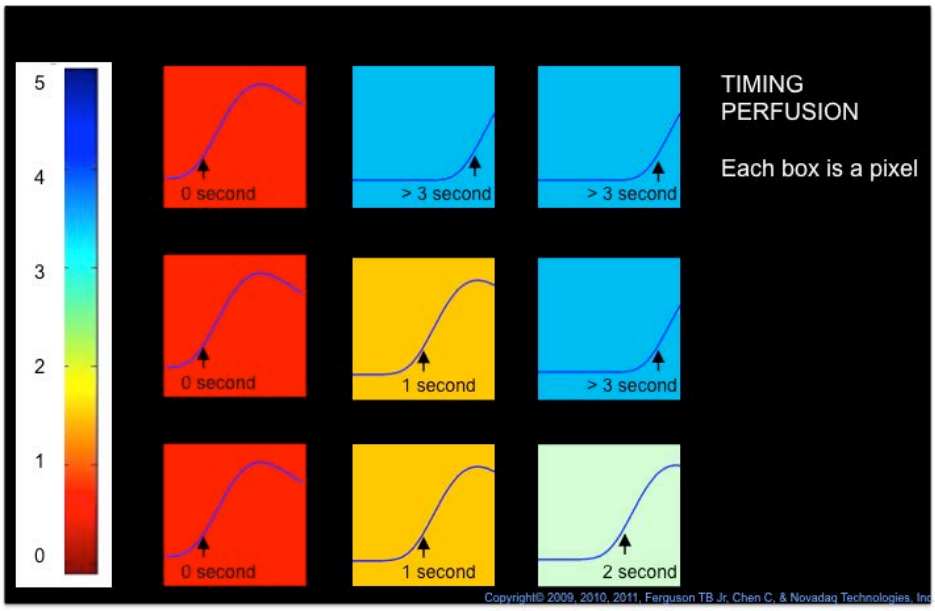

Figure 3.13: Example of LA-ICGFA cumulative perfusion mapping during image capture with SPY Elite® of a hemi-DIEP flap based on a single dominant perforator and graphs of cranio-caudal and medial to lateral perfusion on timing maps (left) and intensity perfusion maps (right).

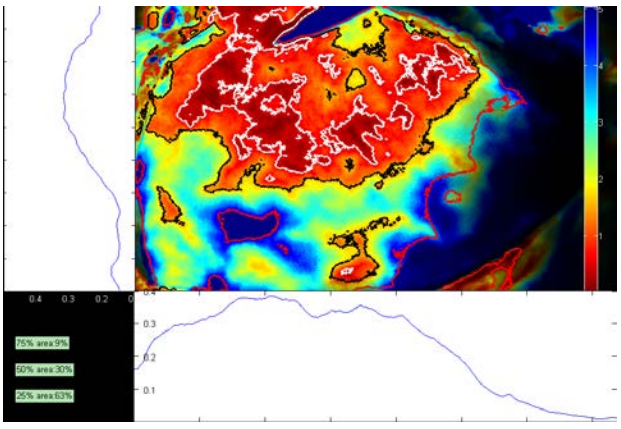

SPY Qc: Timing Perfusion Map of Left Hemi-DIEP

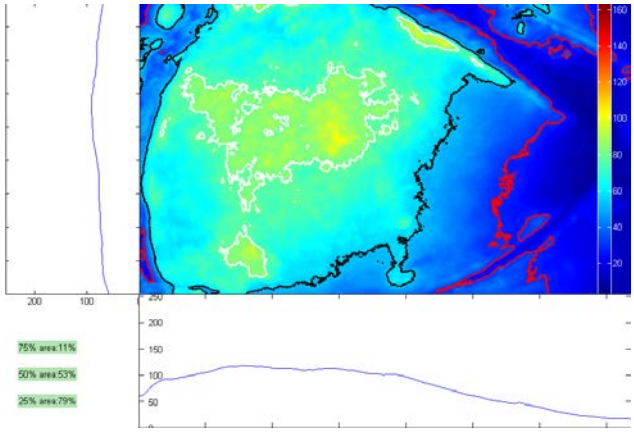

SPY Qc: Perfusion Intensity Map of Left Hemi-DIEP

In addition to the independent analysis of preoperative CTA and LA-ICGFA, a qualitative analysis was performed to characterize the patterns of the in-vivo "dynamic" perforasome. Finally, a comparison of the CTA analysis and LA-ICGFA quantitative and qualitative findings was performed.

3.1.2.4 Statistical Analysis

Descriptive and summary statistics were calculated for the independent variables which included cadaver and patient demographics. Quantitative variables were summarized with median and interquartile range (IQR), or proportions and frequencies as appropriate for categorical variables. All values of the experimental data were reported as the median and interquartile range. The differences in the dependent variables of perforator injection studies or dynamic perforasome assessment were calculated using non-parametric tests for continuous dependent variables (Mann-Whitney and Kruskal-Wallis Tests), and differences between categorical dependent variables were assessed using Chi-Squared or Fisher's Exact Test when appropriate. All analyses were completed with an α-level significance of 0.05 using JMP® Statistical Software Version 11.0

There have been limited clinical studies that specifically review perforasomes and assessment of zonal perfusion in DIEP flaps in-vivo. Based on previous clinical studies of patients undergoing DIEP breast reconstruction to evaluate zonal perfusion zones using ICGFA, Laser Doppler and tissue oxygenation, a sample size of 16-20 flaps for our study was considered to evaluate perforasomes of hemi-DIEP flaps in bilateral breast reconstruction.(55,170,172,173)

3.2 An Experimental Small Animal Model to Evaluate Topical Negative Pressure Pre-treatment and Implications on Flap Vascularity

The **aim** of this study was to determine if negative pressure therapy (NPWT) pre-treatment can be used for perforator flap preconditioning and augment flap vascularity.

The **hypotheses** were:

1. A perforator flap model can be developed in a rodent model for assessment of a flap viability and perfusion.
2. Flaps pre-treated with NPWT will demonstrate augmented perfusion on dynamic imaging studies using laser-assisted indocyanine green fluorescence angiography (LA-ICGFA) and dynamic computed tomographic angiography (4D-CTA), compared to control flaps.
3. Flaps pre-treated with NPWT will demonstrate greater capillary recruitment, vasculogenesis, angiogenic growth factor release compared to control flaps.
4. Flaps pre-treated with NPWT will demonstrate better clinical flap viability and lower degree of complications compared to control flaps.

This study was approved and carried out in accordance to the guidelines of the Institutional Animal Care and Use Committee, Mayo Clinic, Rochester MN, United States (Protocol ID: A57312).

3.2.1 Preliminary Work

The goal for carrying out the preliminary work was to review the literature and examine the perforator anatomy of the rat to develop an appropriate perforator flap model suitable for this study.

Five 200g Sprague Dawley rats were used in a cadaveric pilot study to identify an appropriate perforator flap model to permit the design of a control and intervention flap

model. Posterior thigh perforators were considered too small and the caudal location through the biceps femoris muscle would be more difficult to maintain a reliable seal in the application of the VAC dressing. The iliolumbar perforator arising from the DCIA vessels appear at the cephalad edge of the gluteus muscle. The vessel arose 1.5-2cm from the midline and coursed perpendicular to supply the skin and arborized on reaching the dermal layer with a consistent large axial vessel running in the territory over the gluteus maximus muscle.

The pedicle was surrounded and protected by a layer of fatty issue and lymph nodes. These vessels were easily identified and would permit the design of two small perforator flaps with a control and intervention side per rat, and allow for easier application of VAC dressing. Perforator calibre, location and size of the surrounding tissues made this gluteal area was preferable to a more proximally located perforator, and allowed at least a minimum of a 2-3cm distance between the medial edges of the control and intervention flaps in 400g rats. The planned flap was designed at 3x2 cm and was raised on one 400g male rat in the microsurgery lab to test the flap procedure.

Figure 3.14: Cadaveric dissection of the dorsal rat skin to identify perforators; Cranial Deep Circumflex Iliac Artery (DCIA) perforators arose next to the gluteal maximus (GM) muscle. The caudal biceps femoris (BF) perforators were also consistent but located to caudal to provide a reliable location for NPWT application.

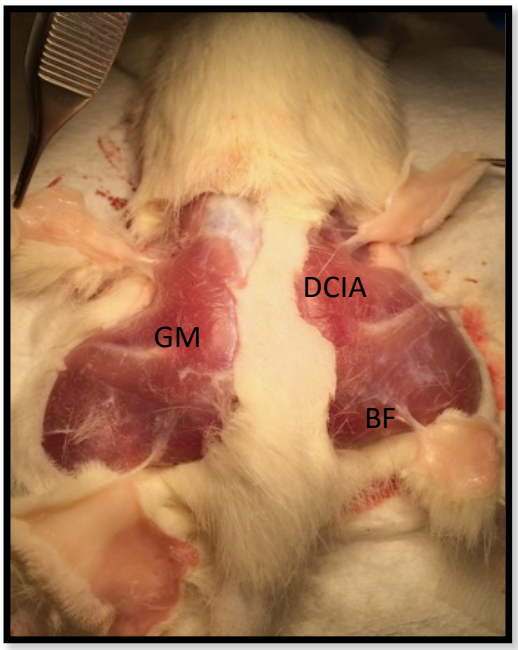

Figure 3.15: Planned gluteal perforator flap design based on the DCIA vessels following hair removal. Two flaps representing the control (rat's left side) and intervention flap (rat's right side) were designed.

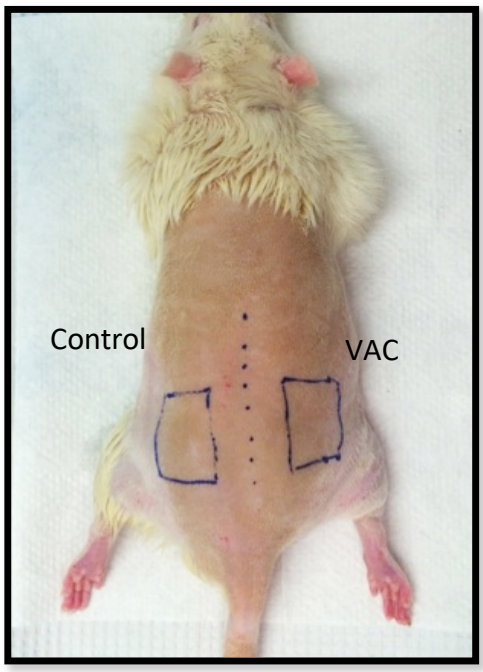

3.2.2 Experimental animals

A total of 23 Sprague Dawley male rats (Charles River Laboratories, Wilmington, MA, USA) weighing 350-400g were used for this study. All animals were obtained and housed in an approved animal care facility. All rats were kept in a single housing following application of VAC dressing. Three of these rats were used as part of the pilot studies described below. Sixteen rats were used in the main study. An additional four rats were added to the study following some loss of data acquisition.

3.2.3 Pilot studies

The goals of the pilot study were:

- Identify suitable method to protect topical negative pressure wound therapy VAC® dressing
- Develop a standard operating procedure and determine the optimum dose for Indocyanine Green (ICG) for laser-assisted ICG fluorescence angiography (LA-ICGFA) to acquire suitable imaging with the SPY ® Elite System (Novadaq Technologies, Florida, USA)
- Trial a new Computed Tomographic Angiography protocol and Micro CT trial injections to develop standard operating procedures.

Application of VAC®

Three rats were used in the initial pilot studies to determine approaches to secure the application of the VAC dressing, optimizing the protection of the dressing and ensuring that the animal was not hindered in movement and could easily access food and water post procedure. In two rats the VAC dressing was applied for 3 days. The biggest limitations that were initially faced included 1) the protection of the VAC system, 2) maintenance of the seal to ensure uninterrupted therapy, and 3) establishing intravenous (IV) access for injection studies which is low morbidity and to avoid open exposure of vessels. In two pilot rats, before the application of a VAC dressing, different rat jackets, modified jackets and dressings were trialled to identify which option would be the most appropriate to maintain mobility and provide protection of the dressing. The resultant dressings used are described in *Animal Procedures* and was successfully applied to the third pilot rat for a total of 5 days without loss of negative pressure seal.

Standard Operating procedure Indocyanine Green and optimization of Imaging Protocols

One rat was used to ascertain the optimum dose of ICG to be administered for fluorescence laser-assisted angiography for dorsal skin perfusion assessment. This was carried out prior to application of the VAC dressing. The tail vein was originally chosen as the site for placement of a 24-gauge butterfly IV catheter, if unsuccessful a posterior thigh or medial thigh vein was chosen based on size. Based on the literature, dosing regimens in rat models to assess perfusion, including random pattern skin flaps, ranged from 0.12-0.4mg for a 300-400mg rat. Using a preparation of ICG which was reconstituted to a concentration of 2.5mg/ml, i.e. 0.25mg per 0.1ml, three test doses were carried out on a 300g rat pilot rat injection 0.05ml, 0.1ml and 0.15ml. Following each injection, a period of 10-15 minutes was allowed to lapse prior to the next injection and imaging was repeated prior to the subsequent injection to ensure no residual ICG was in the skin. Image capture was performed using the SPY Elite® system (Novadaq Technologies, Vancouver, Ca). A 0.1ml injection provided imaging which was not rapidly saturated upon injection and the chosen dose for our protocol.

Finally, one rat was used to test a 4D CTA protocol after three days of VAC therapy. Injection timing, dose and image capture using a newly developed CT protocol was designed in collaboration with the Biomedical Imaging Resource Group, Mayo Clinic. To our knowledge dynamic in-vivo perfusion of skin flaps over time has not been described in the literature for animal studies and the main hurdle faced in this pilot was establishing optimal imaging in a small animal model to allow assessment of the control and preconditioned skin flaps prior to flap harvest. On completion of this study the rat was euthanized with sodium phenobarbital and injected with MicroFil for Micro-CT assessment of the preconditioned and control tissues described in more detail in *Animal Procedures*.

3.2.4 Overview of Experimental Methods

In our initial approach sixteen 400-500g male Sprague Dawley rats were used for the main study, each rat acting as its own control with two dorsal potential skin flap areas designed over the gluteal region. The preconditioned side was always selected on the right and the control tissue designed on the left gluteal region. An overview of the planned methods is shown in Figure 3.16. Topical negative pressure was applied for 5 days on the preconditioned skin flap side, after which the 16 rats were divided into two principle groups: Group A rats (n=8) who underwent flap surgery following 5 days of NPWT and then 7 days of observation, and group B rats (n=8) who underwent CTA assessment and euthanized. Repeat anaesthesia or prolonged inhalation anaesthesia was avoided due to a slight increase in anaesthesia related death postoperatively or intra-operatively, and logistical reasons to perform both procedures in same sitting: therefore, rats who underwent CTA assessment were not subject to flap surgery immediately afterwards.

In the initial methodology, there was concern that flaps used in Micro-CT may produce inferior results if combined with IHC and histology, and this original plan is shown in Figure 3.16. Within each group, flaps were assessed with Micro-CT to assess vessel density per flap (n= 4 rats per group). Histology and immunohistochemistry staining were sent immediately for (n=4 rats per group), but it was decided that the remaining flaps subsequently underwent histological processing *after* Micro-CT evaluation. Specimens assessed following

Micro-CT did not hinder histological or IHC processing, and therefore is a limitation of this current study that would be amended for future experiments.

Figure 3.16: Overview of methods to show animals, groups and outcome measures used at each stage of the study.

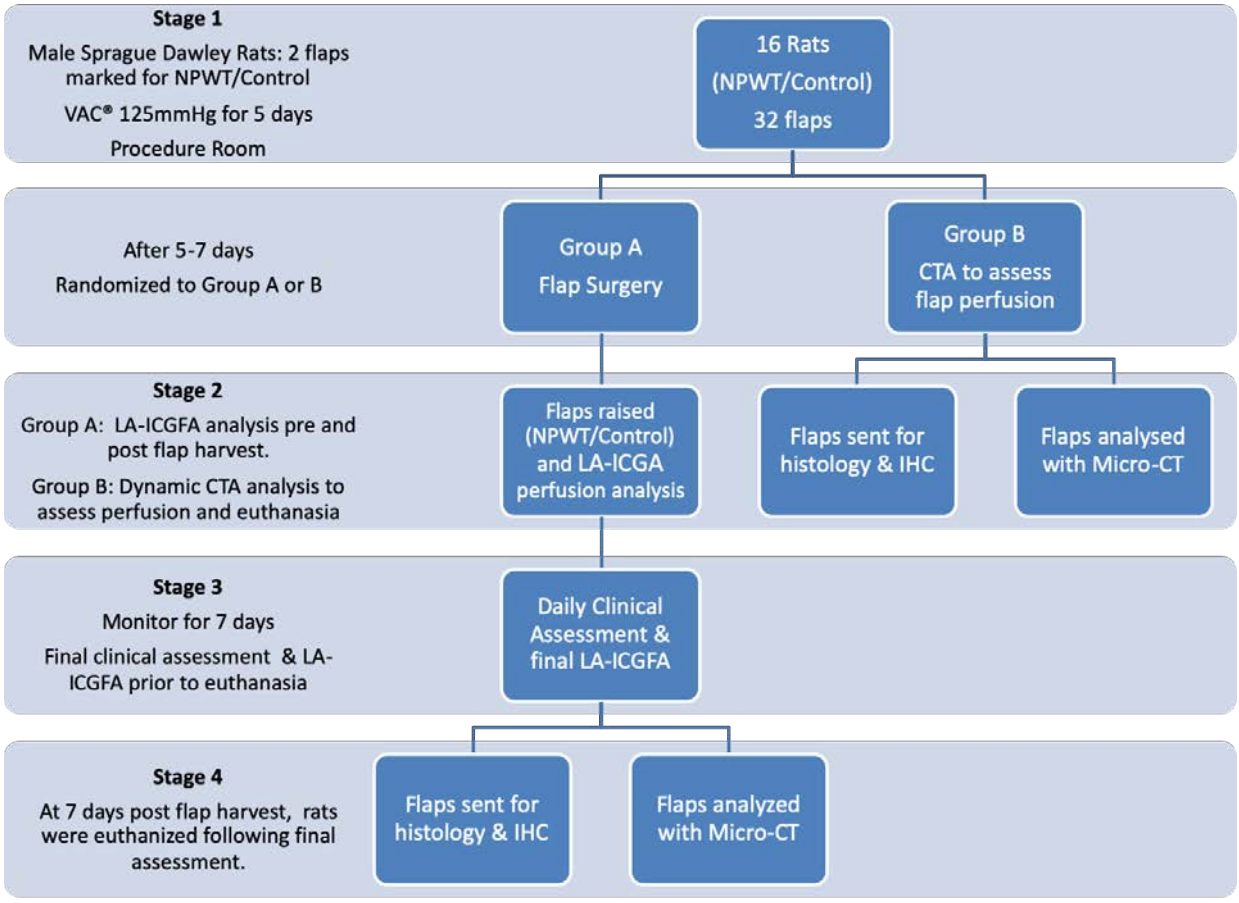

3.2.5 Animal Procedures

For the application of the VAC dressing and for all flap surgeries rats were anaesthetized using 1.5% inhaled Isofluorane for induction and maintenance delivered through nose cone. Procedure time per animal was approximately 30 minutes.

For assessment of perfusion of the skin flaps following 5 days of VAC application, rats were induced using 1.5% inhaled Isoflurane and a mixture of 0.75ml of ketamine (100mg/ml) and 0.075ml of Xylazine (100mg/ml) for 1ml/kg per rat. This induction mixture equates to 40-80mg/kg of ketamine plus 5-10mg/kg of Xylazine. Therefore, for a 400g rat a total of 0.4ml of the aforementioned mixture was given. This allows 45 minutes of anaesthesia with a 1 to 2-hour recovery period. Maintenance was given using a mixture of ketamine 10-20mg/kg + 1.25mg/kg of Xylazine, providing an additional 20-30 minutes of anaesthesia. For application of the VAC dressing and surgery all rats were given Buprenorphine SR (slow release formulation) 0.05-0.1mg/kg administered subcutaneously every 12 hours for 24 hours.

Negative Pressure Wound Therapy V.A.C. system

All rats were anaesthetised with inhaled isoflurane anaesthesia and this was maintained during the entire procedure, which took 30-45 minutes approximately. The dorsum, gluteal region up to the level of the scapulae of the rat was clipped and depilated (Nair®, Church & Dwight CO., Princeton NJ). The rats were cleaned with alcoholic prep followed by normal saline. The flaps were designed with the medial edge 1-1.5cm from the midline, and rectangular 3cm x 2cm, with the proximal edge of the flap starting 1cm cephalad to the edge of the gluteus maximum muscle, which can be palpated (Figure 3.17).

Figure 3.17: Illustration of muscle anatomy and location of perforator vessel exiting proximal to the superficial gluteus and biceps femoris muscles and running in the caudal direction to be included in the flap design (*black dotted square*).

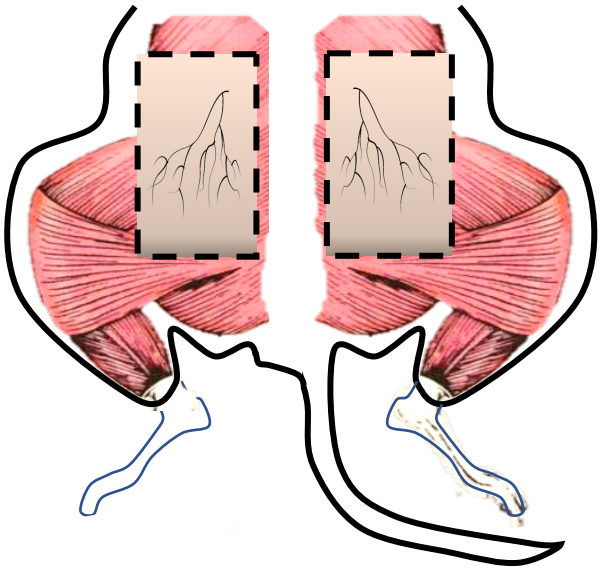

Negative Pressure Wound Therapy (NPWT) is a method of applying topical negative pressure using a Vacuum Assisted Closure Therapy (VAC) device (Kinetic Concepts Inc., San Antonio, Texas) and has been used extensively in wound management and reconstructive surgery. In this study, the portable ActiVAC™ was used. The device consisted of a porous open-cell medical grade black polyurethane sponge VAC® Granufoam ™ (pore size 400-600 microns), which was applied directly to a wound and then subsequently covered with an occlusive dressing (Figure 3.18). For this flap model, the sponge was applied over a non-adherent silicone dressing Adaptic ® (Systagenix, San Antonio, Texas) that was cut to the size of the flap. This provided less irritation, and followed the same principle that is used in clinical practice. The foam dressing was cut to 3 x 2 cm in size and a thickness of 1cm. Double adhesive gel strips (KCl, San Antonio, Texas) were used to maintain seal, allow for better contour and protect the skin from the direct pull of the negative pressure. An occlusive dressing, Tegaderm ™ (3M Health Care, St. Paul, Minnesota) was placed over the control flap and over the sponge with adequate coverage that would provide an adequate seal. Benzoin adhesive spray (Allied Health Products, Inc) was used to assist in securing the Tegaderm dressings to the skin. A small hole was made directly over the sponge and the Sensa T.R.A.C ™ pad (KCl, San Antonio, Texas) was placed over this hole. This pad acted as a

tube that connects the sponge to a vacuum pump, which allowed sub-atmospheric pressure to be applied to the sponge (Figure 3.19). The sponge had multiple pores sized between 400-600 microns, which acted like small suction cups and helped provide uniform distribution of negative pressure at the site. The non-adherent dressing had a similar uniform pore size of 400 microns, therefore should not grossly impact the external suction and microdeformational forces on the intervention side.

Tubing was protected using a long flexible coiled spring to allow movement and flexibility for the rat to walk around freely within its cage. Dressings were protected with a soft elastic adhesive tape over the gluteal region and waterproof adhesive tape over the rat's thorax (Covidien, Mansfield MA). The rat was able to freely walk and eat. Aqua gel packs were placed inside the cage during the first 48 hours post procedure for hydration (Figure 3.20). The negative pressure was initially set at 75mmHg for the first 4 hours, then increased to 100mmHg and up to 125mmHg at 8 hours post NPWT application. This allowed the animal time to acclimatise better and recover following the procedure, compared to direct application of 125mmHg, which was performed in two pilot rats. The NPWT was continued for 5 days. Total hours of treatment were recorded for each rat using the VAC inbuilt treatment history log. Rats were monitored every 4 hours in first 8 hours and then three times daily for the duration of the VAC dressing. Animals were cared for by the Department of Comparative Medicine, and therefore any leaks or problems recognized by the staff were immediately reported for urgent attention.

Figure 3.18: Inhalation anaesthesia set up for induction and maintenance (left); materials for application of VAC dressing (right)

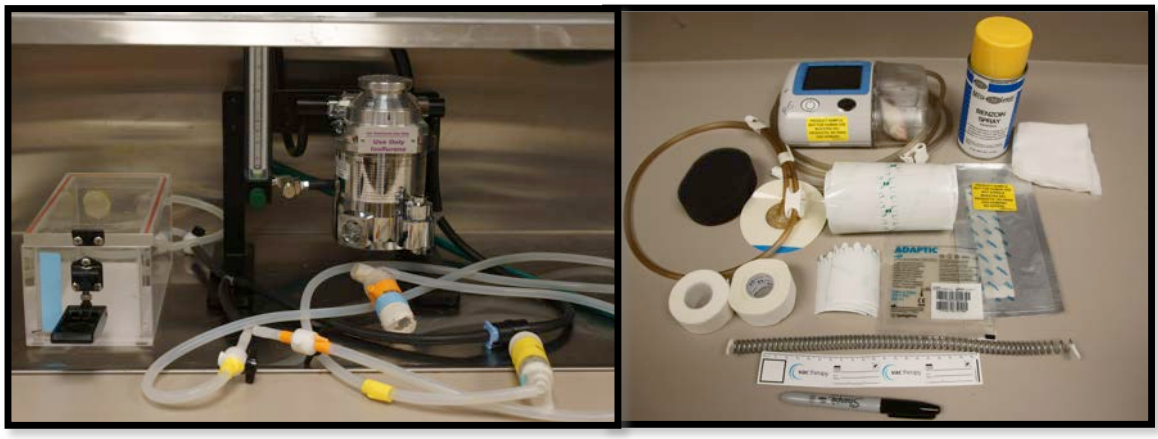

Figure 3.19: Application of VAC Granufoam ™ sponge dressing (A); occlusive dressing applied and Sensa TRAC ™ pad applied (B); further Tegaderm ™ to accommodate rat's movement and maintain seal and flexible spring coil placed to protect tubing (C), and application of a light torso waterproof tape (right).

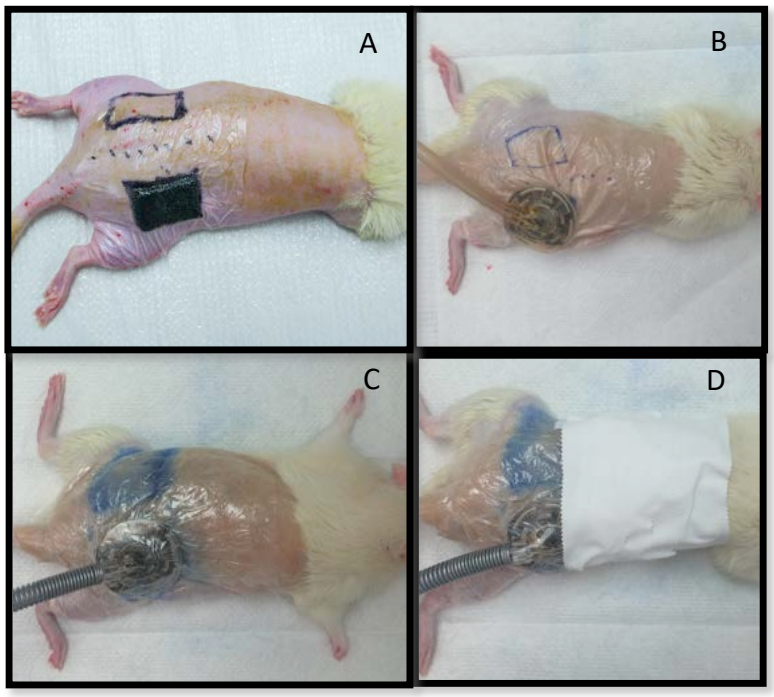

Figure 3.20: Each animal was singly housed and closely monitored to ensure it could freely mobilize around its cage following application of the VAC® dressing.

Laser-Assisted Indocyanine Green Fluorescence Angiography

After 5-7 days of VAC therapy group A rats (n=8) are anaesthetized with inhaled isoflurane and the dressing is removed. The flap outlines are refreshed and an IV catheter is placed in the periphery. The perfusion of the tissue was assessed using indocyanine green laser assisted angiography using the SPY® Elite System (Novadaq Technologies, Florida, USA). Following anaesthesia, 0.1ml of 2.5mg/ml of indocyanine green was injected into the tail catheter. The near infrared light camera was placed over the gluteal region and the fluorescence of this region was displayed on a screen.

Video capture of perfusion were created for the control and preconditioned side simultaneously for each rat. Imaging was acquired before (post VAC) and after flap harvest (post flap) and at 7 days post procedure prior to euthanasia. All the images were analysed using SPYQ software.

Figure 3.21: Flap outlines and SPY imaging demonstrating perfusion during image acquisition for control on the rat's left side and the preconditioned side on the rat's right-hand side.

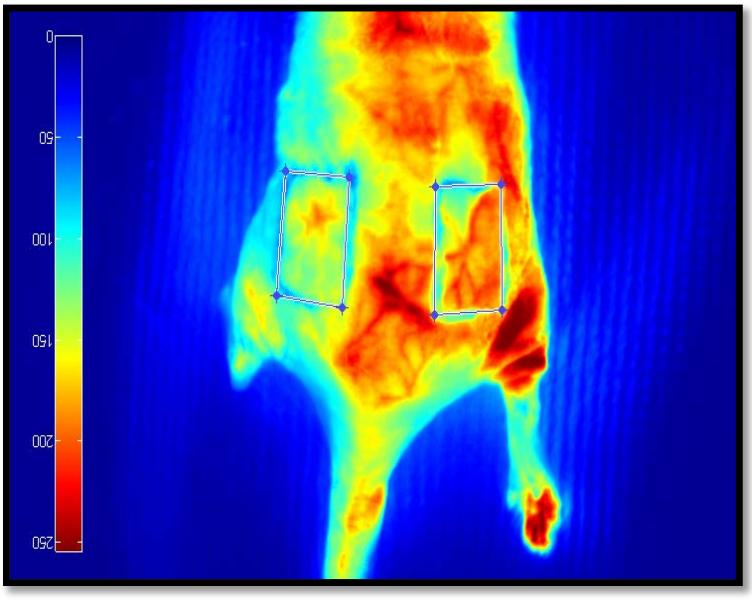

Surgical Procedure

Design

1. Under general anaesthesia, the skin of the gluteal region was shaved using clipper, washed with saline, and prepped with Iodine antiseptic solution.
2. The rat is positioned prone.
3. A line is drawn along the sulcus between the lower limb and gluteal region, starting adjacent to the posterior superior iliac spine (PSIS), to the midpoint of the tail.
4. A vertical line is drawn along the dorsal midline, beginning from the tail upward.
5. A nearly horizontal line is drawn from the PSIS to the midline.
6. A mirror image flap is made on the contralateral side, for the harvest of a contralateral flap.
7. The dimensions of each flap are then 2x3cm.
8. Surgical drapes are secured in place.

Dissection

1. The caudal border of the flap was incised down to the gluteal muscles, using a 15 blade. Bipolar cautery was used if necessary on potential subcutaneous bleedings.
2. The skin flap was raised from caudal to cephalad. The elevation of the flap followed the muscular plane. This dissection was made with micro-scissors. The flap was raised until the desired perforator is seen exiting from the gluteal muscle, just cephalad to the gluteal muscle (the choice will be made based on the size of the perforator, always keeping the largest). Any other encountered perforators will be cauterized. These perforators have a relatively wide diameter compared with those in the deep inferior epigastric artery model, reason why this gluteal model was chosen using the DCIA vessels.
3. Once the perforator was identified, it was necessary to complete a dissection back to the source pedicle and free up the pedicle without skeletonization of the vessels. This dissection was performed to ensure that no other branches will vascularize the flap. Only the main perforator was kept as the vascular supply of the skin flap.

4. Once this dissection was performed, the skin flap relies only on the vascular supply provided by the chosen and dissected perforator. The skin flap therefore becomes an island flap based on a solitary perforator.

5. After this dissection was performed, and the assessment of the flap made with indocyanine green laser-assisted angiography (as described earlier), the flap was re-inset in its wound bed. This means that the flap is sutured back in its original location, using both absorbable 5/0 Vicryl Rapide suture ® (Ethicon, USA).

6. The wound will be washed with saline. Opsite Spray (Smith & nephew, St. Petersburg, FL) will be applied on the wound as dressing.

Figure 3.22: Flaps marked, incised and raised over the gluteal region of rat, and finally re-sutured.

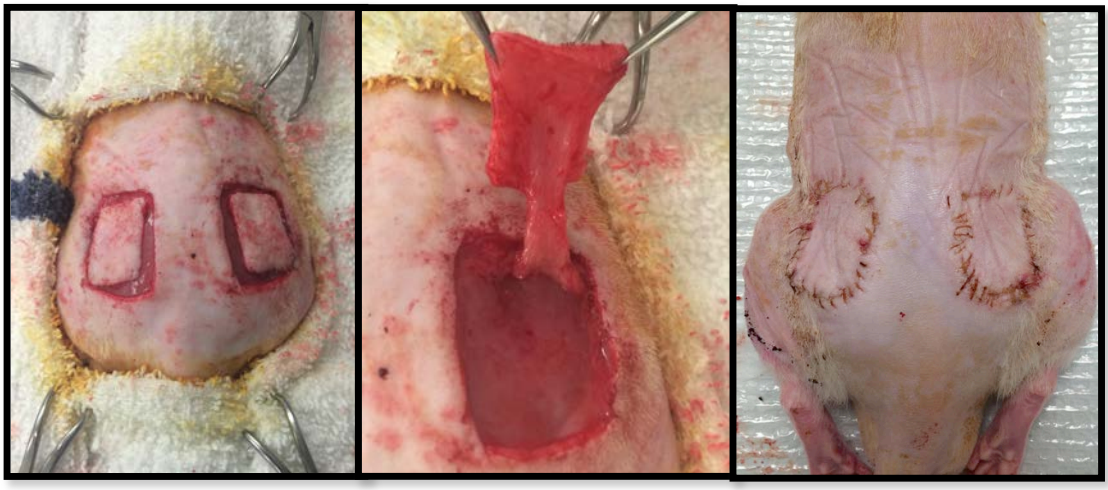

3.2.6 Outcome Assessment of 4D dynamic perfusion CT imaging

8 rats were anaesthetized with Ketamine/Xylazine mixture as previously described, following isoflurane inhalation for induction. A 24G IV catheter was placed in the peripheral vein (tail or leg). For CT scanning 1.5ml of iodinated contrast Omnipaque® 350 (Iohexol) (GE healthcare, USA) was injected over 15 seconds followed by a 1ml saline flush. CT scanning was performed on a Siemens FLASH dual source system. A 4D body volume perfusion

protocol was used to perform CT angiography of the rat's abdomen. A distance of 7 cm ranging from the base of the tail to the mid-abdomen was continuously imaged for 97 seconds while the table moved in and out of the gantry once every 2 seconds obtaining both craniocaudal and caudocranial data. The potential for both x-ray tubes was set at 80kV and the tube current time product was 150 mAs with a 1 second gantry rotation time. The detector collimation was set at 128 x 0.6 mm. 4D data was generated by reconstructing the volume between the proximal and distal localization markers, placed at the edges of the flaps, in 5 mm increments along a distance of 2 cm. A medium smooth kernel (B41f) was used to reconstruct the images in a field of view of 76 mm with a predefined abdomen window level setting of 400/40 HU. Each 5mm slice was analysed using the DynEval software, which generates time-attenuation curves in user defined ROI's drawn over both skin flaps.

Figure 3.23: An axial image of the 4DCT with a Region of Interest (ROI) drawn over the preconditioned area (pink) and control area (red). Graphs represent absolute quantity of contrast detected in Hounsfield units, in the respective ROI**,** against time in seconds.

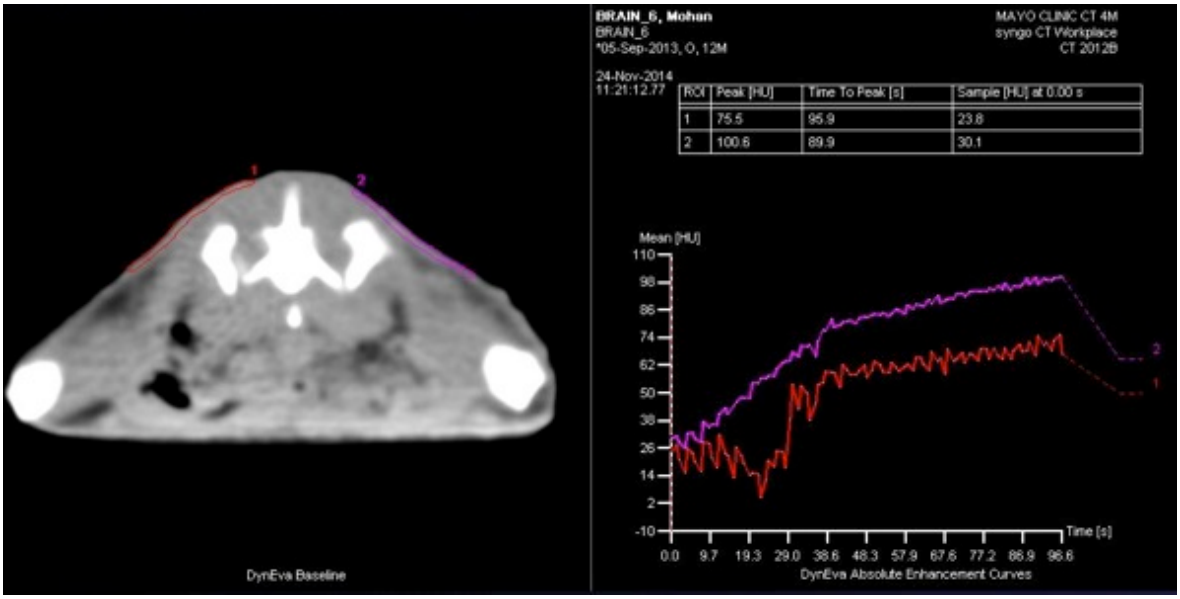

3.2.7 Outcomes Assessment of Indocyanine Green Fluorescence Laser Angiography

All rats in group A underwent assessment with LA-ICGFA of the control and intervention flaps before surgery, immediately following flap harvest and 7 days post procedure (prior to euthanasia) to assess real-time perfusion over two minutes. Direct comparison of control and NPWT pre-treated flaps was analysed by an independent blinded reviewer using newly developed proprietary software (CC). The flap areas were clearly demarcated prior to surgery to define the ROI. Video capture was assessed for quality control and evaluation of perfusion through the angiographic and microcirculation phases was performed. Subsequent intensity maps were assessed to map out the average amount of ICG detected in the ROI of control and intervention flaps. Absolute values were obtained for average perfusion of the entire ROI of both control and intervention flaps. The ratio of intervention to control perfusion was calculated.

3.2.8 Outcomes Assessment of Micro CT

Microvessel density and assessment of the skin flaps Micro CT was performed in 8 rats (4 group A and 4 group B). The rat was injected with 1000units of Heparin intravenously and allowed to circulate for 5 minutes before euthanasia. The abdominal aorta was identified and the proximal aorta and inferior venae cava was tied off below the renal vessels and the aorta was cannulated with a 24G IV catheter and secured with a silk suture and attached to an extension tubing and 3-way Luer-lock tap. A small venotomy was created distally as an outflow mechanism. A flush heparinized saline (10,000u/1000ml) was administered using a 10ml syringe and continued until the effluent was clear, after which a further 10ml was flushed. Then 10ml of 10% formalin was injected, followed by 5ml of heparinized saline, and this step was repeated once more prior to injection of the MicroFil® preparation.

MicroFil ® is a radiopaque silicone rubber compound. The compound (Flow Tech, Inc Carver, MA) were mixed with diluent 50/50 making up a 2ml preparation and mixed evenly and then 5% curing agent was added. 2ml of MicroFil® mixture was prepared. The MicroFil was

slowly injected using a 1ml Luer lock syringe slowly and then allowed to set for 120 minutes. The marked or previously raised skin flaps were then excised and placed in 10% formalin solution for Micro CT. Prior to Micro CT scanning the specimen is placed in paraffin to stabilize the skin flap for the CT scan.

The specimens were mounted on a 360° rotating stage and scanned with a micro-CT scanner (reference) using an x-ray source with a molybdenum anode and zirconium filter to produce 17 keV x-ray photons. The resulting 3-D images consist of 20 micrometre cubic voxels and were analysed using the Analyze® 12.0 software package (Analyze® 12.0, Mayo Clinic College of Medicine, Rochester, MN) (174)

Figure 3.24: Example of 3D reconstruction of microvessel architecture of skin flaps control versus preconditioned.

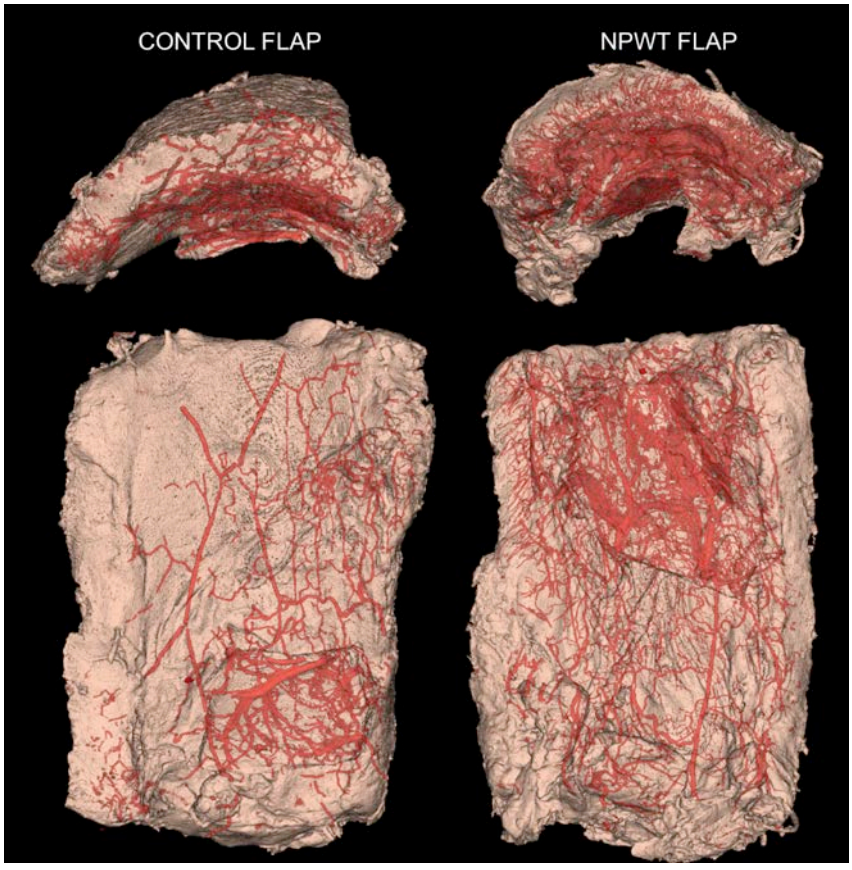

3.2.9 Outcomes Assessment of Histology

Following euthanasia of the animal the control and intervention skin flaps were excised and the central 3mm longitudinal strip of tissue from the flap was excised and fixed immediately in 10% formalin and subsequently paraffin embedded. Longitudinal 5-µm paraffin cross-sections of the tissue were prepared for histological assessment with haematoxylin-and-eosin (H&E) and immunohistochemistry staining, that was performed by the Pathology Research Core, Mayo Clinic.

Immunohistochemistry staining was performed on 5-µm paraffin sections following an initial trial for optimization for CD31, CD68, VEGF and HIF1-alpha. Sections were reviewed following IHC staining and optimization, and all specimens were subsequently stained for CD31.

Immunohistochemical Staining: C31- Pecam 1

Tissue sectioning and IHC staining were performed at the Pathology Research Core (Mayo Clinic, Rochester, MN) using the Leica Bond RX stainer (Leica, Buffalo, IL). Formalin Fixed Paraffin Embedded (FFPE) tissues were sectioned at 5 microns. IHC staining was performed on-line; tissue slides were de-waxed using Bond Dewax (Leica, Buffalo, IL). Slides for CD31 stain were retrieved for 10 minutes using Epitope Retrieval 2 (EDTA, pH9; Leica, Buffalo, IL). CD31-Pecam1, Rabbit Polyclonal antibody (Santa Cruz Biotechnology, CA) was diluted in Bond Antibody Diluent (Leica, Buffalo, IL) to 1:800 and incubated for 30 minutes.

The detection system used was a Polymer Refine Detection System (Leica, Buffalo, IL). This system includes the hydrogen peroxidase block, post primary and polymer reagent, DAB, and Haematoxylin. Immunostaining visualization was achieved by incubating slides 10 minutes in DAB and DAB buffer (1:19 mixture) from the Bond Polymer Refine Detection System. To this point, slides were rinsed between steps with 1X Bond Wash Buffer (Leica, Buffalo, IL). Slides were counterstained for five minutes using Schmidt haematoxylin and

molecular biology grade water (1:1 mixture), followed by several rinses in 1X Bond wash buffer and distilled water. Once the process was completed, slides were removed from the stainer and rinsed in tap water for five minutes. Slides were dehydrated in increasing concentrations of ethyl alcohol and cleared in 3 changes of xylene prior to permanent cover slipping in xylene-based medium.

Sections were evaluated using an Olympus BH-2 microscope (Olympus, Lake Success, NY) and images were captured through an Olympus DP72 camera (Olympus, Lake Success, NY). Quantitative analyses were performed using the cellSens Dimension software version 1.11 (Olympus, Lake Success, NY). Six different random high-power fields of view were examined at x20 magnification, representing three superficial and three deep dermal regions of interest (ROIs). Thresholds were optimized for identification of the stain. The total summed area, percentage area fraction occupied by vessels and a semi-quantitative score (0-3) was recorded for each ROI. A semi-quantitative score was assigned between 0-4 based on the number of positively stained objects in the ROI: minimal (less than 5; score=0), above minimal (5-10 objects; score=1), moderate (10-15 objects; score=2), high moderate (15-20; score=3), high (above 20; score=4). Statistical analyses were performed using a two-sided paired t-Test. A total of 32 flaps (16 control and 16 NPWT flaps) were evaluated.

3.2.10 Statistical analysis

Rats were alternatively assigned to specific treatment groups. Quantitative variables were summarized with means and standard deviations. Categorical data, expressed as proportions and frequencies as appropriate. Matched paired analysis was calculated. For normally distributed continuous data, statistical analyses were conducted with a paired sample t-test. A significance value alpha was set at less than or equal to 0.05. The assessment of skin necrosis and complications was assessed using a chi-square test or Fisher's exact test as appropriate. Statistical analysis was performed using JMP Statistical Software Version 11. 0.

CHAPTER 4: RESULTS

4.1: Anatomical Cadaveric Study of the Perfusion Territories (Perforasomes) of DIEA perforators in the Hemi-Abdomen

4.1.1 DIEA Perforator Mapping in Hemi-Abdominal Flap

A total of 22 hemi-abdomens flaps in 11 fresh cadaveric torsos were harvested for this study, of which 10 flaps were used for assessment of 4D imaging in addition to the 3D CTA assessment. The 4D protocol was developed after the established injection protocol, which accounted for the lower number of flaps used for this assessment. A total of 244 perforators were mapped in 22 hemi-DIEPs and from which 38 perforators were selectively injected for CTA evaluation. Two injections were complicated by an irreparable leak at the most distal part of the perforator and subsequently the injection failed. Hence a total of 36 flaps were simulated for evaluation of the vascular injection territories in the hemi-abdomen: these data included 17 medial row perforators, 15 lateral perforators and 6 DCIA.

The largest perforators from the DIEA source vessel were located within 5cm of the umbilicus which has been previously described(47) and represents the “hot spot” of dominant perforators on the anterior abdominal wall. Fifty-three percent of the perforators greater than 0.5mm on the anterior abdominal wall were found within 5cm of the umbilicus and only 28% within 3cm of the umbilicus. In this study, 88% of medial row perforators (N=15) were located within the 5cm hot spot in comparison to lateral row perforators of which 73% (N=11) were located outside this hot spot zone, and this difference was statistically significant, $p<0.01$ (Fisher’s Exact Test). Perforators within the 5cm “hot spot” demonstrated a greater average external diameter with a median of 2.4mm (IQR=1.4-1.9) versus 1.7mm (IQR=1.8-2.9) of perforators outside this zone (>5cm from umbilicus), $p=0.02$ (Mann Whitney). The median external diameter of the perforators was greatest in the medial row (2.3mm), followed by the lateral row (1.8mm) and smallest in the DCIA perforators (1.55mm), but this was not statistically significant across all three groups, $p=0.38$ (Kruskall-Wallis). Comparison between medial and lateral perforator external diameters was not statistically significant, $p=0.18$ (Mann-Whitney).

4.1.2 Assessment of Perforator Vascular Territories (Perforasome)

Perforator vascular territories areas (perforasomes) were compared between medial row and lateral row perforators shown in the table below. The perforasome areas were comparable between the three groups (medial, lateral and DCIA), p=0.5 (Kruskall-Wallis Test). Paired comparisons did not show any differences between the perforator type and perforasome area.

Table 4.1: Comparison of vascular territories of individual perforators (perforasomes) between medial row, lateral row and DCIA perforators in a hemi-abdominal flap.

	Mean Perforasome Area cm^2(SD)	Median Perforasome Area cm^2 (IQR)	Perforasome cm^2 Min, Max
Medial	210.56(72.4)	206.29(146.57-276.52)	95.31,324.45
Lateral	238.53 (101.10)	218.78(151.87-312.07)	97.6, 410.81
DCIA	195.65(146.79)	149.95(92.42-344.57)	73.59,409.11

Figure 4.1: Maximal Intensity Projection (MIP) images of two perforator injections of a lateral row (left) and medial row (right) perforator in the same flap analyzed using the Syngo® CT workplace (Siemens). Perforator injection areas (perforasomes) were superimposed onto one another and perforasome area, flap area and degree of overlap could be compared.

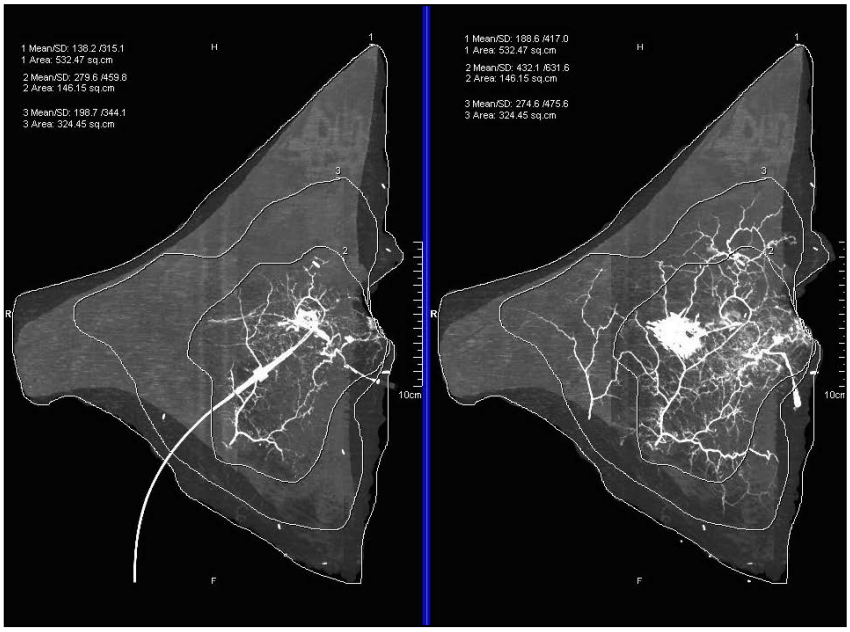

The largest perforators that would be suitable for DIEP reconstruction were selected in each hemi-abdomen. Of these there were 17 medial (53%) and 15 lateral (47%) row perforators. Direct comparison between medial and lateral row perforators demonstrated that the total perforasome area in squared centimetres was 206.3cm^2 (IQR=113-276.5) and 218.8cm2 (IQR=106.8-312.1) respectively, p=0.52 (Mann-Whitney). The percentage area of the perforasome to the total hemi-abdominal area between medial and lateral perforator were also comparable with average coverage of 42.4% and 47.4% respectively, p=0.4 (Mann-Whitney). Caudal and cephalad extension of medial and lateral row perforators in the hemi-abdominal flap from the umbilicus were comparable (p>0.05, Mann-Whitney-U), however lateral row perforators did demonstrate greater lateral extension towards the anterior superior iliac spine (ASIS) (lateral perfusion), which was statistically significant, p<0.01 (Mann-Whitney). The median percentage overlap of the medial and lateral perforasomes was 43%.

Figure 4.2 Graph to show comparison of perforasome area as a percentage of the total hemi-abdominal flap area in medial (M) and lateral row (L) DIEA perforators.

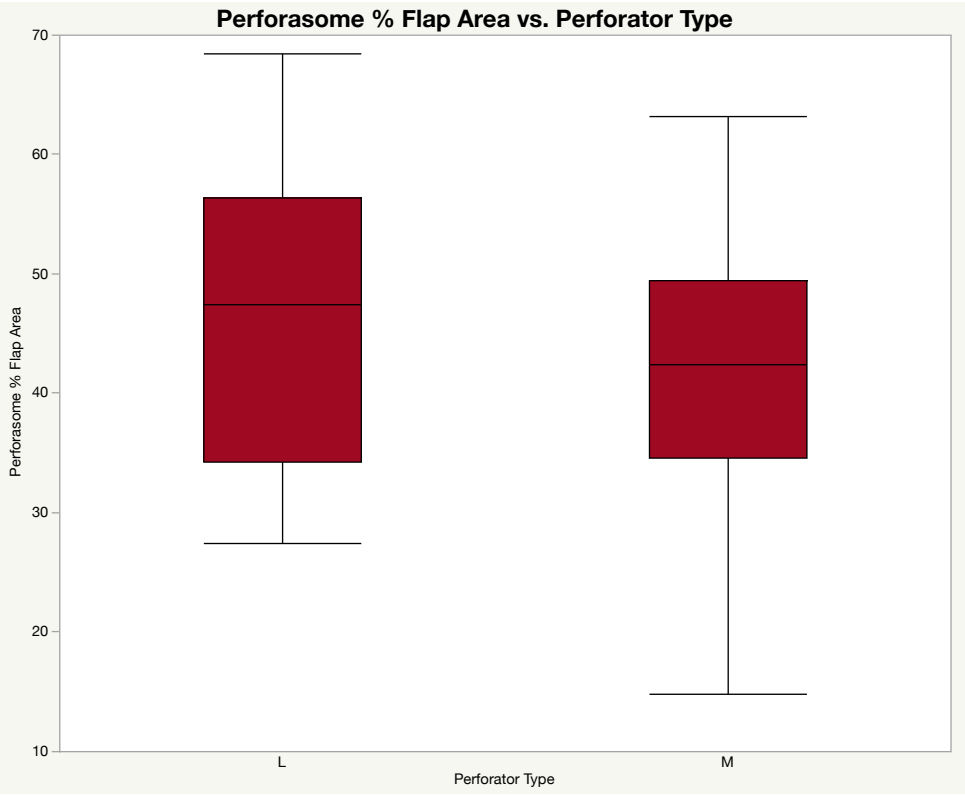

An assessment of the vascularity following perforator injection was then assessed for each hemi-abdominal flap. Comparison of medial and lateral row perforators demonstrated comparable volumes of tissue perfused in the hemi-abdominal flap, $p>0.05$ (Mann-Whitney-U).

Examination of perforators within the 5cm hot spot, demonstrated a median perfusion area of 206.29cm^2 versus 240.9cm^2 in those outside this radius, which was not statistically significant, $p=0.36$ (Mann-Whitney-U). The overall percentage area of the flap covered by perforators within the hot spot versus the cold spot was comparable in both groups, with a median value of 42% and 49% in hot spot and cold spot respectively, $p=0.23$ (Mann-Whitney-U). The extent of the cephalad and caudal perfusion were also comparable with no significant differences, $p>0.05$ (Mann-Whitney-U). Perforators outside the 5cm zone from the umbilicus demonstrated significantly greater lateral perfusion towards the ASIS, $p=0.03$ (Mann-Whitney-U). Assessment of volume of the perforasome within the hemi-abdominal flap between those perforators within 5cm of the umbilicus and those outside this radius were comparable, $p=0.43$ (Mann-Whitney-U).

A simple linear regression was used to evaluate the correlation of the external diameter of a perforator (mm) with the overall perforasome area (cm^2) that demonstrated there was a slight positive correlation ($R=0.30$), however there was insufficient evidence that this relationship was statistically significant, $p=0.17$. Similarly, external diameter of the perforator did not show any significant correlation with perforasome volume, cephalad, caudal or degree of lateral perfusion, $p>0.05$. There was no relationship between the external diameter and total number of perforators in the hemi-abdomen, $p>0.05$.

The relationship of body habitus using body mass index (BMI, kg/m^2) on perforator anatomy and perfusion territories of individual perforators was then evaluated. Using a simple linear regression model there was no correlation seen between increasing BMI and the external diameter of DIEA perforators of the anterior abdominal wall. However, there was strong evidence of a positive linear association ($R=0.48$) between increased BMI and the total number of significant perforators in the hemi-abdomen (>0.5mm), $p<0.01$.

Figure 4.3: Graph to illustrate correlation between body mass index (BMI, kg/m^2) and total number of DIEA perforators of the anterior hemi-abdomen and line of best fit

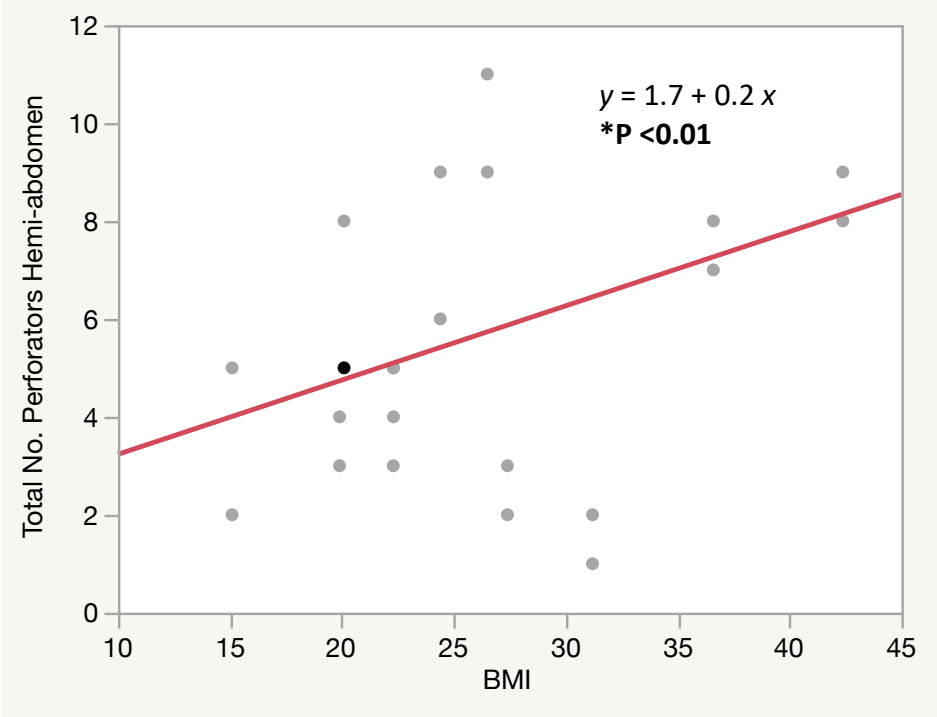

Simple linear regression model was used to assess the relationship of body mass index (BMI, kg/m^2) with the average perforasome area (cm^2) which demonstrated a positive correlation that was statistically significant, p<0.01. Interestingly when the medial versus lateral row DIEA perforators were compared separately for the correlation of increasing BMI on overall perforasome area, lateral row perforators demonstrated a stronger positive linear relationship (R=0.70) between perforasome area and increasing BMI, p<0.01, but this effect was not seen in medial row perforators, p=0.27. When evaluating whether perfusion territory was affected in a cephalad, caudal, or lateral direction with increasing BMI, there were no significant correlations overall, or when lateral and medial row perforators were compared separately, p>0.05.

4.1.3 Assessment of Linking Vessels on Perforator Territories

3D CTA reconstruction were reviewed and capture of specific linking vessels including lateral linking vessels, inter-row and intra-row linking vessels were recorded (Yes/No) from the injected perforator. Lateral linking vessels were dominant linking vessels in the integument that coursed laterally towards the mid-axial line. These vessels may link directly with adjacent source artery territories (e.g. DCIA, SIEA, intercostal artery perforators). The capture and presence of dominant (single large) lateral linking vessels were associated with an increased perforasome area, with an average perforasome area of 272cm^2 (IQR=204.3-333.6) versus 176.8cm^2 (IQR=121.3-264.9), $p<0.01$ (Mann-Whitney-U). This was also associated with a higher relative perfusion of the hemi-abdominal flap when lateral linking vessels were captured (median 51%) following perforator injection compared to when not captured (median 37.6%), that was statistically significant, $p<0.01$ (Mann-Whitney-U). Capture of lateral linking vessels was associated with greater lateral perfusion ($p<0.01$), but did not demonstrate any statistical significance on evaluation of caudal or cephalad perfusion. Lateral row perforators demonstrated a greater associated with capture of lateral linking vessels compared to medial row DIEA perforators that was statistically significant, $p<0.01$ (Chi-squared).

When medial and lateral row perforators were compared, among lateral row perforators the presence of lateral linking vessels was associated with a larger perforasome area that was statistically significant, $p=0.02$ (Mann-Whitney-U); In contrast, among medial row perforators, there was a greater degree of variation in the perforasome areas and although the average perforasome area was greater when lateral linking vessels (median=240.9, IQR=217.7-324.5) were captured, the results were comparable to when the linking vessels were not captured (median=184.1, IQR=131.9-273.8), $p=0.19$.

Figure 4.4: 3D maximal intensity projection (MIP) images of a right hemi-abdominal flap and comparison of a medial and lateral row perforator injection studies; Orange arrows demonstrate capture of dominant linking vessel that courses through the integument.

(ASIS= Anterior Superior Iliac Spine)

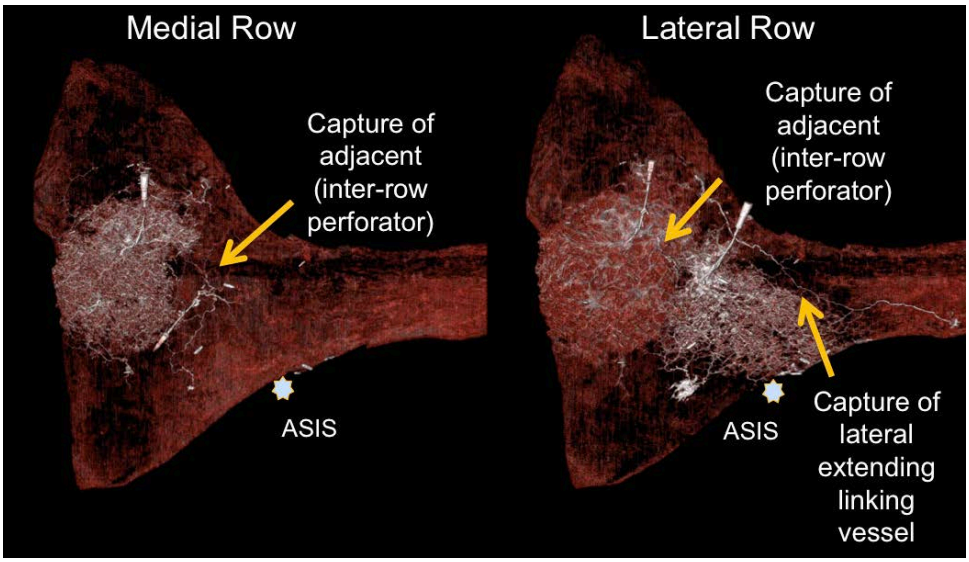

Figure 4.5: 3D Maximal Intensity Projection (MIP) images of a left hemi-abdominal flap and comparison of medial and lateral row DIEA injection studies highlighting how linking vessels course through the integument and overlap with potential adjacent source artery territories of the DCIA and SIEA. (*DCIA=Deep circumflex iliac artery; SIEA=superficial inferior epigastric artery; SCIA superficial circumflex iliac artery)*.

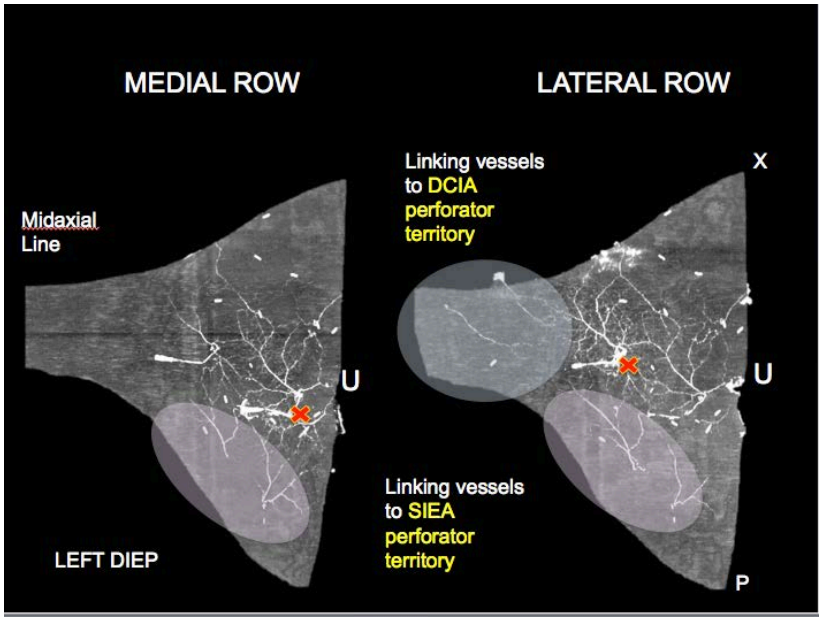

The presence and capture of inter-row and intra-row linking vessels was identified in 91% and 84% of the injected perforators respectively. Further assessment of capture of inter-row and intra-row linking vessels, did not demonstrate a difference among medial and lateral row perforators groups, $p>0.05$ (Chi-squared). Presence of inter-row linking vessels from the injected perforator did not contribute to an increased perforasome area, (median 154.9cm^2 when present versus 135cm^2 when not present), $p=1.0$ (Mann-Whitney). The capture of intra-row perforators did not demonstrate a difference in perforasome area, representing a median perforasome area of 206.3cm^2 (IQR=146.2-365) versus 282.9cm^2 (IQR=187.8-310.7) with presence of dominant intra-row and no intra-row linking vessels respectively, $p=0.29$ (Mann-Whitney-U).

When evaluating the direction of perfusion, the capture of dominant intra-row perforators from the injected perforator was associated with a greater extension of caudal perfusion towards the, $p<0.01$ (Mann-Whitney-U). The dominant linking vessels (inter-row, intra-row, and lateral) or combination of these linking vessels captured was evaluated. The most significant differences were found between “combinations of inter-row, intra-row and lateral” versus “intra-row” only linking vessels, $p=0.05$; “lateral” only versus “intra-row and inter-row”, $p=0.03$, and “combination of inter-row, intra-row and lateral” versus “intra-row and inter-row”, $p=0.05$.

Figure 4.6: Graph to show median and interquartile ranges of perforasome area (cm^2) between different combination of dominant linking vessels (inter-row, intra-row and lateral) captured following DIEA perforator injection.

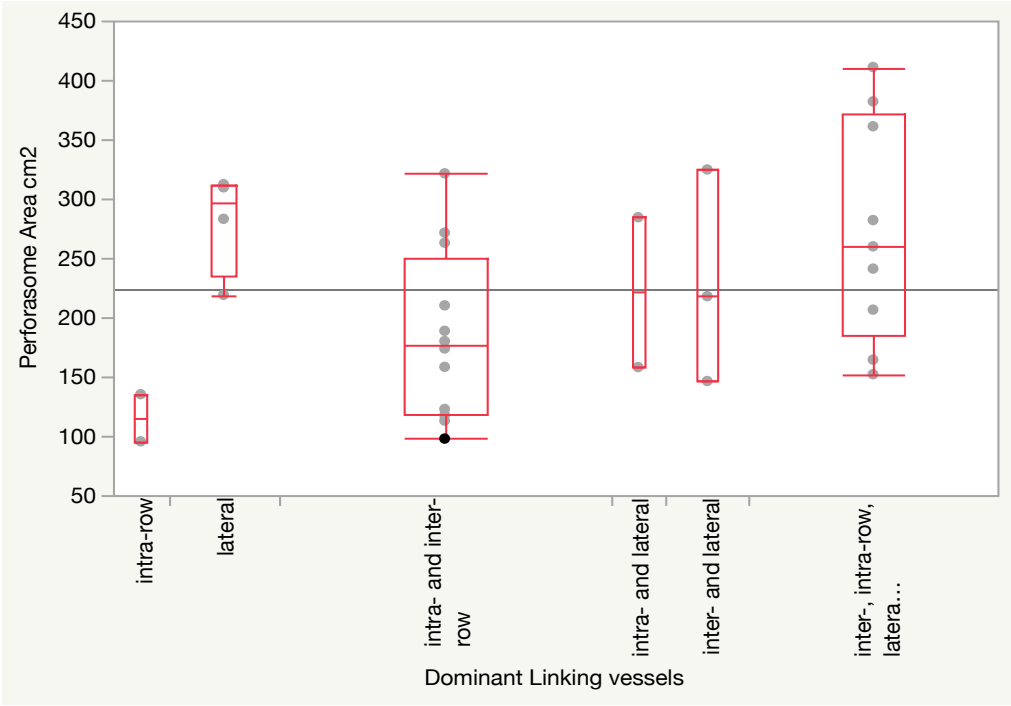

4.1.4 Qualitative analysis of dominant axiality of flow within the perforasome

Axiality of flow, or in other words the dominant direction(s) of distribution of the vascular territory following injection of an individual perforator was assessed on 3D CT imaging qualitatively. The capture of intra-row linking vessels was associated with a significant difference in the axiality of dominant vascular territory distribution of an individual perforasome (bi-directional, medial, or lateral), p=0.02 (Chi-squared) with the greater proportion of bi-directional distribution from the perforator when intra-row perforators were captured. This pattern of perforasome distribution was also seen with on capture of inter-row linking vessel, p<0.01 (Chi-squared), thus when inter-row perforators were captured there was a greater proportion with bi-directional flow. Comparison of axiality of perforasome distribution between medial and lateral row perforators showed a greater

degree of bi-directional (medial and lateral) distribution of the vascular territory in medial perforators compared to a greater degree of lateral based distribution of the vascular territory in lateral perforators, p<0.01 (Fisher's Exact Test). Similarly, a greater degree of bi-directional flow was seen among perforators found within 3cm of the umbilicus compared to outside this radius, p=0.04 (Fisher's Exact Test).

When assessing the perforasome distribution in reference to dominant axiality of flow (bi-directional, medial and lateral) and impact on overall perforasome area, there was no significant differences across all three groups, p=0.08. However, the average perforasome area of bi-directional (206.3cm^2) and lateral (239.2cm^2) was higher than medial axiality of flow (135cm^2) in hemi-abdominal flaps, with the most significant difference seen in the perforasome areas between perforators demonstrating lateral versus medial axiality of flow, p=0.04 (Kruskall-Wallis).

Figure 4.7: Graph to show impact of dominant axiality of flow / perforasome distribution on total perforasome area (cm^2)

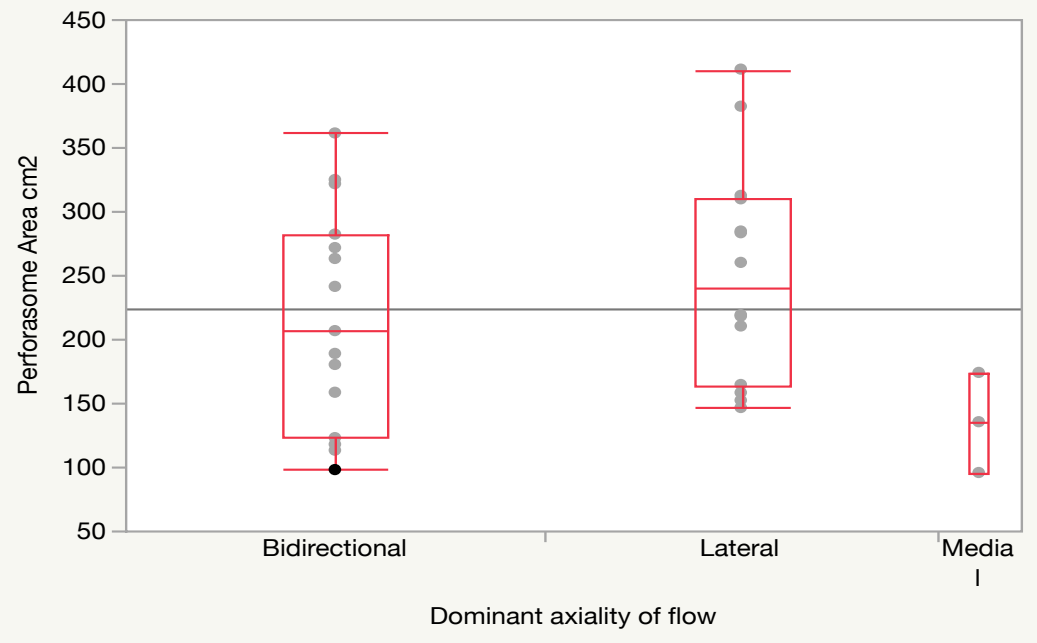

4.1.5 Qualitative analysis of 4-Dimensional perforator vascular territory

Dynamic qualitative assessment of injection of individual perforators was assessed in an axial and coronal plane (N=10 DIEP flap perforators). A 4D CTA was performed for each millilitre of contrast injected in an individual DIEA perforator up to a total of 3ml in the hemi-abdominal flap. The dominant linking vessels captured/perfused following the injection was usually identified following injection of the first 0.5ml of contrast and this was representative and predictive of the pattern of the overall perforasome distribution and area. This protocol was developed following the establishment of our standard injection technique, therefore resulted in a smaller sample size.

Evaluation of individual perforators within the hemi-abdominal flap identified different initial filling patterns based on timing on both coronal and axial planes, hence demonstrated the dynamics of flow. Capturing the speed of flow within microvascular linking vessels within the integument varied but did not demonstrate differences specific to medial or lateral row perforators. Figure 4.8 illustrates differences following injection of a medial row DIEA perforator in two different left hemi-abdominal flaps on coronal view. In contrast to an expected simple radial distribution in the vascular territory from the injected perforator within the flap, it was observed that early capture and filling of adjacent inter-row perforator, SIEA perforator territory, and intercostal perforators (to a lesser degree) via larger linking vessels contributed to rapid distribution of contrast over a wider area and larger overall perforasome.

Observation within the axial video capture revealed pattern of flow to the supra-Scarpa's layer and dermis, and presence of arborization of the perforator as it enters the integument, connections direct to large supra-Scarpa's linking vessels, or recurrent flow through an adjacent inter-row perforator (Figure 4.9A). The presence of these large direct linking vessels and patterns of recurrent flow accounted for rapid and broad early distribution of contrast within the hemi-abdominal flap microvasculature. This is in contrast to smaller direct linking vessels that run along the integument with multiple small contributions to the

dermis along its course (Figure 4.9B). The impact of these initial filling patterns may similarly impact overall perforasome distribution as seen in the examples Figures 4.8 and 4.9.

Figure 4.8: Two examples (A and B) of computed tomographic angiography coronal images captured from 4D scanning following initial 0.5ml injection of contrast into a medial row perforator in left hemi-abdominal flaps. Figures demonstrate initial distribution (left) and final perforasome distribution and area (right).

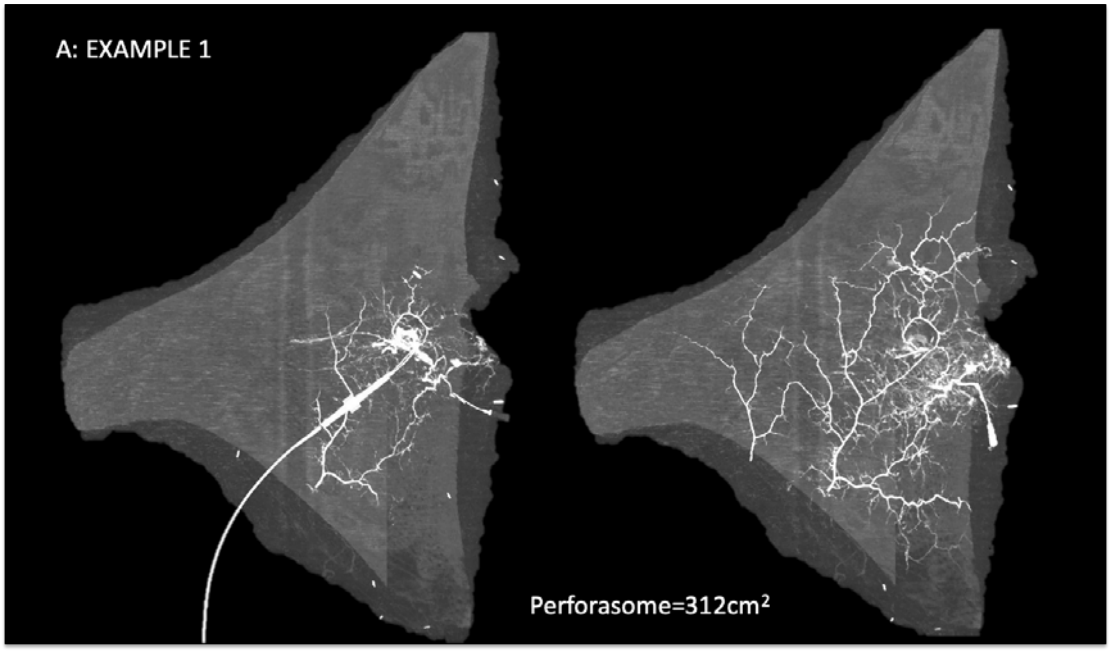

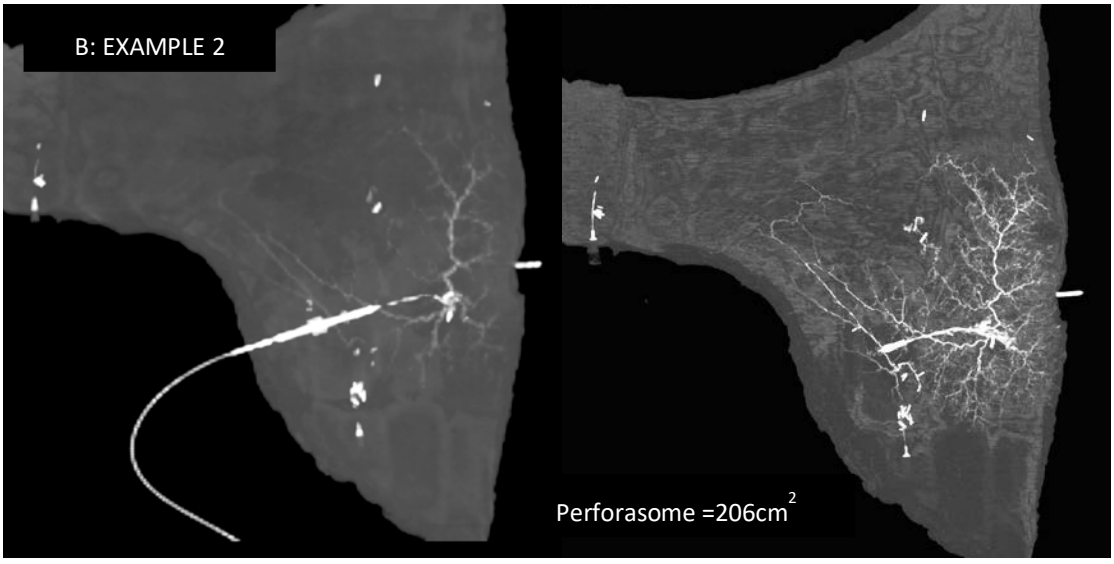

Figure 4.9: Two examples (A and B) of computed tomographic angiography axial images captured from 4D scanning following initial 0.5ml injection of contrast into a medial row perforator in left hemi-abdominal flaps. Figures demonstrate initial distribution (left) and final perforasome distribution and area (right). Initial direction of direct and recurrent flow and capture of principle linking vessels and filling patterns are shown (*red arrows*)

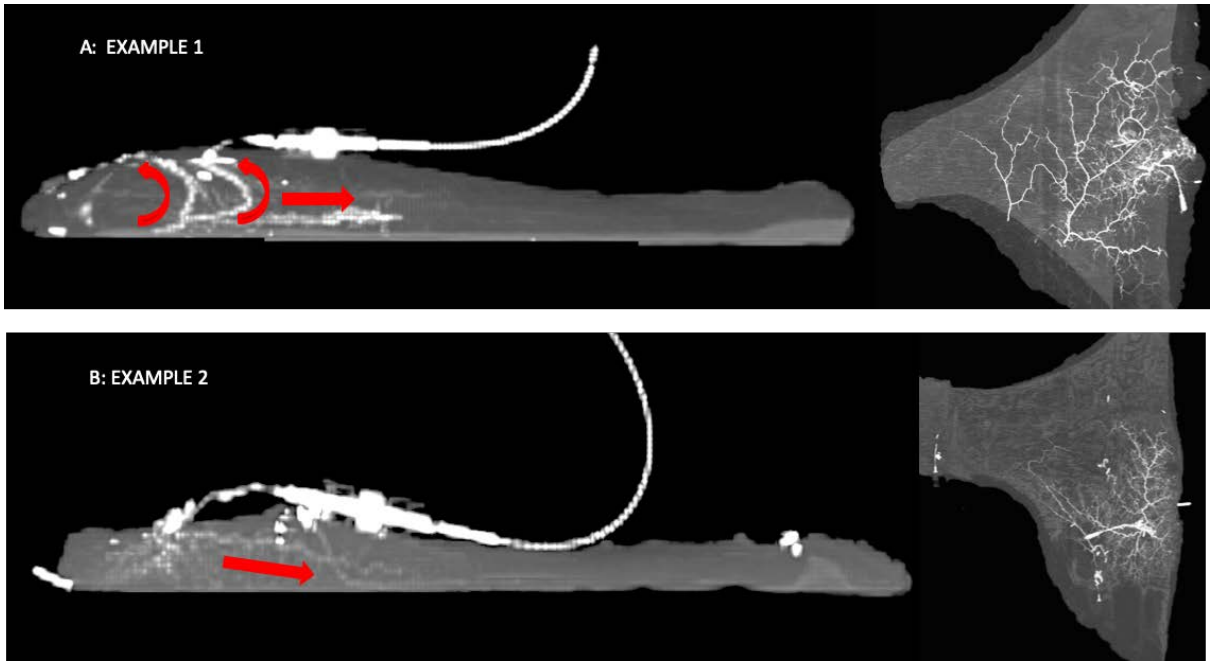

It was observed in this sample of hemi-abdominal flaps that arborisation in the sub-Scarpa's layer from the injected perforator and direct connection with adjacent perforators or a large supra-Scarpa's linking vessel accounted for rapid distribution to boarder areas of the hemi-abdominal flap. This was in contrast to presence of only smaller calibre linking vessels coursing through the integument, or absence of large branching patterns in the sub-Scarpa's layer (Figure 4.10). The absence of larger calibre direct communication with adjacent DIEA perforator territory or SIEA territory, resulted in more radial and slower filling patterns within the integument of the flap. Larger calibre communicating vessels observed travelling predominantly in the supra-Scarpa's or subdermal level was associated with an early broad distribution within the vascular territory. Lateral or oblique larger calibre orientated

communicating vessels, in particular capture of the SIEA territory, was associated with greater degree and more rapid lateral perfusion of the hemi-abdominal flap and broader overall perfusion territory, regardless of perforator row.

Figure 4.10: Example of computed tomographic angiography coronal (top image) and axial (bottom image) screenshots captured from 4D scanning following initial 1ml injection of contrast into a medial row perforator in a right hemi-abdominal flap. Dominant direction of flow and filling distributions shown (*red arrows*).

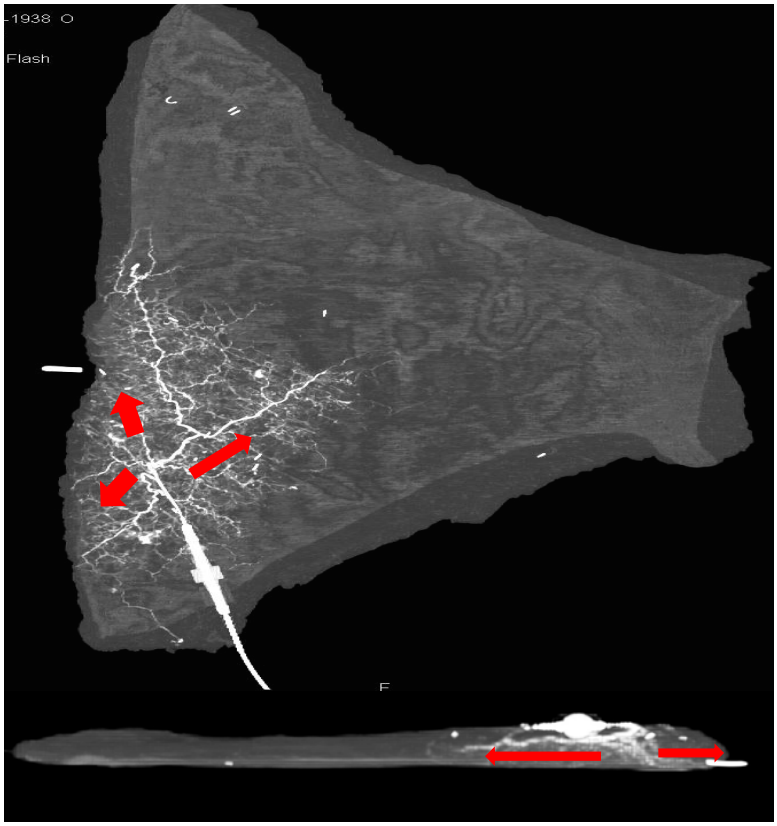

4.2: Clinical Study to Evaluate of Anatomy and Dynamic DIEA Perfusion Territories (Perforasomes) of Hemi-DIEP Flaps in Breast Reconstruction

4.2.1 Patient Population

A total of 98 consecutive women underwent a bilateral DIEP/MSTRAM breast reconstruction between January 2014 and June 2016 performed by a senior surgeon (M.SC)[a] at the Mayo Clinic, Rochester, MN. Data analysis was performed by an independent reviewer (CC)[b] using a protocol that was established to optimize data capture for image analysis and implemented. A total of 44 consecutive flaps were subsequently included in the study following optimization of the data capture protocol. Of these cases, 6 flaps did not have a preoperative CT for evaluation of perforators to compare to the LA-ICGFA imaging.

A total of 38 flaps remained for both CTA and LA-ICGFA analysis, two flaps were converted to MS-TRAM flaps and three flaps were raised with two perforators (1 MSTRAM, 2 DIEPs) while the remaining were all single dominant DIEP free flaps for breast reconstruction (N=34 flaps), using the largest perforator in hemi-abdomen. A medial row perforator was used for the harvest of single perforator hemi-DIEP in 30 flaps (88%) compared to use of a lateral row in 4 flaps (12%). When two perforators were included within the flap (N=3) these all incorporated two perforators from the medial row. Both MSTRAM flaps were harvested on medial row perforators. The average BMI of the women was 29 (IQR=26-32). Average abdominal thickness at the level of the umbilicus was 35mm (IQR=28-41). The mean flap weight was 633g (IQR=542-807).

[a] M.S-C = Michel Saint-Cyr; Consultant Plastic Surgery, Mayo Clinic and Clinical Supervisor of PhD. Dr. Saint-Cyr performed all operations and data acquisition on SPY Elite System ®, and assisted in categorization of SPY perfusion patterns.

[b] CC= Dr. Cheng Chen was an independent and blinded reviewer to assess image quality, and post-processing analysis; He was a developer of the SPY-Qc® software.

4.2.2 Evaluation of Preoperative Computed Tomographic Angiography

A total of 38 hemi-abdominal flaps had available preoperative CT for assessment. The dominant perforator reported on CT was identified at an median of 20mm below the umbilicus (IQR 0-34mm), and 25mm lateral to the umbilicus (IQR 15.7-35mm). 92.1% (N=35 flaps) of dominant perforators within the hemi-abdomens were found within 5cm of the umbilicus and in 55.2% (N=21 flaps) the dominant perforator was found within 3cm of the umbilicus. The origin of the dominant perforator arose from the medial row of the deep inferior epigastric artery in 78.9% of cases (N=30 flaps) and the lateral row in 18.4% (N=7 flaps) and in one hemi-abdomen there was no dominant perforator. Of the medial row dominant perforators, 29% of these were paraumbilical.

The mean perforator size was 2mm (IQR=1.8-3). Looking at density of perforators within an entire hemi-abdomen (from the xiphoid, pubic ramus and laterally towards the ASIS), 52.8% (N=19 flaps) had a moderate density (presence of 3-5 perforators); 44.4% (N=16 flaps) had multiple perforators (presence of greater than 5 perforators), and 1 flap had less than 3 perforators in the hemi-abdomen. A single dominant perforator was present in 63% of hemi-abdomens. When present, the dominant perforator was included in the flap in 95% cases, and the origin of the dominant perforator was the medial row in 82% cases. Using simple linear regression there was no significant correlation between perforator size and abdominal thickness (p=0.88), BMI (p=0.58) or number of perforators in the hemi-abdomen (p=1.0). Interestingly there was no correlation between the number of perforators in the hemi-abdomen and BMI (R= -0.2, p=0.23).

4.2.3 Analysis of Hemi-DIEP perforasome with Laser Assisted Indocyanine Green Fluorescence Angiography

Forty-five hemi-DIEP flap cases were available for analysis using SPY-Qc ® software that captured all three angiographic phases of perfusion (arterial, microvascular and venous circulation).

Figure 4.11: Illustration of the three angiographic phases captures on SPY Elite System® (Novadaq Technologies, Inc.), Image provided by Dr. C Chen and TB Ferguson with permissions.

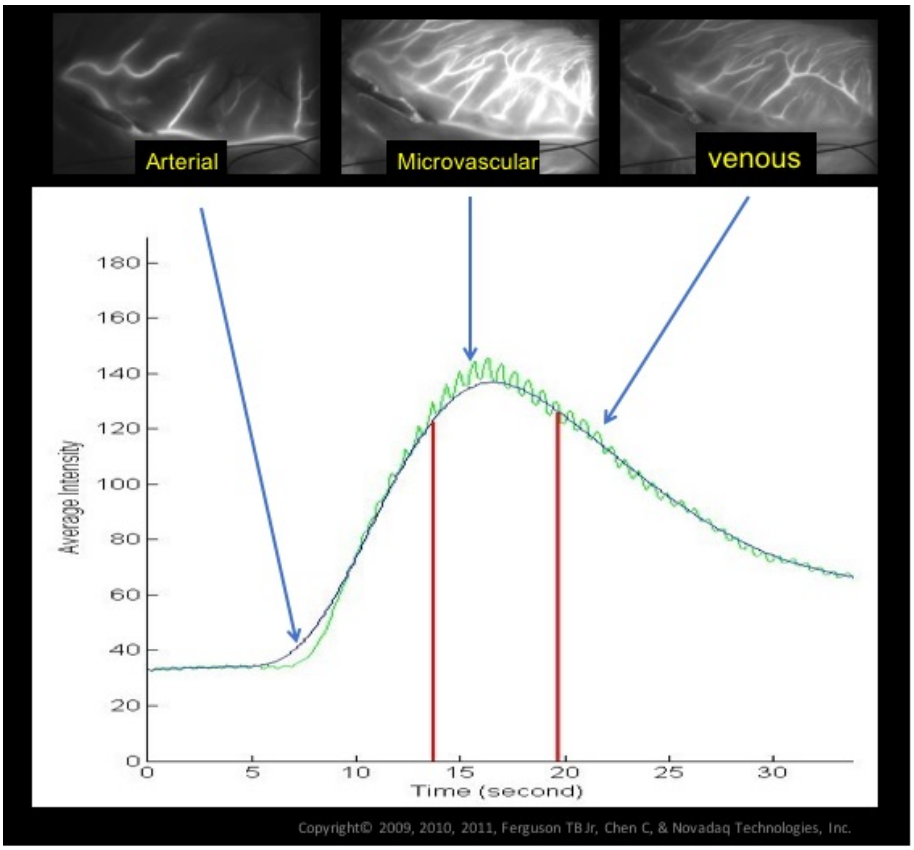

Timing and intensity maps over time were created capturing the ingress, peak concentration of inflow, and egress of the contrast agent into the flap. The region of interest (ROI) included the boundaries of the flap. Maps provided a global quantitative analysis by capturing measurements simultaneously within every pixel of the image captured, and then summated over the entire arterial and microvascular phases of blood flow using the SPY-Qc ® software for analysis (CC)[5]. The relative perfusion within the ROI was determined using the perforator location representing the primary value for comparison (100%).

[5] CC= Cheng Chen

Qualitative analysis of the timing maps captured (ATM[6], M.S-C[7]), that represented the overall rate of inflow into all regions of the DIEP flap, highlighted unique patterns of inflow, and this was apparent even on comparison of only single medial row perforator flaps. Patterns of perfusion were subsequently categorized into three broad patterns based on observed "hot spots" of perfusion and blood flow into the dermis and superficial fat in hemi-DIEP flaps harvested on a single dominant perforator (N=34 flaps): single (N=4 flaps), co-dominance (N=11 flaps) and diffuse (N=19 flaps). Perfusion assessment was made with the flap fully harvested, but remaining in-situ, just prior to transfer to the chest wall. This allows for the flaps to recover from arterial spasm and acclimatise following isolation of the pedicle. The "single" pattern of perfusion described a more concentric pattern of blood flow from the perforator into the remaining portion of the flap (Figure 4.12). The "co-dominant" pattern represented the presence of two hot spots on the timing map, and rapid simultaneous flow into a perforator and possibly adjacent perforator. Finally, the "diffuse" pattern had multiple hot spots across the flap, demonstrating simultaneous rapid inflow likely into adjacent perforating vessels linked to the primary perforator. The flaps converted to MS-TRAM (N=2 flaps) both expressed a diffused pattern of perfusion. Two hemi-DIEP flaps were raised on two medial row perforators that demonstrated a co-dominant pattern of perfusion (N=1 flap) and diffuse perfusion (N=1 flap).

Figure 4.12: Three broad categories of perfusion of single dominant hemi-DIEP flaps illustrated on review of timing maps captured using LA-ICGFA using the SPY Elite System ® (Novadaq Technologies, Inc): Single (*right*), Co-dominance (*centre),* and Diffuse (*left*).

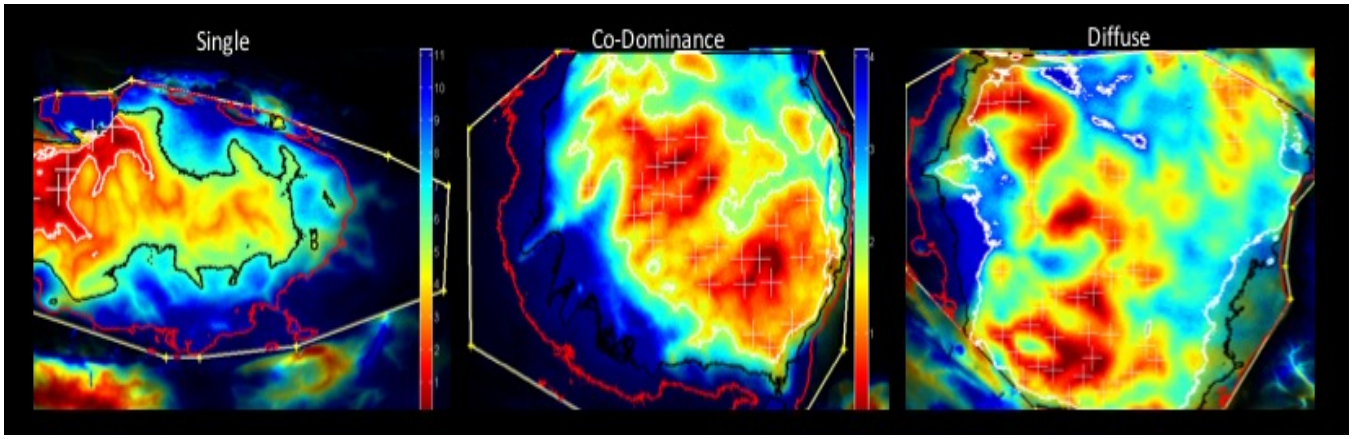

The presence of a single dominant (largest) perforator on preoperative CTA and number of perforators in the hemi-abdomen were comparable in all three perfusion pattern categories ($p>0.05$, Kruskall-Wallis). The three categories of perfusion patterns observed were then compared using both intensity and timing maps to evaluate the flap areas representative of three perfusion thresholds: >25%, >50% and >75% relative to the reference value of the perforator location (Figure 4.13). Comparison of the intensity perfusion maps of the three patterns seen in single dominant hemi-DIEP flaps demonstrated a significant difference in flap areas that were perfused greater than the 25% threshold, with the greatest flap area represented by the diffuse pattern, $p <0.01$ (Kruskall-Wallis). Similarly, comparison of timing maps demonstrated a significant difference between the three groups on evaluation of flap areas perfused greater than the 25% threshold, $p <0.01$ (Kruskall-Wallis): comparison of pairs showed that the diffuse pattern had the greatest flap area compared to single ($p=0.02$, Mann-Whitney) and co-dominant ($p<0.01$, Mann-Whitney) patterns. There were no significant differences seen in the three groups on review of flap areas with greater than 50% and greater than 75% perfusion thresholds ($p>0.05$, Kruskall-Wallis).

An evaluation of cephalad-caudal perfusion gradient across the hemi-DIEP flap on intensity maps showed that there was a significant difference between the three groups ($p=0.03$, Kruskall-Wallis). Comparison between the groups identified that there was a significant difference between the diffuse and single categories ($p=0.02$, Mann-Whitney), but comparable between the diffuse and co-dominant ($p=0.06$, Mann-Whitney), and between single and co-dominant patterns ($p=0.33$, Mann-Whitney). Similarly, upon evaluation of the cephalad-caudal axis in timing maps there was a significant difference between the three perfusion patterns ($p<0.01$, Kruskall-Wallis). This difference was attributed to the diffuse pattern with a greatest area of cephalad-caudal perfusion compared to the two other groups ($p=0.01$, Mann-Whitney), whereas comparison between the single and co-dominant groups were comparable ($p=0.15$, Mann-Whitney). The medial to lateral axis of perfusion in single perforator hemi-DIEPs also demonstrated no significant difference across all three groups in intensity and timing maps ($p=0.33$ and $p=0.07$ respectively, Kruskall-Wallis). These results are summarized in Table 4.2.

Figure 4.13: An example of imaging captured on LA-ICGFA and analysis using SPYQc ® software (Novadaq Technologies, Inc) reproducing intensity map (left) and timing map (right). Cephalad-caudal and medial-lateral gradients of perfusion were assessed on each axis of the map and area under the curve represents area across the flap and marked to show area than is >75% relative to the reference value. Bottom left recorded areas of perfusion that were >75%, >50% and >25% of perfusion relative to the reference value. *Image analysis was provided by Dr C Chen and Dr. TB Ferguson.*

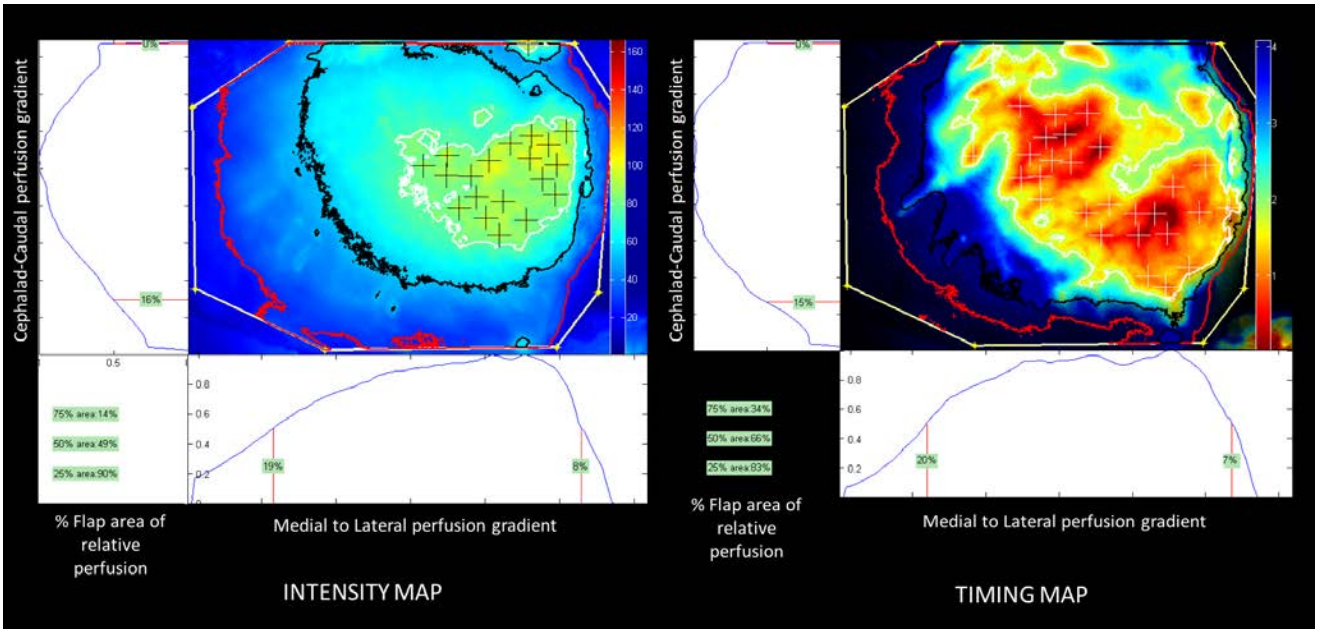

Table 4.2: Table to summarize the perfusion limits and areas on LA-ICGFA as analysed by SPY-Qc ® (Novadaq Technologies, Inc).

	Single Median (IQR) % ROI	**Co-Dominant** Median (IQR) %ROI	**Diffuse** Median (IQR) %ROI	**P-value between groups**[a]
INTENSITY MAPS				
Area of ROI >25% perfusion	73.5 (56-74)	71 (51-90)	91 (89-96)	**<0.01***
Area of ROI >50% perfusion	33.5 (28-43)	26 (12-31)	47 (29-52)	0.13
Area of ROI >75% perfusion	3 (2-8)	2 (0-10)	4 (0-8)	0.86
Cephalad-Caudal Perfusion Gradient >75%	72.5 (63-89)	87 (72-98)	95 (87-100)	**0.02***
Medial-Lateral Perfusion Gradient >75%	70 (61-88)	67 (61-86)	80 (69-87)	0.33
TIMING MAPS				
Area of ROI >25% perfusion	58.5 (48-72)	62 (56-72)	84 (79-89)	**<0.01***
Area of ROI >50% perfusion	41.5 (28-54)	40 (25-49)	54 (39-71)	0.12
Area of ROI >75% perfusion	12 (6-19)	9 (4-24)	12 (6-36)	0.65
Cephalad-Caudal Perfusion Gradient >75%	64 (58-83)	83 (63-87)	93 (77-98)	**<0.01***
Medial-Lateral Perfusion Gradient >75%	63.5 (62-87)	68 (57-80)	77 (70-87)	0.07

a Kruskall Wallis Test

4.2.4 Analysis of Computed Tomographic Angiography and Hemi-DIEP perforasome with Laser Assisted Indocyanine Green Fluorescence Angiography

The dominant perforator as identified on preoperative CTA correlated clinically and included in the hemi-DIEP flaps in 36 out of 38 flaps (95%) of cases. A *single* dominant perforator was identified in the hemi-abdomen on preoperative CTA in 24 out of 38 cases (63%). On review of the single dominant hemi-DIEP flaps, there were no correlations between the number of perforators within the hemi-abdomen and the resultant perfusion areas at the three thresholds (>75%, 50% and 25%), the cephalad-caudal and medial-lateral axes.

4.2.4.1 Medial versus Lateral Row perforators

Analyses of the characteristics of the microvasculature on preoperative CTA based on the selected perforator for flap harvest, and final flap perfusions analysis on SPY-QC® were then subsequently performed. Single dominant hemi-DIEP flaps were included for direct comparison (N=34 flaps). Perforator origin (medial versus lateral row) in these hemi-DIEP flaps had comparable perfusion patterns as (single, co-dominant, diffuse) observed on LA-ICGFA (p=0.86, Fisher's Exact Test). The area of perfusion on both intensity and timing maps were comparable between medial, paraumbilical and lateral row perforators in single dominant hemi-DIEP flaps at all three perfusion thresholds (>75%, >50% and >25%). Similarly, there were no differences in medial to lateral perfusion between the medial, paraumbilical and lateral row perforators in single dominant hemi-DIEP flaps. Similarly, along cephalad-caudal axis, average perfusion was comparable between medial and paraumbilical perforators compared to lateral row perforators, with median areas (%) 90(IQR=78-96), 83 (IQR=75-89) and 68 (IQR=62-88) respectively, p=0.06 (Kruskall-Wallis).

4.2.4.2 Course and characteristics of the DIEA perforator

There were no appreciable differences between the distance of the intramuscular course and perfusion pattern (diffuse, co-dominant or single), areas of perfusion, cephalad-caudal and medial-lateral gradients of perfusion. A comparison of direct and indirect perforators

(multiple branches to muscle and branches at level of fascia prior to entry to the flap) were subsequently compared. From the analysis direct perforators, those with no branching along their route from the underlying source artery to the entry to the flap, were associated with a greater area of flap perfusion that was >75% threshold in both timing and intensity maps ($p=0.05$ and $p=0.03$, respectively). However, these more direct perforators did not influence the flap areas when reviewing areas of perfusion >50% and >25% thresholds ($p>0.05$).

The exit of the perforator from the fascia to supply the integument of the DIEP flap was then reviewed. The perforator was characterized to have a direct or oblique course as it exited the anterior rectus sheath, but there were no differences in perfusion patterns or perfusion gradients or flap areas perfused on SPY-Qc analysis between the two types, ($p>0.05$). Neither the length of the intramuscular course, direct or indirect perforator, nor the exit of the perforator from the fascia (direct or oblique) were associated with any differences in the SPY perfusion pattern (single, co-dominant, diffuse).

4.2.4.3 Branching patterns of the perforator in the Hemi-DIEP flap

On evaluation of the degree of branching in the subscarpa's level (none, minimal, moderate), there were no significant differences in the perfusion areas or perfusion gradients across the hemi-DIEP flaps, except on evaluation of perfusion on intensity maps, which demonstrated perforators with no branching in the subscarpa's had the greatest degree of perfusion (>75% relative to reference value) in the cephalad-caudal axis of the flap, $p=0.01$ (Kruskall-Wallis). On evaluation of the suprascarpa layer branching pattern, the presence of minimal versus multiple branching did not significantly impact the overall perfusion patterns (single, co-dominant, diffuse), $p=0.63$ (Fisher's Exact Test) nor perfusion areas and gradients as previously described on timing or intensity maps, $p>0.05$ (Mann-Whitney).

Semi-quantitative analysis of the microvasculature and density of vertical communicating vessels to the subdermal layer around the perforator (minimal, moderate or multiple) was

associated with a significant difference in SPY patterns (single, co-dominant, diffuse) p=0.02, but this parameter alone did not influence perfusion areas and gradients in hemi-DIEP flaps, p>0.05. Further categorization of the microvascular contribution to the subdermal plexus from the dominant perforator of the hemi-DIEP flap was then evaluated based on the characteristics of the pattern of distribution, which included: (1) via a dominant linking vessel in the suprascarpa's layer with small direct communications; (2) multiple fine direct communications; (3) direct from the perforator; (4) direct from the perforator in addition to a dominant linking vessel with direct communications, and (5) direct from the perforator in addition to multiple fine direct communications to the subdermal plexus. It has been shown that the subdermal plexus anatomically can influence overall perfusion based on previous cadaveric perfusion studies.(175) There is no standardized classification or approach for characterizing the subdermal contributions, but there was great variation, which is a notable limitation with this approach.

On analysis of perfusion areas on intensity and timing maps, only timing maps showed a significant difference in characterization of pattern of contributions to the subdermal plexus on the flap area perfused greater than the 25% threshold, p=0.01 (Kruskall-Wallis), Figure 4.14. The presence of a dominant linking vessel in the suprascarpal layer with small contributions, or a direct perforator with multiple contributions, resulted in larger areas of flap perfusion. Interestingly, the presence of direct communication by the perforator in addition to a dominant linking vessel (group 4) had a slightly lower average compared to the other groups, but only 2 flaps represented this category which may have influenced this result. Creating multiple groups may limit the analysis as there were fewer observations in some categories and this may have influenced our overall results, with a possible type I error. Notably there was variation in the patterns of microvasculature at the subdermal level and further work to validate and characterize these contributions is necessary.

Figure 4.14: Graph to demonstrate impact of contribution to dermal plexus on the area of flap perfusion above the 25% threshold relative to the perforator.

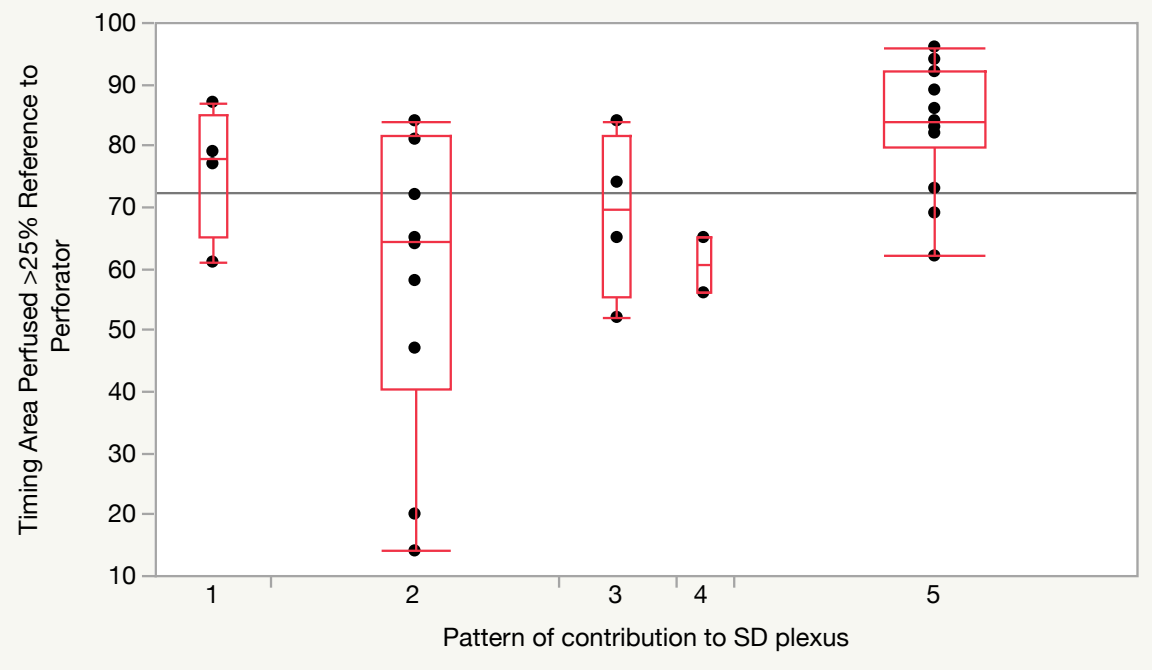

Pattern of contribution: (1) via a dominant linking vessel in the suprascarpa's layer with small direct communications; (2) multiple fine direct communications; (3) direct from the perforator; (4) direct from the perforator in addition to a dominant linking vessel with direct communications, and (5) direct from the perforator in addition to multiple fine direct communications to the subdermal plexus. (Comparison across all groups P=0.01, Kruskal-Wallis)

4.2.4.4 Presence of dominant linking vessels in the Hemi-DIEP flap

The presence of a large calibre dominant linking vessel in the subscarpa's layer and resulting perfusion pattern categorized on SPY-Qc® (single, co-dominant, diffuse) did not demonstrate any significant difference (p=0.51, Fisher's Exact Test). The presence of a dominant linking vessel in the subscarpa's layer did not statistically impact perfusion area on intensity maps of hemi-DIEPs compared to when no dominant linking vessel was present, median 90.5 (IQR=82-96) versus 82 (IQR=71-92), p=0.23 (Mann-Whitney). On timing maps,

however, that evaluates the ingress of blood flow into the hemi-DIEP flap, there was a higher average area of flap perfusion in the presence of a dominant linking vessel in the subscarpa layer (median=84%, IQR=70-94) versus no dominant linking vessel (median 73%, IQR=61-84), which was statistically significant, p=0.05 (Kruskall-Wallis).

Subsequent analysis of the presence of dominant linking vessel in the suprascarpa's layer was then performed. The presence of dominant linking vessel in this layer showed a difference in the category of SPY-Qc ® perfusion patterns of single dominant perforators (single, co-dominant, diffuse), which was statistically significant, p=0.01 (Fisher's Exact Test). The presence of a dominant linking vessel from the dominant perforator used in the hemi-DIEP flap resulted in a higher proportion of flaps with a diffuse pattern (60% flaps) and co-dominant patterns (23% of flaps). Using the same assessment as previously described for the subscarpa's layer, the presence of a dominant linking vessel in the suprascarpa's layer was associated with higher mean perfusion areas with >25% relative to the reference value on intensity maps (median 89.5%, IQR=74-94), compared to absence of dominant linking vessel (median 73%, IQR=41-77), that was statistically significant, p=0.02 (Mann-Whitney). Similarly, on assessment of timing maps the presence of a dominant linking vessel in the suprascarpa's layer had a significantly higher area of perfusion (median 81.5%, IQR=65-85) compared to absence of this linking vessel (median 52, IQR=29-70), p=0.01 (Mann-Whitney).

4.2.4.5 Characteristics of perforator anatomy, branching patterns and linking vessels on SPY perfusion patterns

A multivariate analysis was run to evaluate characteristics of the microvasculature assessed on preoperative CTA and resulting perfusion pattern as previously categorized on SPY-Qc® (single, co-dominant, diffuse) to assess which features may most likely determine the final perfusion pattern seen in single dominant perforator hemi-DIEP flaps. This analysis included branching patterns in the subscarpa's, branching in the suprascarpa's, presence of dominant linking vessel in the subscarpa's and suprascarpa's, presence of inter-row and intra-row

linking vessels, and density of vertical communicating vessels to the subdermal layer around perforator. This demonstrated that the difference in perfusion patterns was correlated with the presence of a dominant linking vessel in the suprascarpa's layer (p=0.02). This multivariate analysis was used to evaluate parameters that may contribute to the area of the flap with inflow >25% on timing perfusion maps, which also demonstrated a dominant linking vessel in the suprascarpa's layer as a significant factor on overall perfusion area, p=0.04.

The presence of inter-row linking vessels (yes/no) from the dominant perforator of single dominant hemi-DIEP flaps was shown to correlate with diffuse patterns (54% flaps) and co-dominant patterns (26% flaps) compared to single patterns (3% flaps), which was statistically significant (p=0.003, Fisher's Exact Test). However, comparison between diffuse and co-dominant patterns only did not demonstrate a significant difference between the two groups, p=0.23 (Fisher's Exact Test). The layers in which the inter-row linking vessels were found were mainly distributed in the suprascarpa's layer (77% flaps).

The presence of intra-row linking vessels on the perfusion pattern was then subsequently evaluated which showed a similar pattern whereby the presence of an intra-row linking vessels was seen in a higher proportion of single dominant perforator hemi-DIEP flaps with a diffuse pattern (57% flaps) and co-dominant pattern (26% flaps) compared to single pattern (11% flaps), however this did not reach statistical significance comparing all three groups, p=0.10 (Fisher's Exact Test). Comparison between the diffuse pattern and co-dominant pattern however, showed that diffuse pattern hemi-DIEP flaps had a higher proportion of intra-row linking vessels, p=0.05 (Fisher's Exact Test). Intra-row linking vessels were found predominantly in the suprascarpa's layer (88% flaps).

The density of vertical communicating vessels to the subdermal layer around the dominant perforator in a single perforator hemi-DIEP flap (categorized semi-quantitatively as minimal, moderate and multiple) demonstrated a significant difference between the three perfusion patterns categories, p=0.007 (Fisher's Exact Test). The diffuse pattern hemi-DIEP flaps were

associated with a significantly higher density of vertical communicating vessels to the subdermal layer.

Table 4.3 Summary of the different parameters analysed on preoperative CTA and categories of perfusion patterns defined on SPY-Qc® (single, co-dominant, diffuse).

PARAMETER EVALUATED	**Single N (%)**	**Co-Dominant N (%)**	**Diffuse N (%)**	**P-VALUE**
Presence of single dominant perforator in the hemi-abdomen *(Yes)*	3 (8%)	5 (13%)	16 (42%)	0.13
Density of perforators in the hemi-abdomen				0.57 [a]
Minimal (<3)	0	1 (3%)	0	
Moderate (3-5)	2 (6%)	6 (17%)	11 (31%)	
Multiple (>5)	2 (6%)	2 (8%)	11 (31%)	
Perforator course (direct/indirect)				1.0
Direct	2 (5%)	6 (16%)	12 (32%)	
Indirect	2 (5%)	5 (14%)	10 (27%)	
Presence of dominant linking vessel in subscarpa's layer *(Yes)*	0 (0%)	3 (8%)	5 (13%)	0.54 [a]
Presence of dominant linking vessel in suprascarpa's layer *(Yes)*	2 (5%)	9 (24%)	22 (58%)	**0.01*** [a]
Presence of an inter-row linking vessel *(Yes)*	1 (3%)	10 (26%)	21(55%)	**0.003*** [a]
Presence of an intra-row linking vessel *(Yes)*	4 (11%)	10 (26%)	22 (58%)	0.09
Density of vertical communicating vessels to the subdermal layer around the perforator				**0.02*** [a]
Minimal	2(6%)	2 (6%)	0 (0%)	
Moderate	1 (3%)	2 (6%)	1 (3%)	
Multiple	1 (3%)	5 (14%)	21 (60%)	

[a] Fisher's Exact Test

A qualitative analysis of the intraoperative videos of ICGFA captured, assessment of timing and perfusion maps and an individualized assessment of underlying perforator anatomy was then performed. Evaluation of the CTA followed evaluation of patterns previously described in Materials and Methods. In the first instance both the dynamic perforasome and the perforator microvascular anatomy was highly variable, even within the same individual.

In single perfusion patterns, video analysis of the ICGFA observed a centralized area of initial perfusion following by diffusion of this region over the area of the flap in a more uniform manner. Blood flow to other areas of the flap was predominantly achieved via the subdermal plexus and recurrent flow to adjacent perforators via the subdermal plexus. An oblique orientation of the principle perforator through the integument or of one of its early branches of comparable calibre (subscarpal branching), may lateralize the perfusion seen even of a medial dominant row perforator. In these grouped patterns of flaps, perfusion is dominated by the subdermal plexus, therefore the supply of contributions to the subdermal plexus then plays a potential role in broadening the zone of higher perfusion of the flap. Communication with the SIEA territory as in the example below (Figure 4.15), seen via a longitudinal linking vessel, allow for rapid distribution of blood flow, even in a centralized pattern dynamic perforasome. These results correlated with findings and results from the cadaveric anatomical studies carried out on hemi-abdominal flaps.

Figure 4.15: Example of imaging technologies used to evaluate a right hemi-DIEP flap and assessment of preoperative perforator anatomy (A) axial slice of preoperative DIEP CTA scan demonstrating a single medial dominant row perforator with minimal lateral linking vessels and minimal branching, however an oblique orientation of one of the subscarpa's branches; (B) sagittal image of direct longitudinal connection with the territory of the SIEA territory within the superficial scarpa's layer; (C-E) Video capture of LA-ICGFA at 6 seconds, 12 seconds and 18 seconds (reaching peak of arterial phase); (F) Timing map during the arterial and microvascular phases demonstrating lateralized dominant perfusion of a single medial row perforator hemi-DIEP and centralized hot spot "single pattern"

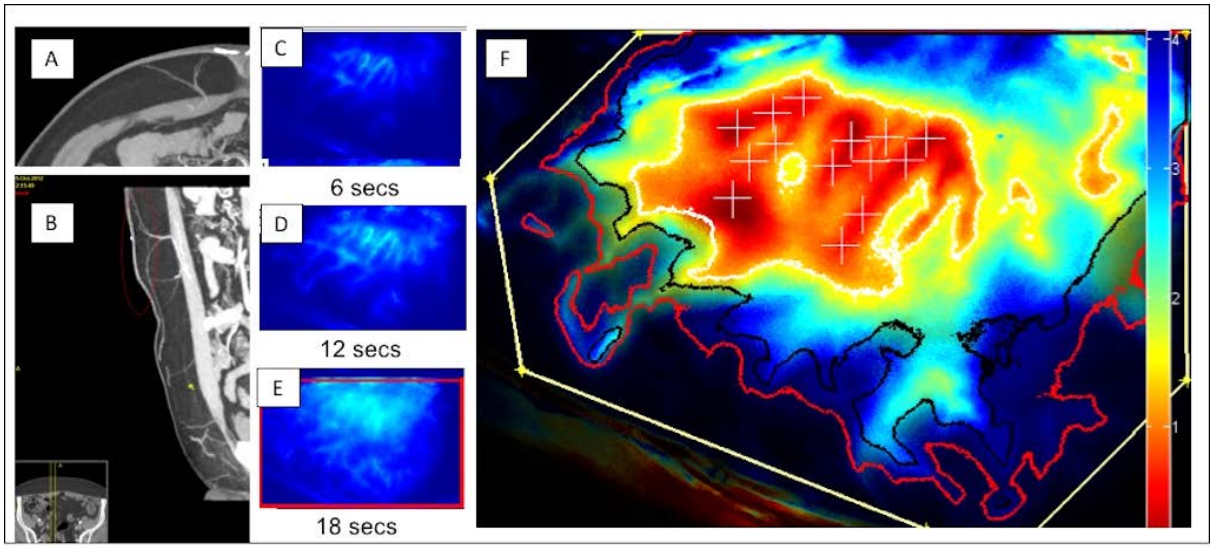

In co-dominant and diffuse patterns, it was hypothesized that hot spots seen on timing maps would indicate higher presence of true anastomosis or dominant linking vessels allowing rapid blood flow through different areas of the flap. Orange and yellow regions may represent a higher degree of contributions to the dermal plexus via a dominant linking vessel or fine contributions to the subdermal plexus, and sometimes a dominant linking vessel within the subdermal plexus. Recurrent flow to adjacent perforators allows distribution of the flow throughout the flap, including linking to the superficial SIEA territory. The difference in these two perfusion patterns on timing maps was related to the presence of two dominant or multiple hot spots, indicating that there is rapid flow into multiple areas of the flap via direct communicating vessels. Perfusion in these flaps was not

primarily dependent on the subdermal plexus. However, on review of the preoperative CTA scan there was a high variability in the presence and patterns of contribution to the subdermal plexus.

The dominant perforator from the flap may directly perfuse the subdermis with either multiple communicating fine branches or a dominant communicating vessel in addition to multiple fine branches. Recurrent flow into adjacent perforators, that was also seen in the anatomical studies, may show more rapid distribution when there is a presence of additional communicating vessel from the dominant perforator to the adjacent network. In other cases, a dominant linking vessel may arise from the dominant perforator and either perfuse the subdermis directly with multiple communications, or join a network of communicating vessels including the superficial system, and often was associated with broader, lateral perfusion of the hemi-DIEP.

The mapping of both intensity and perfusion varied. The intensity maps demonstrated more concentric patterns of perfusion in the flap. However, the timing maps qualitatively represented ingress into the flap and more accurate at depicting perforator hot spots, or the location of true or choke (direct or indirect) linking vessels within the hemi-DIEP integument.

Figure 4.16: Example of imaging technologies used to evaluate a right hemi-DIEP flap and assessment of preoperative perforator anatomy (A) axial slice of preoperative DIEP CTA scan demonstrating a single medial dominant row perforator with large bifurcation at the level of the Scarpa's fascia with an oblique orientation of one of the subscarpa's branches that continues laterally (*green arrow*) with multiple contributions to the subdermal plexus (*orange arrows)* (B) axial magnified image of direct branch from the dominant perforator and connection to the lateral adjacent perforator at the level of the subdermal plexus; (C) Timing map capturing the arterial and microvascular phases demonstrating two initial dominant hot spots of perfusion of a single medial row perforator hemi-DIEP in a "co-dominant pattern", and (D) Video capture of LA-ICGFA at 5 seconds, 10 seconds and 15 seconds (reaching peak of arterial phase).

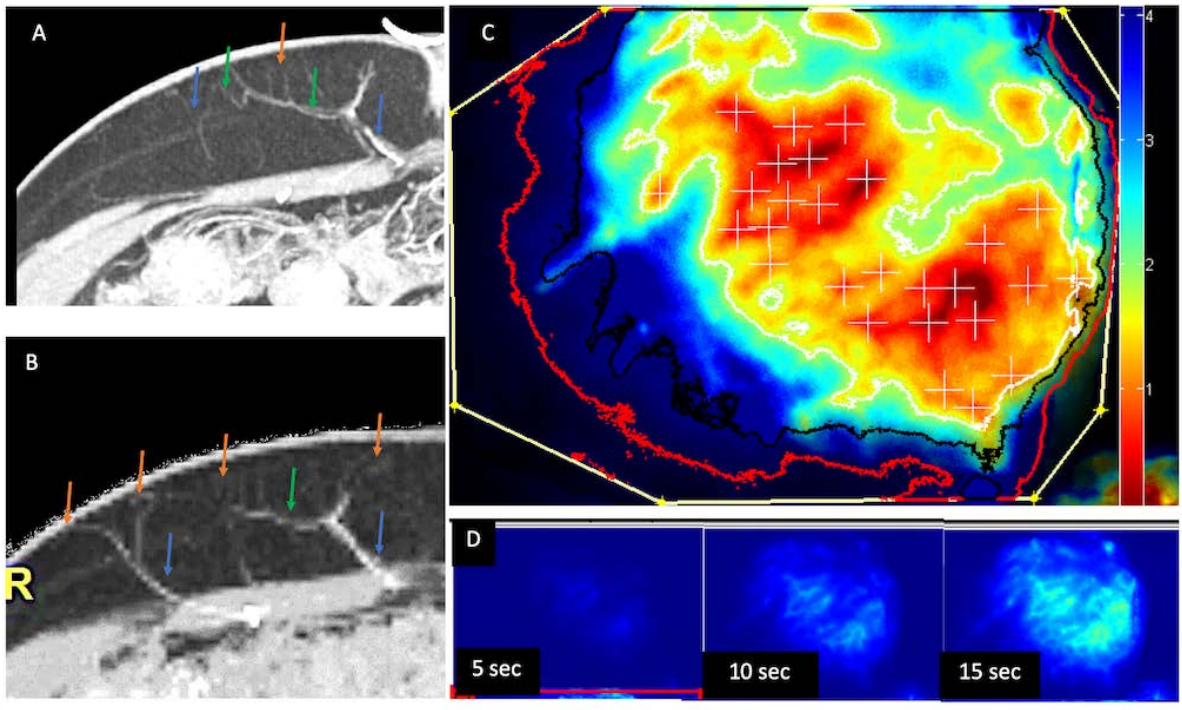

4.2.4.6 Surgical outcomes of DIEP Breast

A total of 41 hemi-DIEP flaps of the 44 flaps were available for analysis with LA-ICGFA and comparing CTA. Based on the surgical reports, the LA-ICGFA imaging of the flaps was deemed OK in 28 (70%) of cases after the pedicle dissection was completed. Following review of LA-ICGFA and based on clinical judgement, areas of hypo-perfusion were estimated between 5-15% of the hemi-DIEP flap. Further resection of hypo-perfused areas was carried out in 7 out of 41 cases (17%), therefore this would be a potential influence on the surgical outcomes and complications.

There were three cases of intraoperative complications and 7 cases of postoperative complications. Venous congestion occurred in three cases intraoperatively, and one case identified postoperatively in the first 24 hours and returned to the OR for exploration. There were 5 cases of documented fat necrosis post operatively and one minor wound dehiscence. The limited sample size and incidence of complications is insufficient to make inferences on LA-ICGFA perfusion patterns or underlying anatomy in relation to incidence of complications. However, evaluation of the angiographic curves which can be visualized by the surgeon in real-time during the intraoperative recording, and incidence of *any* complication was statistically significant (p=0.03, Fishers Exact); Curves that demonstrated sluggish inflow had a higher proportion of complications, and this can be seen by a slow rise on the angiographic curve that deviated from the typical expected curve. However, given that this group was still relatively small (N=5), there were still six incidences of a complication in the group that did demonstrate good arterial inflow. Complications may have originated from venous problems, which are more common, and venous phases were captured on several of the studies, but not all, and has not been analysed in this research as it part of future ongoing work.

4.3 An Experimental Small Animal Model to Evaluate Topical Negative Pressure Pre-treatment and Implications on Flap Vascularity

4.3.1 Animal Experiment and Data Acquisition

Topical continuous negative pressure of -125mmHg was applied onto the intervention side flap area for 5 days. Dressings were maintained for the entire time but may need to be partly replaced if there was a significant leak in the dressing or loss of the seal to permit successful negative pressure. The control flap was covered by a Tegaderm® dressing only. Cumulative hours of 125mmHg of continuous negative pressure were recorded for the intervention side. The median hours of NPWT on the flap was 141 hours, 5.8 days (Interquartile Range (IQR)= 128-165.75 hours, 5.3-6.9 days).

The techniques developed in this animal protocol were new experimental protocols. The biggest limitation in perfusion assessment imaging techniques in a small animal model was maintenance of the peripheral access, in particular, for repeated assessments. This was partly due to the size and nature of the vessel. Peripheral access was maintained either in the lower limb or dorsal vein in the tail, which provided a minimally invasive approach. Intravenous catheters were injected with heparinized saline in an attempt to maintain patency and secured with a temporary splint with a wooden tongue depressor and tape for protection. There was an initial learning curve to optimizing and maintaining peripheral access. This had impact upon the results of some earlier assessments performed:

- During CTA, one set of imaging (n=1) in group B rats was discarded due to inadequate contrast injection picked up in the skin flaps and pooling of contrast within the subcutaneous plane.
- During LA-ICGFA, 5 of 8 rats in group A had adequate SPY imaging for analysis post VAC (N= 10 flaps). However only 2 out of 8 rats (N=4 flaps) had complete image acquisition data at all three time points post VAC, post flap and 7 days post flap surgery.
- There was one premature death of a rat following repeat anaesthesia in group A. Therefore, in group A, only 7 out of the 8 rats (n=14 flaps) could be assessed for flap complications at 7 days post flap surgery.

- During preparation for Micro-CT analysis, 2 out of the 10 had incomplete injections. One was related to technical issues in the earliest stage of learning curve during this technical procedure and the second was due failure of the contrast to reach the dermis.

The table below shows a summary of the final number of rats that were included in final data analysis for the different assessments.

Table 4.4: Summary of data points acquired and final numbers available for each outcome assessment

	Start	**CTA D5**	**Post Vac SPY**	**Post Flap SPY**	**7D Post flap SPY**	**Flap survival assessment**	**Micro CT**	**Histology**
Group A	8	NA	5	3	2	7	4	8*
Group B	8	7	NA	NA	NA	NA	4	8
Additional Group A	4	NA	2	2	2	4	4	0
Total included (No. Flaps)	20 (40)	7 (14)	7 (14)	5 (10)	4 (8)	11 (22)	10** (24)	15 (30)

*Flaps from 1 rat from group A was sent for MicroCT and histology, representing results after VAC therapy only.
** Two flaps on Micro-CT had incomplete injection to permit analysis

4.3.2 Outcome Measurements of Dynamic Computed Tomographic Angiography

A total of 7 rats (14 flaps) from group B were included in this analysis. Data was collected and processed from the DynEva enhancement curves that measured the mean contrast detected in Hounsfield Units (HU) over time (in seconds) in the two Regions of Interest (ROI) at four equal separate regions of the flap measured from the proximal edge of the flap at 25%, 50%, 75% and the most distal extent of the flap region. Measurements were

compared between ROI 1 (Control) represented in red and ROI 2 (NPWT) represented in pink (Figure 4.15).[8]

Figure 4.17: Example of Screenshot of DynEva enhancement curves recording mean Hounsfield Units (HU) detected over time at 0.25cm in the control (red ROI 1) and NPWT treated (pink ROI 2) pre-harvest flap regions.

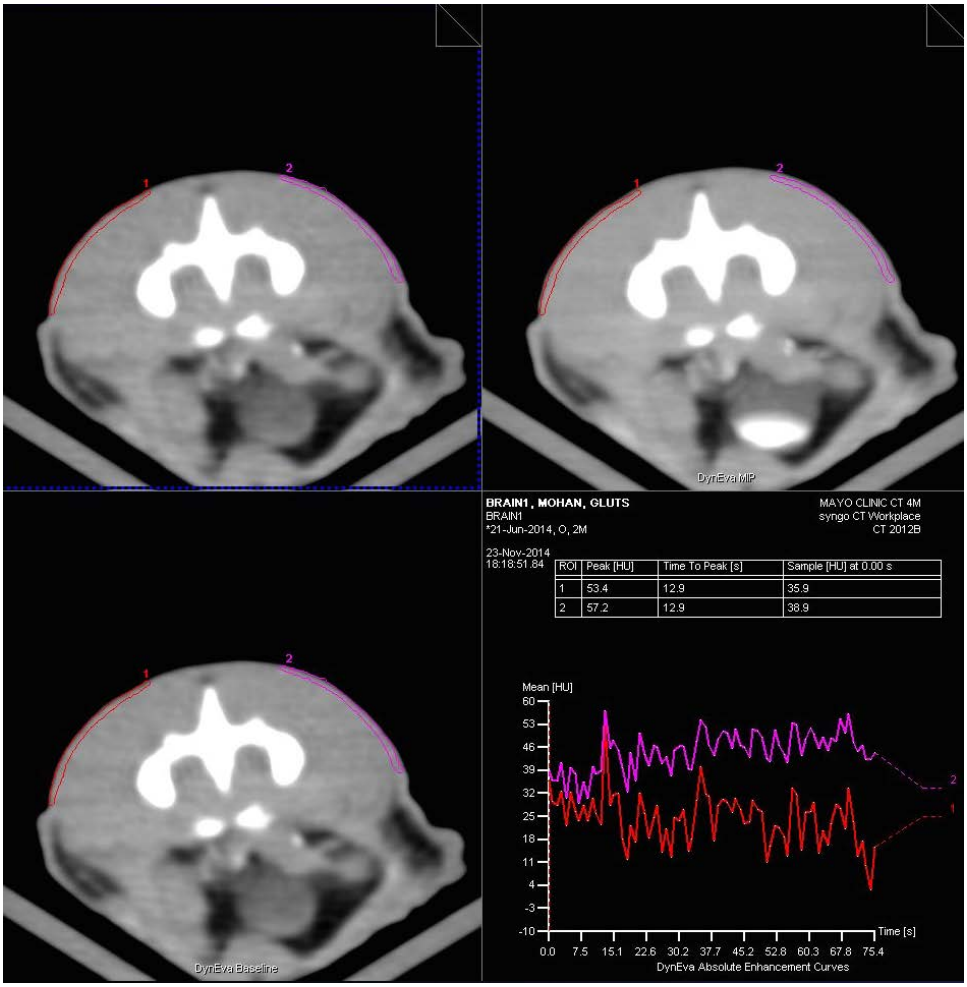

[8] *Dynamic CTA protocols, data acquisition and post-processing analysis were performed by an independent specialist, Dr. Gregory Michalak PhD (see Acknowledgements), who assisted with data interpretation for comparative analysis.*

Matched paired analysis demonstrated a 17% increase in mean tissue perfusion in the ROIs of the intervention (Mean=78.7 HU, SD=8.8) versus matched controls (Mean=67.3 HU, SD=15.7), p=0.001 (Paired T Test). Comparison of peak HU values reached during the time of data acquisition at all four distances showed a mean peak value of 63.01HU (SD=17) in NPWT treated pre-harvest flap regions versus 55.80 HU(SD=12.9) in controls, P<0.001 (Paired T-test). The peak HU reached was then compared at each distance which showed that the average peak value was higher in the NPWT treated flaps versus controls, although this was only significantly different at 0.25cm, P=0.001 (Paired T-Test). There was a slight negative trend in mean peak values towards the more distal regions of the pre-harvest flap (Figure 4.18).

Figure 4.18: Graph to show average peak of contrast in Hounsfield Units (HU) during dynamic CT angiography, detected at different distances along the flap in control and NPWT treated flaps**.** *Significance level set at alpha 0.05, *P=0.001, Paired T-Test*

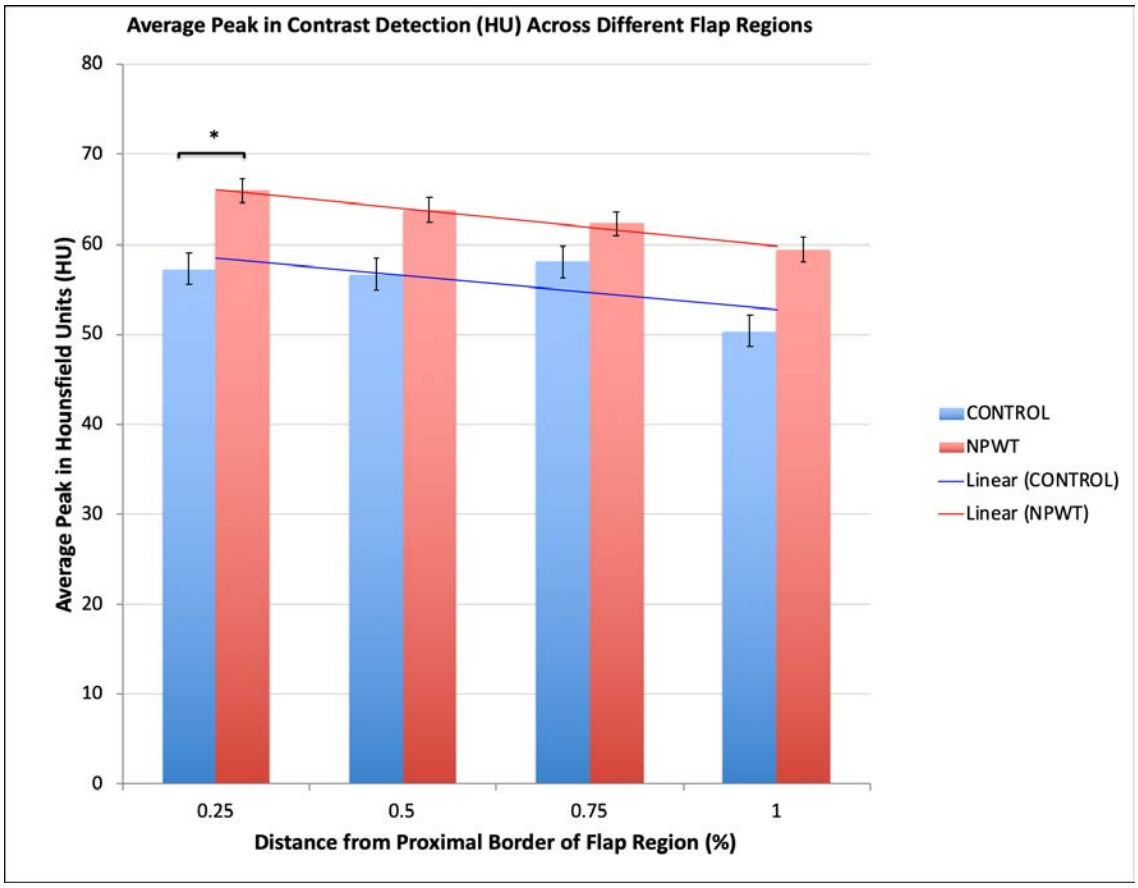

The control and NPWT regions were evaluated at each distance over the course of time, and there was significant difference between the two ROIs at each of the four distances: mean perfusion was significantly different between intervention and control at each distance, P<0.001 (Paired T-tests) (Figure 4.19). The most distal part of the flap region in the NPWT group was better perfused (Mean=51.1, SD=16.7) compared to the control group (Mean=39.4, SD=14.8), that was statistically significant, P<0.001. This demonstrated that the use of NPWT may have an immediate benefit to the perfusion of tissue in the area of flap harvest and potentially improve perfusion in the most distal region of the flap, that would be prone to ischemia. Review of perfusion along the flap from proximal to distal at each distance demonstrated that in the NPWT group there were significant differences noted between the most distal point in the ROI (Mean 51.1) and at 75% (Mean 48.3, P<0.01), 50% (Mean 52.9, P<0.01) and 25% (Mean 55.1, P<0.01). Similarly, there was a difference along the flap in the control group with a significant difference seen in the most distal (Mean 39.4) and at 75% (Mean 42.8, P<0.01), 50% (Mean 43.3, P<0.01) and 25% (Mean 43.4, P<0.01). This showed that in both flaps, control or intervention, there was a noted decrease in along the axiality of the flap.

Figure 4.19: Graph to show comparison of mean perfusion in Control and NPWT treated flaps at all distances along the flap. *Significance level at alpha 0.05, *P<0.001, Paired T-Test.*

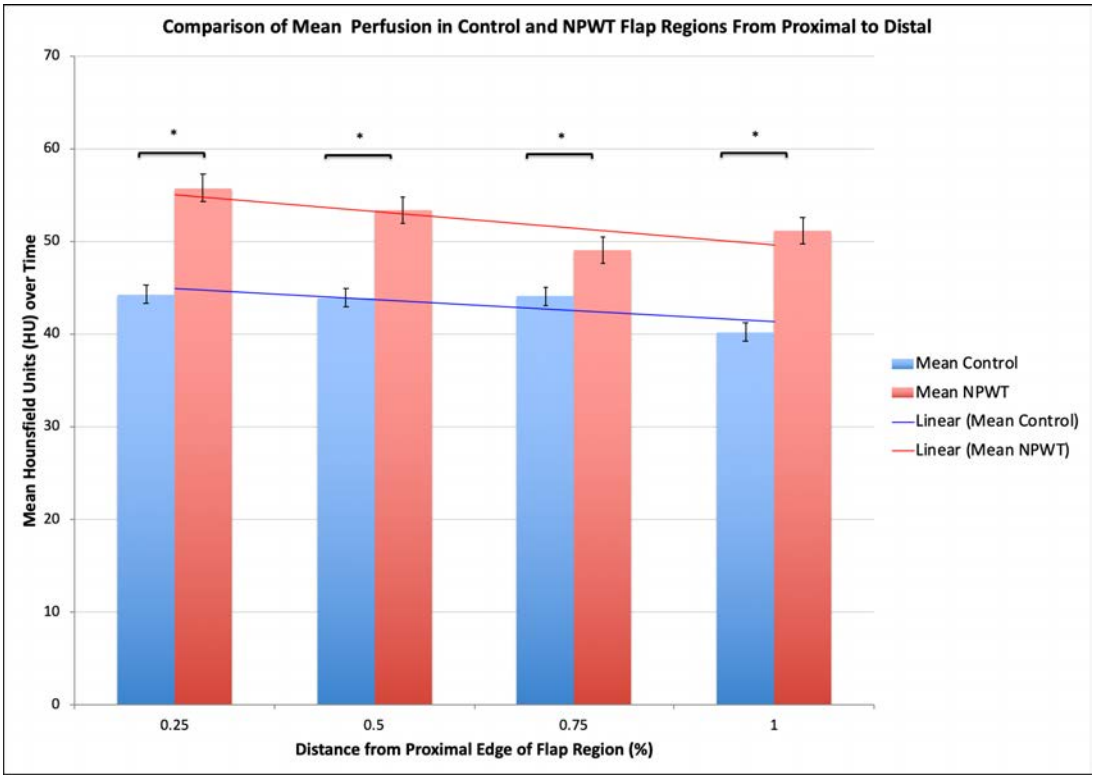

4.3.3 Outcome Measurements of Laser Assisted ICG Fluorescence Angiography

In the main study, animals from Group A were all assessed with LA-ICGFA using the SPY® Elite System that was attempted at three key stages: following the application of topical NPWT for 5-7 days; following flap harvest, and a final image was acquired 7 days post flap harvest. One animal did not recover from repeat anaesthesia following surgery in an attempt to acquire post flap imaging. Due to the limitations described earlier, following the main study all imaging was assessed for quality prior to analysis.[9] There were 5 out of 8 pairs of flaps suitable imaging for analysis post NPWT application, 3 pairs of flaps post flap harvest and 2 pairs at 7 days post procedure. The loss of data was a limitation, and an additional 4 rats were added to the study to increase the sample size for analysis in group A. In total, 7 pairs of flaps post NPWT, 5 pairs of flaps post flap harvest and 4 pairs of flaps 7 days post flap had suitable imaging for final data analysis. The ROIs for the control and NPWT treated flap areas were marked and the average of absolute values of ICG intensity, representative of the degree of perfusion, in each ROI was recorded over the full phases of angiography during course of the data acquisition. Data was analysed by an independent specialist using SPY-Qc® software. This provided a more accurate, comprehensive assessment and comparison of perfusion across all pairs, as the previous software version only permitted analysis at a single chosen time point during the recording.

Following the treatment of NPWT and prior to surgery, assessment showed a mean absolute intensity value of 172.3 (SD=34) in NPWT treated versus 131.1 (SD=24) in controls, with an average increased ratio of perfusion in NPWT treated flaps of 1.3 which was statistically significant, P=0.007 (Paired T-Test). The average in rate of inflow, or ingress rate was assessed in flaps following NPWT before surgical intervention, which showed an average ingress rate of 26.5 and 40.0 in NPWT and control flaps, P=0.03 respectively.

[9] *Analysis was performed by Dr C Chen and Prof TB Ferguson (See Acknowledgements) who are the developers of the software used with SPY® Elite System, using the latest beta version of the SPY-Qc Analysis Toolkit.*

Figure 4.20: Colour maps captured at single time point acquired during LA-ICGFA video assessment in three animals (A-C) prior to surgery, following NPWT treatment. The right flap marked (left of image) was the NPWT treated flap.

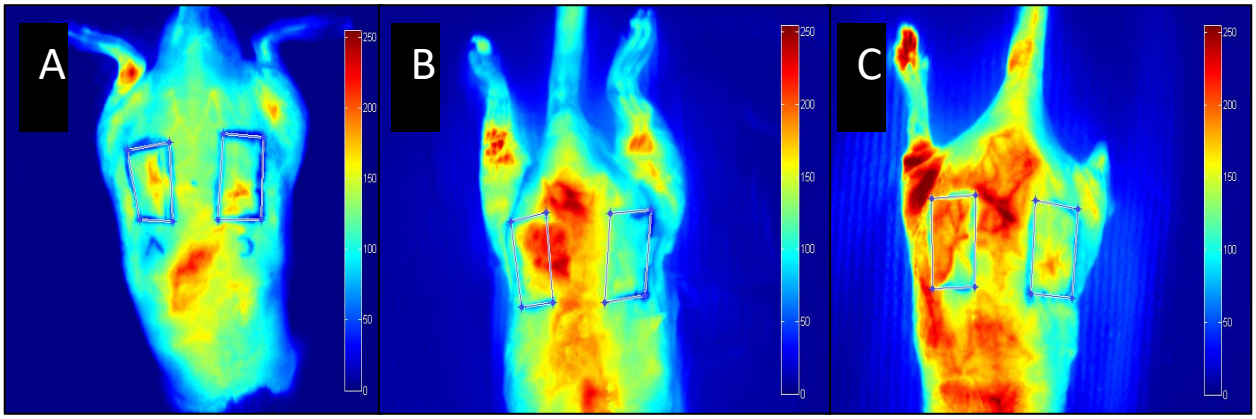

Figure 4.21: Example of an average intensity curve and images of control and NPWT flap captured during the different phases of LA-ICGFA assessment following application of NPWT prior to flap harvest.

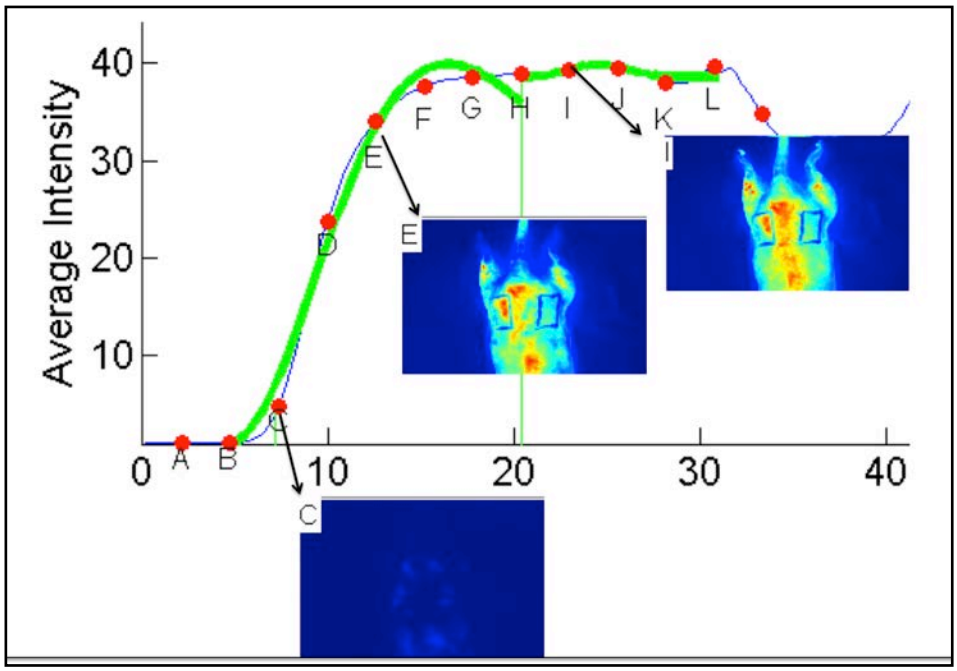

Repeat imaging following flap harvest and inset showed this ratio reduced to 1.1, with a mean perfusion of 98.7 in NPWT versus 83.3 in controls, which was not statistically significant, P=0.20 (Paired T-Test). Upon the final assessment at 7 days post- surgery, 4 pairs of flaps had suitable imaging for final analysis. The average absolute values representative of perfusion in the NPWT group was 189.0 (SD 27) versus 156.9 (SD=31) in controls, with an average increased perfusion ratio of 1.2, that was statistically significant, P=0.03 (Paired T-Test).

Figure 4.22: Video capture using SPY® Elite during LA-ICGFA assessment at seven days following flap procedure. Area of lower or slower perfusion are represented by the darker region (over the control flap) compared to NPWT pre-conditioned flap**.**

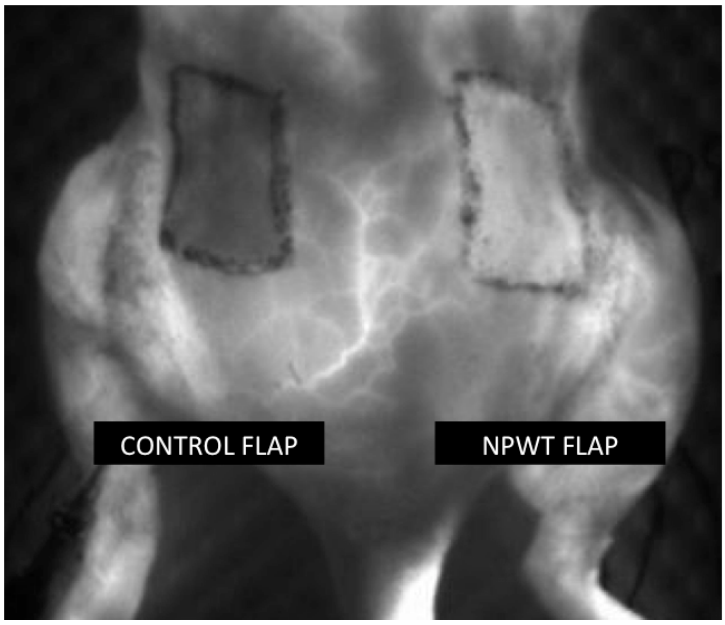

In summary, there is evidence that flaps preconditioned with NPWT prior to flap harvest consistently demonstrated a better perfusion compared to controls, although this difference was smallest immediately following flap harvest. The impact of NPWT effects was sustained even at 7 days post flap surgery. The figure below demonstrates a colour map of imaging acquired with the SPY® Elite System, which was acquired following NPWT treatment and prior to surgery.

4.3.4 Outcome Measurements of Micro-Computed Tomography Angiography

Assessment of injection procedures and final data comparisons were assessed following scanning of all flap (N=12 pairs). A total of 10 pairs of flaps (post-surgery N=6 pairs, post NPWT N=4 pairs) were included in the analysis. Vessels were traced throughout the entire skin flaps and quantitative analysis was performed using Analyze® 12.0 software package (Analyze® 12.0, Mayo Clinic College of Medicine, Rochester, MN) by an independent reviewer (AJV).[10] This allowed assessment of micro vessel density in each flap.

Figure 4.23: Example of assessment of Micro CT using three-dimensional volume rendered skin flaps with microvasculature demonstrating transverse cross-section and longitudinal views of control and NPWT skin flaps.

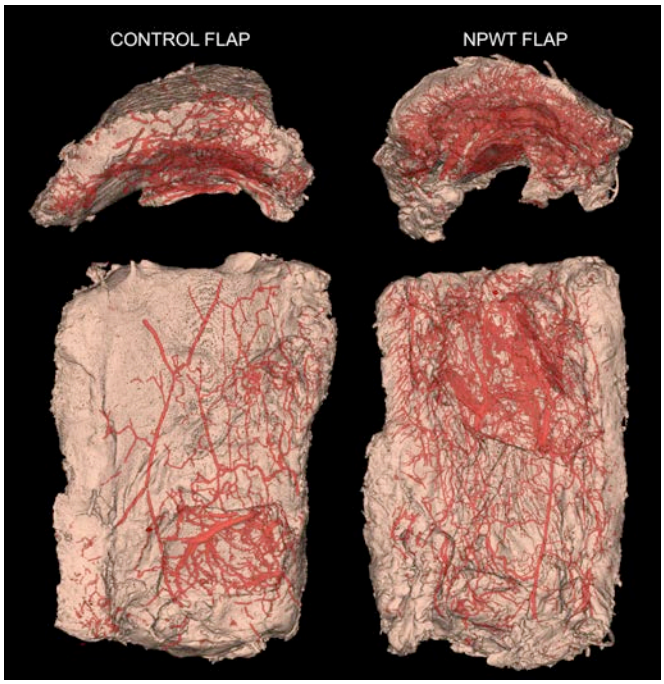

Mean vessel volume (mm^3) in NPWT was 9.14mm^3 versus 4.45mm^3 in control flaps, P=0.04 (Paired T Test). Sub group analysis of specimens was performed within group B rats following removal of NPWT treatment and within group A and additional rats that were assessed 7 days post-surgery. In a subgroup analysis, vessel volumes in the intervention group after treatment (group B rats) showed a 73% higher average (mean=4.4mm3, SD=3)

[10] AJV= *Andrew J Vercnoeke,, Medical Imaging Analyst, (See Acknowledgements).*

versus and control flaps (mean=2.6mm3, SD=2), but this was not statistically significant (p=0.23). This trend was also seen at 7 days post flap surgery (group A rats) with an average vessel volume of 12.3mm3 (SD=8) compared to 5.7mm3 (SD=3) in NPWT and controls respectively, p=0.06. Despite there was a trend of higher average vessel volume and micro vessel density in NPWT treated flaps compared to control flaps, the results were comparable between the two groups after treatment and following surgery. Although these values did not reach statistical significance in all cases, there was a consistent marked difference between the two groups but the limited sample size cannot allow us to draw definitive conclusions. A larger sample size is warranted to determine whether overall microvasculature changes in flaps preconditioned with NPWT and whether this effect is sustained over time.

4.3.5 Outcome Measurements of Clinical Flap Viability

There were no complications directly associated with the application of the VAC® system, however on occasion the flap region pre-treated with NPWT had increased hyperaemia immediately following removal of the VAC®, which mainly settled within a few hours.

Figure 4.24: Photograph example of one case demonstrating evidence of hyperaemia on the treated side immediately following removal of the VAC® following 7 days of therapy.

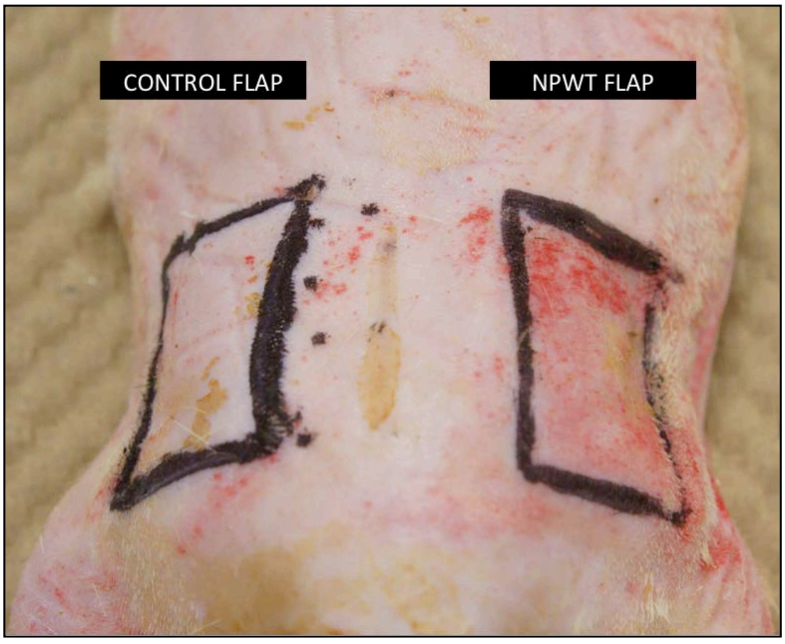

In the main group A all underwent flap surgery (n=8) but only 7 rats (14 flaps) were observed for 7 days post-surgery. An additional four rats were added to the study and underwent the same path as group A. In total 11 rats (22 flaps) were assessed over the course of 7 days following flap harvest and inset. Flaps were assessed clinically and complications were recorded, and flap survival was recorded at 7 days post-surgery. Overall most cases had good flap survival. Three flaps within the control group experienced partial superficial necrosis, that were recorded as 40,60, and 70% of the total flap area; In the NPWT pre-treated treated flaps, 2 flaps experienced partial necrosis but these were both recorded <5%.

Figure 4.25: Photograph to demonstrate control and NPWT pre-treated flap at 7 days post procedure with 100% flap survival.

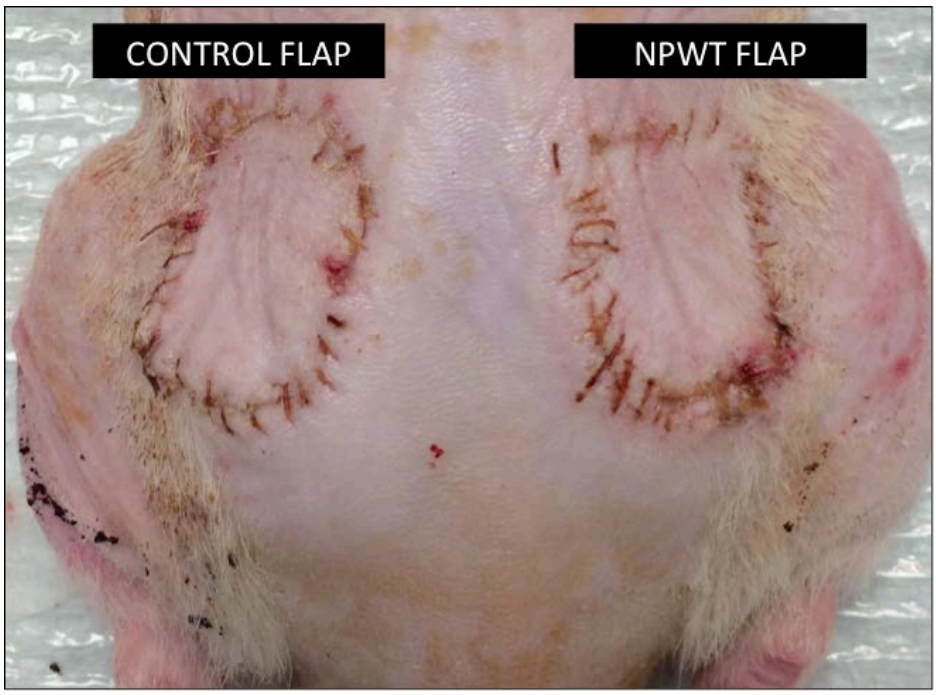

Figure 4.26: Photograph to demonstrate example of case of significant flap necrosis with comparison of control and NPWT pre-treated flaps at 7 days post procedure.

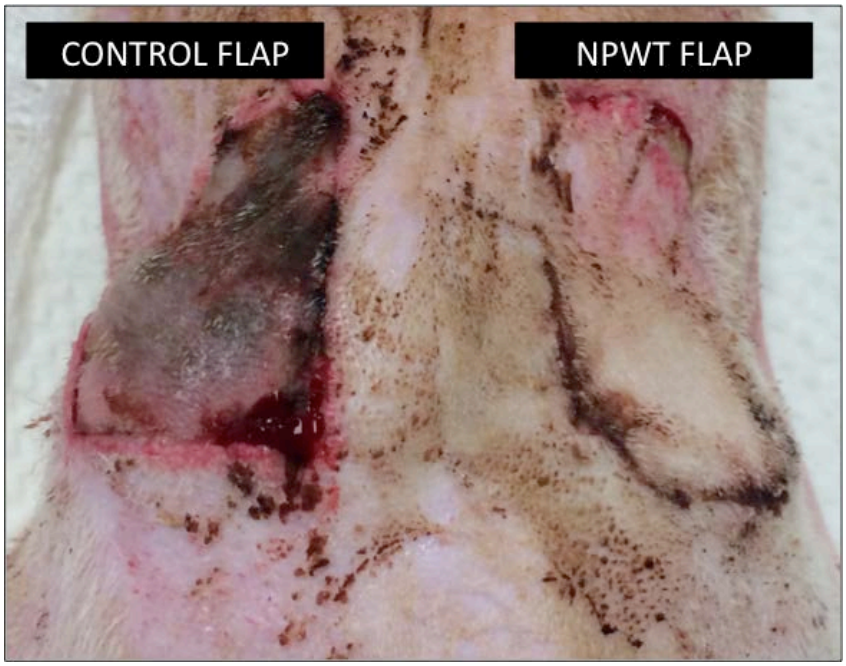

4.3.6 Outcome Measurements of Histological Assessment

A total of 32 flaps were fixed in 10% formalin and subsequently paraffin embedded. Full longitudinal cross-sections were cut and final sections were stained with H&E, and IHC with CD31. A total of 16 rats (post-treatment N=7 rats, post-surgery N=9 rats) had been prepared with MicroFil injection for Micro-CT analysis and then paraffin embedded for sectioning and histological assessment. A total of 16 flaps were directly excised, fixed and paraffin embedded for histology. Longitudinal cross sections represented the central portion of the flap and provided a full thickness cross section of the skin, hypodermis (containing loose areolar tissue and fat) and some specimens included a superficial layer of muscle. Flaps were assessed with standard Haematoxylin & Eosin (H&E) staining to review the general characteristics and morphology of the tissue, epidermal and dermal thickness.

Figure 4.27: Representative H&E stained section to demonstrate layers within a longitudinal cross-section of dorsal rat skin of a control flap. (*A= Epidermis, B= Dermis, C= Hypodermis, D= Muscle, E=Hair Follicle).*

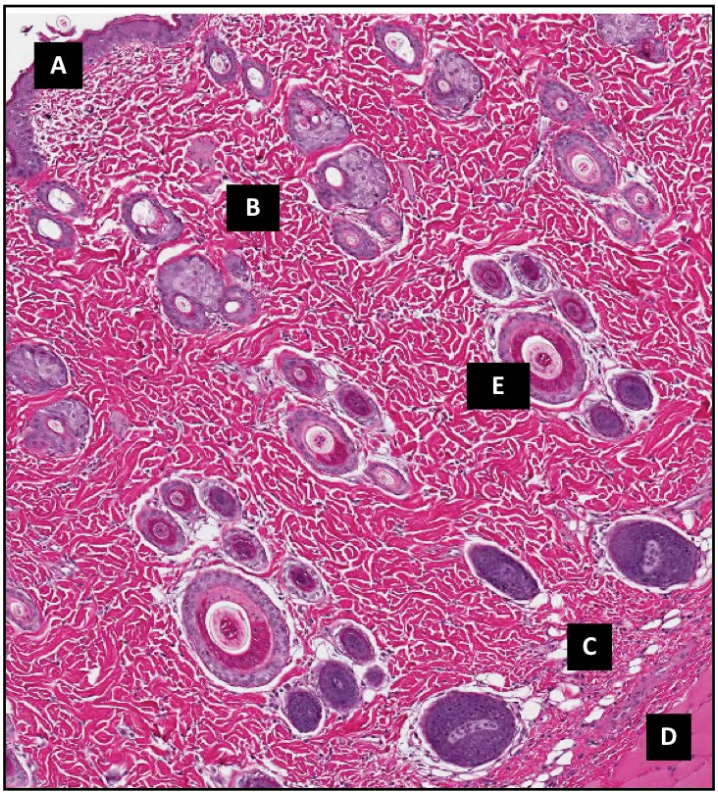

4.3.6.1 Epidermis: H&E Stain

Longitudinal sections were assessed at lower power and x40 magnification for general assessment and more detailed review of representative areas within the section. The epidermis, which is the uppermost part of the dorsal rat skin, consists of four principle layers. The stratum corneum was the most superficial layer containing anucleated dead cells (corneocytes) and the most variable layer. The stratum granulosum is often easily recognizable by their basophilic keratohyalin. The stratum spinosum is a less dominant layer in rat skin histology and the stratum basale is the prominent deepest layer in the epidermis. (176)

Figure 4.28: Representative H&E stained sample in control flap to demonstrate layers of the epidermis in the dorsal rat skin**.**

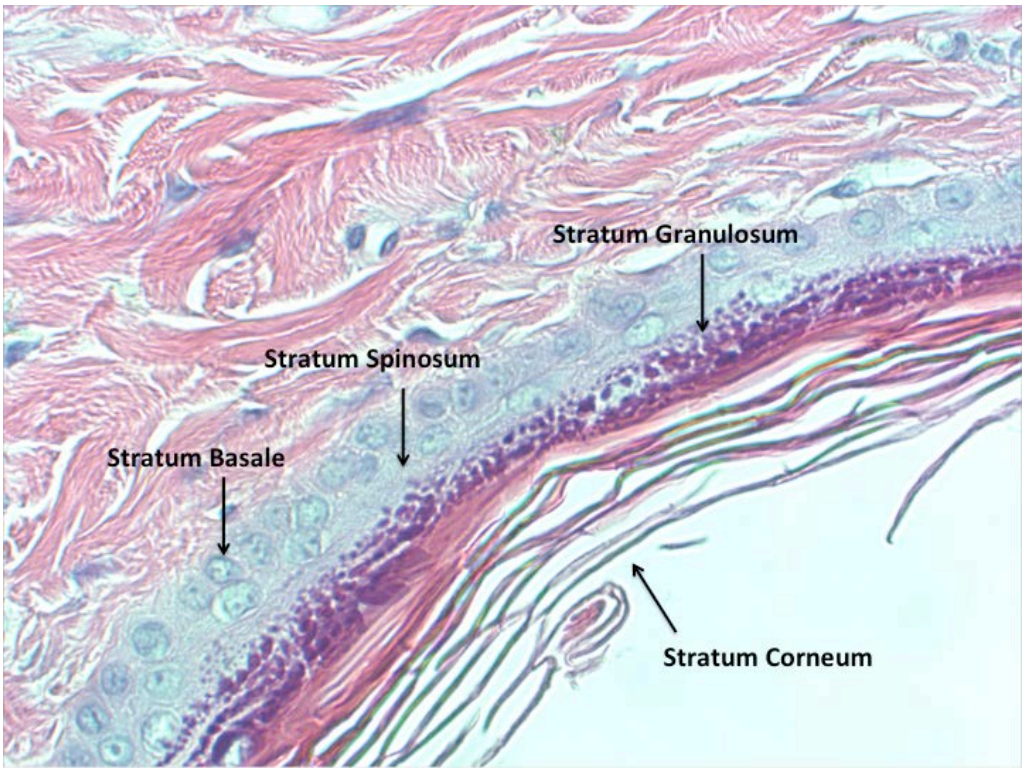

The sections of dorsal rat skin were assessed on low power magnification to assess the whole section and representative areas were selected and assessed at x20 and x40 magnification. An average of three measurements were taken per specimen at x20 magnification. The average epidermal thickness in control flaps had a mean average epidermal thickness of 38.2 µm (SD=9.4) compared to NPWT treated flaps 60.2 µm (SD=8.7), which was statistically significant (P<0.001). The average dermal thickness in the control group had a mean thickness of 1315.74 µm (SD=408.4) compared to a mean of 1381.39 µm (SD=495.2) in the NPWT group, which were comparable (P=0.27).

Figure 4.29: Histogram of mean epidermal thickness and standard deviation in control and NPWT pre-treated skin flaps.

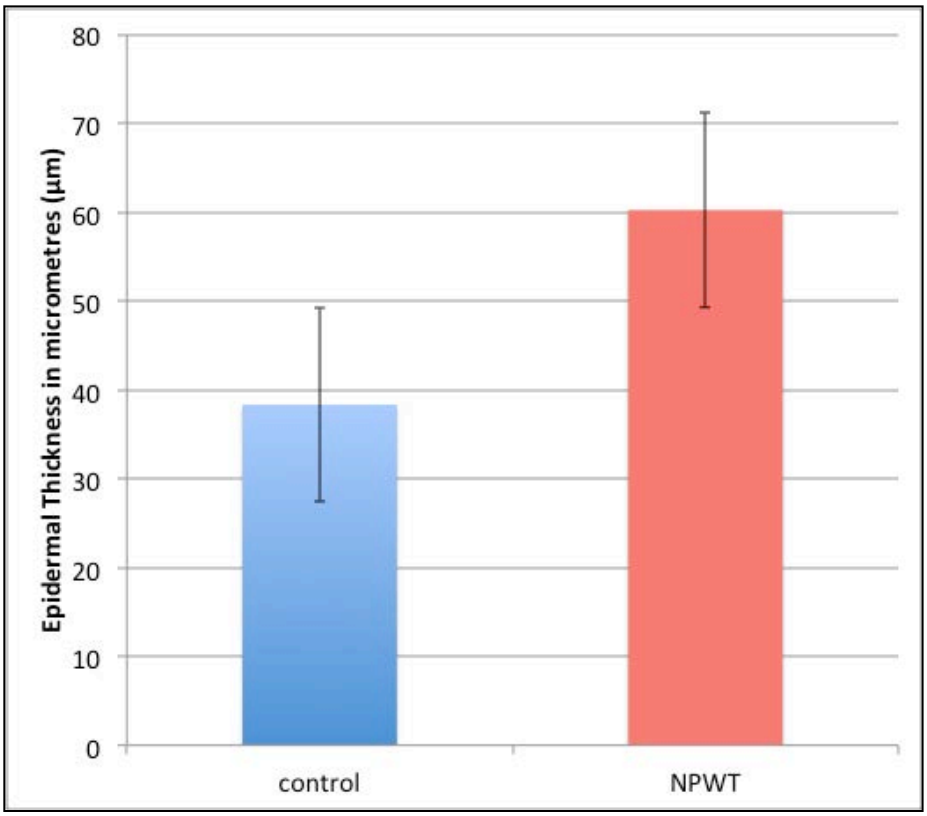

4.3.6.2 Dermis: H&E Stain

Within the dermis, the collagenous fibres predominate, and collagenous type I bundles stained intensely with Eosin. The dermis consists of two principle layers, a more superficial papillary dermal layer and a deeper reticular layer. The reticular dermis provides the overall strength and elasticity as well as incorporating epithelial derived structures such as hair follicles. The hypodermis is the lower most part of the dermis containing loose connective tissue, which may also contain adipose tissue. The dermis contained dense irregular connective tissue, organized into a reticular “basket weave”.

The dermis was assessed qualitatively to assess overall collagen organization at x40 and x60. A qualitative assessment was performed on all H&E sections and overall NPWT treated flaps had improved collagen organization compared to controls. The sections were assessed using a semi-quantitative scoring system at x20 and x40 magnification to assess the density of the arrangement with dermal layer, with lowest score given to less dense arrangement with frequent multiple gaps (score=1), moderate gaps (score=2) and minimal gaps with compact arrangement (score=3). Using this assessment there was an increased overall average density within the dermis in NPWT flaps compared to controls, $P<0.001$. This difference was seen both following NPWT treatment and 7 days following flap elevation, $P=0.02$. However, quantitative assessment following additional staining methods would be preferable to apply for future studies to formally assess and compare collagen content, distribution and elastin content in control versus NPWT flaps.

Figure 4.30: Representative figure of H&E stained sections showing NPWT pre-treated flaps (right) qualitatively demonstrated greater collagen organization that was more densely arranged compared to control flap (left).

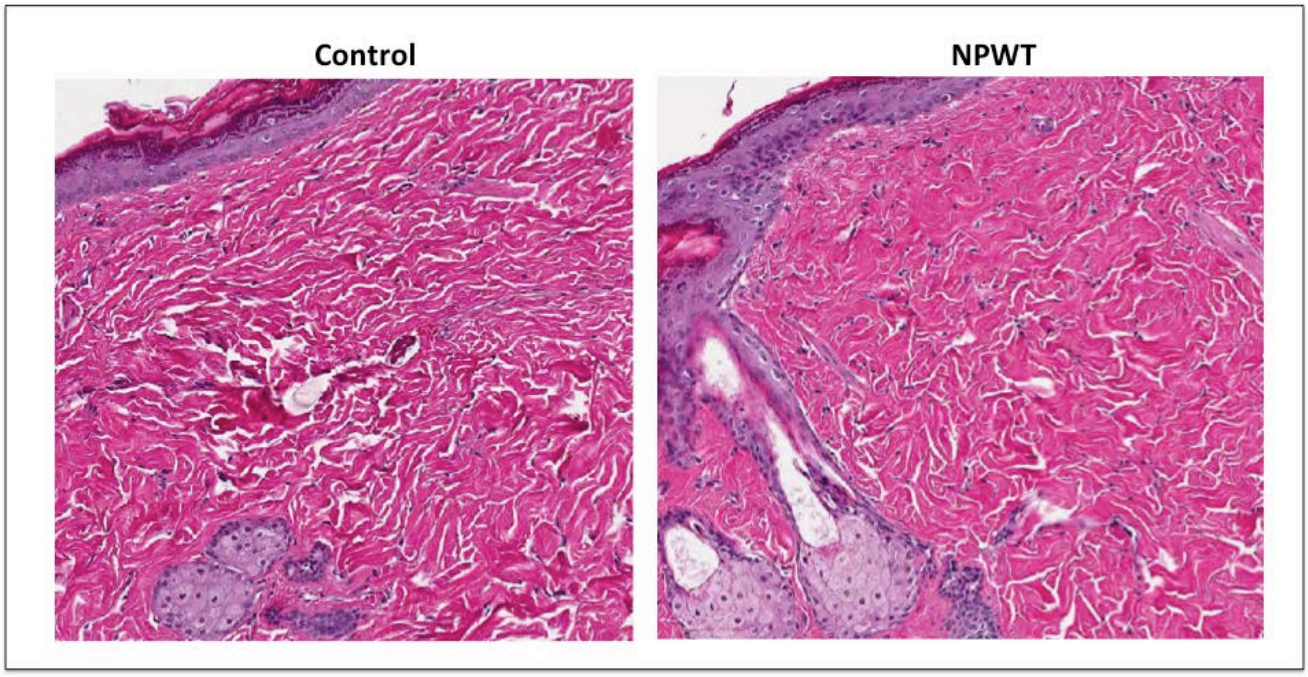

4.3.6.3 CD 31 Immunohistochemical staining

To analyse the presence of endothelial cells, the endothelial cell marker CD31 was used in conjunction with immunohistochemistry (IHC) techniques to assess and compare blood vessels in the sections and their distribution within the skin. Sections were randomly selected for assessment at x10 magnification to provide a general overview of the distribution of the stain. The two regions where vessel distribution was the most prominent was within the superficial dermis and hypodermis. A total of six random high-powered fields (x20) were randomly selected, including three superficial and three deep dermal/hypodermis regions. CellSens Dimension Version 1.11 software (Olympus Corporation) analysis software was used to calculate mean area of fraction and mean area of endothelial stained per high-powered field. A semi-quantitative objective scoring system was also used as an adjunct to the software analysis.

Figure 4.31: Histological representative views to show example of high-powered views x20 magnification regions for comparison of different semi-quantitative scoring assigned

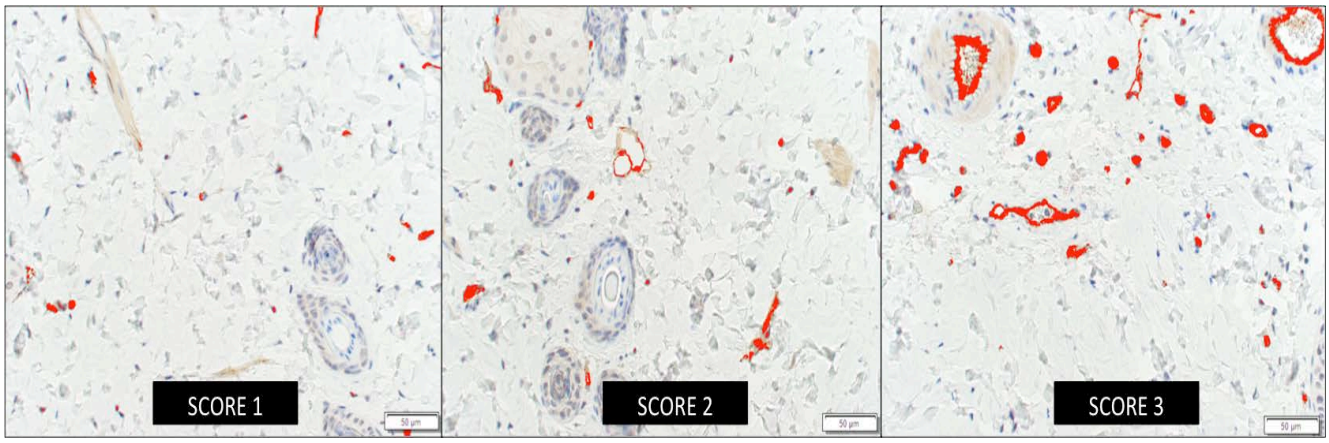

Comparison with all six regions showed a total mean area of CD31 stain per high-power field and percentage mean area fraction was higher in NPWT compared to control flaps, P=0.03 and P<0.01 respectively. The average percentage mean area fraction in the intervention group was 3.9% (SD=3) versus 2.9%(SD=2) in matched controls (P=0.03, Paired T Test). Mean

area of CD 31 staining in the NPWT pre-treated group was 5744 mm^2 versus 4268mm^2 in controls (P=0.03, Paired T-Test). This was concordant with the semi-quantitative scoring that showed an average higher score in NPWT compared to controls, P=0.01. Comparison of superficial and deep dermal regions demonstrated that in the superficial regions there was consistently higher degree of staining in NPWT versus controls, but the main region influencing this difference was the deep dermal region, P=0.05 (Paired T-Test).

Specimens were subdivided and analysed 7 days of NPWT treatment and specimens analysed 7 days following flap surgery. Following NPWT removal the mean area fraction of CD31 stain was 4.1% compared to 2.6% in NPWT and control flaps, P=0.03 at day 7, but this difference was reduced at 7 days following surgery, day 14, P=0.69. Mean summed area of quantified stain was higher in NPWT versus control flaps at day 7, P=0.03 but this did not reach significance at day 14, seven days post-surgery, P=0.63. These results were concordant in the semi-quantitative analysis where a mean scoring was greater in the NPWT group at day 7, immediately following NPWT removal, P=0.03. However, this difference was still apparent at day 14, seven days post-surgery, although trended towards but did not reach statistical significance, P=0.06

There was increased vessel density in NPWT compared to control flaps, which was most prominent in increased vessel formation in the deep dermal layers and immediately following NPWT treatment. This effect was less pronounced at 7 days post flap elevation, although there was still a higher average vessel density in NPWT versus controls.

Figure 4.32: CD31 quantification based on mean area fraction % per high-power field showing increase in the marker following NPWT removal at Day 7, but this difference was smaller 7 days following surgery, at Day 14.

** Significance level set at P=0.05, Paired Test. Data presented with Mean and Standard Error (SE) bars*

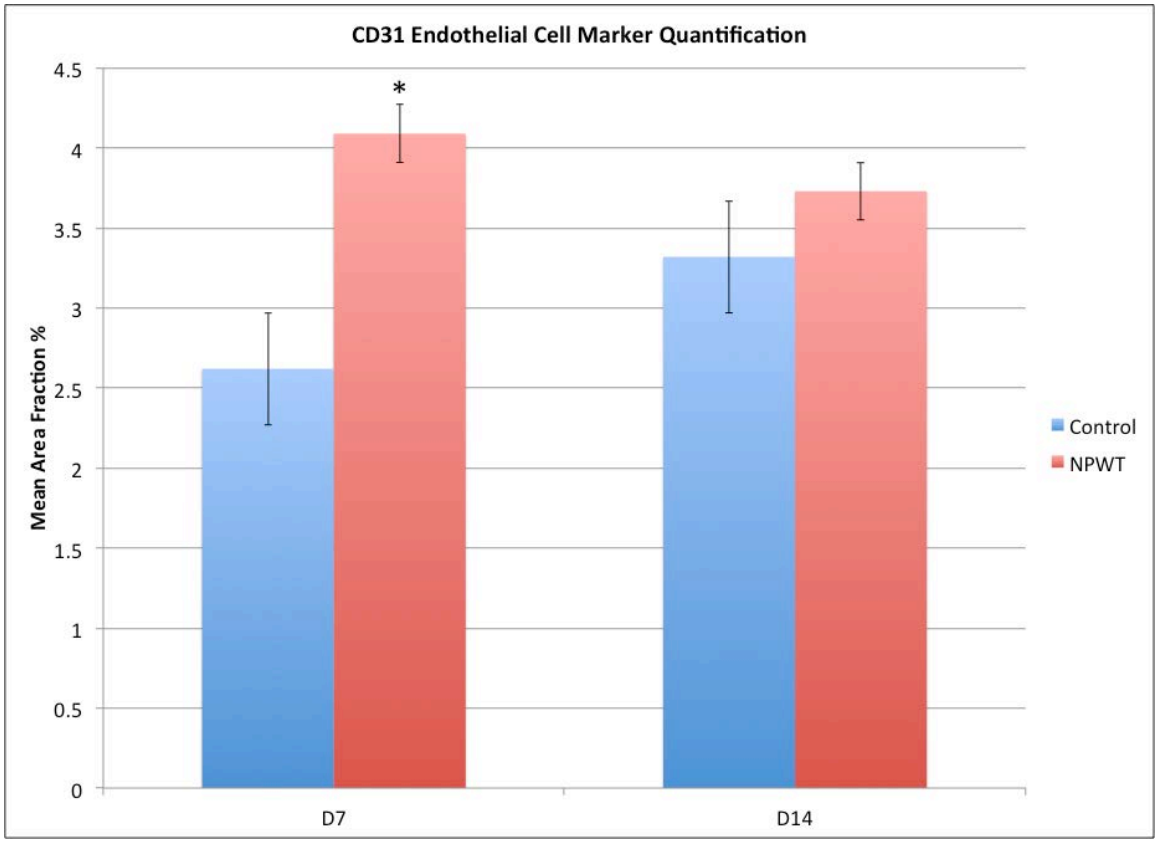

In summary, the dynamic perfusion studies using 4D CTA and LA-ICGFA captured with SPY® Elite system has shown that flaps preconditioned with NPWT prior to flap harvest consistently demonstrated a better perfusion ratio and rate of inflow compared to controls. This effect was not demonstrated immediately flap harvest. At 7 days post flap surgery, however, there was still evidence of increased perfusion in the NPWT treated group. Evaluation of static microvessel density there was a difference overall between the NPWT and control groups. However, on analysis at the relevant time points, microvessel density was comparable between the groups, despite the trend of higher average vessel volumes in the NPWT. Upon histology there was evidence of increased microvasculature in the NPWT group but this was only seen following treatment and not sustained at 7 days post-surgery. There was increased epidermal thickness in NPWT pre-treated flaps, and qualitatively improved collagen rearrangement within the dermis, although further staining techniques or Western blot analysis with quantification for collagen and elastin would be required to determine histological changes. Therefore, there was dynamic changes in perfusion seen following treatment that demonstrated augmentation of flap perfusion, and this may render the tissue more tolerate at the time of surgery to ischemia perfusion. These dynamic changes were still evident following surgery, however at a structural level it was not possible to demonstrated increased microvasculature density on imaging or histology between the two groups at both time points. This may be due to the time interval for development of new vessel formation, or that there was less impact of NPWT on promoting angiogenesis. Further work is required in this area however a proof of concept and establishing multimodal assessment has been established.

CHAPTER 5: DISCUSSION

5.1 Anatomy and Physiology of the Perforasome of Deep Inferior Epigastric Artery Perforators in bilateral breast reconstruction

Perforator selection in DIEP flaps has been previously described based on size and perforator location, and number of perforators to include(27,44,59,177–182) with no specific consensus. Previous anatomical studies performed have assessed perforasomes in DIEP flaps looking specifically at the lower abdomen only reviewing the entire lower abdominal integument, but this is mostly relevant for unilateral reconstructions. (19,26,183) The Hartrampf (18,53) and modified Holm(55) zones of DIEP perfusion have been the standard of selection of tissue and flap design, but it has been increasingly recognized that the dynamics of a perforator are more complex. (17,26,27,57,171) Taking in some of the concepts previously described in the literature in both anatomical and clinical studies, this research focused on bilateral reconstruction which has not been addressed adequately in the current literature. There is very limited progress in the literature of "dynamic perforasomes" in perforator flaps and DIEP breast reconstruction.(38,55) **The aims of this thesis were to evaluate anatomical microvasculature and predict perfusion territories of individual perforators in hemi-abdominal DIEP flaps and then correlate the underlying anatomy to the dynamic perfusion of specific perforators within these flaps for its application of bilateral breast reconstruction.**

5.1.1 Perforator Anatomy and Perforasomes of Hemi-DIEP flaps

The first step of my thesis was to evaluate perforator anatomy in both cadaveric and clinical anatomical studies. In the anatomical studies, the largest perforators in the hemi-abdomen were within a 5cm radius of the umbilicus, which can be considered as a "hot spot" for dominant perforators for DIEP flap reconstruction. (47,182,184) The average external diameter was 2.4mm of those perforators within the 5cm "hot spot" and the majority of perforators within this zone were medial row (88%) compared to 73% of lateral row perforators which are outside this zone. The perforators in the hemi-abdomen originated from the medial row (average 2.3mm) were comparable to lateral row (average 1.8mm).This is similar to anatomical consideration for a full DIEP for unilateral

reconstruction. These patterns were also demonstrated in clinical study patient cohort in this research.

On assessment of perfusion territories in the anatomical studies, medial and lateral row perforators did not show statistical differences in size of the perforasome area or volume. However lateral perforators demonstrated greater lateralized extension of the perforasome territory that was statistically significant ($p<0.01$). This is comparable to previous anatomical studies of DIEP perforators.(26,28)(18,26–28) Lateral row perforators were found to significantly capture lateral linking vessels, with connections seen to the adjacent SIEA territory most commonly. The presence of intra-row linking vessels which had a better degree of caudal perfusion. The direct and indirect linking vessels via the subdermal plexus were found predominantly in the superficial layer of the abdominal flap.

The capture of linking vessels using dynamic 4D-CTA for individual perforasome assessment provided an opportunity to visualize the early distribution of the “dynamic” perforasome within the hemi-abdominal flap. Early capture of dominant linking vessels, flow to the subdermal plexus and recurrent flow into adjacent perforators resulted in a more rapid and larger perforasome distribution. Bi-directional axiality of flow, (seen predominantly in medial row perforators and those within 3cm of the umbilicus) and lateral dominant axiality of flow were both associated with significantly larger perforasome areas. This indicates that the perforasome distribution correlates with characterization of the numerous communicating vessels and adjacent arterial territories. (40,42,185,186)

In our clinical study the surgeon (M.S-C) used an algorithm for perforator selection and harvest which we have previously published.(182) The basis of perforator selection is primarily on perforator size, regardless of row. If a large lateral row perforator was available, this would be chosen for DIEP flap harvest for ease and expeditious flap harvest.(59,178) Assessment of the “dynamic” or “physiological” perforasome in-vivo was assessed using LA-ICGFA and comparison of single medial and lateral dominant perforator flaps showed comparable percentage areas of flap perfusions that was comparable to our anatomical work and previous published studies reconstruction.(187)

This study developed a novel approach in the evaluation of dynamic perfusion patterns in DIEP flaps **with evidence of significant variation in the physiology of the microcirculation in-vivo of flaps, based on qualitative and quantitative analysis using LA-ICGDA intraoperatively, even among single dominant medial row perforator flaps**. This is in stark contrast to the traditional understanding and acceptance of the patterns of perfusion in the DIEP flap and perforasomes(18,40,55,57) and reiterates the gap in knowledge on how branching patterns and characteristics of the direct and indirect linking vessels in the integument may play a critical role in flap perfusion.

5.1.2 A Novel Approach to Evaluate Dynamic Perforasomes of DIEP Flaps in Bilateral Breast Reconstruction In-Vivo

The branching patterns of the DIEA and role in arterial territories of the anterior abdominal wall has been appreciated in extensive anatomical studies.(18,25,26,28,33,42,185,188,189) Although anatomical studies provide the foundation and lay out of the underlying microvascular anatomy they are limited due to the neuronal, hormonal, and local factors that may place an intricate role in perfusion dynamics that may be seen in-vivo. The microcirculation in-vivo of the DIEP flap has been previously assessed in a clinical setting using technologies such as Laser Doppler imaging(21,170,172,173), tissue oximetry, thermal imaging(190) and fluorescence angiography(55,191). However, many of the these studies used the template of the Hartrampf's zones of perfusion, although it is recognized that the dynamics of microcirculatory flow in perforator flaps is different to its TRAM flap counterpart.(25,26,40,57) Although LA-ICGFA and Laser Doppler have been used to assess in-vivo quantification of zonal perfusion(55,108,111,191) these studies used a limited number of quantitative data points within the flap without a clear indication of timing of the angiographic phases captured (Figure 5.1).

Figure 5.1 (A) Example of an assessment of zonal perfusion as measured using LA-ICGFA. (*Source: Losken A, Zenn MR, Hammel J a, Walsh MW, Carlson GW. Assessment of zonal perfusion using intraoperative angiography during abdominal flap breast reconstruction. Plast Reconstr Surg. 2012;129:618-24); (B)* An example of an assessment of zonal perfusion as measured using tissue oximetry *(Source: Rahmanian-Schwarz A, Rothenberger J, Hirt B, Luz O, Schaller H-E. A combined anatomical and clinical study for quantitative analysis of the microcirculation in the classic perfusion zones of the deep inferior epigastric artery perforator flap. Plast Reconstr Surg. 2011;127(2):505-513)*

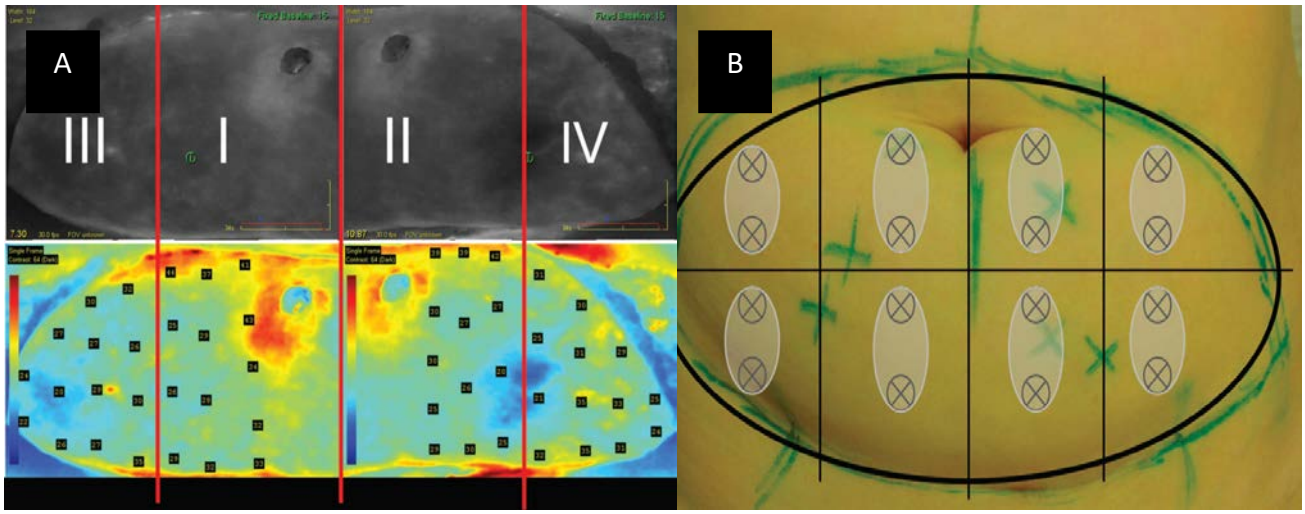

Application of novel techniques for analysis of DIEP flap perfusion using SPY-Qc software created a map of perfusion captured pixel by pixel of total and rate of flow into every area of the flap *throughout* the entire arterial and microcirculatory phase. This eliminated the bias of single time points used in analysis and use of limited data points that does not capture the microcirculatory changes in all areas of the flap. Evaluation of timing maps depicted patterns of inflow within the flap from a single dominant perforator was highly variable, even when based on a large medial row perforator. Rapid ingress of blood flow in adjacent regions of the DIEP flap at the same relative rate as the dominant perforator was characterized by presence of “hot spots” on the flap: single, two (co-dominant) or multiple

spots (diffuse). Observation of this “dynamic perforasome” provided some evidence that even using more modern perfusion concepts of “concentric” perfusion(40,57) may be too rudimentary.

Figure 5.2: An example of LA-ICGFA used intraoperatively following perforator dissection and flap harvest, just prior to start of ischemia time (A) Screen shot of the grey scale video visualized during image capture where by perforators, subdermal linking vessels and flow into the flap can be qualitatively assessed; (B) Intensity maps during the arterial and microcirculatory phases with application of color scaled to the amount of ICG detected per pixel; (C) Timing maps during the arterial and microcirculatory phases with application of color scaled to rate of ingress into the flap detected per pixel. *Images provided by Dr. C Chen and analyzed using SPY-Qc software® (Novadaq Technologies, Inc).*

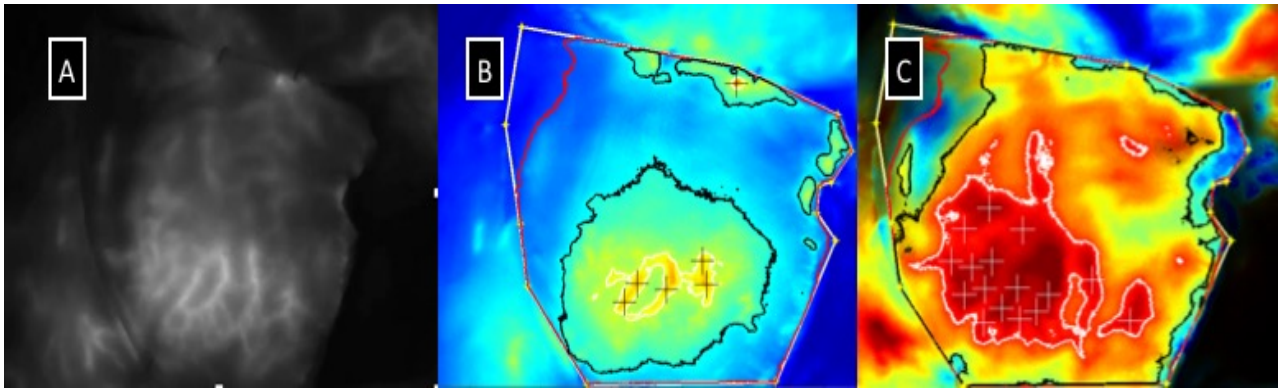

Reviewing this dynamic perforasome may also permit evaluation of inter-perforator zones and the potential to appreciate “true” and “choke” anastomoses that have been previously described by Chubb et al. on assessment of perforasomes using dynamic thermal imaging. (190) Figure 5.3 provides examples of LA-ICGFA images and timing maps reproduced on SPY-Qc ® software with depiction of predicted course of direct inter-row, intra-row and communicating linking vessels.

Figure 5.3: Examples of LA-ICGFA timing maps produced using SPY-Qc software® (Novadaq Technologies, Inc). (A-C) Demonstrate different perfusion patterns in single medial row hemi-DIEP flaps with predicted adjacent perforators (blue arrows) & inter-perforator zones (small black arrow); (D) MS-TRAM flap exhibiting traditional Hartrampf zonal perfusion.

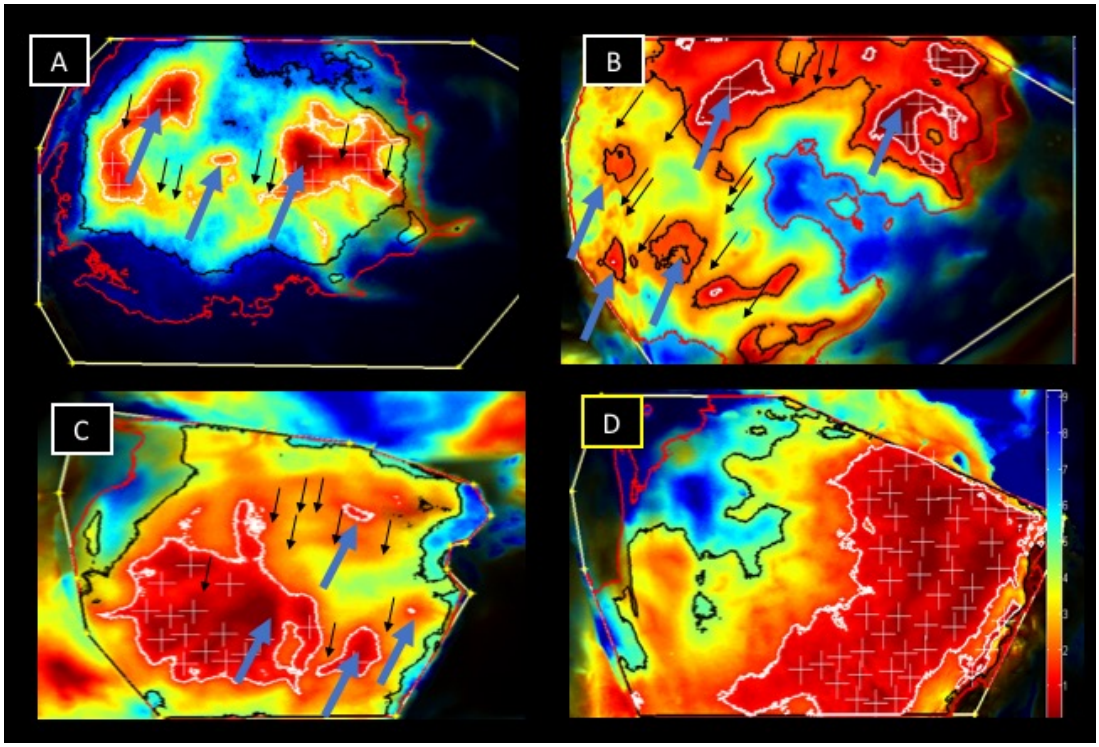

Evaluation of the measured area greater than 25% scale of intensity relative to the reference value 100% (perforator) was used to best indicate the broad area of flap that still remains well vascularized and well above the threshold used for defining hypo-perfusion. There is not enough evidence in the literature to find consensus on the threshold value commonly practiced using 10-15%, but described up to 25%.(192) The diffuse pattern of the dynamic perforasome had significantly greater percentage area of the hemi-DIEP flap perfused above the 25% threshold value both on intensity and timing maps ($p<0.01$). This highlights that there is both a greater concentration of ICG detected over the entire surface of the flap and greater rapid arterial inflow into multiple areas of the flap compared to the single pattern, that exhibited a more radial distribution around the perforator. Diffuse patterns were associated with significantly higher relative blood flow and intensity in the

cephalad-caudal axis of the flap, which may be attributable to greater degree of inter-perforator zones and larger calibre linking vessels, but requires further prospective study.

5.1.3 Bridging the Gap Between Microvascular Anatomy and Impact on Dynamic Perforasomes of DIEP flaps in Bilateral Breast Reconstruction

In our clinical study, we did not identify appreciable differences between the length of the perforator course before it exited the anterior fascia and perfusion patterns or areas. Direct perforators, with no branching in the muscle and level of fascia, demonstrated a higher intensity of perfusion around the perforator on timing and intensity SPY-Qc maps compared to indirect perforators, but this was not statistically significant when reviewing the broader perfusion of the flap (area representing >25% relative to the reference value). The degree of aborization in the subscarpa's and suprascarpa's layer did not significantly impact the area of broader flap perfusion.

The appreciation of the contribution of blood flow to the subdermal plexus (18,25,45,193,194), the presence of a dominant linking vessel in the suprascarpa's layer with either small direct communications to the subdermis, or direct perforator with multiple direct communications to the subdermal plexus, had higher average perfusion areas ($p<0.05$). The presence of the dominant linking vessel in the suprascarpa's layer had the most significant impact on perforasome areas on timing and intensity maps ($p=0.01$ and $p=0.02$ respectively) and resultant dynamic perforasome patterns ($p=0.01$). The presence of inter-row linking vessels also was associated with the difference in perfusion patterns seen ($p=0.003$) with the diffuse pattern with the highest proportion of inter-row linking vessels, followed by co-dominant pattern, with the lowest in the single pattern group. There was a significant difference in the perfusion patterns and the density of vertical communicating vessels to the subdermis immediately around the perforator in the hemi-DIEP flap ($p=0.007$) with the diffuse pattern represented by the highest density. The diffuse pattern for the dynamic perforasome was represented by a higher proportion of inter-row, linking vessels and greater density of vertical communicating vessels contributing to the subdermal plexus. The presence of a dominant linking vessel in the suprascarpa's layer was the most significant

finding on preoperative CTA that correlated with the broadest perfusion patterns (diffuse and co-dominant) and larger perfusion areas. This linking vessel may be an inter-row, intra-row or combination, or may be a linking vessel to the lateral or adjacent territory, however the SIEA and microvasculature could not be assessed as accurately on the preoperative imaging.

In the anatomical studies, BMI also positively correlated with larger perforasome ($p<0.01$) of single perforators. Interestingly when medial versus lateral row perforators were compared separately, the correlation of BMI and total perforasome area showed that only the lateral row perforators demonstrated strong positive linear relationship of a greater perforasome with increased BMI ($p<0.01$). Further study of amalgamation of similar data will help to confirm this finding was not by chance. The clinical application of this would be the preferential selection of a large lateral perforator, when possible, in higher BMI patient. It was also seen that there was evidence of a strong positive linear correlation between increasing BMI and total number of significant perforators (>0.5mm), ($p<0.01$). In our anatomical studies, it has been identified that the harvest of a lateral row perforator may be preferential for safer flap harvest and a more robust flap. Although our anatomical studies only reviewed perforasomes of single perforators, in a clinical setting when operating on patients with a high BMI, or with a large volume flap harvest, if there is concern for vascularity of the flap we have identified that there is usually a higher number of significant perforators available that could be concurrently harvested.

This highlights an important clinical feature, where it has been shown that obesity can increase complications and incidence of fat necrosis in DIEP flap harvest. (195) In obese patients, the increased risk of complications has been attributed to poorer blood supply and it has been suggested that additional perforator harvest would reduce overall complications by providing a more robust blood supply(196), although there has been discord with this theory.(180) In our clinical study, we demonstrated that hemi-DIEP flaps were harvested safely on single dominant perforators and our average patient BMI was 29 (SD=5.6) with a mean flap weight of 691.4 grams. This is analogous to our previously published clinical experience. (182) These flaps were predominantly raised on a dominant medial row

perforator. The evidence in the setting of obesity on perforator choice, or harvest of additional perforators is largely anecdotal based on associations of risk factors in clinical case series. Determination of tissue volume, perforasomes and need for additional perforators in the setting of larger flap volumes needs further study.

The next stage in characterizing the dynamic perforasome of the DIEA in breast reconstruction is how this translates to complications and outcomes in patients. The fundamental understanding of how anatomy may be predictive of flap perfusion would potentially improve the reliability and safety in flap harvest. The use of ICGFA intraoperatively is used in conjunction with clinical judgement with regards to evaluating areas of hypoperfusion that were subsequently resected. The presence of sluggish inflow on analysis of the ICG angiographic curves was significantly related to the incidence of any complication ($p=0.03$). it is appreciated that the risks of complications and morbidity associated with DIEP breast reconstruction is multifactorial, including technical, blood supply and patient factors. This clinical study could not appreciate differences in perfusion types and intraoperative complications, nor postoperative complications such as fat necrosis. The subscarpa's region has been considered the areas of increased risk of fat necrosis. This region is harder to assess using LA-ICGFA when there is limited penetration of the superficial tissue. Therefore, there is limitation of this technology and analysis performed in this research and the ability to assess areas of increased risk of hypoperfusion in a three-dimensional unit. On the other hand, in a clinical setting, assessment of the deep aspects of the flap are often assessed intraoperatively by turning over the flap and objectively evaluating hypoperfusion. However, these actions limit quantitative analysis of the flap and can affect results in the assessment of dynamic perforasomes, which was the primary goal for the research.

Furthermore, complications such as venous congestion are more common than arterial based problems. The understanding of venous anatomy and dynamic venosomes lags further behind its arterial counterparts Study of venous anatomy and perfusion may have more impact on complications of DIEP flap reconstruction and highlights the next stage of research that is required to expand our knowledge and understanding. A larger prospective

clinical study is required to assess the impact of dynamic perforasomes/venosomes on complications, but in addition, a consistent protocol in the reporting and detection of complications, e.g. fat necrosis is required. This will be truly the most translational aspect of the research to assist in flap planning, design, harvest and minimizing complications and increase the predictability and reliability of DIEP flap reconstruction.

In summary in-vivo quantitative and qualitative analysis has identified that the dynamic perforasome of single dominant DIEP flaps are unique compared to musculocutaneous flaps. A step has been made in a new direction to evaluate the "dynamic perforasomes" of perforator flaps. This research attempted to identify some key features on preoperative CTA that would help predict the resulting perfusion pattern and perfusion area.

In the first steps of my PhD thesis the research established concepts to better understand the perforasome or dynamic perforasome in hemi-DIEP flaps for bilateral breast reconstruction, and potential patterns to optimize flap harvest based on the available anatomy. Optimizing blood supply through better understanding of the anatomy and correlation with flap physiology of a perforator flap is fundamental to the success of surgery and reducing morbidity from flap complications. In addition, this research subsequently touched upon the concepts to augment flap vascularity and physiology that may have important clinical applications. The **aim** of this part of the research was to determine if negative pressure wound therapy (NPWT) pre-treatment can be used for perforator flap preconditioning and augment flap vascularity.

5.2 Topical Negative Pressure Pre-treatment and Implications on Flap Vascularity

5.2.1 The Concept of Delay and Pre-conditioning Flaps

The use of traditional surgical delay and ischemic preconditioning that can be applied prior to flap surgery in order to improve survival help to adapt tissue to the subsequent stress of the surgery by improving overall tissue tolerance through increased vascularity and cellular

or signalling pathway modifications. (20) Vascular delay is a well-recognized method of increasing vascularity in pedicled flap and has been a technique studied in numerous experimental studies in animals(118–124) and used clinically(125–127). This manoeuvre promotes hypertrophy and reorganization of vessels to promote axiality of flow along the length of the flap (128) and has been used in the harvest of transverse rectus abdominis myocutaneous (TRAM) flaps for breast reconstruction(125,126,129,130).

Ischemia is a condition of inadequate blood flow to a specific tissue area and when this outruns the tolerance of the tissue implied, there is subsequent inflammation and development of necrosis in addition to a cascade of cellular events following reperfusion that may further increased tissue damage. (172) Ischemia-reperfusion injury always occurs when a free flap is transferred from one region to another and cannot be prevented. It has been shown that ischemic preconditioning can significantly reduce partial necrosis areas caused by ischemia-induced reperfusion injury in skin and myocutaneous flaps with improvement in the survival areas of two to five times those of non-preconditioned flaps (29) The implications of greater vascularity and improved survival(20,116) may permit free fasciocutaneous flaps to be constructed with larger volumes and lower the incidence of partial flap loss if they are preconditioned before transfer. There has been evidence in experimental models that preconditioning can extend critical ischemia time, which represents the time for the onset of 50% flap necrosis (29).

The morbidity of traditional approaches of vascular delay and ischemic preconditioning and additional healthcare costs has stimulated research to identify more elegant approaches that may mimic preconditioning strategies. Numerous pharmacological and alternative strategies have been evaluated in experimental models with very limited translation to clinical applications. Tissue expansion has been described as a form of surgical manipulation that has successfully been adopted into clinical practice and demonstrated changes in microvascular perfusion through the dilation of choke or linking vessels and reorientation of the microvasculature when used as a pre-treatment approach.(156) Although this approach has been used in the clinically setting, it is not always a feasible approach depending on the local environment and is associated with risk of an additional surgical procedure and tissue

expander insertion. Non-invasive strategies ideally would avoid any systemic effects, not increase patient morbidity, be safe and can be applied to the locally to tissue.

5.2.2 Biological Mechanisms of Negative Pressure Wound Therapy

Negative pressure wound therapy (NPWT) is well established in clinical practice over the last 20 years (197,198) as an adjunct in wound management. The biological mechanisms of action although not fully understood are based on the result of chemical and mechanical changes that lead to increase blood flow, formation of more physiological blood vessels(151,199) improved angiogenesis, improved vascularity, capillary density, (146) cell proliferation, local immune modulation (138,140,141,198–200) and can promote circulating stem cells into the wound bed(201). Current knowledge indicates that NPWT can improve vascularization in wound healing both within clinical studies and experimental animal models demonstrating increased perfusion to the wound; fluid removal; (145) stimulation of cellular proliferation, and macrodeformations promoting wound size reduction and maintenance of wound homeostasis. (138) Despite the extensive research that has been carried out in basic science models and clinical practice, there is still a deficiency of large randomized controlled trial and a knowledge gap in underlying biological mechanisms.

Angiogenesis is an intricate process involving the interaction of multiple genes expressed by a variety of cell types that interact in a complex process. Hypoxia is thought to pay a pivotal role as a regulator for the expression of Hypoxia Induced Factor (HIF) 1-alpha, and the physical interactions between cells and extracellular matrix and angiogenic factors including VEGF. (144,148,149) Cells are able to sense mechanical forces may respond through the regulation of specific genes and different interaction pathways(141). Microdeformational transduction forces can influence the microenvironment and stimulate transcriptional cellular mechanisms that controls angiogenesis, but these underlying mechanisms are still generally poorly understood. (149) In experimental models mechanical strain can induce vascular modelling and promote

angiogenesis through increased vessel density, epidermal proliferation and hyperplasia, and increased expression of HIF-1alpha and related angiogenic factors such as VEGF (143,151) that are considered essential in normal blood vessel development and angiogenesis.

There has been comparison of “external volume expansion” and “cupping techniques to apply a negative pressure to wound which have demonstrated similar effects of cellular proliferation and vessel remodelling.(202) The mechanism for this action is based on mechanical stretch. This is considered in contrast to the use of NPWT, which has been described to paradoxically exhibit a positive tissue pressure to the applied area although this effect becomes less pronounced over time.(203) However negative pressure through foam mediated external suction has been shown to create mechanical strain at a cellular level, distributed across the surface, and promote cellular proliferation and vascular remodelling. (144)

5.2.3 The Role of Negative Pressure Wound Therapy Pre-Treatment in Flap Surgery

In our study, the dynamic perfusion studies using 4D CTA and LA-ICGFA captured with SPY® Elite system has shown that flaps preconditioned with NPWT prior to flap harvest consistently demonstrated a better perfusion ratio and rate of inflow compared to controls. This effect was the smallest during flap harvest. At 7 days post flap surgery, there was still evidence of increased dynamic perfusion in the NPWT treated group. Evaluation of static microvessel density assessment on histology and micro-CT demonstrated a notable increase in NPWT pre-treated flaps in vessel volume. This was statistically significant immediately following removal of NPWT and the trend was evident at day 14, seven days following flap surgery, although this did not reach statistical significance on micro-CT or histology, therefore at a structural level. There was increased epidermal thickness in NPWT pre-treated flaps, and qualitatively improved collagen rearrangement within the dermis, although further staining techniques or Western blot analysis with quantification for collagen and elastin would be required to determine histological changes.

This research has provided an initial basis for further research but has recognized limitations. The use of control and intervention flaps was thought to assist to improve the power of the study, however with the loss of some data acquisition points during the study and consideration that outcomes compared histological, micro-CT and dynamic imaging technologies, the power of the sample or final results overall may have been insufficient for all study modalities to achieve statistical significance if a true difference exists. However, the trends towards a significant difference or significant differences shown between NPWT and control groups across all modalities were consistent to infer that there is an improvement in flap vascularity with NPWT pre-treatment.

Although the role of NPWT in as a pre-treatment to improve flap survival was among the original experiments described by Morykwas (1997), there has been limited evaluation of its role to augment flap vascularity in subsequent years and specifically for perforator flaps (147,150,153,154,156,202). Their group demonstrated in their limited sample that there was a statistically significant improvement in the use of NPWT in flap survival based on flap necrosis when applied in the pre- and post-treatment, pre-treatment only and post-treatment only compared to control flaps, although no statistical difference among these three intervention groups. (156). It has been shown to reduce surrounding tissue oedema, permit the egress of inhibitory factors and toxins and improve capillary afterload and microcirculation. The potential however to treat compromised tissues with a modality such as NPWT that can be applied to a limited area, pre- and post-flap surgery, may have a greater value than more elaborate interventions and pharmacological agents.

5.3 Limitations

It is acknowledged that anatomical studies of perforasomes cannot mimic the in-vivo conditions of flap physiology. However, the assessment and use of 4D CTA provides more dynamic assessment of the individual dynamic perforasome. Our studies to correlate with previously published literature and provided some additional new information on perforasome characteristics in the hemi-abdomen and evaluation from the perspective of

bilateral breast reconstructions which has not been previously addressed. Anatomical studies were based on injection of single perforators and therefore a dedicated study to evaluate the impact of additional perforators in the flap harvest has not been performed to determine impact on flap perfusion.

The use of LA-ICGFA can allow one to visualize and qualitatively assess the flow of ICG into the flap. However, in this PhD thesis research we developed new protocols for a non-biased assessment and quantitative analysis of the dynamic perforasome measured throughout the arterial and microcirculatory phases instead of a single time point. We were also able to measure relative flap perfusions in relation to the total flap area as the ROI. This was a novel approach to perforator flap assessment with LA-ICGFA and proprietary software therefore our approach and methodology has not been validated, but followed a systematic approach and provided a foundation for further studies. The assessment and categorization of perforasome categories were based on qualitative analysis by myself and Dr M Saint-Cyr. This type of assessment of the dynamic perforasome based on the timing maps is a novel concept and based on a limited sample of flaps, and with a larger prospective sample, it may be found that other patterns arise and this could potentially lead to different results. However, with the 44 available flaps, we identified among single medial row perforators, there were three broad classifications of the dynamic perforasome, single, co-dominant and diffuse, based on hot spots of rate of flow into the flap. However, there were insufficient data to apply this to lateral row perforators or the inclusion of multiple perforators within the DIEP flap, but this would be an area to further expand the study.

Correlation of ICGFA analysis and the microvasculature as assessed on preoperative CTA was performed through a rudimentary analysis using maximal projection imaging reconstructions of the DIEA protocol. 3D reconstructions of the microvasculature were not performed to quantify or validate the analysis performed using available software, and this was largely related to the time intensive task of processing and ensuring accurate mapping is attained. However, the semi-quantitative analysis performed would have been expected to provide a baseline and indication of the underlying patterns, and would provide a more translatable approach that can be used in clinical practice in DIEP breast reconstruction.

However, we understand the limitation is based on a degree of subjectivity and that an accurate 3D reconstruction would have better validated the findings. Evaluation of the microvasculature connected to the SIEA territory was not consistently reliable to trace in preoperative CTA and this may be related to the methodology of performing the CTA in patients based on detection of blood flow in the femoral artery following contrast administration. A methodical characterization or classification of the microvasculature of the DIEP flap has not been previously described or used in routine reporting. It is recognized that full analysis of patient CTA images was performed by myself, and although approaches were discussed with an expert Consultant Radiologist, it is acknowledged that this is an area of bias. Collaborating in future work with Radiologists, may allow a way to classify and characterize the microvasculature and linking vessels from a dominant perforator and it would be important to test inter-reviewer reliability in scoring systems following assessment to improve reliability and accuracy of the reporting.

In the animal study, for this PhD research new protocols were developed for dynamic imaging using 4D CTA and ICG-LA and their subsequent analysis. Both these modalities required adequate intravenous access for administration of the contrast or dye and this sometimes led to failed acquisition of data points if access was lost and we did not want to increase morbidity with a central venous cut-down procedure which has been previously described. Failed injection of contrast in the imaging modality assessments led to incomplete data acquisition points. However, at every time point and with every modality each intervention was perfectly matched to the control flap, which improved the validity of the results obtained with additional confounding factors eliminated. Another limitation may have been the flap size to assess flap survival. A perforator flap that was extended in length to induce flap necrosis at the tip would allow a comparison of the impact of NPWT pre-treatment in the area of ischemia and provide a better comparison of flap survival. Although 400-500g male rats were used in this study, there is still possibility that there was an influence of the NPWT to the surrounding tissue, which may have included the area of the control flap, and may explain some of the results seen. However, there are previous studied that have applied similar techniques in small rodent models successfully. (147,154,202) Therefore, a larger animal model would be more beneficial to study this flap model or the

use of a larger sample size, but this would then have to be sufficient to account for physiological variability seen between animals when conducting dynamic imaging studies to reliably compare the data.

5.4 General Conclusions

- Anatomical methods and use of advanced imaging technologies including 4D CTA can evaluate dynamic perforator territories and assess the distribution and early capture of dominant linking vessels on perfusion of the DIEA perforator in the hemi-abdomen.
- Medial row perforators and those within 5cm of the umbilicus may be of larger calibre, but for perfusion of the hemi-abdomen, lateral row perforators significantly lateralized their perforasome distribution in anatomical studies.
- The early capture and direct communication and recurrent flow within vessels in the SIEA territory correlated to broader perforasome territories.
- The dynamics of the microcirculation of an individual perforator in DIEP flaps are unique and do not reflect the traditional concepts of perfusion of the lower abdominal tissue based on TRAM flaps.
- The dynamic perforasome as observed in-vivo using LA-ICGFA exhibited variation in perforasome perfusion even when based on a single medial row perforator that can be broadly characterized qualitatively: single, co-dominant and diffuse patterns based on hot spots of within hemi-DIEP flaps.
- Evaluation of the dynamic perforasome based on timing maps was a better predictor for identifying perforators and assessment of inter-perforator connections.
- The diffuse dynamic DIEP perforasome correlated with presence of a dominant large calibre direct linking vessel in the supra-scarpa's layer, and higher degree of inter-row and intra-row linking vessels. Diffuse pattern perforasomes were also associated with the highest robust perfusion areas of hemi-DIEP flaps, that may be related to the microvascular anatomy in the suprascarpal are and contribution to the subdermal plexus.

5.5 Future Work

- 3D characterization of the 3D perforasome and anatomical architecture based around the dominant perforator used in the DIEP flap reconstruction. This may allow a more reliable assessment for linking vessels, and further quantification of density of linking vessels. However, individual mapping of the microvasculature is time consuming, therefore a more efficient approach to perforasome microvascular mapping in individual patients is required.
- Additional assessment and refinement in CTA reviewing methodology and validation of approaches used with intraoperative LA-ICGFA based on currently developed protocols. The goal would be to develop a classification system that summarizes and characterizes the patterns of direct and indirect communicating vessels that may allow better prediction of perfusion. In the absence of intra-operative imaging, we then may be able to subsequently identify key patterns for which we can better predict the physiological perfusion.
- Continue a prospective analysis in DIEP/MS-TRAM flaps with the goal to identify changes in patterns of perfusion and extend the current sample size and extend our analysis to multiple and lateral row perforator flaps.
- Evaluation of dynamic perforasomes of other flaps to develop a better understanding of the microcirculation of individual perforators in the human body.
- The exploration of the venous anatomy of hemi-DIEP breast reconstruction and assessment of dynamic venosomes using LA-ICGFA is an area that also requires simultaneous assessment. is an area that would also require a prospective clinical study to review venosomes, anatomy and determine correlation with intraoperative or post operatively complications.
- The use of a large animal model and longer flap length to width ratios to study the role of NPWT pre-treatment in augmentation of flap vascularity and reduce flap complications.
- The use of NPWT pre-treatment to augment flap vascularity in the context of breast reconstruction patients. This may have a particular role in mastectomy skin flaps, or patients who will undergo radiation treatment.

BIBLIOGRAPHY

1. Breast cancer incidence (invasive) statistics | Cancer Research UK [Internet]. [cited 2017 Jun 1]. Available from: http://www.cancerresearchuk.org/health-professional/cancer-statistics/statistics-by-cancer-type/breast-cancer/incidence-invasive
2. Cancer of the Breast (Female) - Cancer Stat Facts [Internet]. [cited 2017 Jun 1]. Available from: https://seer.cancer.gov/statfacts/html/breast.html
3. Breast Cancer Statistics | Breast Cancer Research Foundation [Internet]. [cited 2018 Mar 8]. Available from: https://www.bcrf.org/breast-cancer-statistics
4. American Cancer Society. Breast Cancer Facts & Figures 2017-2018 [Internet]. American Cancer Society. Breast Cancer Facts & Figures 2017-2018. Atlanta: American Cancer Society, Inc. 2017. 2017 [cited 2018 Mar 8]. Available from: https://www.cancer.org/content/dam/cancer-org/research/cancer-facts-and-statistics/breast-cancer-facts-and-figures/breast-cancer-facts-and-figures-2017-2018.pdf
5. Cromwell D, Browne J, Van Der Meulen J. Fourth annual report of the national mastectomy and breast reconstruction audit [Internet]. Leeds; 2011 [cited 2018 Mar 8]. Available from: http://www.rcseng.ac.uk/surgeons/research/surgical-research/docs/national-mastectomy-and-breast-reconstruction-audit-fourth-report-2011
6. Steiner CA, Weiss AJ, Barrett ML, Fingar KR, Davis PH. Trends in Bilateral and Unilateral Mastectomies in Hospital Inpatient and Ambulatory Settings, 2005–2013. 2013 [cited 2018 Mar 8]; Available from: https://www.hcup-us.ahrq.gov/reports/statbriefs/sb201-Mastectomies-Inpatient-Outpatient.pdf?utm_source=AHRQ&utm_medium=PressRelease&utm_content=1&utm_term=18&utm_campaign=AHRQ_MIG
7. Healy C, Allen RJ. The evolution of perforator flap breast reconstruction: twenty years after the first DIEP flap. J Reconstr Microsurg [Internet]. 2014 Mar 25 [cited 2015 Oct 31];30(2):121–5. Available from: https://www.thieme-connect.com/DOI/DOI?10.1055/s-0033-1357272
8. Angelos P, Bedrosian I, Euhus DM, Herrmann VM, Katz SJ, Pusic A. Contralateral Prophylactic Mastectomy: Challenging Considerations for the Surgeon. Ann Surg

Oncol [Internet]. 2015 Oct [cited 2018 Mar 8];22(10):3208–12. Available from: http://www.ncbi.nlm.nih.gov/pubmed/26259752

9. Kurian AW, Lichtensztajn DY, Keegan THM, Nelson DO, Clarke CA, Gomez SL. Use of and Mortality After Bilateral Mastectomy Compared With Other Surgical Treatments for Breast Cancer in California, 1998-2011. JAMA [Internet]. 2014 Sep 3 [cited 2018 Mar 8];312(9):902. Available from: http://www.ncbi.nlm.nih.gov/pubmed/25182099
10. Neuburger J, Macneill F, Jeevan R, van der Meulen JHP, Cromwell DA. Trends in the use of bilateral mastectomy in England from 2002 to 2011: retrospective analysis of hospital episode statistics. BMJ Open [Internet]. 2013 Aug 1 [cited 2018 Mar 8];3(8):e003179. Available from: http://www.ncbi.nlm.nih.gov/pubmed/23906951
11. Boughey JC, Attai DJ, Chen SL, Cody HS, Dietz JR, Feldman SM, et al. Contralateral Prophylactic Mastectomy (CPM) Consensus Statement from the American Society of Breast Surgeons: Data on CPM Outcomes and Risks. [cited 2018 Mar 8]; Available from: https://associationofbreastsurgery.org.uk/media/1421/contralateral-prophylactic-mastctomy-consensus-stamte-from-the-american-society-of-breast-surgeons-data-on-cpm-outcomes-and-risks.pdf
12. Jeevan R, Cromwell DA, Browne JP, Caddy CM, Pereira J, Sheppard C, et al. Findings of a national comparative audit of mastectomy and breast reconstruction surgery in England. J Plast Reconstr Aesthetic Surg [Internet]. 2014 Oct 1 [cited 2018 Mar 8];67(10):1333–44. Available from: https://www.sciencedirect.com/science/article/pii/S1748681514002009?_rdoc=1
13. Atisha D, Alderman AK, Lowery JC, Kuhn LE, Davis J, Wilkins EG. Prospective Analysis of Long-term Psychosocial Outcomes in Breast Reconstruction. Ann Surg [Internet]. 2008 Jun [cited 2018 Mar 8];247(6):1019–28. Available from: https://insights.ovid.com/crossref?an=00000658-200806000-00016
14. Tsoi B, Ziolkowski NI, Thoma A, Campbell K, O'Reilly D, Goeree R. Systematic Review on the Patient-Reported Outcomes of Tissue-Expander/Implant vs Autologous Abdominal Tissue Breast Reconstruction in Postmastectomy Breast Cancer Patients. J Am Coll Surg [Internet]. 2014 May 1 [cited 2018 Mar 8];218(5):1038–48. Available from: https://www.sciencedirect.com/science/article/pii/S1072751514001409?_rdoc=1&_f

mt=high&_origin=gateway&_docanchor=&md5=b8429449ccfc9c30159a5f9aeaa92ffb#bib10

15. Levine SM, Lester ME, Fontenot B, Allen RJ. Perforator flap breast reconstruction after unsatisfactory implant reconstruction. Ann Plast Surg [Internet]. 2011 May [cited 2015 Apr 28];66(5):513–7. Available from: http://www.ncbi.nlm.nih.gov/pubmed/21301299
16. Hamdi M, Andrades P, Thiessen F, Stillaert F, Roche N, Van Landuyt K, et al. Is a second free flap still an option in a failed free flap breast reconstruction? Plast Reconstr Surg [Internet]. 2010 Aug [cited 2015 Apr 28];126(2):375–84. Available from: http://www.ncbi.nlm.nih.gov/pubmed/20679823
17. Rahmanian-Schwarz A, Rothenberger J, Hirt B, Luz O, Schaller H-E. A combined anatomical and clinical study for quantitative analysis of the microcirculation in the classic perfusion zones of the deep inferior epigastric artery perforator flap. Plast Reconstr Surg. 2011;127(2):505–13.
18. Hartrampf CR, Scheflan M, Black PW. Breast reconstruction with a transverse abdominal island flap. Plast Reconstr Surg [Internet]. 1982 Feb [cited 2015 Apr 28];69(2):216–25. Available from: http://www.ncbi.nlm.nih.gov/pubmed/6459602
19. Wong C, Saint-Cyr M, Arbique G, Becker S, Brown S, Myers S, et al. Three- and four-dimensional computed tomography angiographic studies of commonly used abdominal flaps in breast reconstruction. Plast Reconstr Surg [Internet]. 2009 Jul [cited 2015 Mar 3];124(1):18–27. Available from: http://www.ncbi.nlm.nih.gov/pubmed/19568040
20. Ghali S, Butler PEM, Tepper OM, Gurtner GC. Vascular delay revisited. Plast Reconstr Surg [Internet]. 2007 May [cited 2016 Dec 12];119(6):1735–44. Available from: http://www.ncbi.nlm.nih.gov/pubmed/17440348
21. Figus A, Mosahebi A, Ramakrishnan V. Microcirculation in DIEP flaps: a study of the haemodynamics using laser Doppler flowmetry and lightguide reflectance spectrophotometry. J Plast Reconstr Aesthet Surg [Internet]. 2006 Jun [cited 2017 May 31];59(6):604–12; discussion 613. Available from: http://linkinghub.elsevier.com/retrieve/pii/S1748681506000428
22. Andrades P, Fix RJ, Danilla S, Howell RE, Campbell WJ, De la Torre J, et al. Ischemic

complications in pedicle, free, and muscle sparing transverse rectus abdominis myocutaneous flaps for breast reconstruction. Ann Plast Surg [Internet]. 2008 May [cited 2017 May 31];60(5):562–7. Available from: http://content.wkhealth.com/linkback/openurl?sid=WKPTLP:landingpage&an=00000637-200805000-00017

23. Newman MI, Samson MC, Tamburrino JF, Swartz KA, Brunworth L. An investigation of the application of laser-assisted indocyanine green fluorescent dye angiography in pedicle transverse rectus abdominus myocutaneous breast reconstruction. Can J Plast Surg [Internet]. 2011 Jan [cited 2015 Nov 2];19(1):e1-5. Available from: http://www.pubmedcentral.nih.gov/articlerender.fcgi?artid=3086506&tool=pmcentrez&rendertype=abstract
24. Ducic I, Spear SL, Cuoco F, Hannan C. Safety and risk factors for breast reconstruction with pedicled transverse rectus abdominis musculocutaneous flaps: a 10-year analysis. Ann Plast Surg [Internet]. 2005 Dec [cited 2017 May 31];55(6):559–64. Available from: http://www.ncbi.nlm.nih.gov/pubmed/16327450
25. Saint-Cyr M, Wong C, Schaverien M, Mojallal A, Rohrich RJ. The perforasome theory: vascular anatomy and clinical implications. Plast Reconstr Surg [Internet]. 2009 Nov [cited 2015 Apr 28];124(5):1529–44. Available from: http://www.ncbi.nlm.nih.gov/pubmed/20009839
26. Wong C, Saint-Cyr M, Mojallal A, Schaub T, Bailey SH, Myers S, et al. Perforasomes of the DIEP flap: vascular anatomy of the lateral versus medial row perforators and clinical implications. Plast Reconstr Surg [Internet]. 2010 Mar [cited 2015 Apr 28];125(3):772–82. Available from: http://www.ncbi.nlm.nih.gov/pubmed/20195105
27. Bailey SH, Saint-Cyr M, Wong C, Mojallal A, Zhang K, Ouyang D, et al. The single dominant medial row perforator DIEP flap in breast reconstruction: three-dimensional perforasome and clinical results. Plast Reconstr Surg [Internet]. 2010 Sep [cited 2015 Apr 12];126(3):739–51. Available from: http://www.ncbi.nlm.nih.gov/pubmed/20811209
28. Schaverien M, Saint-Cyr M, Arbique G, Brown SA. Arterial and venous anatomies of the deep inferior epigastric perforator and superficial inferior epigastric artery flaps. Plast Reconstr Surg [Internet]. 2008 Jun [cited 2015 Mar 2];121(6):1909–19. Available

from: http://www.ncbi.nlm.nih.gov/pubmed/18520876

29. Zahir KS, Syed SA, Zink JR, Restifo RJ, Thomson JG. Ischemic preconditioning improves the survival of skin and myocutaneous flaps in a rat model. Plast Reconstr Surg [Internet]. 1998 Jul [cited 2017 May 29];102(1):140–50; discussion 151-2. Available from: http://www.ncbi.nlm.nih.gov/pubmed/9655419
30. Gillies Harold, Jr MD. The Principles and Art of Plastic Surgery. First. Boston, MA: Little, Brown & Co; 1957.
31. Milton SH. Experimental studies on island flaps. 1. The surviving length. Plast Reconstr Surg [Internet]. 1971 Dec [cited 2015 May 19];48(6):574–8. Available from: http://www.ncbi.nlm.nih.gov/pubmed/4946647
32. Cormack GC, Lamberty BGH. The Arterial Anatomy of Skin Flaps [Internet]. Churchill Livingstone; 1994 [cited 2015 Mar 26]. 538 p. Available from: http://books.google.co.uk/books/about/The_Arterial_Anatomy_of_Skin_Flaps.html?id=OxV0QgAACAAJ&pgis=1
33. Taylor GI, Palmer JH. The vascular territories (angiosomes) of the body: experimental study and clinical applications. Br J Plast Surg [Internet]. 1987 Mar 3 [cited 2015 Mar 25];40(2):113–41. Available from: http://www.jprasurg.com/article/0007122687901858/fulltext
34. Morris SF, Tang M, Almutari K, Geddes C, Yang D. The anatomic basis of perforator flaps. Clin Plast Surg [Internet]. 2010 Oct [cited 2015 May 24];37(4):553–70, xi. Available from: http://www.ncbi.nlm.nih.gov/pubmed/20816512
35. Manchot C. The Cutaneous Arteries of the Human Body by C. Manchot | 9781461382232 | Paperback | Barnes & Noble [Internet]. 18th ed. New York: Springer-Verlag; 1983 [cited 2015 Mar 26]. Available from: http://www.barnesandnoble.com/w/the-cutaneous-arteries-of-the-human-body-c-manchot/1013597316?ean=9781461382232
36. Salmon M. Artères de la peau [Internet]. Masson; 1936 [cited 2015 Mar 26]. 246 p. Available from: http://books.google.co.uk/books/about/Artères_de_la_peau.html?id=8d81NAAACAAJ&pgis=1
37. Pontén B. The fasciocutaneous flap: its use in soft tissue defects of the lower leg. Br J

Plast Surg [Internet]. 1981 Apr [cited 2015 Jun 3];34(2):215–20. Available from: http://www.ncbi.nlm.nih.gov/pubmed/7236984

38. Saint-Cyr M, Schaverien M, Arbique G, Hatef D, Brown SA, Rohrich RJ. Three- and four-dimensional computed tomographic angiography and venography for the investigation of the vascular anatomy and perfusion of perforator flaps. Plast Reconstr Surg [Internet]. 2008 Mar [cited 2015 Mar 4];121(3):772–80. Available from: http://www.ncbi.nlm.nih.gov/pubmed/18317127
39. Schaverien M, Saint-Cyr M, Arbique G, Brown SA. Arterial and venous anatomies of the deep inferior epigastric perforator and superficial inferior epigastric artery flaps. Plast Reconstr Surg. 2008;121(6):1909–19.
40. Saint-Cyr M. Assessing perforator architecture. Clin Plast Surg [Internet]. 2011 Apr [cited 2015 Apr 28];38(2):175–202. Available from: http://www.ncbi.nlm.nih.gov/pubmed/21620144
41. McGregor IA, Morgan G. Axial and random pattern flaps. Br J Plast Surg [Internet]. 1973 Jul [cited 2015 Apr 28];26(3):202–13. Available from: http://www.ncbi.nlm.nih.gov/pubmed/4580012
42. Boyd JB, Taylor GI, Corlett R. The vascular territories of the superior epigastric and the deep inferior epigastric systems. Plast Reconstr Surg [Internet]. 1984 Jan [cited 2018 Apr 7];73(1):1–16. Available from: http://www.ncbi.nlm.nih.gov/pubmed/6197716
43. Koshima I, Soeda S. Inferior epigastric artery skin flaps without rectus abdominis muscle. Vol. 42, British journal of plastic surgery. 1989. p. 645–8.
44. Allen RJ, Treece P. Deep inferior epigastric perforator flap for breast reconstruction. Ann Plast Surg [Internet]. 1994 Jan [cited 2015 Apr 28];32(1):32–8. Available from: http://www.ncbi.nlm.nih.gov/pubmed/8141534
45. Taylor G, Watterson P, Zelt R. The Vascular Anatomy of the Anterior Abdominal Wall: The Basis for Flap Design. Semin Plast Surg [Internet]. 2008 Jun 19 [cited 2016 Feb 9];5(01):1–28. Available from: https://www-thieme-connect-de.libproxy.ucl.ac.uk/products/ejournals/html/10.1055/s-2008-1080410
46. Moon HK, Taylor GI. The vascular anatomy of rectus abdominis musculocutaneous flaps based on the deep superior epigastric system. Plast Reconstr Surg [Internet]. 1988 Nov [cited 2015 Apr 28];82(5):815–32. Available from:

http://www.ncbi.nlm.nih.gov/pubmed/2971981

47. Ireton JE, Lakhiani C, Saint-Cyr M. Vascular anatomy of the deep inferior epigastric artery perforator flap: a systematic review. Plast Reconstr Surg [Internet]. 2014 Nov [cited 2015 Apr 28];134(5):810e-821e. Available from: http://www.ncbi.nlm.nih.gov/pubmed/25347657
48. Whitaker IS, Rozen WM, Smit JM, Dimopoulou A, Ashton MW, Acosta R. Peritoneo-cutaneous perforators in deep inferior epigastric perforator flaps: a cadaveric dissection and computed tomographic angiography study. Microsurgery [Internet]. 2009 Jan [cited 2015 Apr 28];29(2):124–7. Available from: http://www.ncbi.nlm.nih.gov/pubmed/19021231
49. Rozen WM, Ashton MW, Taylor GI. Reviewing the vascular supply of the anterior abdominal wall: redefining anatomy for increasingly refined surgery. Clin Anat [Internet]. 2008 Mar [cited 2015 Oct 31];21(2):89–98. Available from: http://www.ncbi.nlm.nih.gov/pubmed/18189276
50. Kikuchi N, Murakami G, Kashiwa H, Homma K, Sato TJ, Ogino T. Morphometrical study of the arterial perforators of the deep inferior epigastric perforator flap. Surg Radiol Anat [Internet]. 2001 Jan [cited 2015 Apr 28];23(6):375–81. Available from: http://www.ncbi.nlm.nih.gov/pubmed/11963619
51. Rozen WM, Chubb D, Ashton MW, Grinsell D. Macrovascular arteriovenous shunts (MAS): a newly identified structure in the abdominal wall with implications for thermoregulation and free tissue transfer. J Plast Reconstr Aesthet Surg [Internet]. 2010 Aug [cited 2015 Mar 3];63(8):1294–9. Available from: http://www.ncbi.nlm.nih.gov/pubmed/19577528
52. Taylor GI, Corlett R, Boyd JB. The extended deep inferior epigastric flap: a clinical technique. Plast Reconstr Surg [Internet]. 1983 Dec [cited 2016 Feb 9];72(6):751–65. Available from: http://www.ncbi.nlm.nih.gov/pubmed/6647599
53. Scheflan M, Dinner MI. The transverse abdominal island flap: part I. Indications, contraindications, results, and complications. Ann Plast Surg [Internet]. 1983 Jan [cited 2015 Apr 28];10(1):24–35. Available from: http://www.ncbi.nlm.nih.gov/pubmed/6219607
54. Scheflan M, Dinner MI. The transverse abdominal island flap: Part II. Surgical

technique. Ann Plast Surg [Internet]. 1983 Feb [cited 2015 Apr 28];10(2):120–9. Available from: http://www.ncbi.nlm.nih.gov/pubmed/6838117

55. Holm C, Mayr M, Höfter E, Ninkovic M. Perfusion zones of the DIEP flap revisited: a clinical study. Plast Reconstr Surg [Internet]. 2006 Jan [cited 2015 Mar 3];117(1):37–43. Available from: http://www.ncbi.nlm.nih.gov/pubmed/16404245

56. Dinner MI, Dowden R V, Scheflan M. Refinements in the use of the transverse abdominal island flap for postmastectomy reconstruction. Ann Plast Surg [Internet]. 1983 Nov [cited 2018 Apr 12];11(5):362–72. Available from: http://www.ncbi.nlm.nih.gov/pubmed/6228179

57. Rozen WM, Ashton MW, Le Roux CM, Pan W-R, Corlett RJ. The perforator angiosome: a new concept in the design of deep inferior epigastric artery perforator flaps for breast reconstruction. Microsurgery [Internet]. 2010 Jan [cited 2015 Mar 2];30(1):1–7. Available from: http://www.ncbi.nlm.nih.gov/pubmed/19582823

58. Laungani AT, Van Alphen N, Christner JA, Lachman N, Pawlina W, Ballman K V, et al. Three-dimensional CT angiography assessment of the impact of the dermis and the subdermal plexus in DIEP flap perfusion. J Plast Reconstr Aesthet Surg [Internet]. 2015 Jan 7 [cited 2015 Mar 2]; Available from: http://www.sciencedirect.com/science/article/pii/S1748681514007062

59. Blondeel PN. One hundred free DIEP flap breast reconstructions: a personal experience. Br J Plast Surg [Internet]. 1999 Mar [cited 2015 Apr 28];52(2):104–11. Available from: http://www.ncbi.nlm.nih.gov/pubmed/10434888

60. Alonso-Burgos A, García-Tutor E, Bastarrika G, Cano D, Martínez-Cuesta A, Pina LJ. Preoperative planning of deep inferior epigastric artery perforator flap reconstruction with multislice-CT angiography: imaging findings and initial experience. J Plast Reconstr Aesthet Surg. 2006;59(6):585–93.

61. Masia J, Navarro C, Clavero JA, Alomar X. Noncontrast magnetic resonance imaging for preoperative perforator mapping. Clin Plast Surg [Internet]. 2011 Apr [cited 2015 Apr 19];38(2):253–61. Available from: http://www.ncbi.nlm.nih.gov/pubmed/21620150

62. Tregaskiss AP, Goodwin AN, Bright LD, Ziegler CH, Acland RD. Three-dimensional CT angiography: a new technique for imaging microvascular anatomy. Clin Anat

[Internet]. 2007 Mar [cited 2015 Oct 31];20(2):116–23. Available from: http://www.ncbi.nlm.nih.gov/pubmed/16795029

63. Mohan AT, Saint-Cyr M. Advances in imaging technologies for planning breast reconstruction. Gland Surg. 2016;5(2).

64. Rozen WM, Ashton MW, Grinsell D. The branching pattern of the deep inferior epigastric artery revisited in-vivo: A new classification based on CT angiography. Clin Anat [Internet]. 2009 Jan [cited 2015 Sep 30];23(1):NA-NA. Available from: http://www.ncbi.nlm.nih.gov/pubmed/19941357

65. Chan JWH, Wong C, Ward K, Saint-Cyr M, Chiu ES. Three- and four-dimensional computed tomographic angiography studies of the supraclavicular artery island flap. Plast Reconstr Surg [Internet]. 2010 Mar [cited 2015 Oct 31];125(2):525–31. Available from: http://www.ncbi.nlm.nih.gov/pubmed/20124838

66. Wong C, Saint-Cyr M, Rasko Y, Mojallal A, Bailey S, Myers S, et al. Three- and four-dimensional arterial and venous perforasomes of the internal mammary artery perforator flap. Plast Reconstr Surg [Internet]. 2009 Dec [cited 2015 Apr 19];124(6):1759–69. Available from: http://www.ncbi.nlm.nih.gov/pubmed/19952631

67. Xue J, Arbique G, Hatef D, Brown S, Saint-Cyr M, Gao JX. Four-Dimensional Vascular Tree Reconstruction Using Moving Grid Deformation. Acad Radiol [Internet]. 2007 Dec [cited 2015 Apr 19];14(12):1540–53. Available from: http://www.sciencedirect.com/science/article/pii/S1076633207003911

68. Sur YJ, Morsy M, Laungani AT, Saint-Cyr M. Three dimensional tomographic angiography of the lower leg: vascular structure and inter-perforator flow mechanism. In: 8th Congress of the World Society for Reconstructive Microsurgery, Mumbai March 2015. Mumbai, India; 2015.

69. Rozen WM, Ashton MW, Stella DL, Phillips TJ, Taylor GI. The accuracy of computed tomographic angiography for mapping the perforators of the DIEA: a cadaveric study. Plast Reconstr Surg [Internet]. 2008 Aug [cited 2015 Jun 28];122(2):363–9. Available from: http://www.ncbi.nlm.nih.gov/pubmed/18626351

70. Rozen WM, Chubb D, Whitaker IS, Grinsell D, Ashton MW. Deep inferior epigastric perforators do not correlate between sides of the body: the role for preoperative

imaging. J Plast Reconstr Aesthet Surg [Internet]. 2010 Dec [cited 2015 Nov 1];63(12):e842-3. Available from: http://www.ncbi.nlm.nih.gov/pubmed/20713316

71. Nahabedian MY. Overview of Perforator Imaging and Flap Perfusion Technologies. Clin Plast Surg [Internet]. 2011 Apr [cited 2015 Apr 19];38(2):165–74. Available from: http://www.ncbi.nlm.nih.gov/pubmed/21620143

72. Man L-X, Selber JC, Serletti JM. Abdominal wall following free TRAM or DIEP flap reconstruction: a meta-analysis and critical review. Plast Reconstr Surg [Internet]. 2009 Sep [cited 2015 Nov 1];124(3):752–64. Available from: http://www.ncbi.nlm.nih.gov/pubmed/19342994

73. Smit JM, Dimopoulou A, Liss AG, Zeebregts CJ, Kildal M, Whitaker IS, et al. Preoperative CT angiography reduces surgery time in perforator flap reconstruction. J Plast Reconstr Aesthet Surg [Internet]. 2009 Oct [cited 2015 Oct 31];62(9):1112–7. Available from: http://www.sciencedirect.com/science/article/pii/S1748681508004580

74. Giunta RE, Geisweid A, Feller AM. The value of preoperative Doppler sonography for planning free perforator flaps. Plast Reconstr Surg [Internet]. 2000 Jun [cited 2015 Nov 1];105(7):2381–6. Available from: http://www.ncbi.nlm.nih.gov/pubmed/10845290

75. Blondeel PN, Beyens G, Verhaeghe R, Van Landuyt K, Tonnard P, Monstrey SJ, et al. Doppler flowmetry in the planning of perforator flaps. Br J Plast Surg [Internet]. 1998 Apr [cited 2015 Nov 1];51(3):202–9. Available from: http://www.ncbi.nlm.nih.gov/pubmed/9664879

76. Berg WA, Chang BW, DeJong MR, Hamper UM. Color Doppler flow mapping of abdominal wall perforating arteries for transverse rectus abdominis myocutaneous flap in breast reconstruction: method and preliminary results. Radiology [Internet]. 1994 Aug [cited 2015 Nov 1];192(2):447–50. Available from: http://www.ncbi.nlm.nih.gov/pubmed/8029413

77. Chang BW, Luethke R, Berg WA, Hamper UM, Manson PN. Two-dimensional color Doppler imaging for precision preoperative mapping and size determination of TRAM flap perforators. Plast Reconstr Surg [Internet]. 1994 Jan [cited 2015 Nov 1];93(1):197–200. Available from: http://www.ncbi.nlm.nih.gov/pubmed/8278479

78. Keys KA, Louie O, Said HK, Neligan PC, Mathes DW. Clinical utility of CT angiography in DIEP breast reconstruction. J Plast Reconstr Aesthetic Surg [Internet]. 2013 Mar [cited 2015 Apr 19];66(3):e61–5. Available from: http://www.ncbi.nlm.nih.gov/pubmed/23084649

79. Cina A, Salgarello M, Barone-Adesi L, Rinaldi P, Bonomo L. Planning Breast Reconstruction with Deep Inferior Epigastric Artery Perforating Vessels: Multidetector CT Angiography versus Color Doppler US 1. Radiology [Internet]. 2010 Jun 1 [cited 2015 Apr 19];255(3):979–87. Available from: http://pubs.rsna.org/doi/abs/10.1148/radiol.10091166

80. Masia J, Clavero JA, Larrañaga JR, Alomar X, Pons G, Serret P. Multidetector-row computed tomography in the planning of abdominal perforator flaps. J Plast Reconstr Aesthet Surg [Internet]. 2006 Jan [cited 2015 Nov 1];59(6):594–9. Available from: http://www.ncbi.nlm.nih.gov/pubmed/16716952

81. Alonso-Burgos A, García-Tutor E, Bastarrika G, Cano D, Martínez-Cuesta A, Pina LJ. Preoperative planning of deep inferior epigastric artery perforator flap reconstruction with multislice-CT angiography: imaging findings and initial experience. J Plast Reconstr Aesthet Surg [Internet]. 2006 Jan [cited 2015 Oct 31];59(6):585–93. Available from: http://www.sciencedirect.com/science/article/pii/S1748681506000350

82. Masia J, Kosutic D, Clavero JA, Larranaga J, Vives L, Pons G. Preoperative computed tomographic angiogram for deep inferior epigastric artery perforator flap breast reconstruction. J Reconstr Microsurg [Internet]. 2010 Jan [cited 2015 Oct 31];26(1):21–8. Available from: http://www.scopus.com/inward/record.url?eid=2-s2.0-76649125536&partnerID=tZOtx3y1

83. Casey WJ, Chew RT, Rebecca AM, Smith AA, Collins JM, Pockaj BA. Advantages of preoperative computed tomography in deep inferior epigastric artery perforator flap breast reconstruction. Plast Reconstr Surg [Internet]. 2009 May [cited 2015 Oct 31];123(4):1148–55. Available from: http://www.ncbi.nlm.nih.gov/pubmed/19337083

84. Casey WJ, Rebecca AM, Kreymerman PA, Macias LH. Computed tomographic angiography: assessing outcomes. Clin Plast Surg [Internet]. 2011 Apr [cited 2015 Apr

19];38(2):241–52. Available from: http://www.sciencedirect.com/science/article/pii/S0094129811000125

85. Chae MP, Hunter-Smith DJ, Rozen WM. Comparative analysis of fluorescent angiography, computed tomographic angiography and magnetic resonance angiography for planning autologous breast reconstruction. Gland Surg [Internet]. 2015 Apr [cited 2015 Nov 1];4(2):164–78. Available from: http://www.pubmedcentral.nih.gov/articlerender.fcgi?artid=4409669&tool=pmcentrez&rendertype=abstract

86. Rozen WM, Garcia-Tutor E, Alonso-Burgos A, Acosta R, Stillaert F, Zubieta JL, et al. Planning and optimising DIEP flaps with virtual surgery: the Navarra experience. J Plast Reconstr Aesthet Surg [Internet]. 2010 Feb [cited 2015 Nov 1];63(2):289–97. Available from: http://www.ncbi.nlm.nih.gov/pubmed/19042174

87. Pacifico MD, See MS, Cavale N, Collyer J, Francis I, Jones ME, et al. Preoperative planning for DIEP breast reconstruction: early experience of the use of computerised tomography angiography with VoNavix 3D software for perforator navigation. J Plast Reconstr Aesthet Surg [Internet]. 2009 Nov [cited 2015 Sep 25];62(11):1464–9. Available from: http://www.sciencedirect.com/science/article/pii/S1748681508006475

88. Gacto-Sánchez P, Sicilia-Castro D, Gómez-Cía T, Lagares A, Collell T, Suárez C, et al. Computed tomographic angiography with VirSSPA three-dimensional software for perforator navigation improves perioperative outcomes in DIEP flap breast reconstruction. Plast Reconstr Surg [Internet]. 2010 Jan [cited 2015 Nov 1];125(1):24–31. Available from: http://www.ncbi.nlm.nih.gov/pubmed/20048587

89. Malhotra A, Chhaya N, Nsiah-Sarbeng P, Mosahebi A. CT-guided deep inferior epigastric perforator (DIEP) flap localization -- better for the patient, the surgeon, and the hospital. Clin Radiol [Internet]. 2013 Feb [cited 2015 Nov 1];68(2):131–8. Available from: http://www.ncbi.nlm.nih.gov/pubmed/22889458

90. Rozen WM, Garcia-Tutor E, Alonso-Burgos A, Corlett RJ, Taylor GI, Ashton MW. The effect of anterior abdominal wall scars on the vascular anatomy of the abdominal wall: A cadaveric and clinical study with clinical implications. Clin Anat [Internet]. 2009 Oct [cited 2015 Nov 1];22(7):815–22. Available from:

http://www.ncbi.nlm.nih.gov/pubmed/19644965

91. Cina A, Barone-Adesi L, Rinaldi P, Cipriani A, Salgarello M, Masetti R, et al. Planning deep inferior epigastric perforator flaps for breast reconstruction: a comparison between multidetector computed tomography and magnetic resonance angiography. Eur Radiol [Internet]. 2013 Aug [cited 2015 Oct 31];23(8):2333–43. Available from: http://www.ncbi.nlm.nih.gov/pubmed/23571697
92. Rozen WM, Ashton MW, Stella DL, Phillips TJ, Grinsell D, Taylor GI. The accuracy of computed tomographic angiography for mapping the perforators of the deep inferior epigastric artery: a blinded, prospective cohort study. Vol. 122, Plastic and reconstructive surgery. 2008.
93. Phillips TJ, Stella DL, Rozen WM, Ashton M, Taylor GI. Abdominal wall CT angiography: a detailed account of a newly established preoperative imaging technique. Radiology [Internet]. 2008 Oct 1 [cited 2015 Sep 15];249(1):32–44. Available from: http://pubs.rsna.org/doi/full/10.1148/radiol.2483072054
94. Rozen WM, Whitaker IS, Stella DL, Phillips TJ, Einsiedel PF, Acosta R, et al. The radiation exposure of Computed Tomographic Angiography (CTA) in DIEP flap planning: low dose but high impact. J Plast Reconstr Aesthet Surg [Internet]. 2009 Dec [cited 2015 Nov 23];62(12):e654-5. Available from: http://www.ncbi.nlm.nih.gov/pubmed/19121614
95. Niumsawatt V, Debrotwir AN, Rozen WM. Reducing radiation dose without compromising image quality in preoperative perforator flap imaging with CTA using ASIR technology. Int Surg [Internet]. Jan [cited 2015 Nov 23];99(4):485–91. Available from: http://www.pubmedcentral.nih.gov/articlerender.fcgi?artid=4114385&tool=pmcentrez&rendertype=abstract
96. Hummelink S, Hameeteman M, Hoogeveen Y, Slump CH, Ulrich DJO, Schultze Kool LJ. Preliminary results using a newly developed projection method to visualize vascular anatomy prior to DIEP flap breast reconstruction. J Plast Reconstr Aesthet Surg [Internet]. 2015 Mar [cited 2015 Aug 31];68(3):390–4. Available from: http://www.ncbi.nlm.nih.gov/pubmed/25498828
97. Ahn CY, Narayanan K, Shaw WW. In vivo anatomic study of cutaneous perforators in

free flaps using magnetic resonance imaging. J Reconstr Microsurg [Internet]. 1994 May [cited 2015 Nov 2];10(3):157–63. Available from: http://www.ncbi.nlm.nih.gov/pubmed/8071902

98. Chernyak V, Rozenblit AM, Greenspun DT, Levine JL, Milikow DL, Chia FA, et al. Breast Reconstruction with Deep Inferior Epigastric Artery Perforator Flap: 3.0-T Gadolinium-enhanced MR Imaging for Preoperative Localization of Abdominal Wall Perforators. Vol. 250, Radiology. 2009. p. 417–24.
99. Mathes DW, Neligan PC. Preoperative Imaging Techniques for Perforator Selection in Abdomen-Based Microsurgical Breast Reconstruction. Clin Plast Surg [Internet]. 2010 Oct [cited 2015 Apr 19];37(4):581–91. Available from: http://www.sciencedirect.com/science/article/pii/S0094129810000702
100. Aubry S, Pauchot J, Kastler A, Laurent O, Tropet Y, Runge M. Preoperative imaging in the planning of deep inferior epigastric artery perforator flap surgery. Skeletal Radiol [Internet]. 2013 Mar [cited 2015 Apr 19];42(3):319–27. Available from: http://www.ncbi.nlm.nih.gov/pubmed/22729378
101. Schaverien M V, Ludman CN, Neil-Dwyer J, McCulley SJ. Contrast-enhanced magnetic resonance angiography for preoperative imaging of deep inferior epigastric artery perforator flaps: advantages and disadvantages compared with computed tomography angiography: a United Kingdom perspective. Ann Plast Surg [Internet]. 2011 Dec [cited 2015 Jun 15];67(6):671–4. Available from: http://www.ncbi.nlm.nih.gov/pubmed/21407061
102. Greenspun D, Vasile J, Levine JL, Erhard H, Studinger R, Chernyak V, et al. Anatomic imaging of abdominal perforator flaps without ionizing radiation: Seeing is believing with magnetic resonance imaging angiography. J Reconstr Microsurg. 2010;26(1):37–44.
103. Pauchot J, Aubry S, Kastler A, Laurent O, Kastler B, Tropet Y. Preoperative imaging for deep inferior epigastric perforator flaps: a comparative study of computed tomographic angiography and magnetic resonance angiography. Eur J Plast Surg [Internet]. 2012 Jun 15 [cited 2015 Nov 1];35(11):795–801. Available from: http://link.springer.com/10.1007/s00238-012-0740-0
104. Schaverien M V, Ludman CN, Neil-Dwyer J, Perks AGB, Raurell A, Rasheed T, et al.

Relationship between venous congestion and intraflap venous anatomy in DIEP flaps using contrast-enhanced magnetic resonance angiography. Plast Reconstr Surg [Internet]. 2010 Aug [cited 2015 Mar 3];126(2):385–92. Available from: http://www.ncbi.nlm.nih.gov/pubmed/20679824

105. Agrawal MD, Thimmappa ND, Vasile J V, Levine JL, Allen RJ, Greenspun DT, et al. Autologous breast reconstruction: preoperative magnetic resonance angiography for perforator flap vessel mapping. J Reconstr Microsurg [Internet]. 2015 Jan [cited 2015 Apr 19];31(1):1–11. Available from: http://www.ncbi.nlm.nih.gov/pubmed/24875438
106. Scott JR, Liu D, Said H, Neligan PC, Mathes DW. Computed tomographic angiography in planning abdomen-based microsurgical breast reconstruction: a comparison with color duplex ultrasound. Plast Reconstr Surg [Internet]. 2010 Mar [cited 2015 Oct 31];125(2):446–53. Available from: http://www.ncbi.nlm.nih.gov/pubmed/20124830
107. Rozen WM, Phillips TJ, Ashton MW, Stella DL, Gibson RN, Taylor GI. Preoperative imaging for DIEA perforator flaps: a comparative study of computed tomographic angiography and Doppler ultrasound. Plast Reconstr Surg [Internet]. 2008 Jan [cited 2015 Nov 1];121(1):9–16. Available from: http://www.ncbi.nlm.nih.gov/pubmed/18176200
108. Liu DZ, Mathes DW, Zenn MR, Neligan PC. The application of indocyanine green fluorescence angiography in plastic surgery. J Reconstr Microsurg [Internet]. 2011 Jul [cited 2015 Nov 1];27(6):355–64. Available from: http://www.ncbi.nlm.nih.gov/pubmed/21717392
109. Nahabedian MY. Overview of Perforator Imaging and Flap Perfusion Technologies. Clin Plast Surg [Internet]. 2011 Apr [cited 2015 Apr 19];38(2):165–74. Available from: http://www.sciencedirect.com/science/article/pii/S0094129811000149
110. Pestana IA, Zenn MR. Correlation between abdominal perforator vessels identified with preoperative CT angiography and intraoperative fluorescent angiography in the microsurgical breast reconstruction patient. Ann Plast Surg [Internet]. 2014 Jan [cited 2015 May 9];72(6):S144-9. Available from: http://www.ncbi.nlm.nih.gov/pubmed/24835872
111. Komorowska-Timek E, Gurtner GC. Intraoperative perfusion mapping with laser-assisted indocyanine green imaging can predict and prevent complications in

immediate breast reconstruction. Plast Reconstr Surg [Internet]. 2010 Apr [cited 2015 Nov 1];125(4):1065–73. Available from: http://www.ncbi.nlm.nih.gov/pubmed/20335859

112. Duggal CS, Madni T, Losken A. An outcome analysis of intraoperative angiography for postmastectomy breast reconstruction. Aesthet Surg J [Internet]. 2014 Jan 1 [cited 2015 Nov 1];34(1):61–5. Available from: http://www.ncbi.nlm.nih.gov/pubmed/24396073

113. Holm C, Dornseifer U, Sturtz G, Ninkovic M. Sensitivity and specificity of ICG angiography in free flap reexploration. J Reconstr Microsurg [Internet]. 2010 Jul [cited 2015 Nov 2];26(5):311–6. Available from: http://www.ncbi.nlm.nih.gov/pubmed/20183789

114. Yamaguchi S, De Lorenzi F, Petit JY, Rietjens M, Garusi C, Giraldo A, et al. The "perfusion map" of the unipedicled TRAM flap to reduce postoperative partial necrosis. Ann Plast Surg [Internet]. 2004 Sep [cited 2015 Nov 1];53(3):205–9. Available from: http://www.ncbi.nlm.nih.gov/pubmed/15480004

115. Wapnir I, Dua M, Kieryn A, Paro J, Morrison D, Kahn D, et al. Intraoperative imaging of nipple perfusion patterns and ischemic complications in nipple-sparing mastectomies. Ann Surg Oncol [Internet]. 2014 Jan [cited 2015 Nov 2];21(1):100–6. Available from: http://www.ncbi.nlm.nih.gov/pubmed/24046104

116. Harder Y, Amon M, Laschke MW, Schramm R, Rücker M, Wettstein R, et al. An old dream revitalised: preconditioning strategies to protect surgical flaps from critical ischaemia and ischaemia-reperfusion injury. J Plast Reconstr Aesthet Surg [Internet]. 2008 Jan [cited 2015 Apr 28];61(5):503–11. Available from: http://www.ncbi.nlm.nih.gov/pubmed/18166506

117. Carroll CM, Carroll SM, Schuschke DA, Barker JH. Augmentation of skeletal muscle flap survival using platelet derived growth factor. Plast Reconstr Surg [Internet]. 1998 Aug [cited 2017 May 29];102(2):407–15. Available from: http://www.ncbi.nlm.nih.gov/pubmed/9703077

118. SC D, GI T. The delay phenomenon: the story unfolds. Plast Reconstr Surg. 1999;104(7):2079–91.

119. Myers MB CG. Augmentation of tissue survival by delay: an experimental study in

rabbits. Myers MB, Cherry G. Plast Reconstr Surg . 1967;39(4):397–401.

120. Mcfarlane R, Deyoung G, Henry R. The Design of a Pedicle Flap in the Rat to Study Necrosis and its Prevention. Plast Reconstr Surg. 1965;35:177–82.
121. Komorowska-Timek E, Timek T, Brady S, Buncke H. Perfusion, viability, and pedicle dependence in acute and delayed rat island skin flaps. Microsurgery. 2007;27:146–51.
122. Coşkunfirat O, Okşar H, Ozgentaş H. Effect of the delay phenomenon in the rat single-perforator-based abdominal skin flap model. Ann Plast Surg. 2000;45:42-7.
123. Myers M, Cherry G. Differences in the delay phenomenon in the rabbit, rat, and pig. Plast Reconstr Surg. 1971;47:73–8.
124. Milton SH. Experimental studies on island flaps. II. Ischemia and delay. Plast Reconstr Surg [Internet]. 1972 Apr [cited 2015 May 19];49(4):444–7. Available from: http://www.ncbi.nlm.nih.gov/pubmed/4552357
125. Jensen J, Handel N, Silverstein M, Waisman J, Gierson E. Extended skin island delay of the unipedicle TRAM flap: experience in 35 patients. Plast Reconstr Surg. 1995;96(6):1341–5.
126. Codner M, Bostwick III J, Nahai F, Bried J, Eaves F. TRAM flap vascular delay for high-risk breast reconstruction. Plast Reconstr Surg. 1995;96:1615–22.
127. Ribuffo D, Muratori L, Antoniadou K, Fanini F, Martelli E, Marini M, et al. A hemodynamic approach to clinical results in the TRAM flap after selective delay. Plast Reconstr Surg. 1997;99:1706–14.
128. Taylor GI, Corlett RJ, Caddy C., Zelt RG. An anatomic reivew of the delay phenonomen: II. Clinical applications . Plast Reconstr Surg. 89(3):408–16.
129. O'Shaughnessy KD1 MT. The surgical TRAM flap delay: reliability of zone III using a simplified technique under local anesthesia. Plast Reconstr Surg. 2008;122:1627–30.
130. Restifo R, Ward B, Scoutt L, Brown J, Taylor K. Timing, magnitude, and utility of surgical delay in the TRAM flap: II. Clinical studies. Plast Reconstr Surg. 1997;99(5):1217–23.
131. Pang C, Forrest C, Neligan P, Lindsay W. Augmentation of blood flow in delayed random skin flaps in the pig: effect of length of delay period and angiogenesis. Plast Reconstr Surg. 1986;78(1):68-74.
132. Morris SF, Taylor GI. The time sequence of the delay phenomenon: when is a surgical

delay effective? An experimental study. Plast Reconstr Surg [Internet]. 1995 Mar [cited 2016 Dec 12];95(3):526–33. Available from: http://www.ncbi.nlm.nih.gov/pubmed/7870778

133. Murry CE, Jennings RB, Reimer KA. Preconditioning with ischemia: a delay of lethal cell injury in ischemic myocardium. Circulation [Internet]. 1986 Nov [cited 2017 May 29];74(5):1124–36. Available from: http://www.ncbi.nlm.nih.gov/pubmed/3769170

134. Küntscher M V., Hartmann B, Germann G. Remote ischemic preconditioning of flaps: A review. Microsurgery [Internet]. 2005 [cited 2017 May 29];25(4):346–52. Available from: http://www.ncbi.nlm.nih.gov/pubmed/15880486

135. Tepper OM, Galiano RD, Kalka C, Gurtner GC. Endothelial progenitor cells: the promise of vascular stem cells for plastic surgery. Plast Reconstr Surg [Internet]. 2003 Feb [cited 2015 Apr 28];111(2):846–54. Available from: http://www.ncbi.nlm.nih.gov/pubmed/12560713

136. Forster NA, Künzi W, Giovanoli P. The reoperation cascade after breast augmentation with implants: what the patient needs to know. J Plast Reconstr Aesthet Surg [Internet]. 2013 Mar [cited 2015 Nov 14];66(3):313–22. Available from: http://www.ncbi.nlm.nih.gov/pubmed/23102610

137. Küntscher M V, Schirmbeck EU, Menke H, Klar E, Gebhard MM, Germann G. Ischemic preconditioning by brief extremity ischemia before flap ischemia in a rat model. Plast Reconstr Surg [Internet]. 2002 Jun [cited 2017 May 29];109(7):2398–404. Available from: http://www.ncbi.nlm.nih.gov/pubmed/12045567

138. Lancerotto L, Bayer LR, Orgill DP. Mechanisms of action of microdeformational wound therapy. Semin Cell Dev Biol [Internet]. 2012 Dec [cited 2015 Apr 13];23(9):987–92. Available from: http://www.ncbi.nlm.nih.gov/pubmed/23036531

139. Argenta LC, Morykwas MJ. Vacuum-assisted closure: a new method for wound control and treatment: clinical experience. Ann Plast Surg [Internet]. 1997 Jun [cited 2015 Apr 21];38(6):563–76; discussion 577. Available from: http://www.ncbi.nlm.nih.gov/pubmed/9188971

140. Argenta LC, Morykwas MJ, Marks MW, DeFranzo AJ, Molnar JA, David LR. Vacuum-assisted closure: state of clinic art. Plast Reconstr Surg [Internet]. 2006 Jun [cited 2015 Apr 21];117(7 Suppl):127S-142S. Available from:

http://www.ncbi.nlm.nih.gov/pubmed/16799380

141. Saxena V, Hwang C-W, Huang S, Eichbaum Q, Ingber D, Orgill DP. Vacuum-assisted closure: microdeformations of wounds and cell proliferation. Plast Reconstr Surg [Internet]. 2004 Oct [cited 2015 Mar 25];114(5):1086–96; discussion 1097-8. Available from: http://www.ncbi.nlm.nih.gov/pubmed/15457017
142. Chen S-Z, Li J, Li X-Y, Xu L-S. Effects of vacuum-assisted closure on wound microcirculation: an experimental study. Asian J Surg [Internet]. 2005 Jul [cited 2016 May 28];28(3):211–7. Available from: http://www.ncbi.nlm.nih.gov/pubmed/16024319
143. Heit YI, Lancerotto L, Mesteri I, Ackermann M, Navarrete MF, Nguyen CT, et al. External volume expansion increases subcutaneous thickness, cell proliferation, and vascular remodeling in a murine model. Plast Reconstr Surg [Internet]. 2012;130(3):541–7. Available from: http://www.ncbi.nlm.nih.gov/pubmed/22929239
144. Erba P, Ogawa R, Ackermann M, Adini A, Miele LF, Dastouri P, et al. Angiogenesis in wounds treated by microdeformational wound therapy. Ann Surg [Internet]. 2011 Feb [cited 2015 Apr 21];253(2):402–9. Available from: http://www.pubmedcentral.nih.gov/articlerender.fcgi?artid=3403722&tool=pmcentrez&rendertype=abstract
145. Orgill DP, Bayer LR. Update on negative-pressure wound therapy. Plast Reconstr Surg [Internet]. 2011 Jan [cited 2015 Apr 29];127 Suppl:105S-115S. Available from: http://www.ncbi.nlm.nih.gov/pubmed/21200280
146. Chen S-Z, Li J, Li X-Y, Xu L-S. Effects of vacuum-assisted closure on wound microcirculation: an experimental study. Asian J Surg. 2005;28(3):211–7.
147. Rhodius P, Haddad A, Matsumine H, Sakthivel D, Ackermann M, Sinha I, et al. Noninvasive Flap Preconditioning by Foam-Mediated External Suction Improves the Survival of Fasciocutaneous Axial-Pattern Flaps in a Type 2 Diabetic Murine Model. Plast Reconstr Surg [Internet]. 2018 Dec [cited 2019 Apr 12];142(6):872e-883e. Available from: http://www.ncbi.nlm.nih.gov/pubmed/30188471
148. Pugh CW, Ratcliffe PJ. Regulation of angiogenesis by hypoxia: role of the HIF system. Nat Med [Internet]. 2003 Jun [cited 2015 Mar 25];9(6):677–84. Available from: http://www.ncbi.nlm.nih.gov/pubmed/12778166

149. Mammoto A, Connor KM, Mammoto T, Yung CW, Huh D, Aderman CM, et al. A mechanosensitive transcriptional mechanism that controls angiogenesis. Nature [Internet]. 2009 Feb 26 [cited 2015 Apr 17];457(7233):1103–8. Available from: http://www.pubmedcentral.nih.gov/articlerender.fcgi?artid=2708674&tool=pmcentrez&rendertype=abstract

150. Wei S, Orgill DP, Giatsidis G. "Delivery of External Volume Expansion (EVE) through Micro-deformational Interfaces Safely Induces Angiogenesis in a Murine Model of Intact Diabetic Skin with Endothelial Cell Dysfunction (ECD)." Plast Reconstr Surg [Internet]. 2018 Nov [cited 2019 Apr 7];143(2):1. Available from: http://www.ncbi.nlm.nih.gov/pubmed/30531623

151. Erba P, Miele LF, Adini A, Ackermann M, Lamarche JM, Orgill BD, et al. A morphometric study of mechanotransductively induced dermal neovascularization. Plast Reconstr Surg [Internet]. 2011 Oct [cited 2015 Apr 21];128(4):288e-299e. Available from: http://www.pubmedcentral.nih.gov/articlerender.fcgi?artid=3350091&tool=pmcentrez&rendertype=abstract

152. Nissen NN, Polverini PJ, Koch AE, Volin M V, Gamelli RL, DiPietro LA. Vascular endothelial growth factor mediates angiogenic activity during the proliferative phase of wound healing. Am J Pathol [Internet]. 1998 Jun [cited 2015 Apr 21];152(6):1445–52. Available from: http://www.pubmedcentral.nih.gov/articlerender.fcgi?artid=1858442&tool=pmcentrez&rendertype=abstract

153. Hong YG, Kim SC, Koh KS. Flap Preconditioning with the Cyclic Mode (Triangular Waveform) of Pressure-Controlled Cupping in a Rat Model. Plast Reconstr Surg [Internet]. 2019 Jan [cited 2019 Apr 7];143(1):88e-98e. Available from: http://www.ncbi.nlm.nih.gov/pubmed/30325895

154. Giatsidis G, Cheng L, Haddad A, Ji K, Succar J, Lancerotto L, et al. Noninvasive induction of angiogenesis in tissues by external suction: sequential optimization for use in reconstructive surgery. Angiogenesis [Internet]. 2018 Feb 17 [cited 2019 Apr 7];21(1):61–78. Available from: http://www.ncbi.nlm.nih.gov/pubmed/29147813

155. Fourman MS, Gersch RP, Phillips BT, Nasser A, Rivara A, Verma R, et al. Comparison of

Laser Doppler and Laser-Assisted Indocyanine Green Angiography Prediction of Flap Survival in a Novel Modification of the McFarlane Flap. Ann Plast Surg [Internet]. 2014;00(00). Available from: http://www.ncbi.nlm.nih.gov/pubmed/24401807

156. Morykwas MJ, Argenta LC, Shelton-Brown EI, McGuirt W. Vacuum-assisted closure: a new method for wound control and treatment: animal studies and basic foundation. Ann Plast Surg [Internet]. 1997 Jun [cited 2015 Apr 21];38(6):553–62. Available from: http://www.ncbi.nlm.nih.gov/pubmed/9188970

157. Baldea BI, Toader S, Orbai P, Barsan S, Olariu R, Grigorescu DO, et al. The influence of diabetes mellitus on survival of abdominal perforator flaps: an experimental study in rats with slowly induced diabetes mellitus. J Reconstr Microsurg [Internet]. 2015 Feb [cited 2015 Apr 24];31(2):145–53. Available from: http://www.ncbi.nlm.nih.gov/pubmed/25360858

158. Wang Y, Chen S-Y, Gao W-Y, Ding J, Shi W, Feng X-L, et al. Experimental study of survival of pedicled perforator flap with flow-through and flow-end blood supply. Br J Surg [Internet]. 2015 Mar [cited 2015 Apr 24];102(4):375–81. Available from: http://www.ncbi.nlm.nih.gov/pubmed/25689293

159. Kelahmetoglu O, Demir R, Okten G, Demir A, Alpaslan Pinarli F, Diraman E. The effect of mesenchymal stem cells and sildenafil on flap viability in perforator-based flaps for ischemia/reperfusion injury: An experimental study. Microsurgery [Internet]. 2015 Feb 27 [cited 2015 Apr 24]; Available from: http://www.ncbi.nlm.nih.gov/pubmed/25726839

160. Lee H-J, Lim S-Y, Pyon J-K, Bang S-I, Oh K-S, Shin MS, et al. The influence of pedicle tension and twist on perforator flap viability in rats. J Reconstr Microsurg [Internet]. 2011 Sep [cited 2015 Apr 24];27(7):433–8. Available from: http://www.ncbi.nlm.nih.gov/pubmed/21717393

161. Coşkunfirat OK, Islamoğlu K, Ozgentaş HE. Posterior thigh perforator-based flap: a new experimental model in rats. Ann Plast Surg [Internet]. 2002 Mar [cited 2015 Apr 24];48(3):286–91. Available from: http://www.ncbi.nlm.nih.gov/pubmed/11862034

162. Rodríguez A, Alvarez A, Aguirrezabalaga J, Martelo F. The anteromedial thigh flap as a training model of a perforator flap in rat. J Reconstr Microsurg [Internet]. 2007 Jul [cited 2015 Apr 29];23(5):251–5. Available from:

http://www.ncbi.nlm.nih.gov/pubmed/17876727

163. Kayano S, Nakagawa M, Nagamatsu S, Koizumi T, Akazawa S. Why not perforator flap training models in rats? J Plast Reconstr Aesthet Surg [Internet]. 2010 Feb [cited 2015 Apr 24];63(2):e134-5. Available from: http://www.sciencedirect.com/science/article/pii/S1748681509002927

164. Zhuang Y, Hu S, Wu D, Tang M, Xu DC. A novel in vivo technique for observations of choke vessels in a rat skin flap model. Plast Reconstr Surg [Internet]. 2012 Aug [cited 2015 Apr 24];130(2):308–17. Available from: http://www.ncbi.nlm.nih.gov/pubmed/22842407

165. Yang D, Morris SF. An extended dorsal island skin flap with multiple vascular territories in the rat: A new skin flap model. J Surg Res [Internet]. 1999 Dec [cited 2015 Apr 24];87(2):164–70. Available from: http://www.ncbi.nlm.nih.gov/pubmed/10600345

166. Syed SA, Tasaki Y, Fujii T, Hirano A, Kobayashi K. A new experimental model: the vascular pedicle cutaneous flap over the dorsal aspect (flank and hip) of the rat. Br J Plast Surg [Internet]. 1992 Jan [cited 2017 May 29];45(1):23–5. Available from: http://www.ncbi.nlm.nih.gov/pubmed/1737202

167. Ahmed SS, Pierce J, Reid M, Thomson JG, Restifo RJ. A new experimental model: the vascular pedicled cutaneous flap over the mid-dorsum of the rat. Ann Plast Surg [Internet]. 1997 Nov [cited 2017 May 29];39(5):495–9. Available from: http://www.ncbi.nlm.nih.gov/pubmed/9374146

168. Mohan AT, Laungani AT, Rammos CK, Lachman N, Saint-Cyr M. Profunda artery perforator flap perforasome territories: implications of vascular anatomy for optimal flap design in reconstructive microsurgery. In: World Society of Reconstructive Microsurgery (WSRM). Mumbai, India; 2015. p. 24.

169. Sur Y-J, Morsy M, Mohan AT, Zhu L, Michalak GJ, Lachman N, et al. Three-dimensional computed tomographic angiographic study of the inter-perforator flow of the lower leg. Plast Reconstr Surg [Internet]. 2016 Jan 18 [cited 2016 Jan 29]; Available from: http://www.ncbi.nlm.nih.gov/pubmed/26796376

170. Rahmanian-Schwarz A, Rothenberger J, Hirt B, Luz O, Schaller H-E. A combined anatomical and clinical study for quantitative analysis of the microcirculation in the

classic perfusion zones of the deep inferior epigastric artery perforator flap. Plast Reconstr Surg [Internet]. 2011 Feb [cited 2015 May 9];127(2):505–13. Available from: http://www.ncbi.nlm.nih.gov/pubmed/21285755

171. Erić M, Ravnik D, Zic R, Dragnić N, Krivokuća D, Lekšan I, et al. Deep inferior epigastric perforator flap: an anatomical study of the perforators and local vascular differences. Microsurgery [Internet]. 2012 Jan [cited 2015 Apr 19];32(1):43–9. Available from: http://www.ncbi.nlm.nih.gov/pubmed/22113874
172. van den Heuvel MGW, Mermans JF, Ambergen AW, van der Hulst RRWJ. Perfusion of the deep inferior epigastric perforator flap measured by laser Doppler imager. Ann Plast Surg [Internet]. 2011 Jun [cited 2015 May 9];66(6):648–53. Available from: http://www.ncbi.nlm.nih.gov/pubmed/21233705
173. Tindholdt TT, Saidian S, Pripp AH, Tønseth KA. Monitoring microcirculatory changes in the deep inferior epigastric artery perforator flap with laser Doppler perfusion imaging. Ann Plast Surg [Internet]. 2011 Aug [cited 2017 Jun 1];67(2):139–42. Available from: http://content.wkhealth.com/linkback/openurl?sid=WKPTLP:landingpage&an=00000637-201108000-00013
174. Jorgensen SM, Demirkaya O, Ritman EL. Three-dimensional imaging of vasculature and parenchyma in intact rodent organs with X-ray micro-CT. Am J Physiol [Internet]. 1998 Sep [cited 2015 Apr 28];275(3 Pt 2):H1103-14. Available from: http://www.ncbi.nlm.nih.gov/pubmed/9724319
175. Laungani AT, Van Alphen N, Christner JA, Lachman N, Pawlina W, Ballman K V., et al. Three-dimensional CT angiography assessment of the impact of the dermis and the subdermal plexus in DIEP flap perfusion. J Plast Reconstr Aesthetic Surg [Internet]. 2015 Apr [cited 2018 Apr 12];68(4):525–30. Available from: http://www.ncbi.nlm.nih.gov/pubmed/25665491
176. Wells MY, Voute H, Bellingard V, Fisch C, Boulifard V, George C, et al. Histomorphology and vascular lesions in dorsal rat skin used as injection sites for a subcutaneous toxicity study. Toxicol Pathol [Internet]. 2010 Feb 1 [cited 2016 May 28];38(2):258–66. Available from: http://tpx.sagepub.com/content/38/2/258.long
177. Damen THC, Morritt AN, Zhong T, Ahmad J, Hofer SOP. Improving outcomes in

microsurgical breast reconstruction: lessons learnt from 406 consecutive DIEP/TRAM flaps performed by a single surgeon. J Plast Reconstr Aesthet Surg [Internet]. 2013 Aug [cited 2015 Oct 31];66(8):1032–8. Available from: http://www.sciencedirect.com/science/article/pii/S1748681513002246

178. Granzow JW, Levine JL, Chiu ES, Allen RJ. Breast reconstruction with the deep inferior epigastric perforator flap: History and an update on current technique. J Plast Reconstr Aesthetic Surg [Internet]. 2006 Jun [cited 2015 Jun 28];59(6):571–9. Available from: http://www.ncbi.nlm.nih.gov/pubmed/16716950
179. Schaverien M, Saint-Cyr M. Perforators of the lower leg: analysis of perforator locations and clinical application for pedicled perforator flaps. Plast Reconstr Surg [Internet]. 2008 Jul [cited 2015 Jun 13];122(1):161–70. Available from: http://www.ncbi.nlm.nih.gov/pubmed/18594401
180. Gill PS, Hunt JP, Guerra AB, Dellacroce FJ, Sullivan SK, Boraski J, et al. A 10-year retrospective review of 758 DIEP flaps for breast reconstruction. Plast Reconstr Surg [Internet]. 2004 Apr 1 [cited 2015 May 24];113(4):1153–60. Available from: http://www.ncbi.nlm.nih.gov/pubmed/15083015
181. Baumann DP, Lin HY, Chevray PM. Perforator Number Predicts Fat Necrosis in a Prospective Analysis of Breast Reconstruction with Free TRAM, DIEP, and SIEA Flaps. Plast Reconstr Surg [Internet]. 2010 May [cited 2015 Jun 27];125(5):1335–41. Available from: http://www.ncbi.nlm.nih.gov/pubmed/20440154
182. Mohan AT, Zhu L, Wang Z, Vijayasekaran A, Saint-Cyr M. Techniques and Perforator Selection in Single, Dominant DIEP Flap Breast Reconstruction: Algorithmic Approach to Maximize Efficiency and Safety. Plast Reconstr Surg. 2016;138(5).
183. Schaverien M, Saint-Cyr M, Arbique G, Brown SA, Rohrich RJ. Three- and four-dimensional arterial and venous anatomies of the thoracodorsal artery perforator flap. Plast Reconstr Surg [Internet]. 2008 May [cited 2015 Apr 19];121(5):1578–87. Available from: http://www.ncbi.nlm.nih.gov/pubmed/18453980
184. Boyd Taylor The vascular territories of the superior epigastric and the deep inferior epigastric systems.pdf.
185. Taylor GI, Tempest M. Michel Salmon: Arteries of the skin. Taylor GI, Tempest M., editors. New York: Churchill Livingstone; 1988. 72–80 p.

186. Taylor GI, Chubb DP, Ashton MW. True and “choke” anastomoses between perforator angiosomes: part i. anatomical location. Plast Reconstr Surg [Internet]. 2013 Dec [cited 2015 Jun 5];132(6):1447–56. Available from: http://www.ncbi.nlm.nih.gov/pubmed/24281575
187. Garvey PB, Salavati S, Feng L, Butler CE. Perfusion-Related Complications Are Similar for DIEP and Muscle-Sparing Free TRAM Flaps Harvested on Medial or Lateral Deep Inferior Epigastric Artery Branch Perforators for Breast Reconstruction. Plast Reconstr Surg [Internet]. 2011 Dec [cited 2015 Sep 30];128(6):581e-589e. Available from: http://www.pubmedcentral.nih.gov/articlerender.fcgi?artid=3226762&tool=pmcentrez&rendertype=abstract
188. El-Mrakby HH, Milner RH. The vascular anatomy of the lower anterior abdominal wall: a microdissection study on the deep inferior epigastric vessels and the perforator branches. Plast Reconstr Surg. 2002;109(2):539–43; discussion 544-547.
189. Rozen WM, Grinsell D, Koshima I, Ashton MW. Dominance between angiosome and perforator territories: A new anatomical model for the design of perforator flaps. J Reconstr Microsurg. 2010;26(8):539–45.
190. Chubb DP, Taylor GI, Ashton MW. True and “Choke” Anastomoses between Perforator Angiosomes. Plast Reconstr Surg [Internet]. 2013 Dec [cited 2017 Jun 1];132(6):1457–64. Available from: http://www.ncbi.nlm.nih.gov/pubmed/24281576
191. Losken A, Zenn MR, Hammel J a, Walsh MW, Carlson GW. Assessment of zonal perfusion using intraoperative angiography during abdominal flap breast reconstruction. Plast Reconstr Surg [Internet]. 2012;129(4):618e-24e. Available from: http://www.ncbi.nlm.nih.gov/pubmed/22456376
192. Yeoh MS, Kim DD, Ghali GE. Fluorescence angiography in the assessment of flap perfusion and vitality. Oral Maxillofac Surg Clin North Am [Internet]. 2013 Feb 1 [cited 2018 Apr 7];25(1):61–6, vi. Available from: http://www.ncbi.nlm.nih.gov/pubmed/23399396
193. Taylor GI, Corlett RJ, Boyd JB. The versatile deep inferior epigastric (inferior rectus abdominis) flap. Br J Plast Surg [Internet]. 1984 Jul [cited 2016 Feb 9];37(3):330–50. Available from: http://www.ncbi.nlm.nih.gov/pubmed/6234962
194. Moon HK, Taylor GI. The vascular anatomy of rectus abdominis musculocutaneous

flaps based on the deep superior epigastric system. [Internet]. Vol. 82, Plastic and reconstructive surgery. 1988. p. 815–32. Available from: http://www.ncbi.nlm.nih.gov/pubmed/2971981

195. Lee K-T, Mun G-H. Effects of Obesity on Postoperative Complications After Breast Reconstruction Using Free Muscle-Sparing Transverse Rectus Abdominis Myocutaneous, Deep Inferior Epigastric Perforator, and Superficial Inferior Epigastric Artery Flap. Ann Plast Surg [Internet]. 2016 May [cited 2018 Apr 7];76(5):576–84. Available from: http://www.ncbi.nlm.nih.gov/pubmed/25536199
196. Nahabedian MY, Momen B, Galdino G, Manson PN. Breast Reconstruction with the free TRAM or DIEP flap: patient selection, choice of flap, and outcome. Plast Reconstr Surg [Internet]. 2002 Aug [cited 2018 Apr 7];110(2):466–75; discussion 476-7. Available from: http://www.ncbi.nlm.nih.gov/pubmed/12142662
197. Orgill DP, Bayer LR. Negative pressure wound therapy: past, present and future. Int Wound J [Internet]. 2013 Dec 20 [cited 2015 Mar 22];10(s1):15–9. Available from: http://www.ncbi.nlm.nih.gov/pubmed/24251839
198. Glass GE, Murphy GF, Esmaeili A, Lai L-M, Nanchahal J. Systematic review of molecular mechanism of action of negative-pressure wound therapy. Br J Surg [Internet]. 2014 Dec [cited 2015 Apr 28];101(13):1627–36. Available from: http://www.ncbi.nlm.nih.gov/pubmed/25294112
199. Lu F, Ogawa R, Nguyen DT, Chen B, Guo D, Helm DL, et al. Microdeformation of three-dimensional cultured fibroblasts induces gene expression and morphological changes. Ann Plast Surg [Internet]. 2011 Mar [cited 2015 Apr 28];66(3):296–300. Available from: http://www.pubmedcentral.nih.gov/articlerender.fcgi?artid=3909952&tool=pmcentrez&rendertype=abstract
200. Huang C, Leavitt T, Bayer LR, Orgill DP. Effect of negative pressure wound therapy on wound healing. Curr Probl Surg [Internet]. 2014 Jul 1 [cited 2016 May 29];51(7):301–31. Available from: http://www.currprobsurg.com/article/S0011384014000847/fulltext
201. Mustoe TA, O'Shaughnessy K, Kloeters O. Chronic wound pathogenesis and current treatment strategies: a unifying hypothesis. Plast Reconstr Surg [Internet]. 2006 Jun

[cited 2015 Feb 24];117(7 Suppl):35S-41S. Available from: http://www.ncbi.nlm.nih.gov/pubmed/16799373

202. Koh KS, Park SW, Oh TS, Choi JW. Flap preconditioning by pressure-controlled cupping in a rat model. J Surg Res [Internet]. 2016 Aug [cited 2016 Dec 13];204(2):319–25. Available from: http://www.sciencedirect.com/science/article/pii/S002248041630083X

203. Kairinos N, Solomons M, Hudson DA. Negative-pressure wound therapy I: the paradox of negative-pressure wound therapy. Plast Reconstr Surg [Internet]. 2009 Feb [cited 2016 Dec 13];123(2):589–98; discussion 599-600. Available from: http://www.ncbi.nlm.nih.gov/pubmed/19182617

APPENDIX

APPENDIX 1: List of Products

V.A.C®, KCI, San Antonio, Texas, United States

V.A.C.® GranuFoam™ Sponge dressing KCI, San Antonio, Texas, United States

Sensa T.R.A.C pad, KCI, San Antonio, Texas, United States

VAC® Gel Strips, KCI, San Antonio, Texas, United States

SPY Elite System®, Novadaq Technologies Inc, Florida, United States

Indocyanine Green, Novadaq Technologies Inc Florida, United States

Adaptic ®, Systagenix, San Antonio, Texas

MicroFil ®, Flow Tech, Inc Carver, MA

Iodinated contrast medium (Omnipaque 240, GE Healthcare, Little Chalfont, UK)

24-gauge intravenous catheters (BD InsyteTM, Becton Dickinson, NJ)

Metal vessel clips (HorizonTM, Teleflex, Wayne, PA)

APPENDIX 2: List of Presentations

ORAL PRESENTATIONS

Mohan AT, Rammos C, Michalak G, Lachman N, Saint-Cyr M. Quantitative In-Vivo Assessment of Single Dominant Perforasomes for Bilateral DIEP Breast Reconstruction: Implications on Current Practice. Association of Plastic Reconstructive Surgeons of South Africa, APRSSA, Cape Town, S. Africa. P — 2014

Mohan AT, Rammos C, Michalak G, Lachman N, Saint-Cyr M. Profunda Artery Perforator Flap Perforasome Territories: implication of vascular anatomy for optimal flap design in reconstructive microsurgery. Association of Plastic Reconstructive Surgeons of South Africa, APRSSA, Cape Town, S. Africa. P — 2014

Mohan AT, Rammos C, Gaba P, Schupbach J, Saint-Cyr M. Impact of drain free donor site closure on patient outcomes in DIEP breast reconstruction. Society of Academic and Research Surgery (SARS) 2015, Durham, UK. P — 2015

Mohan AT, Hwang S, Laungani A, Zhu L, Bishop A, Saint-Cyr M. The impact of negative pressure therapy to enhance vascularity and wound healing in perforator flap preconditioning: an experimental rat model. Society of Academic and Research Surgery (SARS) 2015, Durham, UK. P — 2015

Mohan AT, Rammos C, Laungani A, Sur YJ, Morsy M, Michalak G, Lachman N, Saint- Cyr M. Evaluating perforasome and clinical applications of the superficial femoral artery perforator flap in loco-regional reconstruction. World Society of Reconstructive Microsurgery WSRM, India.P — 2015

Mohan AT, Hwang S, Zhu L, Laungani A, Friedrich P, Bishop A, Saint-Cyr M. Assessment of vascularization of a perforator flap after preconditioning negative pressure therapy in a rat model. World Society of Reconstructive Microsurgery WSRM, India .P — 2015

Mohan AT, Zhu L, Sur YJ, Morsy M, Rammos C, Michalak G, Lachman N, Saint-Cyr M Profunda Artery Perforator Flap Perforasome Territories: Implications of vascular anatomy for optimal flap design in reconstructive microsurgery. World Society of Reconstructive Microsurgery WSRM, India. P — 2015

Mohan AT, Sur YJ, Morsy M, Laungani AT, Saint-Cyr M. Three dimensional computed tomographic angiography of the lower leg; vascular structure and inter-perforator flow mechanism. World Society of Reconstructive Microsurgery WSRM, India 2015. P — 2015

Mohan AT, Rammos C, Gaba P, Schupbach J, Saint-Cyr M. Drain-free donor site DIEP flap: Comparative analysis with traditional abdominal drain closure in autologous breast reconstruction. American Society of Plastic Surgery, ASPS senior resident conference, Chicago, USA.NP 2014

Mohan AT, Rammos C, Laungani A, Michalak G, Lachman N, Saint-Cyr M. Evaluating Perforasome and Clinical Applications of the Superficial Femoral Artery Perforator Flap. American Society of Reconstructive Microsurgery, Bahamas, 2015.P 2015

Mohan AT, Rammos C, Michalak G, Lachman N, Saint-Cyr M Profunda Artery Perforator Flap Perforasome Territories: Implications of vascular anatomy for optimal flap design in reconstructive microsurgery. American Society of Reconstructive Microsurgery, ASRM, Bahamas, 2015.P 2015

Mohan AT, Akhavan A, Martinez-Jorge J, Wu P, Moran S, Saint-Cyr M. Strategies in oncological reconstruction: modification to the keystone perforator flap concept and maintaining vascular integrity. American Society of Reconstructive Microsurgery, ASRM, Bahamas, 2015.P 2015

Mohan AT, Zhu L, Mardini S, Moran S, Saint-Cyr M. Appraisal Of Perforasomes And Venosomes Of Perforators In Bilateral DIEP Breast Reconstruction Using Updated SpyQ Analysis. Plastic Surgery Research Council (PSRC), Seattle, USA. P 2015

Mohan AT, Zhu L, Rammos CK, Michalak G, Lachman N, Moran S, Saint-Cyr M. Profunda Artery Perforator Flap Perforasome Territories: Implications of Vascular Anatomy for Optimal Flap Design in Reconstructive Microsurgery. Plastic Surgery Research Council (PSRC), Seattle, USA. P 2015

Mohan AT, Zhu L, Vijaysekaran A, Wang Z, Saint-Cyr M. The Single Dominant Perforator DIEP Breast Reconstruction: A Review of Clinical Outcomes and Risk Factors. Accepted to American Society of Reconstructive Microsurgery ASRM 2016, Arizona, USA.

Mohan AT, Hwang SM, Zhu L, Michalak G, Laungani AT, Vernocke A, Anderson JL, Grande J, Bishop A, Moran SL, Saint-Cyr M. Radiological and Histological Assessment in Perforator Flap Microvasculature Following Pretreatment with Topical Negative Pressure Therapy: An Experimental Rat Model. American Society of Plastic Surgeons (ASPS), 2016 2016

Mohan AT, Chen C, Ferguson TB, Mardini S, Moran SL, Saint-Cyr M. Novel Assessment of Intraoperative venous outflow with near infrared indocyanine green angiography in bilateral DIEP breast reconstruction. American Society of Plastic Surgeons ASPS, Chicago, USA 2018

Mohan AT, Michalak GJ, Lachman N, Mardini S, Moran SL, Saint-Cyr M. Refinements in Microcirculation of the Deep and Superficial Venous Territories & Contribution of the Dermal Plexus in DIEP flap reconstruction: An Anatomical study. American Society of Plastic Surgeons ASPS, Chicago, USA 2018

POSTER PRESENTATIONS

Mohan AT, Zhu L, Michalak G, Chen C, Ferguson TB, Saint-Cyr M. Re-appraisal of angiosome territories in abdominal based perforator flap breast reconstruction using SPY-Q analysis and indocynanine green laser angiography in-vivo: lessons learnt to improve reconstructive outcomes. 20th Annual Balfour Surgery Research Symposium Mayo Clinic. 2014

Mohan AT, Hwang S, Zhu L, Laungani A, Friedrich P, Michalak G, Bishop A, Grande J, Saint-Cyr M. The impact of preconditioning in perforator flap surgery in an experimental rat model: negative pressure therapy on vascularity and wound healing. 20th Annual Balfour Surgery Research Symposium, Mayo Clinic 2014

Mohan AT, Hwang S, Lin Z, Lachman N, Saint-Cyr M. Reappraisal of arterial and venous perforator territories using SPY indocyanine green laser angiography in abdominal based perforator flap breast reconstruction. Society of Academic and Research Surgery (SARS) 2015, Durham, UK. 2015

Mohan AT, Zhu L, Michalak G, Lachman N, Saint-Cyr M. Quantitative assessment of single dominant perforator territories in bilateral DIEP breast reconstruction using indocyanine green fluorescence angiography and 4D CT imaging. World Society of Reconstructive Microsurgery WSRM, Mumbai, India 2015

APPENDIX 3: Publications

1. Mohan AT, Saint-Cyr M. Anatomic and physiological fundamentals for autologous breast reconstruction. Gland Surg. Apr 2015;4 (2):116-33. PMID 26005644

2. Mohan AT, Rammos CR, Akhavan A, Martinez-Jorge J, Wu P, Moran S, Behan F, Mardini S, Sim F, Saint-Cyr M. Evolving Concepts of Keystone Perforator Flap: Principles of Perforator Anatomy, Design Modifications and Extended Clinical Applications. Plast Reconstr Surg *ePub Feb 2016*
3. Sur YJ, Morsy M, Mohan AT, Zhu L, Lachman N, Saint-Cyr M. The first perforating branch of the deep femoral artery - a reliable receipient vessel for vascularized fibular grafts: An anatomical study. J Plast Reconstr Aesth Surg. 2016;69:351-8. doi: 10.1016/j.bjps.2015.10.024.

4. Mohan AT, Saint-Cyr M. Advances in Imaging Technologies for Planning Breast Reconstruction. Gland Surg. 2016;5:242-54. doi: 10.3978/j.issn.2227-684X.2016.01.03.

5. Mohan AT, Zhu L, Wang Z, Vijayasekaran A, Saint-Cyr M. Techniques and Perforator Selection in Single Dominant DIEP breast reconstruction: Algorithmic approach to maximize efficiency and safety has been built ad requires approval. Plast Reconstr Surg. *Accepted December 2015*
6. Sur YS, Morsy M, Mohan AT, Zhu L, Michalak GJ, Lachman N, Laungani AT, Alphen NV, Saint-Cyr M. Three-dimensional computed tomographic angiographic study of the inter-perforator flow of the lower leg. Plast Reconstr Surg: 2016;137:1615-28.

7. Mohan AT, Zhu L, Sur YJ, Morsy M, Michalak GJ, Lachman N, Rammos CK, Saint-Cyr M. Application of Posterior Thigh 3D Profunda Artery Perforator (PAP) Perforasomes in Refining Next Generation Flap Designs: T-PAP, V-PAP, S-PAP. Plast Recon Surg. 2017:139834-45. doi: 10.1097/PRS.0000000000003224.

8. Mohan AT, Zhu L, Morsy M, Sur YJ, Michalak GJ, Lachman N, Mardini S, Saint-Cyr M. Re-appraisal of Perforasomes of the Superficial Femoral Artery, Descending Genicular and Saphenous Artery and Clinical Applications to Loco-Regional Reconstruction. Plast Recon Surg *Accepted* 2017

9. Tomouk T, Mohan AT, Azizi A, Conci E, Brickley EB, Malata CM. Donor site morbidity in DIEP free flap breast reconstructions: A comparison of unilateral, bilateral and bipedicled surgical procedure types. J Plast Recon Surg. 2017. Epub doi.org/10.1016/j.bjps.2017.05.044

APPENDIX 4: Preoperative CTA DIEP protocol

PROTOCOL V05_00A

SIEMENS E-128
06/30/17

Elizmab
6 LIST 3

PRE OP CTA FOR DIEP FLAP

GENERAL: This protocol is used for Pre-Op planning for breast reconstruction. They are looking at the anatomy of the DIEP (Deep Inferior Epigastric Perforators) Arteries.

***Place two Beekley markers together to make an "x". Place the "x" directly on the umbilicus. Not around it, right over it. The surgeons use this for measuring purposes.**

Patient supine, feet first, arms above head.

A CT chest may be requested by the referring physician or radiologist. If requested by radiologist, you will have to call scheduling and have it put on the CHESTX calendar. Arrive the chest in RIMS and use study split. Append on a routine chest and scan immediately after the CTA. Chest is read by the chest Radiologist..

MEDICATION: Medication Protocol

TOPO: PA, 512 Top of liver through greater trochanters. **STOP SCAN** when below greater trochanters.
If chest ordered too: PA, 768 Top of chest through greater trochanters.

PREP DELAY	Monitor Location	mA(s)	Monitoring Delay	Monitoring ISD	Enhancement (Trigger)	Diagnostic Delay (post-threshold)
Siemens CARE Bolus	Descending Aorta, 2 cm above start location	50	10 sec	2 sec	150	11 sec

CTA SCAN: Scan from 5cm above the umbilicus (*you can measure this off the topo from the beekley "x") through the lesser trochanters.

SIEMENS	E-128
Scan Type	Spiral
Rotation Time (s)	0.5
Collimation	128 x 0.6
Pitch	0.4
kVp	120
Quality ref. mAs	350
CARE Dose 4D	ON
CARE kV / Slider	ON / 11
Prep Delay	CARE Bolus
AI*	inspiration
Min. Rotro(sec)	*0.6*
CTDIvol (mGy)	*17*
Base Protocol	*BodyAngioVol*

SAMPLE IMAGES: Located at the end of the protocol

	RECON 1	RECON 2	RECON 3	RECON 4	RECON 5	RECON 6	RECON 7
Series description	CTA DIEP	CTA DIEP 250 FOV (center FOV to include anterior skin)	Cor CTA DIEP	Axial MIPS	Coronal MIPS	Rt Sag MIPS	Left Sag MIPS
Type	Axial	Axial	3D-MIP	3D-MIP	3D-MIP	3D-MIP	3D-MIP
Recon Axis	---	---	Coronal	---	Coronal	Sagittal	Sagittal
Start	5cm above the umbilicus	5cm above the umbilicus	anterior to beekly marker	Pubic symphysis	Anterior to Beekley	Midline	Midline
End	Through lesser trochanters	Through lesser trochanters	posterior to aortic bifurcation	Through umbilicus with marker	Cover epigastrics	Rt Abdominal Wall	Left Abdominal Wall
Angle	None	None	None	None	To visualize most of the arteries in one plane	None	None
Image Order	Craniocaudal	Craniocaudal	Anterior to Posterior	**Inferior to Superior**	Anterior to Posterior	Medial to lateral	Medial to lateral
SAFIRE / Strength	---	---	---	---	---	---	---
Kernel	I40	I40	I40	I40	I40	I40	I40
Slice (mm)	1.5	1.5	2	30	20	20	20
Increment (mm)	0.8	0.8	2	5	2	2	2
FOV (mm)	Patient	*250	Patient	Patient	Patient	Patient	Patient
:-Q/-D	---	---	---	---	---	---	---
Network	IAU and Radiologist	IAU and Radiologist	IAU and Radiologist	IAU and Radiologist	IAU and Radiologist	IAU and Radiologist	IAU and Radiologist
FILMING							
Format	20:1	---	---	---	---	---	---
WW, WC	550/60	550/60	550/60	550/60	550/60	550/60	550/60
Images	Every 4th	---	---	---	---	---	---

CHARGE	# Charges	Scan Sequence No.'s	w/ or w/o 3D
CTA Pelvis	1	1	72191

Images read by a vascular radiologist.